Characterizing Polymers with Complex Architecture using Pyrene Excimer Fluorescence

by

Janine Lydia Thoma

A thesis
presented to the University of Waterloo
in fulfillment of the
thesis requirement for the degree of
Doctor of Philosophy
in
Chemistry

Waterloo, Ontario, Canada, 2021

Examining Committee Membership

The following served on the Examining Committee for this thesis. The decision of the Examining Committee is by majority vote.

External Examiner	**Dr. Elizabeth Gillies** Professor, Department of Chemistry and Chemical and Biochemical Engineering Western University, London, Canada
Supervisor	**Dr. Jean Duhamel** Professor, Department of Chemistry University of Waterloo, Waterloo, Canada
Internal Member #1	**Dr. Mario Gauthier** Professor, Department of Chemistry University of Waterloo, Waterloo, Canada
Internal Member #2	**Dr. Xiaosong Wang** Professor, Department of Chemistry University of Waterloo, Waterloo, Canada
Internal-External Member	**Dr. Michael Tam** Professor, Department of Chemical Engineering University of Waterloo, Waterloo, Canada

Author’s Declaration

This thesis consists of material all of which I authored or co-authored: see Statement of Contributions included in the thesis. This is a true copy of the thesis, including any required final revisions, as accepted by my examiners. I understand that my thesis may be made electronically available to the public.

Statement of Contributions

I completed all work and writing presented in this thesis with consultation with my supervisor Prof. Jean Duhamel. This thesis consists of one manuscript written for publication.

Chapter 2: Thoma, J. L.; McNelles, S. A.; Adronov, A.; Duhamel, J. Direct Measure of the Local Concentration of Pyrenyl Groups in Pyrene-Labeled Dendrons Derived from the Rate of Fluorescence Collisional Quenching. *Polymers* **2020**, *12*, 1-14.

Abstract

This thesis combines two different models, namely the model free analysis (MFA) and the fluorescence blob model (FBM), that were used to study the conformation and internal dynamics of two highly branched macromolecules, that were fluorescently labeled with the dye pyrene. Pyrene was selected due to its ability to form an excimer upon encounter between an excited and a ground-state pyrene. The effects of branching on the dynamics of the chain ends of 2,2-bis(hydroxymethyl)propionic acid backbone dendrons were first studied. Six generations of the dendrons, G(1)-G(6), were prepared with their terminal ends covalently labeled with a pyrenyl moiety (Py_x-G(N), $x = 2^N$). The MFA was used to calculate the average rate constant $<k>$ of excimer formation, which was found to be proportional to the local concentration of pyrene $[Py]_{loc}$. To account for the presence of aggregated pyrenyl groups, whose contribution was found to be significantly larger for the G5 and G6 dendrons, $<k>$ was divided by the fraction of pyrenyl groups forming excimer through diffusion, f_{diff}. $<k>$ was found to depend on the solvent, due to different solvent viscosity (η) and probability (p) of pyrene excimer formation (PEF). Consequently, different trends were obtained by plotting $<k>$ as a function of $[Py]_{loc}$ in tetrahydrofuran (THF), toluene, *N*,*N*-dimethylformamide (DMF), and dimethylsulfoxide (DMSO). To account for these differences in $<k>$ with solvent, the model compound ethyl 4-(1-pyrene)butyrate (PyBE) was prepared. The rate constant for PEF through diffusive intermolecular encounters, k_{diff}, was determined for PyBE in each of the 4 solvents and used to normalize $<k>$. $<k>/f_{diff} \times k_{diff}$–*versus*–$[Py]_{loc}$ was then plotted and the data in each of the 4 solvents collapsed onto a single master trend, which passed through the origin,

thus confirming the direct relationship between $<k>$ and $[Py]_{loc}$ and suggesting that the dendron side chains obeyed Gaussian statistics.

The chain end dynamics of a polymer with a different branching architecture, namely polymeric bottle brushes (PBBs), were then investigated. Four poly(oligo(ethylene glycol) methyl ether methacrylates) (P(PyEG$_y$MA), y = 3, 5, 8, and 12) with side chain lengths containing 12, 18, 27, and 39 atoms, respectively, were end-labeled with a 1-pyrenemethoxy group. $<k>$ was then determined in THF, DMF, dioxane, and DMSO. $[Py]_{loc}$ was calculated assuming that each side chain probed a spherical *blob*, whose diameter was represented by the end-to-end distance of the side chains, $r_{ee,SC}$, assuming a Gaussian conformation in solution with $r_{ee,SC} = n^{0.5} \times l$. The model compound 1-pyrenemethoxy di(ethylene glycol) methyl ether (PyEG$_2$ME) was synthesized and k_{diff} was determined to normalize for η and p. A plot of $<k>/f_{diff} \times k_{diff}$–*versus*–$[Py]_{loc}$ was considered again and the data obtained in THF, DMF, and dioxane were found to converge onto a single trend. Unfortunately, DMSO was found to be too polar to study the fully pyrene labeled P(PyEG$_y$MA) PBBs, and it is believed that the hydrophobic pyrene pendant was not fully solvated and resided closer to the polymethacrylate (PMA) main chain. Excellent agreement was found when comparing the results obtained between the PBBs and the dendrons, even though the two families of macromolecules exhibited a very different branching architecture.

The PBB architecture was then investigated in more detail in organic and aqueous environments. A series of poly(oligo(ethylene glycol) methyl ether methacrylate) PBBs were synthesized by randomly copolymerizing an oligo(ethylene glycol) methyl ether methacrylate with penta(ethylene glycol) 1-pyrenemethyl ether methacrylate) to yield a series of PyEG$_5$-

PEG_nMA samples, where n = 0, 3, 4, 5, 7, 9, and 19). The change in main chain flexibility in organic solvents was probed as a function of increasing side chain length using the FBM. The FBM retrieves the number of structural units, N_{blob}, encompassed per unit volume or *blob*. As the side chain length of a PBB increases, there is an increase in steric repulsion between the side chains, which causes stiffening of the polymer main chain. This increase in polymer stiffness is reflected by a decrease in N_{blob} and an increase in the persistence length, l_p, of the PBBs. In an attempt to quantify the change in N_{blob} with increasing side chain length, a *blob*-based approach was suggested, which combines the FBM and the Kratky-Porod worm like chain (KPWLC) model to obtain l_p. The l_p values obtained from the FBM approach were plotted as a function of the number of atoms, N_S, in the side chain, where it was found that l_p increased linearly with N_S^2, as had been proposed theoretically. l_p was also determined from conformation plots based on intrinsic viscosity, $[\eta]$, using gel permeation chromatography (GPC). Using a Bohdanecky linearization, the l_p was extracted from the GPC traces and found to be 1.8 times larger than the l_p found using the FBM. This discrepancy was attributed to the difference in length scales probed by each technique.

The $PyEG_5$-PEG_nMA PBBs were then studied in an aqueous solution to investigate the shielding effects afforded by the oligo(ethylene glycol) side chains of PBBs to the hydrophobic pyrenyl groups. The FBM was used to investigate the level of aggregation of the pyrenyl moieties as well as the effect that the side chain length had on shielding pyrene from the aqueous environment. The change in the volume probed by pyrene was studied using N_{blob} obtained from the FBM of the fluorescence decays and comparing the results obtained in organic solvents, where both the polymer and pyrene were fully soluble, to those obtained in

an aqueous solution, where the polymer is soluble but pyrene is only slightly soluble. When compared to a series of poly(alkyl methacrylates) labeled with a shorter 1-pyrenebutyl methacrylate linker, the N_{blob} values obtained for $PyEG_5$-PEG_nMA PBBs in water were found to overlap perfectly. These results suggested that even though pyrene is attached onto a 16 atom-long linker, it can only probe a volume similar to that afforded by a 4 atom-long linker in water. This study also indicated that the oligo(ethylene glycol) side chains of the PBBs generate an organic-like environment around the main chain, that shields the hydrophobic pyrenyl labels from interacting with the aqueous phase.

Acknowledgements

I would like to thank Prof. Jean Duhamel for giving me the opportunity as an undergraduate student to work in his research laboratory as a CHEM 494 student 6 years ago. Working in the Duhamel laboratory, I found my passion for research in polymer chemistry, which has driven me throughout my graduate studies career. His mentorship, patience, and dedication have been crucial to my success.

I would like to thank my committee members Prof. Mario Gauthier, Prof. Michael Tam, and Prof. Xiaosong Wang for their support and feedback throughout the years.

I would also like to thank all of the past and current members of both the Duhamel and Gauthier laboratories who have offered me guidance, assistance, and friendship.

Dedication

I would like to dedicate this thesis to my parents Sharon and Rene, my stepfather Guy, my siblings Rina and Marcel and my fiancé Remi. I would also like to dedicate this thesis to my twin nephews Lukas and Domenic. Throughout the last 6 years of graduate school, they have supported me and kept me grounded. I am happy to finally have an answer to the age old question “When are you going to be done school?”.

Table of Contents

List of Figures

List of Tables

List of Schemes

List of Abbreviations

2-D	two-dimensional
3-D	three-dimensional
AFM	atomic force microscopy
ATRP	atom transfer radical polymerization
DCM	dichloromethane
DDS	drug delivery systems
DMF	*N*,*N*-dimethylformamide
DMSO	dimethylsulfoxide
DP	degree of polymerization
DRI	differential refractive index
EEC	end-to-end cyclization
EFDs	excimer forming dyes
EG	ethylene glycol
FBM	fluorescence blob model
FCQ	fluorescence collisional quenching
FDA	food and drug administration
FRET	fluorescence resonance energy transfer
G(*N*)	generation number
GPC	gel permeations chromatography
HASE	hydrophobically modified alkali swellable emulsion polymer

ICAR-ATRP	Initiators for Continuous Activator Regeneration Atom Transfer Radical Polymerization
IRF	instrument response function
KPWLC	Kratky-Porod worm-like chain
MALLS	multi-angle laser light scattering
MFA	model free analysis
MMOs	molecular mechanics optimizations
MWD	molecular weight distribution
NAF	nanosized amylopectin fragment
NMP	nitroxide mediated polymerization
NMR	nuclear magnetic resonance
OLD	organic-like domain
PA	poly(aryl ether)
PAMAM	poly(amido amine)
PBBs	polymeric bottle brushes
PDMA	poly(*N*,*N*-dimethylacrylamide)
PEF	pyrene excimer fluorescence/formation
PEG	poly(ethylene glycol)
PEG_nMA	poly(oligo(ethylene glycol) methyl ether methacrylate)
PGA	poly(*L*-glutamic acid)

PGMA-Py/PNIPAM	poly(glycidyl methacrylate) with a bivalent linker onto which a 1-pyrenebutyroyl group and a poly(*N*-isopropyl acrylamide) side chain were attached
PIMA	poly(isobutylene-*alt*-maleic anhydride)
PMA	polymethacrylate
PMA-*g*-P*n*BA	polymethacrylate backbone with poly(*n*-butyl acrylate) side chains
PMA-*g*-PS	polymethacrylate backbone with polystyrene side chains
PMMA	poly(methyl methacrylate)
PMMA-*g*-Py/PEG	polymethacrylate main chain with pyrene labels and poly(oligoethylene glycol) side chains
PMPA	poly(2,2-bis(hydroxymethyl)-propanoic acid)
P(PyEG$_y$MA)	poly(oligo(ethylene glycol) 1-pyrenemethyl ether methacrylate)
PS-*g*-P*n*HIC	polystyrene main chain with poly(*n*-hexyl isocyanate) side chains
PyBE	ethyl 4-(1-pyrene)butyrate
PyC4-PC$_n$MA	poly(alkyl methacrylate)s labeled with 1-pyrenebutanol
PyEG$_2$ME	1-pyrenemethoxy di(ethylene glycol) methyl ether
PyEG$_5$-OH	1-pyrenemethyl ether penta(ethylene glycol)
PyEG$_5$-PEG$_n$MA	poly(oligo(ethylene glycol) methyl ether methacrylate)s labeled with 1-pyrenemethyl ether penta(ethylene glycol)

$Py_x(G(N))$	2,2-bis(hydroxymethyl)propionic acid backbone dendrons labeled with x ($=2^N$) molecules of pyrene
Py-WSP	pyrene-labeled water-soluble polymer
QTP	quasi-two-parameter
RAFT	reversible addition-fragmentation chain transfer polymerization
RBF	round bottom flask
RI	refractive index
ROMP	ring-opening metathesis polymerization
SANS	small angle neutron scattering
SAXS	small angle X-ray scattering
SI	supporting information
SLS	static light scattering
SSF	steady-state fluorescence
SUs	structural units
THF	tetrahydrofuran
TRF	time-resolved fluorescence
UV	ultraviolet
WLC	worm-like chain

List of Symbols

$[Py]_{loc}$	local concentration of pyrene
$[Q]_{loc}$	quencher concentration experienced locally by the excited dye
a_i	pre-exponential factors
A_η	*y*-intercept of a conformation plot
A_0	Function equal to $0.46 - 0.53 \times log(d/2l_p)$
A_2	second virial coefficient
b	length of a structural unit
B_η	slope of a conformation plot
B_0	constant equal to 1.05
C_∞	characteristic ratio
C_m	mass concentration
C-*C*	carbon – carbon bond
D	diffusion coefficient
$Đ$	dispersity
D^*	excited dye
dn/dc	refractive index increment
d_{PS}	diameter of the PS main chain
f_{agg}	molar fraction of aggregated pyrenes
f_D	molar fraction of improperly stacked aggregated pyrene species

f_{diff}	molar fraction of pyrenyl groups forming excimer through diffusion
f_{E0}	molar fraction of properly stacked aggregated pyrene species
f_{free}	molar fraction of pyrenyl groups which do not form excimer
f_{Mfree}	fraction of pyrenyl groups, that are isolated along the chains and do not form excimer
$I(q)$	experimental excess scattering intensity
I_1	first peak of the monomer emission
I_3	third peak of the monomer emission
I_E	fluorescence intensity of the pyrene excimer
I_M	fluorescence intensity of the pyrene monomer
$<k>$	average rate constant of excimer formation
k	pseudo-unimolecular rate constant
k_B	Boltzmann constant
k_{blob}	rate constant of excimer formation inside a blob
k_{cy}	rate constant of cyclization
k_{diff}	rate constant of excimer formation through diffusive encounters
k_{diff}[inter]	bimolecular rate constant for intermolecular pyrene excimer formation
k_{PEF}	rate constant of pyrene excimer formation
k_Q	quenching rate constant

k_{rad}	radiative rate constant
K	optical constant
K_{eq}	equilibrium constant
l	length of a bond
l_b	contour length per monomer unit
l_g	distance between two P*n*HIC side chain joints to the main chain
l_k	Kuhn length
l_p	persistence length
l_p(fluo)	persistence length obtained from the fluorescence blob model
l_p^o	persistence length obtained at an infinitely high viscosity
$<L^2>^{1/2}$	Square root of the square of the average distance between two pyrenyl groups
L	contour length
M	molar mass
M_0	molar mass of a structural unit or side chain
M_L	molar mass per unit contour length
M_n	number-average molecular weight
M_w	weight-average molecular weight
$<n>$	average number of ground-state pyrenyl groups
n	number of bonds
N_A	Avogadro's number

N_{blob}	number of monomer units encompassed within a blob
N_{blob}^{exp}	experimentally determined N_{blob}
N_{blob}^{theo}	theoretically determined N_{blob}
N_k	number of Kuhn segments
N_S	number of non-hydrogen atoms in the side chain
p	probability of forming an excimer
$P(\theta)$	particle scattering factor
Py_{diff}*	pyrenes that form an excimer through diffusive encounters
Py_{free}*	pyrenes that are isolated in solution and cannot form excimer
q	scattering vector
Q	quencher
$\langle r_{ee}^2 \rangle$	average squared end-to-end distance of a linear chain
r	radius
r_{EE}	end-to-end distance of a polymer coil
$r_{ee,SC}$	end-to-end distance of the side chains
R	molecular diameter of pyrene
$\langle R^2 \rangle_0$	unperturbed mean squared end-to-end distance
$\langle R_g^2 \rangle$	average squared radius of gyration of a polymer coil
$\langle R_G^2 \rangle_C$	average squared cross-sectional radius of gyration of the main chain
$\langle R_g^2 \rangle_M$	average squared radius of gyration of the main chain

$\langle R_g^2 \rangle_z$	*z*–average squared radius of gyration
R_θ	excess Rayleigh ratio
R_c	radius of curvature of a comb molecule with flexible side chains
R_G	radius of gyration
S-S	sulfur – sulfur bond
T	absolute temperature
V_{blob}	volume of a blob
V_{coil}	volume of a polymer coil
$V_{dendron}$	volume of a dendron
V_{Py}	volume probed by pyrene
x	molar fraction of subunits bearing a pyrenyl label
δ	contribution of the side chains at the ends of the main chain
ΔF	free energy for bending of the comb molecule
ε_b	molar extinction coefficient of bound pyrene
ε_f	molar extinction coefficient of free pyrene
η	viscosity
$[\eta]$	intrinsic viscosity
θ	angle
λ	wavelength
λ_0	short range contributions to the persistence length between the main chain and the side chain units near the main chain

λ^{-1}	main chain stiffness parameter
λ_b	contributions to the persistence length from the side chains
ν	Flory exponent
σ	grafting density
$<\tau>$	average lifetime
τ_0	natural lifetime of a dye
τ_D	lifetime of the improperly stacked excimer
τ_{E0}	lifetime of the properly stacked excimer
τ_E	lifetime of the excimer
τ_i	decays time
τ_M	lifetime of the monomer
τ_S	short lifetime
Φ	crowding parameter
$\Phi_{o,\infty}$	theoretical Flory constant
ϕ_E	quantum yield of the excimer
ϕ_M	quantum yield of the monomer

Chapter 1

Introduction

The conformation of macromolecules in solution has a major effect on their properties. For example, a linear chain in a good or poor solvent will reach the semi-dilute regime, where the viscosity of the polymer solution increases rapidly with increasing polymer concentration, at a lower or higher concentration, respectively.[1] A structured or denatured polypeptide can yield a catalytically active protein or an amorphous coil made of more or less folded segments, respectively.[2] Linear chains with short or long side chains are coiled or elongated in solution, yielding concentrated solutions that have a high and low number of entanglements, resulting in high and low modulus, respectively.[3] The profound impact that macromolecular conformation has on the solution properties of macromolecules has resulted in a sustained effort to develop techniques that could probe macromolecular conformations in solution. ^{1}H NMR,[4,5] circular dichroism,[6] rheology,[1] intrinsic viscosity,[7,8] and light scattering[9,10] represent a small list of techniques that have been applied over the years to solve macromolecular conformations in solution. Perhaps not as intensively used, fluorescence-based methods such as fluorescence anisotropy and fluorescence resonance energy transfer (FRET) are also well-established techniques, that are applied to study the conformations of macromolecules in solution by monitoring the delocalization of the emission dipole moment of an appropriate dye with respect to its excitation dipole moment or the transfer of energy of a donor to an acceptor, respectively.[11] In these fluorescence experiments, the dyes are physically or covalently bound to the macromolecule so that the behavior of the dyes directly reflects the behavior of the macromolecule. The main advantage of using fluorescence to probe macromolecules resides in its outstanding sensitivity, which allows the study of macromolecules at concentrations that are 2-to-3 orders of magnitude lower than for any other technique.

One fluorescence technique, that is not known for its capability to probe the conformation of macromolecules in solution is pyrene excimer fluorescence/formation (PEF).[12,13] PEF is a chemical reaction where an excimer is formed from the encounter between an excited and a ground-state pyrene. Consequently, the rate constant for PEF (k_{PEF}), which can be determined from steady-state and time-resolved fluorescence measurements, is proportional to the concentration of ground-state pyrenes experienced by an excited pyrene.[13] But if a macromolecule happens to be covalently labeled with a pyrene derivative, then k_{PEF} equals $k_{diff} \times [Py]_{loc}$, where k_{diff} is the PEF rate constant for diffusive encounters and $[Py]_{loc}$ is the local concentration of ground-state pyrenyl labels experienced by an excited pyrene.[14] In turn, $[Py]_{loc}$ is proportional to the local density of the pyrene-labeled macromolecule in solution since the pyrenyl labels are covalently attached to it, and as such k_{PEF} yields quantitative information about the conformation of a macromolecule. However, the tricky part in a PEF experiment consists in disentangling the contributions to k_{PEF}, that arise from the internal dynamics of the macromolecule (k_{diff}) and its local conformation ($[Py]_{loc}$). Over the past 25 years, the Duhamel Laboratory has introduced two new methodologies[15] that have shown promising results for determining the conformation in solution of rigid biological macromolecules such as polysaccharides[16,17] and polypeptides.[18–21] In this context, the purpose of this thesis is to assess whether the same PEF-based methodology, that worked so well for biological macromolecules, could be applied to the study of highly branched synthetic macromolecules, namely dendrimers and polymeric bottle brushes (PBBs). This Introduction will go over the principles of PEF and how it can be applied to probe the conformation of

macromolecules in solution, and provide an overview of the properties of dendrimers and PBBs.

1.1 Pyrene Excimer Fluorescence

Excited pyrene dimers, or excimers, were discovered in 1955 by Förster and Kasper.[12] Birks demonstrated in 1963 that the kinetics of excimer formation in solution for excimer-forming dyes (EFDs) like pyrene could be described by a simple kinetic scheme, now known as the Birks Scheme, that involved a rate constant of formation (k_{diff}) and dissociation (k_{-diff}), and the natural lifetime of the monomer (τ_M) and excimer (τ_E).[13] It was also acknowledged early on that excimer formation could be generated intramolecularly by linking two EFDs with a short linker.[22–24] A 1974 theoretical report, where Wilemski and Fixman demonstrated that quenching of one dye attached to one end of a monodisperse chain by a quencher at the other end could be handled by a single quenching rate constant,[25,26] led to a series of studies where the rate of end-to-end cyclization (EEC) was characterized by monitoring PEF between two pyrenyl labels attached at the ends of alkyl chains[27,28] and poly(ethylene oxide)s.[29] In these studies, the fluorescence spectra of the pyrene end-labeled chains were acquired and relationships about the EEC rate constant (k_{cy}) were inferred from the ratio I_E/I_M of the fluorescence intensity of the pyrene excimer (I_E) over that of the pyrene monomer (I_M), since the I_E/I_M ratio is proportional to k_{cy} according to Equation 1.1. In a major advance to the field, M. A. Winnik applied the Birks Scheme (see Scheme 1.1) to analyse the fluorescence decays acquired with a series of pyrene end-labeled monodisperse polystyrenes and determine k_{cy} in a direct manner (see Scheme 1.1).[30]

$$\frac{I_E}{I_M} \sim k_{cy} \tag{1.1}$$

The Birks Scheme analysis of pyrene end-labeled monodisperse chains could then be applied to other polymers to assess the effect that the backbone composition would have on k_{cy}. These experiments represented a first attempt at applying PEF to probe the internal dynamics of macromolecules.[31–35] For instance, for a same degree of polymerization k_{cy} was much larger for poly(ethylene oxide)[31] and polydimethylsiloxane[32] than for polystyrene, reflecting the larger flexibility of the two former chains.[30]

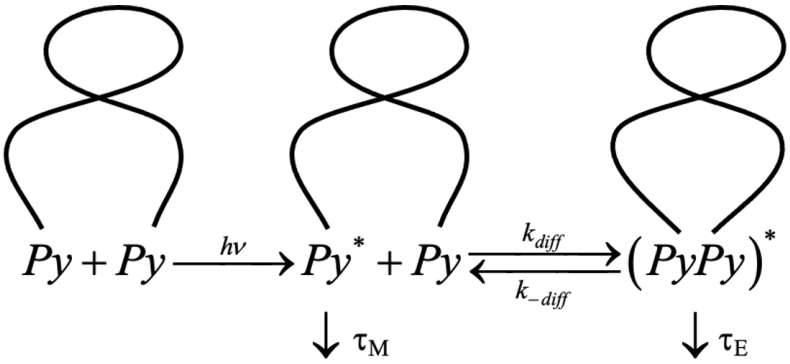

Scheme 1.1. Birks' scheme of a macromolecule end-labeled with two pyrenes.

The kinetic studies of end-labeled monodisperse oligomers to investigate the EEC of linear chains, while synthetically challenging due to the requirement of labeling the polymer at two specific positions, were mathematically simple since k_{cy} could be extracted from the

Birks scheme analysis of the fluorescence decays acquired with the pyrene end-labeled polymers. Although PEF is a bimolecular reaction, k_{cy} is a pseudo-unimolecular rate constant, whose expression is shown in Equation 1.2. In the case of a monodisperse chain labeled at both ends with pyrene, $[Py]_{loc}$ in Equation 1.2 corresponds to the concentration of one ground-state pyrene inside the volume V_{coil} defined by the polymer coil, since the other pyrenyl label must be excited to form an excimer. Due to the difficulty of measuring V_{coil} experimentally, $1/V_{coil}$ is usually lumped with k_{diff} and k_{cy} is being considered. Since V_{coil} scales as $DP^{3\nu}$, where ν is the Flory exponent equal to 0.5 and 0.6 in a theta or good solvent, respectively, scaling laws such as $V_{coil} \sim DP^{\alpha}$ were observed experimentally with α ranging between 0.9 and 1.9.[36]

$$k_{cy} = k_{diff} \times [Py]_{loc} = k_{diff} \times \frac{1}{V_{coil}} \tag{1.2}$$

The discrepancy between the α–exponents obtained experimentally and the predicted 3ν values of 1.5 and 1.8 can be traced back to the short range of *DP*s available to conduct EEC experiments. As *DP* increases, the probability of forming an excimer decreases, which leads to the eventual disappearance of PEF. These experiments can be better understood by considering that a pyrenyl label can only probe a finite volume referred to as a *blob* while it remains excited. EEC will result in PEF only for those chains, whose end-to-end distance (r_{EE}) is smaller than the diameter of a *blob*. As *DP* increases, the fraction of chains whose r_{EE} is larger than the *blob* diameter, cannot form excimer and the excited pyrene will emit with its own lifetime τ_M.[37,38] This phenomenon limits the range of *DP*s over which EEC can be carried

out. For instance, a *DP* larger than 170 would be the upper limit to conduct EEC experiments for polystyrene in toluene.[38] As a result, these early EEC experiments aimed at characterizing macromolecules in solution by PEF led to the untold conclusion that the pyrenyl labels would need to be brought closer to each other, if PEF were applied to probe large macromolecules whose backbone would be stiffer than that of polystyrene. Instead of targeting the chain ends, such conditions could be easily achieved by randomly labeling a polymer with pyrene. Unfortunately, such a labeling scheme would introduce a distribution of distances for each pyrene pair, which would result in an intractable distribution of PEF rate constants corresponding to each chain length spanning every two pyrenyl labels based on the work by Wilemski and Fixmann.[25,26] These considerations were discussed in an earlier review.[39]

A solution to this mathematical deadlock was proposed in 1999 by considering that an excited pyrenyl label could not probe the entire polymer coil during its finite lifespan, but rather a sub-volume referred to as a *blob*.[40] The polymer coil could then be divided into a cluster of identical *blobs*, where the randomly attached pyrenyl labels would distribute themselves according to a Poisson distribution. Since an ensemble of pyrene moieties randomly distributed inside polymeric *blobs* or surfactant micelles are conceptually identical, the robust mathematical treatment used to determine the aggregation number of micelles[41] was then applied to determine the number of structural units (N_{blob}) constituting a *blob*.[40] This mathematical model was referred to as the fluorescence *blob* model (FBM) and has been applied to a wide variety of macromolecules randomly labeled with pyrene.[16,17,19,36,38,39] The FBM also yields the average number $<n>$ of ground-state pyrenyl groups per *blob*, the rate constant, k_{blob}, of diffusive encounters between two structural units (SUs) bearing an excited

and a ground-state pyrene inside a same *blob*, and the molar fraction f_{Mfree} of pyrenyl labels that are isolated along the chains and do not form excimer. N_{blob} is determined by combining $<n>$, f_{Mfree}, and the molar fraction of SUs bearing a pyrenyl label, x, according to Equation 1.3.

$$N_{blob} = \frac{(1 - f_{Mfree}) \times < n >}{x} \tag{1.3}$$

Based on its definition, k_{blob} is equal to the product $k_{diff} \times (1/V_{blob})$, where V_{blob} is the volume of a *blob* so that the product $k_{blob} \times N_{blob}$ in Equation 1.4 is proportional to the local pyrene concentration ($[Py]_{loc} = <n>/V_{blob}$) in the macromolecule. Since the pyrenyl labels are covalently attached onto the macromolecule, the product $k_{blob} \times N_{blob}$ has been found to respond to the internal dynamics of macromolecules.[42] This product is also proportional to the local density of the macromolecule, as shown in Equation 1.4, and should thus be capable of probing the conformation of macromolecules in solution.

$$k_{blob} \times N_{blob} = k_{diff} \frac{1}{V_{blob}} \times \frac{(1 - f_{Mfree}) < n >}{x} = \left[k_{diff} \frac{(1 - f_{Mfree})}{x} \right] \times \frac{< n >}{V_{blob}} \tag{1.4}$$

As a matter of fact, N_{blob}^{exp} experimentally determined by PEF experiments on randomly labeled macromolecules has been found to equal the maximum number (N_{blob}^{theo}) of structural units separating two pyrene-labeled SUs, while still allowing for PEF to occur. This

feature has been recently applied to characterize the conformation of several polysaccharides (amylose[16] and amylopectin)[17] and polypeptides.[18–21]

While the FBM is ideally suited to study macromolecules randomly labeled with pyrene, it does not apply to macromolecules whose chemical composition does not provide reactive groups for labeling or that are not randomly distributed throughout the macromolecule. Examples of such macromolecules would be linear polymers with two reactive groups at the ends such as condensation polymers or dendritic macromolecules, whose many chain ends are inherently reactive. The realization that numerous macromolecular architectures could not be studied with the FBM led to the development of the model free analysis (MFA), which can be applied to any pyrene-labeled macromolecules.[15,43] The MFA is based on the mere observation that any fluorescence decay can be fit with a sum of exponentials. Consequently, the fluorescence decays of any pyrene-labeled macromolecule can be fit with a sum of exponentials, whose pre-exponential factors (a_i) and decay times (τ_i) can be re-arranged into Equation 1.5 to yield the average rate constant for PEF.

$$< k >= \frac{\sum_{i=1}^{n} a_i}{\sum_{i=1}^{n} a_i \tau_i} - \frac{1}{\tau_M} \tag{1.5}$$

Like k_{cy} in the Birks Scheme or k_{blob} in the FBM, $<k>$ is a pseudo unimolecular rate constant, which depends on both the rate constant, k_{diff}, of PEF through diffusive encounters and the local concentration of pyrene, $[Py]_{loc}$.

$$\langle k \rangle = k_{\text{diff}} \left[Py \right]_{\text{loc}} \tag{1.6}$$

Unlike the FBM, the MFA cannot deconvolute information on the dynamics of the macromolecule (k_{diff}) from information on its conformation ($[Py]_{\text{loc}}$) in solution. However, $\langle k \rangle$ has been shown to increase linearly with increasing $[Py]_{\text{loc}}$ by studying a series of pyrene-labeled bis(hydroxymethyl) propionic acid backbone dendrons (Py_x-G(N)) of generation N ranging from 1 to 6 with x pyrenyl labels ($x=2^N$) covalently attached to its terminal ends.[44] Dendrons are symmetrical and well-defined tree-like macromolecules with many terminal ends. If a pyrenyl group is covalently bound to each terminal end of the dendron, then the number (2^N) and location of pyrenyl labels are precisely known. The $[Py]_{\text{loc}}$ should thus equal $(2^N - 1)/V_{\text{dendron}}$. As long as V_{dendron} can be determined, $[Py]_{\text{loc}}$ is known. Duhamel derived an expression to calculate the average distance between two pyrenyl groups, $\langle L^2 \rangle^{1/2}$, for the series of Py$x$-G($N$) dendrons, allowing for the determination of $V_{\text{dendron}} \sim \langle L^2 \rangle^{3/2}$.[44] $\langle k \rangle$ was found to be proportional to $(2^N - 1)/\langle L^2 \rangle^{3/2}$, and thus $[Py]_{\text{loc}}$ in tetrahydrofuran (THF). Not only could $\langle k \rangle$ probe the local density of dendrimers, but it has also been shown to reflect the flexibility of a macromolecule in a study involving a 'stiff' poly(isobutylene-*alt*-maleic anhydride) (PIMA) and 'flexible' polysiloxane.[45,46]

Scattering techniques are the dominating techniques for the characterization of macromolecules due to their ability to determine the internal density of macromolecules in solution. Yet, the examples discussed above and based on the application of the FBM and MFA

to the analysis of PEF data suggest that PEF should respond to the local density of the macromolecule through $[Py]_{loc}$. In turn, PEF studies of pyrene-labeled macromolecules should be able to characterize the conformation of macromolecules in solution in a manner similar to scattering techniques, since both techniques can probe the internal density of macromolecules. Both dendrons and polymeric bottle brushes (PBBs) exhibit highly branched and complex architectures which, once covalently labeled with pyrenyl groups, can be studied using PEF. The purpose of the research conducted in this thesis was thus to investigate whether the PEF signal of pyrene-labeled dendrons and PBBs could be employed to probe their internal dynamics and conformations in a variety of solvents having different viscosities and polarities. But before considering the feasibility of this proposal, a brief overview of dendrimers and PBBs is presented hereafter.

1.2 Dendrimers

Dendrimers are ideal candidates to study the $[Py]_{loc}$ of their pyrene-labeled analogues in solution because of their monodisperse and perfectly well-defined tree-like structure. Their reactive terminal ends provide obvious locations for pyrene labeling, while the number of terminal ends can be tailored by increasing or decreasing the generation number, *N*. Dendrimers can either be grown divergently or convergently, and include a focal point or core, interior branching, and terminal functional groups.[47] Introduced by Vögtle in 1978,[48] the divergent method was first utilized by Denkewalter,[49] Tomalia,[50,51] and Newkome,[52] beginning with a single core molecule and then diverging outwards in successive cycles of monomer addition to each functional group, followed by a deprotection step.[53] The exponential increase

in the number of terminal ends with increasing *N* allows for the synthesis of dendrimers with high molecular weights. However, increased congestion at the dendrimer periphery and high concentrations of reactive groups results in incomplete growth, causing defects in the higher generation dendrimers obtained by divergent methods.[47,53,54] The convergent method was proposed by Fréchet[55] and Millerand and Neeman[56] to circumvent the congestion observed in the higher generation dendrimers resulting in defect formation. It begins with a condensation reaction of the terminal ends, followed by deprotection. Cycles of condensation and deprotection are repeated until a single monomer unit is connected to make the core of the dendrimer.[53] While higher molecular weight dendrimers are often difficult to prepare due to steric hindrance at the final coupling step of the dendritic arms to the core, convergent dendrimers often produce perfectly monodisperse structures.[53] Unlike the divergent method, the convergent method allows for purification at each round of coupling, which eliminates the accumulation of side products with incomplete coupling.[47] The two most common types of dendrimers are Tomolia-type poly(amido amine)s (PAMAM) [51] and Fréchet-type poly(benzyl ether)s.[55]

The multitude of terminal ends and a protected core which are present in dendrimers makes them ideal candidates in applications such as in light harvesting systems,[57] nanomedicine,[58] gene delivery,[59] catalysis,[60] and optical sensors.[61] The ability of dendrimers to generate large local concentrations of compounds of interest also led to some conceptual discussions by de Gennes and Hervet, about the location of the terminal ends.[62] It was initially postulated that the terminal ends of a dendrimer remained at the outer periphery of the

macromolecule, creating a core and shell domain, where each additional increase in *N* resulted in an increase in segmental density.[62] De Gennes believed that the crowding generated by the terminal ends would limit the dendrimer growth to a finite number of generations[62] as is the case for highly branched glycogen.[63] This theory was initially readily accepted by researchers prompting a discussion by Lescanec and Muthukumar,[64] who conducted simulations based on a kinetic growth method. They found that the calculated density distributions suggested instead, a core dense model with the terminal ends of a dendrimer at a given generation size being buried withing the macromolecule.[64] Theoretical studies of shell–*versus*–core dense models have shown that the core dense model is correct, and it is believed by Ballauff, that all other models should be disregarded.[65] The driving force of the core dense model stems from entropic effects, which favor the search of the entire 3 dimensional (3-D) conformational dendrimer interior by the terminal ends, rather than their localization at the periphery.[65] A second factor stems from the difference in the rate of growth between the number of terminal ends and the volume of the dendrimer. While the chain ends grow exponentially, the volume of a dendrimer grows linearly as a function of *N*.[47] As a result, lower *N* dendrimers tend to be open and flexible, while higher *N* dendrimers become less deformable spheres, ellipsoids, or cylinders.[47] Tomalia describes three phases undergone by the density and accessibility to the interior of a dendrimer as a function of generation number.[47] The molecular weight, generation number, and type of core, interior, and terminal ends all contribute to the scaffolding properties of a dendrimer.[47] Lower generations, G(*0*)-G(*3*), contain a flexible scaffolding, mid-generations, G(*4*)-G(*6*), have container properties, and higher generations, larger than G(*7*),

have rigid surface scaffolding or de Gennes dense packing.[47] While the de Gennes shell dense model has been disproven,[64] the surface area available per terminal group becomes increasingly smaller with increasing *N*, until it reaches the physical cross-sectional area of the terminal group, at which point the dendrimer has reached the de Gennes dense packed regime.[66] The recognition that the accessibility of small molecules to the dendrimer interior and the internal dynamics of the terminal ends change in each of the three phases mentioned above was important, as it helped define the limits of applications for dendrimers of a given generation.

While fluorescence spectroscopy techniques can take advantage of the intrinsic fluorescence of amino acids such as tryptophane or tyrosine to probe protein folding,[67] there have been much fewer studies that use the intrinsic fluorescence of some dendrimers to probe the internal dynamics and conformation of dendrimers.[68] Of course, dendrimers have been labeled with dyes to study their properties by fluorescence resonance energy transfer,[69,70] time-resolved fluorescence,[69–71] steady-state fluorescence (SSF),[72] pyrene excimer fluorescence (PEF),[44,73] and florescence anisotropy.[68] Among these spectroscopic techniques, PEF has been used to characterize the long-range internal dynamics of a wide variety of macromolecules with architectures ranging from polymer coils, α–helices, to dendrimers.[74] Unfortunately, results obtained for pyrene-labeled dendrons solely through SSF spectra can be plagued by artifacts, as described in a review by Duhamel.[36] These inconsistencies arise mainly from the presence of free unattached pyrene derivatives which are not completely removed during the purification of the pyrene-labeled dendrimers. PEF is in effect a quenching mechanism for the pyrene monomer, which shortens its lifetime. As highlighted in two studies by the Duhamel

laboratory,[73,75] the extremely large $[Py]_{loc}$ found in pyrene-labeled dendrimers results in efficient PEF associated with the strong quenching of the pyrenyl labels attached to the dendrimer, but not of the free pyrenyl derivatives in solution. A reduction in pyrene lifetime from 200 ns for a pyrenyl derivative in solution to 5 ns for the same pyrenyl label attached on a dendrimer is not unusual. Yet, since the quantum yield equals $k_{rad} \times \tau_M$, where k_{rad} is the radiative rate constant, a 40-fold decrease in τ_M results in a 40-fold decrease in fluorescence quantum yield, implying that one unattached free pyrenyl derivative emits as strongly as 40 pyrenyl derivatives covalently attached to the dendrimer. In essence, if 2.5 mol% of the pyrenyl labels are not attached to the dendrimer, or if the pyrene-labeled dendrimer is 97.5% pure, the fluorescence of the monomer, which is typically used to draw conclusion about the fluorescence response of a pyrene-labeled macromolecule, will be 100% off! Reducing the error on the pyrene monomer fluorescence to 20%, which still represents a large error, would require a 99.5% pure dendrimer. As discussed by Duhamel, the origin of the most surprising results reported for pyrene-labeled dendrimers in the literature can be traced back to the presence of unattached pyrenyl derivatives, and the MFA of the fluorescence decays acquired with pyrene-labeled dendrimers can eliminate this artefact, thanks to the ability of the MFA to isolate the contribution of pyrenyl derivatives that are free in solution.[36] To date, the MFA has been applied to probe PEF[44,73,76] but also FRET[77,78] in fluorescently labeled dendrimers.

The first application of the MFA to pyrene-labeled dendrimers was conducted on a series of four generations of pyrene-labeled aliphatic polyester dendrons with a poly(2,2-bis(hydroxymethyl)-propanoic acid) (PMPA) backbone.[73] The average rate constant for PEF, $\langle k \rangle$, was calculated and shown to increase linearly with increasing N. If $\langle k \rangle$ was proportional

to $[Py]_{loc}$, then the volume probed by pyrene, V_{Py}, was expected to scale as $N^{0.9}$ for $N = 1 – 4$. However, this scaling law was smaller than what had been discussed in the literature regarding the scaling of the volume of a dendron $V_{dendron} \sim N^{1.9}$.[73] The authors suggested that the smaller exponent of the scaling law arose from the branched architecture of the dendrons, which holds the ends of the dendron closer than expected and does not allow an excited pyrene to probe the entire volume of the dendrimer before forming an excimer.[73] Two generations of a pyrene end-labeled poly(aryl ether) dendron (PA) were also prepared and studied with the MFA.[78] Comparison of the $<k>$ values retrieved with the PMPA and PA dendrons showed that the internal dynamics of the PA dendrons were significantly lower than those of the PMPA dendrons, as expected from the rigid phenyl rings incorporated in the PA backbone.[78] Unfortunately, only two generations of the PA dendrons were prepared so the trend of $<k>$ vs. N could not be investigated. The original study with pyrene-labeled PMPA dendrons of generations 1 – 4 was extended to include a generation 5 and 6 pyrene-labeled PMPA dendrons.[44] The dendrons were analyzed with the MFA to yield $<k>$ and the molar fraction of pyrenes that were aggregated, f_{agg}. The average squared end-to-end distance, $<L_{Py}^2>$, between any two pyrenyl labels was calculated and used to determine $[Py]_{loc}$. This study represented the first example where $<k>$ was found to be proportional to $[Py]_{loc}$. The f_{agg} was also calculated for each N and found to remain below 5 mol % for generations 1 through 4 but increased to 10 % and then 35 % for the generations 5 and 6, respectively. The rapid increase in aggregated terminal ends for the generation 6 dendrimer was taken as evidence that de Gennes dense packing regime[62] was observed for the high generation dendrimers as discussed by Tomalia.[66]

1.3 Polymeric Bottle Brushes

Over the last 20 years, advances in controlled radical polymerization techniques have allowed the synthesis of polymers with a variety of architectures, chemical compositions, and functionalities, which can be tuned depending on the desired application.[79–81] Architectures vary from the standard linear chain to branched macromolecules or mixtures of the two. Polymeric bottle brushes (PBBs) are a class of branched polymers which are characterized by having a high grafting density and large molecular weight side chains. Some of the advantages to the PBB architecture is a high degree of control over the chemical structure, molecular weight of the side chains, and grafting density, which affords a high degree of functionality and large controlled sizes, that can be finely tuned to achieve a desired application.

The preparation of PBBs can be achieved using three different techniques shown in Figure 1.1 and referred to as grafting-*to*, grafting-*from*, and grafting-*through*. Each technique has specific pros and cons.[80] The first grafting-*to* technique involves the separate synthesis of a polymer backbone and side chains, which are coupled together at a later stage. The benefit of the grafting-*to* technique is that the polymer backbone and side chains can be synthesized with a large degree of polymerization (DP) and fully characterized independently of one another. Unfortunately, coupling efficiencies decrease as the molecular weight of the side chain increases due to steric hindrance. As a result, the grafting density can be low and uneven. In the second grafting-*from* technique, the polymer backbone is synthesized first and acts as a macroinitiator, from which the side chains are grown. Since the polymer backbone is synthesized first it can be characterized on its own. If the side chains can be grown using a controlled polymerization technique they are likely to be monodisperse, although they cannot

be characterized once grown from the macroinitiator. The final technique is the grafting-*through* technique, which involves the synthesis of a macromonomer, which is then polymerized. The benefits of the grafting-*through* technique are that the side chains can be synthesized beforehand with a narrow dispersity $Đ$ and fully characterized prior to polymerization. Furthermore, the grafting-*through* technique ensures that all structural units bear a side chain. However, one notorious drawback of this technique is that the preparation of PBBs with a high DP is more challenging to achieve with larger macromonomers. For instance, Cho et al. found that an oligo(ethylene glycol) methyl ether methacrylate monomer with 45 ethylene glycol units could only be polymerized up to a maximum main chain DP of 88 using atom transfer radical polymerization (ATRP).[82]

Different polymerization techniques have been utilized with the three grafting techniques.[80,81,83–85] Living polymerizations such an anionic polymerization or ring-opening metathesis polymerization (ROMP) produce low $Đ$ polymers ($Đ < 1.1$) and achieve a great level of control.[86] However, *pseudo*-living or controlled-living radical polymerization techniques such as ATRP, reversible addition–fragmentation chain transfer (RAFT), and nitroxide mediated polymerization (NMP) are also able to produce polymers with low $Đ$ and with less demanding synthetic protocols.[81,86]

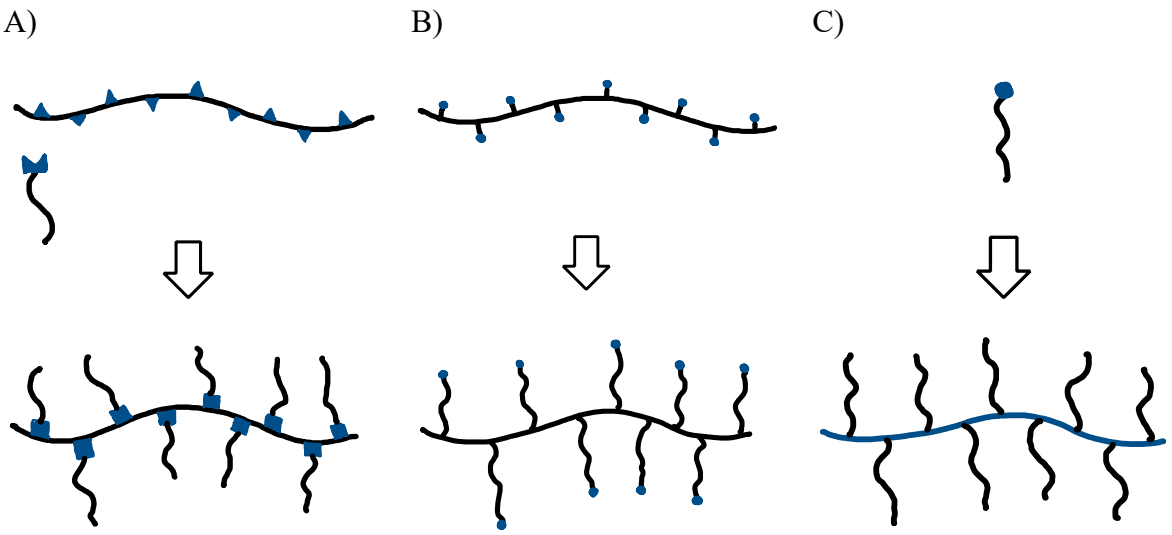

Figure 1.1. Schematic representation of the A) grafting-*to*, B) grafting-*from*, and C) grafting-*through* techniques.

Polymer stiffness and how it is affected by changes in side chain length, grafting density, and chemical composition, are central questions for the characterization of PBBs. The chain stiffness of a polymer is defined by the main chain stiffness parameter, λ^{-1}, which represents either the Kuhn length, l_k, or the persistence length ($l_p = 2 \times l_K$). Kuhn described a polymer coil as a freely jointed chain constituted of N_k Kuhn segments of length l_k.[87] This model assumed that there were no restrictions to the bond angle between, or rotation of, the Kuhn segments which were made of several structural units. The unperturbed mean squared end-to-end distance, $\langle R^2 \rangle_0$, of this freely jointed chain was equal to $N_k \times l_k^2$. The expression of the effective length l_k of a Kuhn segment is given in Equation 1.7 as the ratio of $\langle R^2 \rangle_0$ to the contour length of the polymer, L, equal to the product $n \times l$, where n is the *DP* of the chain and l is the length of a structural unit in the chain.

$$l_k = \frac{< R^2 >_0}{L} \tag{1.7}$$

Flory also defined the characteristic ratio, C_∞, which is a dimensionless constant. C_∞ equals $(N_K \times l_K^2)/(n \times l^2)$ and is related to l_k through Equation 1.8.[88]

$$< R^2 >_0 = C_\infty n l^2 = N_k l_k^2 \tag{1.8}$$

l_k is related to the persistence length, l_p, and both l_p and l_k are typically expressed in nanometers. l_p represents the length required to decorrelate the projection of the tangent to the contour length of the main chain at position x from its original orientation at x=0 as shown in Equation 1.9.

$$< \cos[\theta(x)] > = \exp(-x / l_p) \tag{1.9}$$

In Equation 1.9, $\theta(x)$ is the angle between the tangents taken at positions x and x=0 along the contour of the chain. The determination of l_p will be discussed in further detail hereafter.

Numerous theoretical, computational, and experimental studies have been conducted on PBBs to determine the effect of side chain length, grafting density, and chemical composition on l_k or l_p using the worm-like chain (WLC) model. The most common WLC

model was described by Kratky and Porod, which results in the expression given in Equation 1.10 of the squared end-to-end distance of a linear chain $<r_{ee}^2>$ as a function of l_p and its contour length, L.[89]

$$< r_{ee}^2 >= 2l_p L - 2l_p{}^2 \left[1 - \exp(-L / l_p)\right] \qquad (1.10)$$

As it turns out, numerous theoretical studies predict that l_k scales with the molar mass M_0 of the side chain. In this context, Fredrickson published a study in 1993 where binding of an ionic surfactant to an oppositely charged polyion would induce the stiffening and extension of the polyion main chain to an extent that would depend on the length of the surfactant alkyl tail and the percentage coverage of the polyion.[90] At the high coverage limit, l_p was found to scale as $M_0^{15/8}$. Since the structure of a complex formed in solution between surfactants and a polyion is conceptually the same as that of a PBB with flexible side chains, the scaling laws obtained by Fredrickson are often used to rationalize experimental results obtained with PBBs. Using a self-consistent field approach, Subbotin reached a similar conclusion for PBBs with a semi-flexible backbone and flexible side chains, finding that l_p scaled as M_0^2.[91] Subbotin also suggested that l_p was the product of the persistence length of the main chain and a second term, which is related to the side chains. A similar result was obtained by Nakamura, who introduced the terms λ_0^{-1} and λ_b^{-1}, which reflect the short-range contributions between the main chain and the side chain units near the main chain, and the contributions from the side chains.[92] As shown in Equation 1.11, the main chain stiffness parameter, λ^{-1}, is simply the sum of λ_0^{-1} and λ_b^{-1}.

Nakamura derived the expression given in Equation 1.12 for λ_b^{-1}, where R_c, ΔF, k_B, and T are the radius of curvature of a comb molecule with flexible side chains, the free energy accompanying the bending of the comb molecule, the Boltzmann constant, and the absolute temperature.

$$\lambda^{-1} = \lambda_0^{-1} + \lambda_b^{-1} \tag{1.11}$$

$$\lambda_b^{-1} = 4R_c^2 \frac{\Delta F}{Lk_B T} \tag{1.12}$$

Binder and coworkers have extensively studied PBBs using Monte Carlo simulations.[93–96] They used a bond fluctuation model on a simple cubic lattice to study both backbone and side chain length variations for a flexible PBB in good solvent conditions.[94] Comparison of the simulated data to experimental work conducted by Rathgeber[97] showed quantitative agreement for the different length scales investigated.[94] l_p determined from these simulations was shown to increase with side chain length, unfortunately, a less than linear increase was shown.[94] This finding contradicted the experimental results of Rathgeber, which showed that l_p did not change with side chain length, remaining constant for side chain length increasing from 22 to 98 butyl acrylate monomers.[97] One conclusion of these theoretical studies was that the scaling predictions were not useful for the experimentally accessible side chain lengths.[94] However, the authors provided a few explanations for the possible differences in simulations versus experiments. Firstly, one must consider that experimental measurements

provide data that reflect the conformation of the entire polymer, from which l_p for the backbone is being extracted, whereas simulations directly probe the l_p of the backbone. Secondly, the standard definition of l_p is well defined only for Gaussian chains and not for real chains with excluded volume interactions. Finally, the simulations use very good solvent conditions to model a polymer chain, which might not be the case experimentally. The authors did conclude that the main chain stiffness of a PBB can be changed to a large extent by varying the length of its side chains.[93,94] The inconsistencies mentioned above both experimental and theoretical predictions were the driving force for Chatterjee and Vilgis to study the scaling laws of PBBs using molecular dynamics simulations.[98] Similarly to the work conducted by Fredrickson, the authors identified two regimes depending on the number of atoms in the side chains. In the low coverage limit or for shorter side chains, l_p was found to scale as $N_S^{3/5}$ and in the high coverage limit or for longer side chains, the polymer became semiflexible and l_p scaled as $N_S^{15/8}$.[98]

The remarkable stiffening of a flexible polymer with the addition of long enough side chains stemmed from research conducted on comb polymer synthesis in the 60's and 70's[99–101] and the synthesis of macromers or macromonomers in the 80's and 90's.[102–105] Since then, many groups have investigated the effect of side chain length on PBB flexibility. The Schmidt and Tsukahara groups combined their PBBs made of a polymethacrylate backbone with polystyrene side chains (PMA-*g*-PS) prepared by radical polymerization of methacryloyl end-functionalized polystyrene macromonomers to study the effect of side chain molecular weight on l_k.[106] The results obtained by small angle X-ray scattering (SAXS) and with a gel permeation chromatography (GPC) system equipped with a multiangle laser light scattering (MALLS) and viscosity detector were combined to determine the cross-sectional radius of gyration, $\langle R_g^2 \rangle_C$,

and l_k of the PMA-*g*-PS PBBs. Using eight samples prepared with side chain number-average molecular weights, M_n, ranging from 720 g/mol to 4,940 g/mol, l_k was found to increase with increasing M_n. The l_k values taken from the Schmidt and Tsukahara study[106] plotted in Figure 1.2 as a function of M_0^2 demonstrate that l_k increases linearly with M_0^2. Zhang et al. working on PMA-*g*-PS PPBs found a similar scaling relationship between l_k and M_n using a combination of light and small angle neutron (SANS) scattering techniques.[107] The side chains ranged in molar mass from 800 g/mol to 3,600 g/mol, however, the l_k calculated by Zhang et al. was half the l_k determined by Wintermantel.[106,107] Changing the chemical composition of the polymer backbone, Terao and Hokajo synthesized three PBBs consisting of a polystyrene backbone with polystyrene side chains (PS-*g*-PS) containing 15, 33, and 65 styrene units.[108,109] Characterization of the PBBs was conducted in toluene using static light scattering (SLS) of monodisperse fractions of each PBB obtained through fractional precipitation. After successive doubling of the number of styrene units in the side chain, l_k was found to increase from 16 nm to 36 nm to 75 nm. In this case, l_k increased linearly with M_0. However, the data set consisted of only three samples. Interestingly, l_k also increased linearly with M_0^2 in Figure 1.2, albeit without passing through the origin. Unlike the previous authors, Rathgeber found no dependence of l_k on side chain length and reported an l_k value of 70 nm in toluene for three poly(alkyl methacrylate) backbones bearing poly(*n*-butyl acrylate) side chains (PMA-*g*-P*n*BA), which were studied by SLS and SANS.[97] After including more samples in their data set, an increase was observed in l_k going from P*n*BA to PMA-*g*-P*n*BA with 9 *n*BA units.[110] The plateau in l_k, shown in Figure 1.2 for the PMA-*g*-P*n*BA PBBs, is observed for side chains having more than 22 *n*BA units and this effect was also investigated using Monte-Carlo

simulations. The authors believe that the saturation effect observed at higher side chain length arises from the fact that the inner side chain segments are more sterically hindered and contribute more to the stiffening of the polymer backbone versus the outer segments of the side chains, which have more conformational freedom to arrange themselves in the much less crowded environment generated away from the main chain.[110]

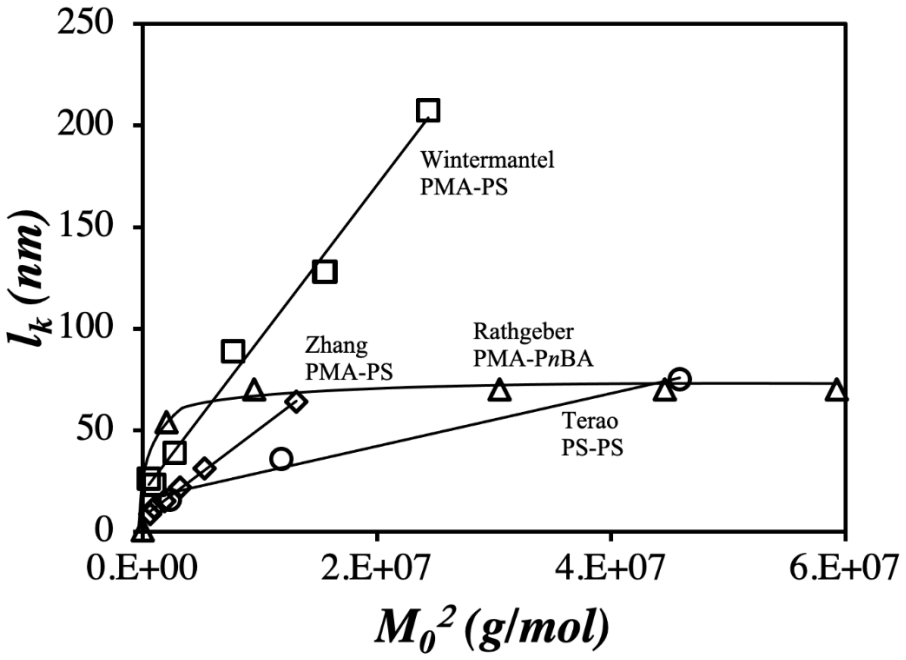

Figure 1.2. Plot of l_k versus M_0^2 from work published by (□) Wintermantel,[106] (◇) Zhang,[107] (△) Rathgeber,[110] and (○) Terao.[108,109]

Unlike the previous authors, Kikuchi synthesized a PBB consisting of rod-like *n*-hexyl isocyanate side chains.[111] These stiff cylindrical brushes were characterized using a combination of GPC-MALLS to calculate the radius of gyration $\langle R_g^2 \rangle$ of the polymer and

SAXS to determine $<R_g^2>_C$. l_k was then extracted by fitting the $<R_g^2>$ according to the WLC model based on the Benoit-Doty equation, which is discussed in more detail afterwards. l_k for the stiff PBBs was found to scale linearly with M_0, which was different from the $l_k \sim M_0^2$ expected for PBBs with flexible side chains.[91,92]

When determining the structural parameters defining a PBB from a scattering technique, the length, l_b, per monomer unit in the backbone must be considered and can be determined experimentally from the Holtzer[112] analysis or if the molar mass per unit contour length, M_L, is known. The maximum value expected for an alkyl chain in the all *trans*-conformation is 0.25 nm, since it equals $2\times0.154\times\sin(109.5^o/2)$, as illustrated in Figure 1.3.

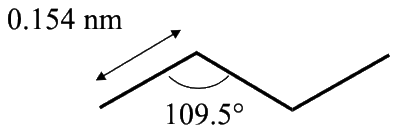

Figure 1.3. Schematic representation of an alkyl chain in the fully extended *trans*-conformation.

Multiple accounts report that the contour length per monomer unit, l_b, was insensitive to the backbone and side chain length. [97,108] For a PMA backbone, l_b was found to equal 0.253 nm[97] and 0.241 nm[107], and for a PS backbone 0.27 nm[108] in toluene, with all values being close to the theoretical value of 0.25 nm. Earlier reports by Schmidt and co-workers found different and much lower values of 0.071 nm and 0.145 nm in tetrahydrofuran (THF) for the l_b of a polymer obtained by polymerizing methacryloyl end-functionalized oligo methacrylate

(M_0=2410 g/mol) and a PMA-*g*-PS (M_0=3624 g/mol), respectively.[113,114] However, it was later explained that the smaller l_b values obtained were not correct because they had been derived from the Benoit–Doty formula, which neglects excluded volume.[107] The effect of solvent quality was also investigated by Zhang et al. and Fisher et al.[107,114] A decrease in l_b was observed when going from a good to a θ solvent, with the PMA-*g*-PS PBBs showing a decrease in l_b from 0.241 nm in toluene to 0.207 nm in cyclohexane and from 0.145 nm in THF to 0.110 nm in cyclohexane. There has been agreement in the literature about the change of l_b with solvent quality, with a coiled backbone conformation in a theta solvent giving rise to a smaller l_b versus the l_b obtained for a swollen backbone conformation in a good solvent, with an l_b approaching the maximum value of 0.25 nm for a fully extended backbone in the trans conformation.

The effect of grafting density on l_k has also been studied experimentally and computationally. Kikuchi synthesized a series of PBBs with PS main chain and poly(*n*-hexyl isocyanate) side chains (PS-*g*-P*n*HIC) with varying grafting densities.[115] The PBBs were characterized using GPC-MALLS and SAXS and both l_k and $\langle R_G^2 \rangle_C$ were studied as a function of the grafting density, σ. σ is defined as the inverse of the area occupied by a side chain and can be calculated using Equation 1.13.

$$\sigma = \frac{1}{\pi d_{PS} l_g} \tag{1.13}$$

In Equation 1.13, d_{PS} and l_g are the diameter of the PS main chain and the distance between two P*n*HIC side chain joints to the main chain, respectively. For low σ, $\langle R_G^2 \rangle_C$ was found to increase with increasing σ as expected, however, $\langle R_G^2 \rangle_C$ reached a plateau in the high σ region corresponding to the $\langle R_G^2 \rangle_C$ value expected for the homopolymers. λ_M^{-1} or l_k was shown to increase linearly with increasing σ, with the y-intercept approaching the l_k value of a linear PS chain. The contribution from the side chains, λ_b^{-1}, which was first introduced in Equation 1.11, was also calculated and was found to be proportional to σ. The effect of grafting density on l_k was investigated by Liang et al. for PBBs using a combination of coarse-grained molecular dynamics simulations and scaling analysis for polymers in a melt by determining a crowding parameter, Φ, describing the overlap between neighboring macromolecules.[116] Polymers with a low grafting density, also called comb polymers, were represented by a $\Phi < 1$, corresponding to conditions where side chains and backbone were able to interpenetrate (comb regime).[116] At high grafting densities, $\Phi \geq 1$, steric repulsions between the side chains prevented interpenetration and the polymers were viewed as PBBs (bottlebrush regime).[116] In the comb regime, l_k was found to be equivalent to that found for a linear chain, and as Φ was increased, interactions between the side chains caused a local stiffening of the polymer backbone and l_k became proportional to Φ in the bottlebrush regime.[116] Experimental and computational simulations conducted by Kikuchi et al. and Liang et al., respectively, found that l_k is expected to increase linearly with the grafting density σ.[115,116] In contrast Chatterjee, who also used molecular dynamics simulations to investigate the effect of the grafting density on l_p, found that in the high coverage limit, l_p scaled as $\sigma^{17/8}$.[98]

With the vast variety of choices in PBB composition along with the added complexity of solvent quality, it is very difficult to fully understand the implications of the PBB architecture on the flexibility of the main chain. Unfortunately, the above discussion indicates that theoretical, experimental, and computational simulations do not fully agree yet on the effect, that side chain length should have on the l_p or l_k. Other factors such as solvent quality and temperature have also not been fully understood. The techniques used for the characterization of PBBs will now be discussed in detail. While scattering techniques are by far the most common tool used in the characterization of PBBs, it is clear from the discrepancies in the results reported in the literature that other techniques, such as pyrene excimer fluorescence, could offer a unique contribution to the field.

1.4 Polymeric Bottle Brush Characterization

The DP of a PBB and its side chains as well as its l_p are all essential parameters, that need to be characterized, when designing a polymer for a desired application. While these parameters are typically obtained by using a combination of static light scattering (SLS), small angle X-ray or neutron scattering (SAXS or SANS), and gel permeation chromatography (GPC), both atomic force microscopy (AFM) and fluorescence measurements can also be used to support the conclusions drawn from these other techniques.

Static light scattering

Static light scattering (SLS) is a well-established technique for determining the weight-average molecular weight, M_w, and z−average radius of gyration, $<R_g^2>_z$, of a macromolecule

in solution.[117] SLS measurements are conducted on a polymer solution at multiple angles and concentrations. A light source, typically a laser, is set up at a known distance from the sample cell and the detector is set at an angle, θ, to the transmitted beam ranging from 25° to 150° as displayed in Figure 1.4.

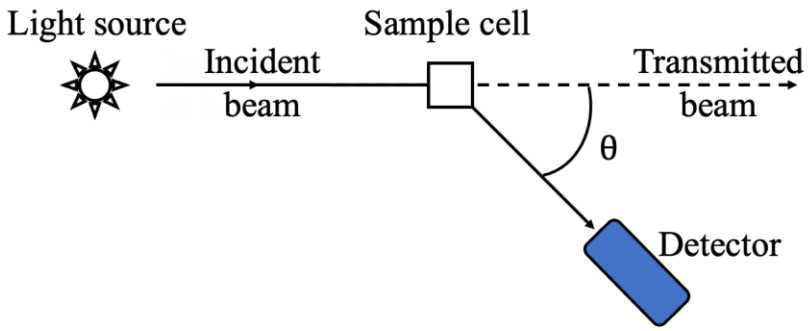

Figure 1.4. Traditional set up for a SLS instrument.

Unlike small molecules, macromolecules with a size that is larger than a twentieth of the wavelength of the incident light have an asymmetrical scattering envelope, whereby the intensity of scattered light is stronger for forward scattering than backward scattering, being largest when θ = 0°.[117] Interference effects are caused by the phase differences of the light scattered by different parts of the macromolecule.[117,118] Interference effects decrease the intensity of scattered light and their contribution to the scattering signal is greater at larger θ.[118] A particle scattering factor, $P(\theta)$, is introduced, which depends on θ, the size of the polymer, and its general shape (coil or rod-like).[118] A Zimm plot is constructed with 5-6 polymer mass concentrations (C_m) and several viewing angles to obtain all of the characteristic information

pertaining to the polymer including M_w, $\langle R_g^2 \rangle_z$, and the second virial coefficient, A_2. All of these parameters are related through Equation 1.14.

$$\lim_{c \to 0} \frac{KC_m}{R_\theta} = \left(\frac{1}{M_w} + 2A_2 C_m + \ldots \right) \left(1 + \frac{16\pi^2}{3\lambda^2} \left\langle R_g^2 \right\rangle_z \sin^2 \frac{\theta}{2} + \ldots \right) \tag{1.14}$$

In Equation 1.14, K, R_θ, and λ, are the optical constant, the excess Rayleigh ratio at the scattering angle θ, and the wavelength of the light from the incident beam.

The persistence length, l_p, of a polymer can be obtained from an SLS measurement by determining the $\langle R_g^2 \rangle_z$ of a monodisperse polymer. Assuming that the polymer behaves as a worm-like chain,[89] the Benoit-Doty equation,[119] shown in Equation 1.15, can be applied.

$$\frac{\langle R_g^2 \rangle_z}{l_p^2} = \frac{L}{3l_p} - 1 + \frac{2l_p}{L} - \frac{2l_p^2}{L^2} \left[1 - \exp\left(-\frac{L}{l_p} \right) \right] \tag{1.15}$$

In Equation 1.15, L is the contour length of the polymer chain ($=n \times l$). Through the careful preparation of multiple monodisperse polymers, a plot of $\langle R_g^2 \rangle_z$ versus M_w can be constructed and then fit with Equation 1.15 to extract l_p.[108] Polydisperse polymers can also be characterized in this manner by using a gel permeation chromatography (GPC) instrument equipped with a differential refractive index (DRI) and a multi-angle laser light scattering (MALLS) detector, that enables the analysis of thin slices of the molecular weight distribution, where the polymer can be considered to be monodisperse.[111,115] The $\langle R_g^2 \rangle_z$ of a wormlike chain can be described

as the sum of two contributions including the squared radius of gyration of the cross section, $\langle R_g^2 \rangle_C$, and the squared radius of gyration of the main chain, $\langle R_g^2 \rangle_M$, as shown in Equation 1.16.[120]

$$\langle R_g^2 \rangle_z = \langle R_g^2 \rangle_C + \langle R_g^2 \rangle_M \tag{1.16}$$

The effect of chain thickness becomes more important with decreasing molecular weight.[120] It was found by Kikuchi that the contribution of $\langle R_g^2 \rangle_C$ to $\langle R_g^2 \rangle$ became negligible for M_w larger than 20,000 g/mol.[111] Small angle X-ray scattering (SAXS) is typically employed to determine the $\langle R_g^2 \rangle_C$ of a polymer and will be discussed further in the SAXS section.[111] This methodology needs also to consider chain end effects, when working with low molecular weight polymers. This is accomplished by introducing the contribution of the side chains at the ends of the main chain by adding δ to the main chain contour length.[115] The last factor to consider, when determining the l_p from the $\langle R_g^2 \rangle_z$ of a polymer is solvent quality. If the polymer is studied in good solvent conditions, then the data might not be fit well using Equation 1.15. To account for intramolecular excluded-volume effects, the $\langle R_g^2 \rangle_z$ data can be re-fit with the quasi-two-parameter (QTP) theory for a wormlike chain.[121–123] The QTP theory uses a radius expansion factor, α, to account for excluded volume effects.

Small angle X-ray scattering and small angle neutron scattering

Small angle X-ray (SAXS) and neutron (SANS) scattering techniques both stem from the basic theory that was already presented for SLS, but with differences in the source and scattering involved for the different radiations. While scattering of visible light results in differences in polarizability, which are accounted for by introducing the refractive index and the change in refractive index of the solution with polymer concentration (dn/dc), the scattering of X-rays and neutrons results in differences in electron density and neutron scattering-length density, respectively.[117] The wavelengths of X-ray and neutrons are in the 0.1 nm and 0.1 nm – 2 nm range, respectively, and are 2-3 orders of magnitude smaller than for visible light, and therefor, provide information on a smaller length scale.[117] Measurements are made at very small angles, typically less than 2°, to reduce interference effects.[117]

X-rays can be generated by using either a synchrotron, with wavelengths ranging from 0.06 to 0.3 nm, or a laboratory instrument with a CuKα source at a set wavelength of 0.154 nm.[117] The source of radiation determines the upper limit for measuring $\langle R_g^2 \rangle_z$, which can only be measured if it is less than q^{-1}, where q is the scattering vector defined in Equation 1.17.

$$q = \frac{4\pi \sin\theta}{\lambda} \tag{1.17}$$

Typically, the $\langle R_g^2 \rangle_z$ can be extracted from SAXS measurements, if the polymer is less than 5 nm in size for $\lambda = 0.154$ nm and $\theta = 0.5°$, but this upper limit can be pushed by decreasing θ.[117] The Kawaguchi laboratory has used SAXS to determine the cross-sectional radius of

gyration, $\langle R_g^2 \rangle_C$, of cylindrical rod brushes.[111] $\langle R_g^2 \rangle_C$ was determined from cross-section Guinier plots obtained by representing $\ln[q\Delta I(q)]$ as a function of q^2, where I(q) is the experimental excess scattering intensity.[111] For polymers with a small enough $\langle R_g^2 \rangle_z$, a plot of $I(q)$ versus q can be constructed. The l_p of a polymer can then be extracted in two different ways from an $I(q)$-versus-q scattering plot, either through graphical determination or by fitting the data with a model such as the one developed by Sharp and Bloomfield.[124]

Depending on the $\langle R_g^2 \rangle_z$ of a macromolecule, either thermal ($\lambda \sim 0.1$ nm) or cold neutrons ($\lambda \sim 1$ nm) can be employed. Increasing λ increases the upper limit to 20 nm for the determination of $\langle R_g^2 \rangle_z$ by SANS in the Guinier region, making it a complementary technique to SLS.[117] Macromolecules studied by SANS either need to be labeled with deuterium or be dissolved in a deuterated solvent. The difference between the neutron scattering lengths of hydrogen and deuterium is what affords the necessary contrast.[117] The in-depth study by Zhang et al. on the conformation of PBBs prepared with a polymethacrylate main chain and polystyrene side chain represents an example of the application of SANS to the study of PBBs.[107] The SANS and SLS techniques were combined to determine l_b, L, and l_p.[107] These parameters were extracted from fitting a Holtzer[112] plot, where $q \times I(q)/C$ obtained from SANS experiments was plotted as a function of q, with the Pedersen-Schurtenberger[125] fitting routine.

Gel permeation chromatography

Gel permeation chromatography (GPC) is the most commonly used analytical technique to determine the number- (M_n) and weight- (M_w) average molecular weights and dispersity ($Đ$ =

M_w/M_n) of a polymer. GPC works by separating polymers according to their hydrodynamic size. A GPC instrument consists of a pump, an autoinjector, and a set of columns followed by a series of detectors. GPC systems typically contain one or more concentration detectors, based on differential refractive index (DRI) or UV absorption, as well as right angle, low angle, or multi angle light scattering, and viscosity detectors. A GPC instrument with all three types of detectors is coined a triple detection system.

In a GPC experiment, separation occurs when the polymer solution flows through the pores of the columns. Polymers with a larger hydrodynamic radius will interact less with the pores compared to a smaller polymer, which will spend more time and get caught inside the pores. As a result, larger polymers will elute at a shorter elution time than polymers with a smaller hydrodynamic radius. A column set has an upper exclusion and lower exclusion limit. The upper exclusion limit occurs when a polymer is too large and does not interact with the pores. The polymer can no longer be separated by the columns and is immediately eliminated from the system. The lower exclusion limit is observed when the polymer is too small and interacts with all the pores in the columns. These polymers will elute close to or with small molecule impurities.

One of the benefits of GPC is that a polydisperse polymer can be analyzed in monodisperse slices without the need to fractionate the sample. GPC can be used to investigate the flexibility of polymers by constructing conformation plots using $<R_g^2>_z$ and the intrinsic viscosity, $[\eta]$, of the polymer to calculate l_p.[126] Conformation plots utilizing GPC coupled with a MALLS detector have been used by Mourey and the Kawaguchi group to investigate polymer flexibility.[111,115,126] By carefully selecting the high molecular weight region of the polymer

trace, the $\langle R_g^2 \rangle_z$ of each slice can be plotted as a function of M_w and fit with Equation 1.15 to determine l_p. One of the main disadvantages of light scattering techniques is the dependence of R_g on the refractive index increment, dn/dc, of the polymer. A weak signal from the light scattering detector translates into a large error in the conformation plots.[126] A viscosity detector can also be used to construct a $[\eta]$-*versus*-molecular weight conformation plot. $[\eta]$ is more sensitive to lower molecular weight polymer species and offers a higher signal-to-noise ratio.[126] Yamakawa, Fujii, and Yoshizaki[127,128] derived a WLC model for intrinsic viscosity, which was linearized by Bohdanecky[129] in Equation 1.18.

$$\left(\frac{M^2}{[\eta]}\right)^{1/3} = A_\eta + B_\eta M^{1/2} \tag{1.18}$$

Plotting $(M^2/[\eta])^{1/3}$ as a function of $M^{1/2}$ yields a straight line, whose y-intercept and slope are taken as A_η and B_η, respectively, which are related to the l_p of the polymer through Equations 1.19 and 1.20, respectively.

$$A_\eta = \frac{A_0 M_L}{\Phi_{0,\infty}^{1/3}} \tag{1.19}$$

$$B_\eta = \frac{B_0}{\Phi_{0,\infty}^{1/3}} \left(\frac{2l_p}{M_L}\right)^{-1/2} \tag{1.20}$$

In Equation 1.19, A_0, M_L, $\Phi_{o,\infty}$, equal $0.46 - 0.53\times log(d/2l_p)$, where d is the hydrodynamic diameter of the PBB, M_0/b, where M_0 and b (=0.25 nm) are the molar mass and length of the structural unit, and 2.87×10^{23} mol^{-1}, which is the theoretical Flory constant for infinitely large molecular weights, respectively. In Equation 1.20, B_0 equals 1.05 for $M/(2l_pM_L)$ values ranging from 0.4 to 300.

Atomic force microscopy

Atomic force microscopy (AFM) is a popular technique used by many researchers to visualize the rod or worm-like conformations so famously afforded by PBBs.[83,115,130–132] The high density of flexible or rigid side chains allows researchers to visualize PBBs by increasing their cross-sectional diameter and $<R_g^2>_z$. Since the polymers are adsorbed onto a substrate, characterization is done in a two-dimensional (2D) space. AFM studies are also complicated by the fact that adsorption of a PBB onto a substrate has been shown to cause backbone scission over time.[133–135] Park et al. studied droplets of a PBB polymer melt consisting of a polymethacrylate backbone with a disulfide linker in the middle and with poly(*n*-butyl acrylate) side chains. In these experiments, a drop of the PBB was spread across the mica plate and the distribution of PBB lengths was monitored as a function of the distance from the point, where the drop had been originally spread into a film. Spontaneous chain scission of S–S bonds and C–C bonds were observed at distinct distances of r ~ 20-50 μm and r ~ 140 μm, respectively, from the drop edge.[133]

Sheiko also visualized a PBB consisting of a polymethacrylate (PMA) backbone and poly(methyl methacrylate) (PMMA) side chains.[130] The PBBs had an extended conformation

with collapsed backbone segments that were measured to be 1/3 of the fully extended length. Contraction of the polymer backbone is believed to occur as the polymer transitions from a solvated state in a good solvent to the dry state, which is more akin to poor solvent conditions.[130] The determination of l_p from AFM images has also been investigated and can be determined using two complementary methods.[132] The first method uses the local curvature of the PBB, as shown in Equation 1.21.[136]

$$< \cos(\theta) >= \exp(\frac{-s}{l_p}) \tag{1.21}$$

In Equation 1.21, $\cos(\theta)$ and s are the cosine of the angle, θ, between two unit vectors tangent to the chain contour and the distance separating the two vectors, respectively.

The second method is based on the KPWLC model applied to a 2D-space with Equation 1.22.[132,136]

$$\left\langle R_g^2 \right\rangle_{2D} = 4l_p L\left(1-\frac{2l_p}{L}\left(1-\exp(\frac{-L}{2l_p}\right)\right) \tag{1.22}$$

To account for the loss of one degree of freedom in the molecule, l_p is multiplied by a 2× factor.[136] Equation 1.22 holds only if the molecules deposited onto a substrate have equilibrated prior to the measurements.[136]

Pyrene excimer fluorescence

Pyrene excimer fluorescence or formation (PEF) has been used to study a handful of PBB systems, where a pyrenyl label was either covalently attached[42,137,138] or loaded[139–144] into the PBB. Zhao et al. reported the synthesis of a PBB with a backbone consisting of a poly(glycidyl methacrylate) used to generate a bivalent linker for attachment of a 1-pyrenebutyroyl group and a poly(*N*-isopropyl acrylamide) side chain (PGMA-*g*-Py/PNIPAM).[137] The PNIPAM hydrophilic linker had a degree of polymerization of 53 and could be dissolved in both organic and aqueous media. Concentration studies were conducted to investigate the level of interpenetration of the side chains in tetrahydrofuran (THF), a good solvent for PNIPAM and pyrene, and in water, a good solvent for PNIPAM and a poor solvent for pyrene. Steady-state fluorescence (SSF) was used to calculate the efficiency of excimer formation based on the I_E/I_M ratio, by taking the intensity (I_E) measured at 476 nm for the excimer and dividing it by the intensity (I_M) measured at 397 nm for the pyrene monomer. The polarity of the microenvironment of pyrene was also probed through the I_1/I_3 ratio, where the I_1 and I_3 peaks of the monomer emission were found at approximately 377 and 388 nm, respectively. Unfortunately, the authors analyzed the I_E/I_M and I_1/I_3 ratios at concentrations in THF that were so high that they observed both the inner filter effect and reabsorption and therefore, their results obtained for pyrene concentrations above 10^{-5} M are not reliable. The inner filter effect occurs when the concentration of the chromophore is so high that the excitation light cannot completely pass through the solution, so that only the section of the solution located next to the cell wall in direct contact with the incoming beam is being irradiated, resulting in the absence of excitation at the center of the cell, where fluorescence is detected. Consequently,

the fluorescence observed is much less than expected. Reabsorption is also observed at high chromophore concentrations and occurs when the fluorescence of the chromophore is re-absorbed by a neighbouring chromophore distorting the monomer emission. In the case of pyrene, the I_1 peak becomes smaller, and the overall monomer emission becomes distorted as shown in Figure 7 of the manuscript.[137] At pyrene concentrations lower than 10^{-5} M the I_E/I_M ratio is constant, indicating that only intramolecular excimer formation, and thus no interpenetration of PBBs, is taking place. A similar issue is found in water and only the data for pyrene concentrations smaller than 10^{-5} M are reliable. The I_E/I_M ratio begins to increase with increasing pyrene concentration, indicating interpenetration and the formation of PBB aggregates. Gadwal et al. also synthesized a PBB with a PGMA backbone, where each glycidyl moiety was used to generate a bifunctional linker connected to one 1-pyrenebutanoyl group and oligo(ethylene glycol)s to yield a series of PGMA-*g*-Py/PEG samples.[138] The fluorescence spectra of the PGMA-*g*-Py/PEG with 1 and 16 ethylene glycol (EG) units were acquired. While not discussed in the manuscript, the I_E/I_M ratios could have been calculated, and it is evident from the spectra acquired in chloroform that the PBB with 1 EG unit shows a substantial enhancement in excimer formation compared to the PBB with 16 EG units. The PBB with the longer side chains experiences more steric interactions between the side chains causing a stiffening of the polymer backbone. As a result, the local concentration of pyrene decreases, which causes a decrease in the I_E/I_M ratio as expected from Equation 1.1. A similar experiment was conducted by Farhangi et al. for a series of PBBs with increasing side chain length.[42] The PBBs were constituted of a poly(methyl methacrylate) (PMMA) backbone with alkyl side chains ranging in length from 1 to 18 carbon atoms. They were randomly labeled with 1-

pyrenebutanol throughout the polymer to yield a series of PMMA-*g*-Py/C_n samples. Dilute PMMA-*g*-Py/C_n solutions were studied in THF using both SSF and time-resolved fluorescence (TRF). The results showed that extension of the alkyl side chains led to a pronounced decrease in PEF attributed to the stiffening and extension of the main chain, as had been observed in the study by Gadwal et al.[42,138] The TRF decays were analyzed using the fluorescence blob model (FBM), which was developed in the Duhamel laboratory.[40] The FBM retrieves N_{blob}, which is the number of monomer units encompassed within a *blob*. N_{blob} is expected to decrease as the number of atoms in the side chain increases and the polymer backbone becomes less flexible. This was indeed the case, as N_{blob} was shown to decrease and plateau similarly to the trend shown for the I_E/I_M ratios. The plateau observed in both the I_E/I_M and N_{blob} values occurred for the PBBs with 12 and 18 carbon atoms in the side chain. The authors believe that this trend demonstrates a saturation of the local volume, where a side chain made of more than 12 carbon atoms no longer affects the dynamics of the main chain probed by PEF.

While PEF remains a powerful technique, which has been applied to characterize a variety of polymer architectures,[16–21] very few studies have been conducted using pyrene excimer fluorescence to study polymers with a PBB architecture. PEF is a characterization technique which extracts information about the structure and conformation of a macromolecule as well as its internal dynamics. The driving force for this thesis was to extend the applications of PEF to be able to determine the local concentration of pyrene of a pyrene-labeled macromolecule in solution and to draw conclusions about the conformation of the macromolecule in a manner similar to what is currently done with scattering techniques.

1.5 Research Goals and Thesis Outline

The main objective was to investigate whether a different technique, namely pyrene excimer fluorescence (PEF), can be used to characterize the conformation and internal dynamics of macromolecules with complex architecture, a field typically dominated by scattering techniques. This thesis has focused on two specific branched macromolecular architectures, namely dendrons and polymeric bottle brushes (PBBs). The first research goal was to apply our PEF-based methodology to dendrons and PBBs that had been homogenously end-labeled with the chromophore pyrene. The dynamics of the terminal ends of dendrons and PBBs were investigated by determining the average rate constant $<k>$ of excimer formation, which was then related to the local concentration of pyrene $[Py]_{loc}$ calculated for each construct. Few studies have related the dynamics experienced by the chain ends of highly branched macromolecules to their local concentration. Pyrene, with its ability to form an excimer, was an ideal candidate to conduct these studies, and the relationship between the two was investigated using PEF. The second research goal was to conduct an in-depth study of PBBs in both organic and aqueous solutions. The first goal was to study the change in PBB flexibility with increasing side chain length. To this end, a new *blob*-based approach was introduced to quantitatively measure the persistence length, l_p, for a series of pyrene-labeled PBBs with a poly(methyl methacrylate) main chain and poly(oligoethylene glycol) side chains (PMMA-*g*-Py/PEG). The second goal was to study the ability of the densely grafted side chains of the PMMA-*g*-Py/PEG samples to protect the hydrophobic pyrenyl pendants as well as the fraction of aggregated pyrenyl groups. This research was completed by a study of the loading capacity in water of unlabeled PMMA-*g*-PEG samples with molecular pyrene.

This thesis is composed of six chapters. The first chapter sets out to introduce PEF and describe how it has been used in the literature to characterize macromolecules in solution. Two of the models currently used by the Duhamel laboratory, namely the model free analysis (MFA) and the fluorescence blob model (FBM), were presented and discussed. The dendritic and bottle brush architectures were discussed along the synthetic routes and their characterization in solution. Chapter 2 focusses on the study of six generations of pyrene-labeled dendrons. A calibration curve was constructed to compare the dynamics of the pyrene-labeled terminal ends of the dendrons to the local concentration of pyrene in a variety of solvents. This curve set the stage for Chapter 3, which involved the synthesis and characterization of four PBBs, whose side chains had been homogenously labeled with pyrene. A grafting-through method was adopted, which ensured that each side chain was monodisperse in length. The volume probed by the side chains of the PBBs with 12, 18, 27, and 39 non-hydrogen atoms in their side chains were investigated in 4 different solvents. The internal dynamics of each PBB were then studied, and $<k>$ was calculated and plotted as a function of $[Py]_{loc}$. The results were compared to those obtained in Chapter 2 and good agreement was found between the two different branched architectures. Chapter 4 introduces a new series of PBBs, which were randomly labeled with pyrene and contained a variety of side chain lengths ranging from 3, 12, 15, 18, 24, 30, to 60 non-hydrogen atoms. The flexibility of these polymers was investigated using the Fluorescence Blob Model (FBM) and a *blob*-based approach was used, for the first time, to determine the l_p of these polymers. The flexibility of the PBBs was also investigated using gel permeation chromatography and an image of the PBB with 60 atoms in the side chain could be obtained using atomic force microscopy. The pyrene labeled PBBs

were fully characterized in organic solvents in Chapter 4, and Chapter 5 is a study of these same polymers in water. The pyrene pendant can be viewed as a hydrophobic drug, which would have been covalently bound to PBBs and studied for drug delivery applications. The effects that the length of the spacer attached to the pyrenyl moiety, as well as the length of the PBB side chains, have on the behavior of the PBBs were thoroughly investigated using a variety of fluorescence-based techniques. The concluding chapter, Chapter 6, summarizes the main conclusions and discoveries from each of the above-mentioned chapters and discusses future work.

Chapter 2

Direct Measure of the Local Concentration of Pyrenyl Groups in Pyrene-Labeled Dendrons Derived from the Rate of Fluorescence Collisional Quenching

Adapted with permission from Thoma, J. L.; McNelles, S. A.; Adronov, A.; Duhamel, J. Direct Measure of the Local Concentration of Pyrenyl Groups in Pyrene-Labeled Dendrons Derived from the Rate of Fluorescence Collisional Quenching. *Polymers* **2020**, *12*, 1-14.

2.1 Abstract

The model-free analysis (MFA) was applied to measure the average rate constant (<*k*>) for pyrene excimer formation (PEF) in a series of pyrene-labeled dendrons referred to as Py_x-G(*N*), where *x* (= 2^N) is the number of pyrenyl labels born by a dendron of generation *N* ranging from 1 to 6. <*k*> was measured in four different solvents, namely tetrahydrofuran (THF), toluene, *N*,*N*-dimethylformamide (DMF), and dimethylsulfoxide (DMSO). <*k*> was found to increase linearly with increasing local pyrene concentration ($[Py]_{loc}$), where $[Py]_{loc}$ had been determined mathematically for the Py_x-G(*N*) dendrons. The slope of each straight line changed with the nature of the solvent and represented k_{diff}, the bimolecular rate constant for PEF. k_{diff} depended on the solvent viscosity (η) and the probability (*p*) for PEF upon encounter between an excited and a ground-state pyrene. In a same solvent, k_{diff} for the Py_x-G(*N*) dendrons was about 360 ± 30 times smaller than k_{diff} obtained for ethyl 4-(1-pyrene)butyrate (PyBE), a pyrene model compound similar to the pyrene derivative used to label the dendrons. The massive decrease in k_{diff} observed for the Py_x-G(*N*) samples reflected the massive loss in mobility experienced by the pyrenyl labels after being covalently attached onto a macromolecule compared to freely diffusing PyBE. Interestingly, the k_{diff} values obtained for the Py_x-G(*N*) dendrons and the PyBE model compound followed similar trends as a function of solvent, indicating that the difference in behavior between the k_{diff} values obtained in different solvents were merely due to the changes in the η and *p* values between the solvents. Normalizing the <*k*> values obtained with the Py_x-G(*N*) dendrons by the k_{diff} values obtained for PyBE in the same solvents accounted for changes in η and *p*, resulting in a master curve upon plotting $<k>/(f_{diff} \times k_{diff})$ as a function of $[Py]_{loc}$, where f_{diff} was introduced to account for some pyrene aggregation in the higher generation dendron (Py_{64}-G(6)). This result demonstrates that <*k*> represents a direct measure of $[Py]_{loc}$ in pyrene-labeled macromolecules.

2.2 Introduction

Techniques such as viscometry, light scattering (LS), and small angle X-ray (SAXS) or neutron (SANS) scattering have traditionally played a critical role in the characterization of macromolecules due to their ability to determine the internal density of macromolecules in solution. Since the internal density of a macromolecule can be related to its volume after the molecular weight has been determined, such measurements provide a means to assess the dimensions of macromolecules in solution. For instance, the existence of excluded volume experienced by macromolecules in solution is readily detected by a marked decrease in the internal density of macromolecules, which can be mathematically predicted and experimentally confirmed through intrinsic viscosity ($[\eta]$) and LS measurements.[1] These measurements are typically conducted with polymer concentrations in the 1 – 10 g/L range, a concentration range that is suitable for well-soluble samples, but that can lead to aggregation and challenging data analysis for less soluble macromolecules.

In contrast, fluorescence is better known for its ability to probe fast photochemical processes, which has led to the implementation of many fluorescence-based applications to characterize the internal dynamics of macromolecules in solution.[2] In a typical fluorescence collisional quenching (FCQ) experiment, where quenching occurs solely upon contact between the excited dye and its quencher, a macromolecule is covalently labeled with a dye and its quencher at two specific positions, followed by the acquisition of the monoexponential fluorescence decay of the fluorescently labeled macromolecule. Analysis of the decay yields the decay time (τ) corresponding to the quenching of the dye by the quencher, which is equal to $(1/\tau_o + k_{diff}\times[Q]_{loc})^{-1}$, where τ_o, k_{diff}, and $[Q]_{loc}$ are the dye natural lifetime, the bimolecular quenching rate constant describing the diffusive encounters between the excited dye and the quencher, and the quencher

concentration experienced locally by the excited dye, respectively. Because $[Q]_{loc}$ is deemed impossible to measure experimentally, the fluorescence decay analysis yields the product $k_{diff} \times [Q]_{loc}$, which is referred to as the pseudo-unimolecular rate constant k. Information about the internal dynamics of the macromolecule is retrieved from k, a larger k reflecting a more flexible macromolecule. Yet, this interpretation of k overlooks the fact that k is not only a function of k_{diff} but also of $[Q]_{loc}$, which is related to the internal density of the macromolecule, since the quencher is covalently attached to the macromolecule.

The difficulty in establishing the relationship between k and $[Q]_{loc}$ for fluorescently labeled macromolecules is rooted in a number of technical and theoretical hurdles that must be overcome, as described in an earlier review.[3] First, most photophysical processes like FCQ occur over short distances of less than 5 nm.[3] This constraint requires that the dye and quencher be relatively close to each other, limiting the application of FCQ experiments to oligomers, not macromolecules. To study macromolecules by FCQ and resolve this first hurdle, the dye and quencher must be brought closer to each other, typically by increasing the number of dyes and quenchers attached to the macromolecule. Unfortunately, this practice leads to the second hurdle of FCQ experiments, whereby each polymer segment spanning a dye and a quencher results in a different quenching rate constant, which leads to a complex distribution of quenching rate constant (k_i).[3] In turn, the fluorescence decay of the randomly labeled macromolecules turns into a sum of exponentials associated with a distribution of decay times τ_i equal to $(1/\tau_o + k_i)^{-1}$. Since no multiexponential decay analysis can resolve all the τ_i values resulting from the distribution of the k_i rate constants, the average rate constant for quenching $\langle k \rangle$ is typically determined. The relationship between $\langle k \rangle$ and $[Q]_{loc}$ now needs to be established, and this represents the third hurdle in FCQ experiments

because $[Q]_{loc}$ is difficult to predict for a macromolecule labeled with more than one dye and one quencher.[3]

For reasons that have been presented in several reviews,[3–5] excimer formation upon encounter between an excited and a ground-state pyrenyl group covalently attached onto a macromolecule is a well-known and often used FCQ application to probe the internal dynamics of macromolecules. The multiexponential fluorescence decays acquired with macromolecules labeled with more than two pyrenes can be satisfyingly fit according to the model-free analysis (MFA), which yields the average rate constant $<k>$ of pyrene excimer formation (PEF).[3,6] In this case, the ground-state pyrenes act as quenchers, and $<k>$ is related to the local pyrene concentration ($[Py]_{loc}$) experienced by an excited pyrene according to Equation 2.1. Equation 2.1 is well accepted in the literature because it has been shown to hold for homogeneous pyrene solutions,[7] it agrees with the results obtained with end-labeled monodisperse polymers,[8,9] and it has been predicted for polymers randomly labeled with pyrenes.[10] The MFA has been shown to be a superior analytical tool[11] compared to other procedures that have been applied previously to study the fluorescence of pyrene-labeled dendrimers,[12–28] as was reported in an earlier review.[4] Yet, validation of Equation 2.1 is essential to demonstrate that FCQ experiments such as those based on PEF yield parameters that report on $[Py]_{loc}$, and thus on the internal density of the macromolecule onto which the pyrenyl labels are attached.

$$< k >= k_{diff} \times [Py]_{loc} \qquad (2.1)$$

The only study to have indicated that Equation 2.1 is valid was conducted in tetrahydrofuran (THF) with a series of pyrene labeled dendrons referred to as Py_x-G(N). The Py_x-

G(*N*) dendrons were prepared with a 2,2-bis(hydroxymethyl) propionic acid backbone, the generation number (*N*) of the dendrons ranged from 1 through 6, and *x* (= 2^N) represented the number of pyrenyl labels covalently attached to the terminal ends of a dendron of generation *N*.[29] The published derivation of the average squared end-to-end distance, $<L_{Py}^2>^{1/2}$, of the highly branched Py_x-G(*N*) dendrons was employed to estimate $[Py]_{loc}$ for each Py_x-G(*N*) dendron. The MFA of the fluorescence decays acquired with the Py_x-G(*N*) dendrons yielded $<k>$, which was found to increase linearly with increasing $[Py]_{loc}$ as predicted by Equation 2.1. This original study is now extended to the three additional solvents toluene, *N*,*N*-dimethylformamide (DMF), and dimethylsulfoxide (DMSO), which provide, after including THF, a series of four solvents with a broad range of polarity and viscosity. In turn, polarity and viscosity affected the probability (*p*) of forming an excimer and the diffusion coefficient (*D*) of the pyrene labels in a different manner, which affected the results obtained by PEF. Fortunately, these effects could be accounted for by studying PEF with homogeneous solutions of ethyl 4-(1-pyrene)butyrate (PyBE) in the same solvents, which provided a means to assess how k_{diff} in Equation 2.1 was affected by solvent polarity and viscosity. After accounting for the changes in k_{diff} due to solvent polarity and viscosity, all $<k>$ vs. $[Py]_{loc}$ plots obtained for the Py_x-G(*N*) samples in the different solvents merged into a single master curve, thus demonstrating the validity and generality of Equation 2.1.

2.3 Experimental

Materials: The six 2,2-bis(hydroxymethyl)propionic acid backbone dendrimers bearing pyrenyl labels at each terminal end have been previously synthesized, and their synthesis and characterization in THF can be reviewed in a previous publication.[29] The chemical structure of the pyrene-labeled dendrons (Py_x-G(*N*)) used in this study is provided in Table 2.1.

Table 2.1. Chemical structure and $[Py]_{loc}$ for each Py_x-G(N) dendron.[29]

Sample	**Py_2-G(1)**	**Py_4-G(2)**	**Py_8-G(3)**	**Py_{16}-G(4)**
Structure	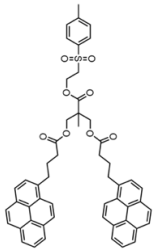	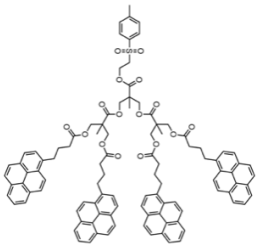	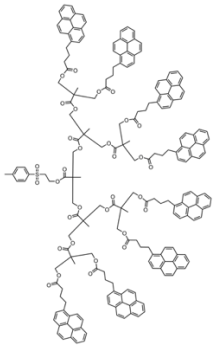	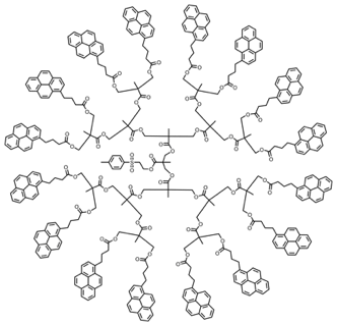
$[Py]_{loc}$ (M)	34	62	94	140

Sample	**Py_{32}-G(5)**	**Py_{64}-G(6)**
Structure	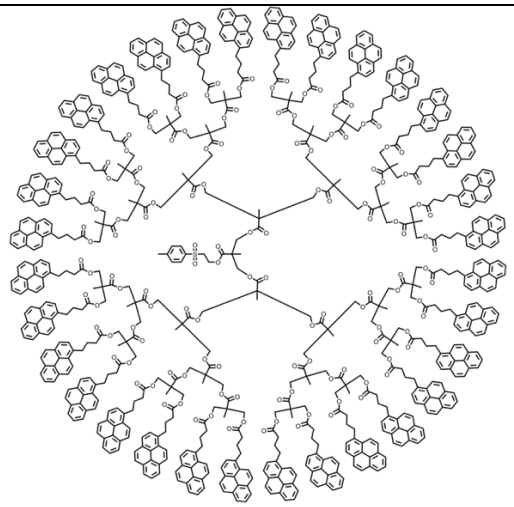	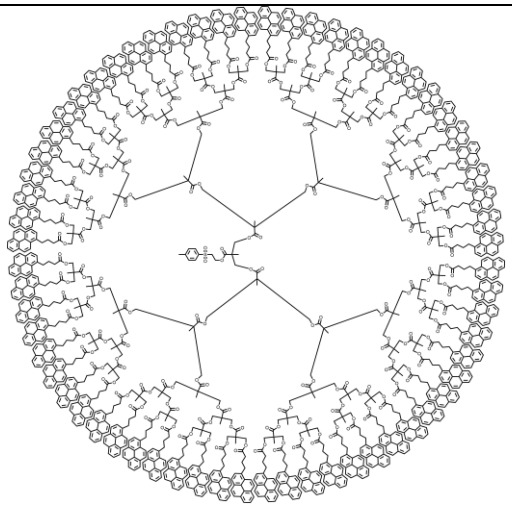
$[Py]_{loc}$ (M)	212	330

Dichloromethane (DCM, ≥ 99.8 %), *N,N'*-dicyclohexylcarbodiimide (DCC, ≥ 99.0 %), 4-(dimethylamino)pyridine (DMAP, ≥ 99%), *N,N*-dimethylformamide (DMF, ≥ 99.8%), dimethylsulfoxide (DMSO, ≥ 99.9%), ethanol (reagent grade), 1-pyrenebutyric acid (97%), sodium hydroxide (≥ 97.0 %), and sodium sulfate (anhydrous, ≥ 99.0 %) were obtained from

Sigma (Oakville, ON, Canada). Sodium bicarbonate (≥ 99.7 %), tetrahydrofuran optima (≥ 99.9%), and toluene (distilled in glass) were supplied by VWR (Mississauga, ON, Canada), Fisher Scientific (Ottawa, ON, Canada), and Caledon Laboratories (Halton Hills, ON, Canada), respectively. All chemicals were used as received.

Synthesis of ethyl 4-(1-pyrene)butyrate (PyBE): The synthesis of the model compound ethyl 4-(1-pyrene)butyrate (PyBE) follows the reaction scheme outlined in Scheme 2.1 and is described in more detail hereafter. Freshly distilled DCM (25 mL) was added to a 50 mL round bottom flask (RBF) equipped with a magnetic stir bar. 1-Pyrenebutyric acid (1.00 g, 3.5 mmol), ethanol (1.60 g, 34.7 mmol), and DMAP (0.08 g, 0.7 mmol) were added to the RBF. The RBF was then placed in an ice water bath under a gentle flow of nitrogen (Praxair, 4.0). DCC (0.72 g, 3.5 mmol) was dissolved in 5 mL of DCM, and the solution was added dropwise to the RBF over 30 min. The reaction was left stirring under a nitrogen atmosphere at room temperature for 18 hours. The next day, the reaction solution was filtered using suction filtration to remove the urea precipitate. The reaction solution was then washed with 0.5 M HCl, a saturated solution of sodium bicarbonate, and a saturated solution of sodium chloride. The organic layer was extracted after each wash and dried with sodium sulfate. Silica gel chromatography was then used to purify PyBE using a 1:10 ethyl acetate:hexane mixture. The final product was isolated as a colourless solid and dried *in vacuo* overnight (0.68 g, 62 %). The ^{1}H NMR spectrum is shown in Figure S2.1 in the Supporting Information (SI), and its molar absorbance coefficient at 344 nm equals 42,600 ± 140 $M^{-1}\cdot cm^{-1}$ in THF.

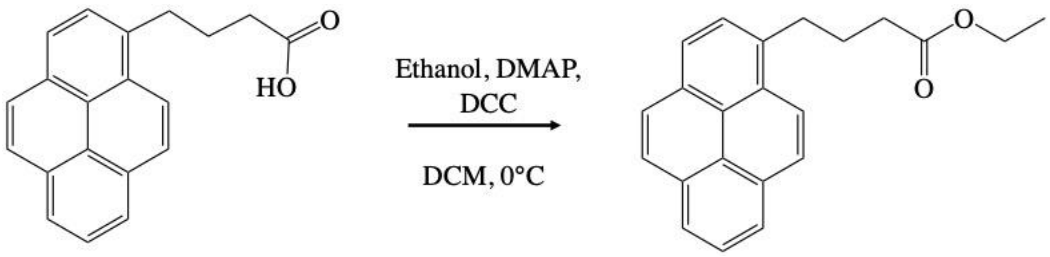

Scheme 2.1. Chemical reaction scheme of the synthesis of the model compound ethyl 4-(1-pyrene) butyrate (PyBE).

UV-Vis Spectroscopy: All absorption measurements were carried out on a Varian Cary 100 Bio spectrophotometer (Varian, Palo Alto, CA, USA). The Py(*x*)-G(*N*) solutions were prepared with a pyrene concentration of 2.5×10^{-6} M equivalent to an optical density of 0.1. The absorbance measurements were made using a quartz cuvette with a 10 mm path length.

Steady-State Fluorometer: All steady-state fluorescence (SSF) measurements were performed on a QM-400 spectrofluorometer equipped with a Xenon arc lamp (HORIBA, London, ON, Canada). The different pyrene solutions in organic solvents were degassed for 30 – 45 min depending on the organic solvent. Their spectra were acquired with a 344 nm excitation wavelength and over wavelengths ranging from 350 to 600 nm. The SSF measurements with the Py_x-G(*N*) dendrons were conducted using the conventional right-angle geometry, and the measurements carried out with more concentrated solutions of the PyBE model compound were performed using the front face geometry to avoid the inner filter effect and reabsorption. The intensity of the excimer emission, I_E, was divided by the intensity of the monomer emission, I_M, to obtain the I_E/I_M ratio, which is a measure of PEF efficiency. I_M was calculated by integrating the area under the first fluorescence peak of the monomer fluorescence spectrum from $\lambda_{0\text{-}0}$ – 4 nm to $\lambda_{0\text{-}0}$ + 4 nm, where $\lambda_{0\text{-}0}$ corresponds to the wavelength of the 0-0 transition of the pyrene derivative in a given solvent.

Since I_E was much less sensitive to solvent differences, it was calculated by integrating the excimer fluorescence intensity under the spectrum from 500 to 530 nm.

Time-Resolved Fluorometer: A FluoroHub fluorometer (HORIBA, Piscataway, NJ, USA) equipped with a DeltaDiode at 336 nm was used to acquire the monomer and excimer time-resolved fluorescence (TRF) decays of the degassed solutions of the Py_x-G(*N*) dendrons and PyBE in the different solvents at 375 and 510 nm with a 370 and 490 nm cut off filter, respectively. The cut off filters prevented stray light from reaching the fluorescence detector. All decays had 20,000 counts at their maximum and were acquired over 1,024 channels with times-per-channel of 0.435, 0.0514 or 0.102 ns/ch. A 2.04 ns/ch time-per-channel was used for the fluorescence decays of 2.5×10^{-6} M dilute solutions of the PyBE and Py_1-G(0) model compounds acquired to determine the natural lifetime (τ_M) of the pyrene derivatives. The instrument response function (IRF) was obtained with an aluminum reflective monolith by setting the emission wavelength at 336 nm. The IRF was then convoluted with the mathematical expressions for the time-dependent concentration of the pyrene monomer and excimer given in SI as Equations S2.1 and S2.2 for the MFA[3,6] and as Equations S2.3 and S2.4 for the Birks scheme analysis.[7,9] The parameters in Equations S2.1 – S2.4 were optimized according to the Marquardt-Levenberg algorithm.[30] The quality of the fits was gauged from a low χ^2 (< 1.20) and residuals and autocorrelation of the residuals randomly distributed around zero.

Model Free Analysis (MFA) of the Fluorescence Decays: The model free analysis (MFA) is a global analysis tool which can be used to simultaneously fit monomer and excimer decays.[3–6,29] The MFA can be used to fit the decays of any molecule or macromolecule labeled with the chromophore pyrene. When pyrene becomes excited by a photon of light, it can decay to the ground state using one of two pathways. It can either fluoresce with its monomeric lifetime,

τ_M, or it can encounter another ground-state pyrene and form one of two excimers. An excimer can be the result of the proper (E0) and improper (D) stacking of two pyrenyl groups and they have their own lifetime, τ_{E0} and τ_D, respectively. Three different pyrene species are expected to co-exist in solution, namely those pyrenes that are isolated in solution cannot form excimer (Py_{free}*), form an excimer through diffusive encounters (Py_{diff}*), and are pre-aggregated (*E0** or *D**). The MFA yields the molar fractions f_{free}, f_{diff}, and f_{agg} (= f_{E0} + f_D) of the pyrene species Py_{free}*, Py_{diff}*, *E0**, and *D**, respectively. In some instances, a contribution from residual scattering or possibly short-lived pyrene dimers is seen in the excimer decays, and an exponential with a short lifetime (τ_S) of 4 ns is added to the expression of the excimer decay during the decay analysis. More information about the details of the MFA can be found in the SI, along with the equations used to fit the pyrene monomer and excimer TRF decays.

Using the decay times, τ_i, and pre-exponential factors, a_i, calculated by the MFA, the average lifetime, $<\tau>$, as well as the average rate constant of excimer formation, $<k>$, can be calculated as shown using Equations 2.2 and 2.3, respectively.

$$<\tau> = \sum_{i=1}^{3} a_i \tau_i \tag{2.2}$$

$$<k> = \frac{1}{<\tau>} - \frac{1}{\tau_M} \tag{2.3}$$

Using the molar fractions of the different pyrene species along with $<\tau>$ and $<k>$, the $I_E/I_M{}^{TRF}$ ratio representing the absolute I_E/I_M ratio shown in Equation 2.4 can be calculated.[31]

$$\left(I_E/I_M\right)^{TRF} = \frac{(f_{diffE0}\tau_{E0} + f_{diffD}\tau_D) < \tau >< k > + f_{E0}\tau_{E0} + f_D\tau_D}{f_{diff} < \tau > + f_{free}\tau_M} \qquad (2.4)$$

Birks Scheme Analysis of the Fluorescence Decays:[7] The pyrene monomer and excimer fluorescence decays of PyBE were also fitted globally with Equations S2.3 and S2.4, respectively. In this case, the excimer is assumed to be produced by diffusive encounters between an excited and a ground-state pyrene label with a single rate constant k_{diff}. The excimer can then fluoresce with its natural lifetime τ_{E0} or dissociate by returning an excited and ground-state pyrene with a dissociation rate constant k_{-1}. Global analysis of the decays yields k_{diff}×[*PyBE*], k_{-1}, and τ_{E0}, where [*PyBE*] is the concentration of the PyBE model compound.[7,9,32]

2.4 Results

The average squared end-to-end distance, $<L_{Py}^2>^{1/2}$, of a series of 2,2-bis(hydroxymethyl)propionic acid backbone dendrons labeled with 1-pyrenebutyric acid at their terminal ends (Py_x-G(N)) is shown in Equation 2.5, which has been derived in an earlier publication.[29] The parameters a (= 6) and b (= 8) in Equation 2.5 represent the number of atoms connecting the pyrene label to the first junction point and the number of atoms resulting from the incorporation of each bis(hydroxymethyl)propionic acid in the construct, respectively. In Equation 2.5, l represents the projection of a C-C bond length taken to equal 0.125 nm.

$$< L_{Py}^2 > = l^2\left(1 + 2a + b\frac{N \times 2^N - 2^{N+1} + 2}{2^N - 1}\right) \qquad (2.5)$$

$[Py]_{loc}$ could then be determined with Equation 2.6, where N_A is the Avogadro number and the term $(2^N - 1)$ represents the number of ground-state pyrenes in the Py_x-G(N) dendron after considering that one pyrenyl label must be excited in a PEF experiment. The $[Py]_{loc}$ concentrations corresponding to the different Py_x-G(N) dendrons are provided in Table 2.1. The very large $[Py]_{loc}$ concentrations reported in Table 2.1 are a result of the short distances separating the ends of the dendrons in comparison to their overall size. For instance, a linear chain made of 16 bonds would have an end-to-end distance equal to $16^{0.5} \times l = 0.5$ nm using an l value of 0.125 nm. This end-to-end distance would result in a molar concentration for one chain end according to Equation 2.6 equal to 25 M, which is much larger than many organic solvents, but is a consequence of dealing with the end-to-end distance of a molecule instead of its overall size that is much larger. With their much higher number of chain ends, the Py_x-G(N) dendrons have considerably higher local concentrations of chain ends, as reported in Table 2.1.

$$[Py]_{loc} = \frac{2^N - 1}{\frac{4}{3}\pi\left(\frac{< L_{Py}{}^2 >}{2^2}\right)^{3/2} \times N_A} \tag{2.6}$$

The steady-state fluorescence (SSF) spectra for each Py_x-G(N) sample were acquired in the different solvents and are shown in Figure 2.1 for toluene, DMF, and DMSO. Py_2-G(1), which contains two pyrenyl groups, produces the least amount of excimer in each solvent, and PEF was found to increase with generation number and the number of pyrenyl groups present in a given Py_x-G(N) dendron, thus reflecting a direct relationship between the PEF efficiency and $[Py]_{loc}$. The SSF spectra shown in Figure 2.1 are typical of a pyrene-labeled macromolecule, and the PEF efficiency can be better quantified by considering the I_E/I_M ratio, which is proportional to k_{diff} and

$[Py]_{loc}$, as shown in Equation 2.7. The expression of k_{diff} is given in Equation 2.8, where R, D, and p are the molecular diameter of pyrene, the diffusion coefficient of pyrene, and the probability of having PEF upon a diffusive encounter between an excited and a ground-state pyrene, respectively.[2] The expression of the diffusion coefficient (D_{Py}) for one pyrene molecule is given in Equation 2.9, where k_B, T, η, and R_h are the Boltzmann constant, the absolute temperature, the solvent viscosity, and the hydrodynamic radius of the dye, respectively. Based on Equations 2.7 – 2.9, k_{diff}, and thus the I_E/I_M ratio, is proportional to the ratio p/η, which depends critically on the dielectric constant (reported at 20 ^oC) and viscosity (reported at 25 ^oC) of the solvent, which equal 2.4 and 0.56 mPa.s, 7.5 and 0.46 mPa.s, 38 and 0.79 mPa.s, and 47 and 1.99 mPa.s for toluene, THF, DMF, and DMSO, respectively.[33]

$$\frac{I_E}{I_M} \propto k_{diff} \times [Py]_{loc} \tag{2.7}$$

$$k_{diff} = 4\pi N_A RDp \tag{2.8}$$

$$D = \frac{k_B T}{6\pi\eta R_h} \tag{2.9}$$

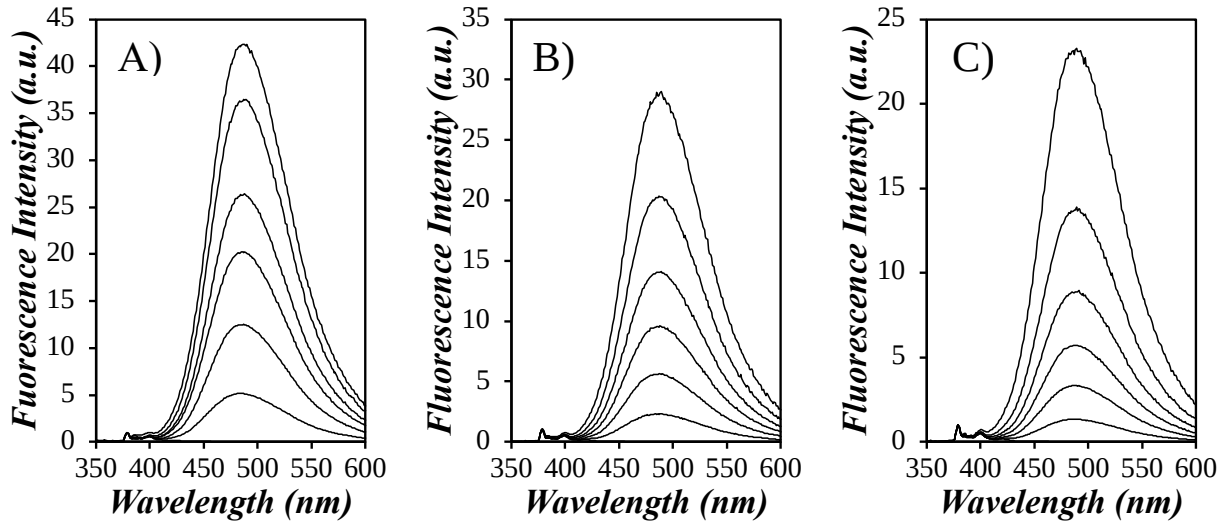

Figure 2.1. SSF spectra of the Py_x-G(N) dendrons normalized at the 0-0 transition of pyrene (~378 nm) in (A) toluene, (B) DMF, and (C) DMSO. From top to bottom: Py_{64}-G(6), Py_{32}-G(5), Py_{16}-G(4), Py_8-G(3), Py_4-G(2), and Py_2-G(1). λ_{ex} = 344 nm, [Py] = 2.5×10^{-6} M.

The I_E/I_M ratios of the Py_x-G(N) dendrons were plotted in Figure 2.2A for each solvent. The I_E/I_M ratio increased with increasing generation number. However, and as predicted by Equations 2.7 – 2.9, the I_E/I_M ratio did not depend solely on the viscosity of the solvent. For instance, toluene with a viscosity higher than THF was found to form excimer more efficiently, followed by THF, DMF, and finally DMSO. THF, which is more than 4 times less viscous than DMSO, yielded I_E/I_M ratios that were only 2.4-fold larger than those obtained in DMSO. This behaviour was a result of the different p values taken in Equation 2.8 for different solvents. The I_E/I_M ratios were also plotted as a function of $[Py]_{loc}$ in Figure 2.2B. Fairly linear trends were obtained between I_E/I_M and $[Py]_{loc}$ up to Py_{32}-G(5), but clear deviations from linearity were observed for Py_{64}-G(6). The linear increase of I_E/I_M with increasing $[Py]_{loc}$ agreed with the behavior expected from Equation 2.7.

The somewhat odd behavior observed in Figure 2.2B for Py_{64}-G(6), whereby the I_E/I_M ratio is smaller than anticipated, has two most plausible causes. One would be the presence of a small but strongly emissive amount of unattached pyrenyl labels, that would artificially increase the pyrene monomer emission, thus reducing the I_E/I_M ratio as was illustrated in an earlier publication.[11] The second would be the enhanced crowding of the terminal pyrenyl groups for the Py_{64}-G(6) sample leading to a reduction in the number of pyrenyl groups available for diffusive PEF, and thus resulting in less efficient PEF as was suggested earlier for the trends obtained in THF.[29] To address these concerns as well as the somewhat erratic behavior shown in Figure 2.2B where each solvent yielded a different trend, a more detailed analysis of the fluorescence data is required by applying the model free analysis (MFA) to the fluorescence decays of the Py_x-G(N) samples. The MFA dissects the PEF process into its dynamic and structural components, given by the average rate constant <k> for PEF (see Equation 2.1) and the molar fractions of the different pyrene species contributing to PEF, respectively.

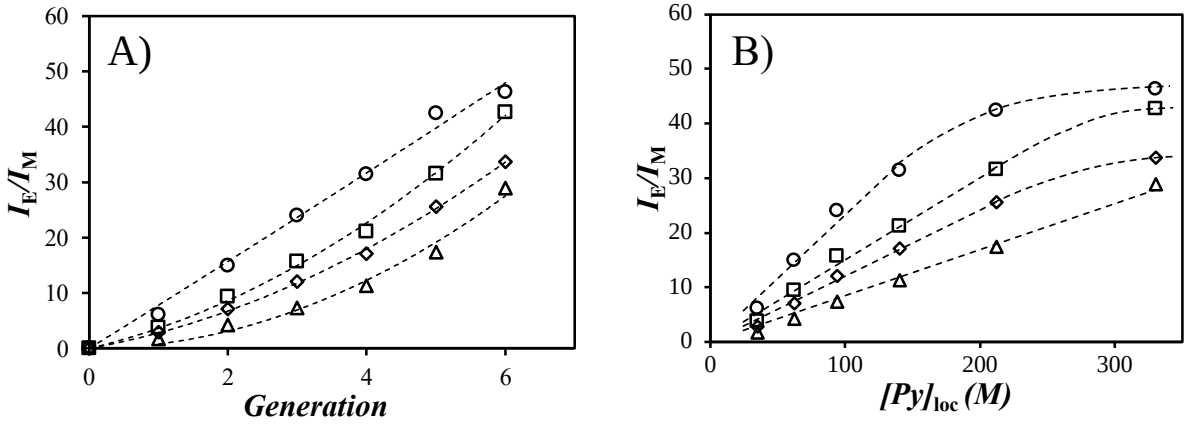

Figure 2.2. Plot of the I_E/I_M ratios for each Py_x-G(N) dendron in (○) toluene, (□) THF,[29] (◇) DMF, and (△) DMSO versus (A) generation number and (B) the $[Py]_{loc}$.

The TRF decays of each Py_x-G(N) dendron were acquired in toluene, DMF, and DMSO and then analysed using the MFA. The global MFA of the decays gave excellent fits with a $\chi^2 \leq$ 1.2 and residuals and autocorrelation of the residuals randomly distributed around zero. A sample fit is shown in Figure S2.2. A detailed explanation of the MFA can be found in the supporting information (SI) as well as all the parameters retrieved from the fits in Tables S2.3-2.5. The MFA parameters were used to calculate $<k>$ from Equation 2.3 and the molar fractions of the different pyrene species. These molar fractions f_{free}, f_{diff}, and f_{agg} represent the pyrenes that do not form excimer in solution and are usually free unattached pyrene derivatives, form excimer through diffusive encounters, and form excimer through direct excitation of a pyrene aggregate, respectively. To ensure that the parameters retrieved from the MFA provided an accurate representation of the fluorescence spectra shown in Figure 2.2, the parameters retrieved from the MFA of the decays were used to calculate the absolute I_E/I_M^{TRF} ratios using Equation 2.4. The absolute I_E/I_M^{TRF} ratios calculated from Equation 2.4 should be proportional to the relative I_E/I_M^{SSF} ratios obtained from the analysis of the SSF spectra. The linear relationship observed in Figure 2.3 between the I_E/I_M^{TRF} and I_E/I_M^{SSF} ratios demonstrated that the MFA parameters retrieved from the global analysis of the fluorescence decays agreed with the analysis of the fluorescence intensities in the fluorescence spectra. The average rate constant $<k>$ could now be studied in more detail.

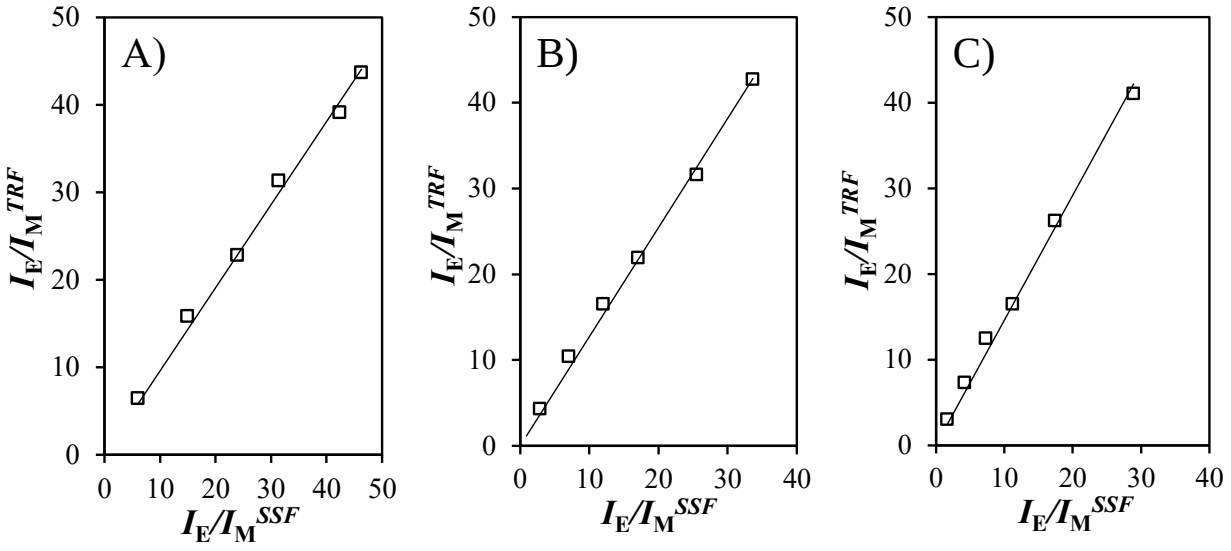

Figure 2.3. Plot of I_E/I_M^{TRF} versus I_E/I_M^{SSF} for the Py$_x$-G(N) samples in A) toluene, B) DMF, and C) DMSO.

Figure 2.4A is a plot of <k> vs. $[Py]_{loc}$ for the Py$_x$-G(N) samples in the three solvents. As for the I_E/I_M^{SSF} ratios in Figure 2.2B, <k> increased linearly with increasing $[Py]_{loc}$ for N values ranging from 1 to 5 but showed a clear downward curvature for Py$_{64}$-G(6). The same behavior had been observed earlier in THF, and this behavior had been attributed to increased aggregation of the pyrenyl labels, which lowered the local concentration of active pyrenyl labels that could form excimer by diffusive encounters between an excited and a ground-state pyrene.[29] The notion that the pyrenyl labels were strongly aggregated in the Py$_{64}$-G(6) sample was easily illustrated by plotting the molar fraction of aggregated pyrenes (f_{agg}) as a function of the generation number in Figure 2.4B. While the Py$_x$-G(N) samples with $1 \le N \le 5$ yielded f_{agg} values that were smaller than 0.06, f_{agg} for the Py$_{64}$-G(6) sample took a value that was larger than 0.17 in all solvents studied. Since <k> is unaffected by the presence of free pyrene derivatives, this result confirmed our earlier

analysis[29] that the unexpected behavior observed for Py_{64}-G(6) in Figure 2.2B and 2.4A was probably a consequence of extensive aggregation of the pyrenyl labels due to overcrowding. Dividing <*k*> by the molar fraction of pyrenyl groups, which form excimer exclusively though diffusive encounters (f_{diff}),[29] accounts for this artefact by increasing <*k*> to the value that it should take if all its pyrenyl groups were dissolved in the solution, as assumed by Equation 2.6 for the calculation of $[Py]_{loc}$.

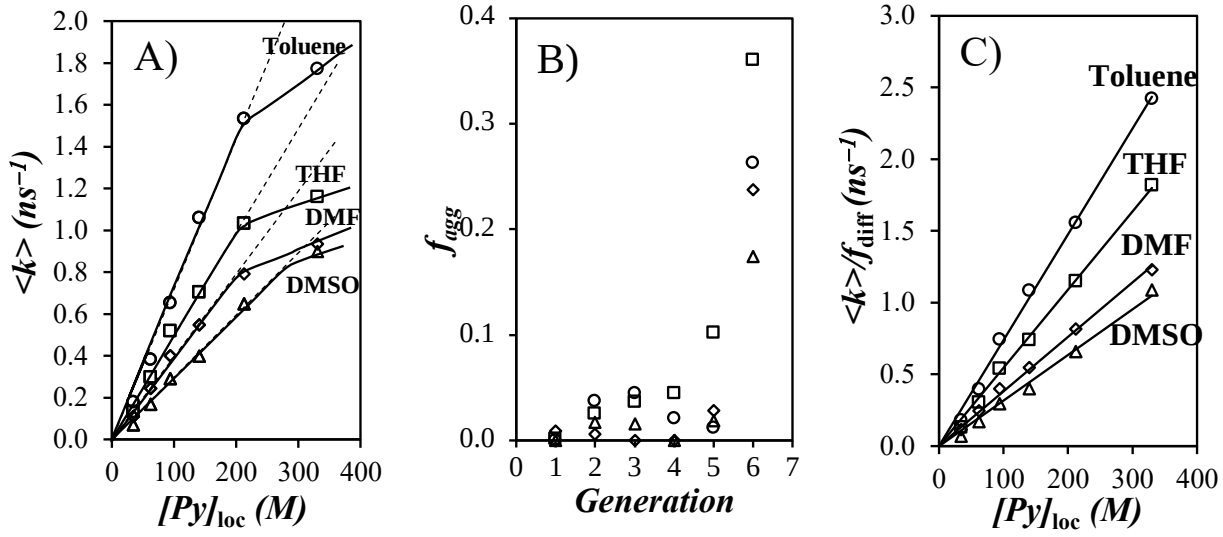

Figure 2.4. Plot of (A) <*k*> versus $[Py]_{loc}$ for the Py_x-G(*N*) dendrons, (B) f_{agg} calculated by the MFA for each generation, and (C) <*k*>/f_{diff} versus $[Py]_{loc}$ for the Py_x-G(*N*) dendrons in (○) toluene, (□) THF,[29] (◇) DMF, and (△) DMSO.

This correction was applied, and the ratio <*k*>/f_{diff} was plotted as a function of $[Py]_{loc}$ in Figure 2.4C. The linear relationships obtained in the plots shown in Figure 2.4C for all Py_x-G(*N*) dendrons in toluene, THF, DMF, and DMSO validated the proposal that the unexpected behavior observed for the I_E/I_M^{SSF} and <*k*> parameters in Figures 2.2B and 2.4A was due to extensive aggregation of the pyrenyl groups in Py_{64}-G(6). Similarly to the trends obtained in Figure 2.2B

with the I_E/I_M^{SSF} ratios, $<k>$ was found to be larger in the more viscous toluene than in THF. In an effort to identify the origin of this phenomenon and assess whether it was general or specific to the family of Py_x-G(N) dendrons, the PEF process was investigated further with ethyl 4-(1-pyrene)butyrate (PyBE), which was used as a model compound, since it resembles the pyrene derivative covalently bound to the Py_x-G(N) samples.

The fluorescence spectra of PyBE solutions with concentrations ranging from 6 to 14 mM were acquired in toluene, THF, DMF, and DMSO and are presented in Figure S2.3 of SI. The fluorescence spectra showed the expected spectral features of a pyrene derivative forming excimer, with a set of sharp peaks observed between 370 and 410 nm indicative of the pyrene monomer and a broad structureless emission centered at 480 nm for the excimer. Increasing the PyBE concentration resulted in increased pyrene-pyrene encounters that resulted in increased PEF. The fluorescence spectra shown in Figure S2.3 were analyzed to obtain their I_E/I_M^{SSF} ratios, which were plotted as a function of the PyBE concentration in Figure S2.4. The plots were linear as expected for PEF, but they also displayed the same unexpected trend observed with the Py_x-G(N) dendrons that showed more viscous toluene yielding larger I_E/I_M^{SSF} ratios than less viscous THF.

The fluorescence decays of the pyrene monomer and excimer of all the PyBE solutions were acquired and analyzed according to the Birks scheme and the MFA. The parameters retrieved from the Birks scheme analysis and MFA for the PyBE solutions have been listed in Tables S1 and S2, respectively. The fluorescence decay fits were excellent with the MFA in all solvents and for the Birks scheme in toluene and THF but showed some slight deviations at the early times in DMF and DMSO, possibly due to the increased viscosity of the two latter solvents. Nevertheless, the product $k_{diff}\times[PyBE]$ obtained from the Birks scheme analysis of the fluorescence decays and $<k>$ obtained from the MFA were plotted as a function of the PyBE concentration in Figure 2.5A.

Both $<k>$ and $k_{diff}\times[PyBE]$ increased linearly with increasing PyBE concentration, with $<k>$ being always slightly smaller than the product $k_{diff}\times[PyBE]$, probably a consequence of the different assumptions made for the derivation of each model. The Birks scheme assumes that the pyrene excimer dissociates with a dissociation rate constant that is typically small compared to $1/\tau_{E0}$, as found experimentally in Table S1, whereas the MFA neglects the excimer dissociation altogether. The Birks scheme also assumes a single rate constant for excimer formation, whereas the MFA assumes that the excimer can be formed by several rate constants. The poorer fits obtained for the fit of the fluorescence decays with the Birks scheme analysis in DMF and DMSO suggests that the MFA is a more robust analysis method. Nevertheless, the slopes of the plots of $<k>$ and $k_{diff}\times[PyBE]$ as a function of PyBE concentration in Figure 2.5A and of $<k>$ versus $[Py]_{loc}$ in Figure 2.4C yielded the bimolecular rate constant (k_{diff}[inter]) for intermolecular diffusive encounters between two pyrene molecules for PyBE and the pyrenyl labels of the Py_x-G(N) dendrons, respectively. They are plotted in Figure 2.5B as a function of the inverse of the solution viscosity.

The three plots for k_{diff} show some striking similarities with a sharp maximum for a $1/\eta$ value of 1.79 $(mPa\cdot s)^{-1}$ obtained in toluene. The common behavior observed for the pyrenyl labels of the Py_x-G(N) dendrons and PyBE demonstrates that this behavior is a result of the pyrene dye and not of its attachment onto the dendrons. k_{diff} was found to be 360 ± 30 times larger for the PyBE model compound than for the pyrenyl labels covalently attached to the dendrons. This massive reduction in k_{diff} reflects the equally massive loss in mobility experienced by a pyrene derivative upon covalent attachment to a macromolecule versus the same pyrene derivative freely diffusing in solution.

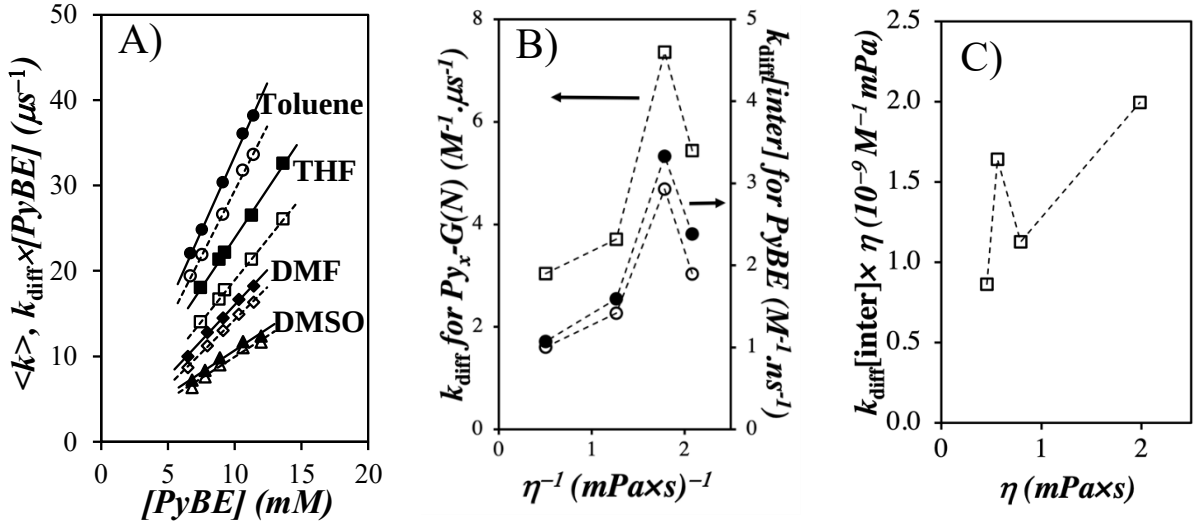

Figure 2.5. (A) <*k*> and k_{diff}×[*PyBE*] versus [PyBE] in (○,●) toluene, (□,■) THF, (◇,◆) DMF, and (△,▲) DMSO; solid and hollow symbols are for the fluorescence decay analysis according to the Birks scheme and MFA, respectively. B) Plot of k_{diff} for (□) the Py$_x$-G(*N*) dendrons and k_{diff}[inter] for the PyBE model compound when the fluorescence decays were fitted according to (○) the MFA and (●) the Birks scheme. C) k_{diff}×η of PyBE versus solvent viscosity.

Another important feature of Figure 2.5B is that k_{diff} is not inversely proportional to the solution viscosity, because PEF depends also on the probability (*p*) of forming an excimer upon encounter between two pyrene moieties, as discussed in Equations 2.7 – 2.9. This aspect is further illustrated with Figure 2.5C, which shows the product $\eta \times k_{diff}$[inter], which is proportional to *p*, plotted as a function of the solvent viscosity. For the four solvents investigated, $\eta \times k_{diff}$[inter] fluctuates from 0.86×10^9 M^{-1}·mPa in THF to 2.00×10^9 M^{-1}·mPa in DMSO. Additionally, the $\eta \times k_{diff}$[inter] value of 1.13×10^9 M^{-1}·mPa for DMF was almost half that of 2.00×10^9 M^{-1}·mPa in DMSO, suggesting a similar relationship for *p* as had been suggested earlier with two other pyrene model compounds, namely 1-pyrenemethylacetamide[34] and *n*-butyl-1-pyreneacetamide[35].

For the sake of consistency, the $\langle k \rangle / f_{diff}$ values obtained for the Py_x-G(N) dendrons in different solvents were divided by the k_{diff}[inter] values of 1.90, 2.93, 1.42, and 1.00 $M^{-1} \cdot ns^{-1}$ obtained from the MFA of the PyBE decays acquired in THF, toluene, DMF, and DMSO (see Figure 2.5B) to account for the changes in the ratio p/η between the different solvents. The quantity $\langle k \rangle / (f_{diff} \times k_{diff}[\text{inter}])$ was plotted as a function of $[Py]_{loc}$ in Figure 2.6 for the four solvents considered. All data points in Figure 2.4C collapsed along a master line in Figure 2.6, indicating that this correction accounted for the different p/η values of the solvents. The data points showed more scatter for the higher generation dendrimers, possibly because the pyrenyl labels were more aggregated, but also because the larger dendrons might have been subject to more excluded volume effects, which are not accounted for by the derivation of Equation 2.4. The smaller dendrons are likelier to be devoid of solvent effects and their behavior is well-described by Equation 2.4, which assumes that each chain segment behaves like a Gaussian chain. Finally, the straight line obtained between $\langle k \rangle / (f_{diff} \times k_{diff}[\text{inter}])$ and $[Py]_{loc}$ demonstrates that $\langle k \rangle$ responds directly to $[Py]_{loc}$ for the pyrene-labeled dendrons regardless of the nature of the solvent.

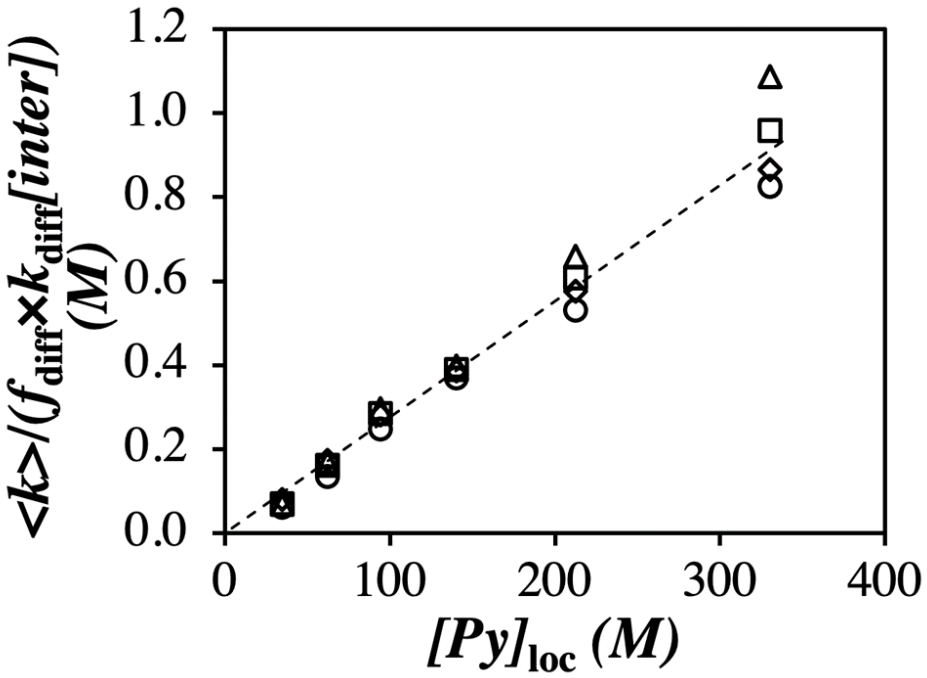

Figure 2.6. Plot of $\langle k \rangle/(f_{diff} \times k_{diff}[\text{inter}])$ as a function of $[Py]_{loc}$ for the Py_x-G(N) dendrons where the $\langle k \rangle$ values obtained for the dendrimers in a given solvent are divided by f_{diff} to account for possible aggregation of the pyrenyl labels and k_{diff}[inter] obtained from the MFA of the PyBE fluorescence decays in the same solvent to account for the p/η term in Equation 2.8 – 2.9; (○) toluene, (□) THF,[29] (◇) DMF, and (△) DMSO.

2.5 Conclusion

A series of six pyrene end-labeled dendrons (Py_x-G(N)) were studied in toluene, THF, DMF, and DMSO. These four solvents had different polarities and viscosities, which affected PEF through diffusive encounters between the pyrenyl labels differently. Accounting for the ratio p/η, by dividing the $\langle k \rangle$ values obtained for each Py_x-G(N) sample in different solvents by k_{diff} obtained for the model compound PyBE in the same solvents, yielded a straight line between $\langle k \rangle/(f_{diff} \times k_{diff}[\text{inter}])$ and $[Py]_{loc}$. This relationship was found to hold regardless of the nature of

the solvents, particularly for the smaller dendrons that are devoid of solvent effects. It also demonstrates that $<k>$ obtained from the MFA of the fluorescence decays acquired with pyrene-labeled macromolecules depends directly on $[Py]_{loc}$ and can thus be used to probe the internal density of macromolecules in the same manner as other techniques like intrinsic viscosity or static light scattering. The main difference between PEF and these other techniques is that it takes advantage of the extreme sensitivity of fluorescence, which allows fluorescence measurements to be performed with pyrene labeled macromolecule solutions as low as 1 mg/L, two to three orders of magnitude lower than all other standard techniques that are used to characterize macromolecules in solution.

Chapter 3

Probing the Local Concentration Experienced by the Side Chain Ends of Poly(oligo(ethylene glycol) 1-Pyrenemethyl Ether Methacrylate) Bottle Brushes in Solution Using Pyrene Excimer Fluorescence

3.1 Abstract

Four poly(oligo(ethylene glycol) 1-pyrenemethyl ether methacrylate) (P(PyEG$_y$MA) samples, with y = 3, 5, 8, and 12) were synthesized, where each side chain was terminated with a 1-pyrenemethoxy moiety. The efficiency of excimer formation between an excited and a ground-state pyrene was used to assess the conformation of the PyEG$_y$ side chains in these polymeric bottle brushes by conducting time-resolved fluorescence measurements in tetrahydrofuran (THF), *N*,*N*-dimethylformamide (DMF), dioxane, and dimethylsulfoxide (DMSO). These experiments took advantage of the dependency of the average rate constant $<k>$ of pyrene excimer formation (PEF) on the local pyrene concentration $[Py]_{loc}$ experienced by an excited pyrene bound to the P(PyEG$_y$MA) samples. $[Py]_{loc}$ could be estimated theoretically by assuming that the EG$_y$ side chains adopted a Gaussian conformation. Linear plots of $<k>/f_{diff}$ as a function of $[Py]_{loc}$, where f_{diff} is the molar fraction of pyrenyl labels forming excimer by diffusion, introduced to account for residual pyrene aggregation, were obtained in all four solvents with slopes that depended on solvent viscosity and the probability of PEF upon diffusive encounter between two pyrenyl labels. Solvent-induced differences in PEF efficiency could be accounted for by determining the bimolecular rate constant, k_{diff}[inter], for intermolecular PEF with the model compound 1-pyrenemethyl diethylene glycol methyl ether in the four solvents. Except for DMSO, which was too polar and led to the segregation of the pyrenyl labels close to the polymethacrylate backbone, the data obtained for all P(PyEG$_y$MA) samples in THF, DMF, and dioxane collapsed on a master line, similarly to the one obtained in Chapter 2 with a series of pyrene-labeled dendrons when plotting $<k>/(f_{diff}\times k_{diff}[\text{inter}])$ vs. $[Py]_{loc}$. The $<k>/(f_{diff}\times k_{diff}[\text{inter}])$ vs. $[Py]_{loc}$ master line confirmed the direct relationship that exists between the PEF efficiency and $[Py]_{loc}$, a relationship that could be used effectively to probe the conformation of highly branched macromolecules in solution.

3.2 Introduction

The end-to-end distance (r_{EE}) of linear polymer chains is a most important mathematical tool to represent the dimension of a chain without having to account for the molecular details associated with the chemical structure of the monomer used to prepare the polymer under study.[1] Theoretically, r_{EE} is expected to scale as n^{ν}, where n is the number of bonds of the chain and ν is the Flory exponent equal to 0.5 for a linear chain in the bulk or in a theta solvent or 0.6 for a chain in a good solvent.[2] Experimentally however, it is usually not r_{EE} that is determined but the radius of gyration (R_G) using scattering techniques.[3,4] R_G can then be related to r_{EE} by taking advantage of the well-known relationship $r_{EE}^2 = 6 \times R_G^2$, that applies to linear chains. The main advantage of using R_G over r_{EE} in the case of linear chains resides in the small number of chain ends that need to be detected for r_{EE} measurements, compared to the much larger number of structural units constituting the linear chain that are probed in an R_G measurement. This explains why experimental techniques that probe the ends of a linear chain must enhance the chain end signal to facilitate their detection, typically by labeling the two chain ends with fluorescent dyes such as a pair of FRET donor and acceptor dyes[5–11] or two pyrene labels.[12–14] The dyes are selected for the ability of their fluorescence signal to report on either r_{EE} directly for a FRET pair, or the local concentration of the chain ends within the macromolecular volume for the pyrene labels. r_{EE} can then be derived from the analysis of the pyrene fluorescence.

While the ability of fluorescence experiments to probe r_{EE} from fluorescently end-labeled linear chains is well-established,[5–14] the r_{EE}-concept is more difficult to visualize in the case of dendrimers and polymeric bottle brushes, whose many chain ends beg the question as to which chain ends should be considered to characterize the r_{EE} of such macromolecules. For these more complex macromolecules, the R_G-concept is particularly well-suited, as it characterizes the spatial

mass distribution of a macromolecule within the macromolecular volume with respect to its center of mass without having to consider its chain ends.[15,16] Yet a mathematical procedure was proposed in two recent studies to determine the average end-to-end distance $\langle r_{EE} \rangle$ for the terminals of dendrimers that had been labeled with pyrenyl groups.[17,18] $\langle r_{EE} \rangle$ was applied to predict the local pyrene concentration ($[Py]_{loc}$) generated by a series of six pyrene end-labeled dendrons. These dendrons were prepared with a 2,2-bis(hydroxymethyl) propionic acid backbone and were referred to as Py_x-G(N), where the generation number (N) ranged from 1 to 6 and the number of pyrene molecules (x) equaled 2^N. For each Py_x-G(N) sample, the fluorescence decays of the pyrene monomer and its excimer, generated through the diffusive encounters between an excited and a ground-state pyrene, were fitted globally according to the model free analysis (MFA). These studies yielded the average rate constant $\langle k \rangle$ for PEF for the Py_x-G(N) samples in four different solvents. $\langle k \rangle$ equals the product $k_{diff} \times [Py]_{loc}$, where k_{diff} is the bimolecular rate constant for PEF by diffusion. Accounting for solvent-induced differences in the fluorescence response of the pyrene derivatives of the Py_x-G(N) samples led to a master line, along which all $\langle k \rangle$ values obtained for the Py_x-G(N) samples clustered when plotted against $[Py]_{loc}$.[18] The coalescence of all $\langle k \rangle$ values along a master line suggested that the calculated $\langle r_{EE} \rangle$ values led to predictions for $[Py]_{loc}$, that reflected the conformation of the dendrons in solution.

Emboldened by this early success, the present study illustrates how the same PEF-based methodology can be applied to predict the conformation of the side chains of another family of highly branched macromolecules, namely a series of polymeric bottle brushes (PBBs) belonging to the PEGMA-type, introduced by the Lutz group due to their interesting thermoresponsive properties.[19,20] In solution, PBBs adopt an extended conformation as the main chain becomes more crowded with increasing side chain length.[21,22] The topology of the PBBs generates two length

scales, one related to the main chain, which is often described by its persistence length (l_p), and another by the side chains, which is described by the average squared cross-sectional radius of gyration of the main chain ($R_{g,C}$) or the end-to-end distance of the side chains ($r_{EE,SC}$).[23–35] The parameters l_p, $R_{G,C}$, and $r_{EE,SC}$ are typically extracted from scattering data, whose analysis requires "dividing out" the contribution of the side chains from the overall scattering signal to isolate the signal pertaining to the main chain. In turn, this mathematical process involves making some assumptions about the density profiles of the side chains.[35] Isotopic labeling of specific sections of PBBs (backbone or side chains) could distinguish between both contributions in a more definitive manner, but to the best of our knowledge such experiments have not been conducted yet.

In contrast, the backbone and side chains of PBBs can be labeled separately with a pyrenyl derivative, whose fluorescence response would provide information about the internal density of the targeted section of the fluorescently labeled PBB. In the present study, four poly(oligo(ethylene glycol) 1-pyrenemethyl ether methacrylate)s (P(PyEG$_y$MA) samples, with *y* being the number of ethylene glycol units in the side chain equal to 3, 5, 8, and 12), were prepared where each side chain was end-labeled with a pyrenyl group. The design of the P(PyEG$_y$MA) constructs, where each side chain was pyrene end-labeled, was utilized to probe the conformation of the side chains based on the fluorescence of the pyrenyl derivative. The monomer and excimer decays of the P(PyPEG$_y$MA) samples were acquired in tetrahydrofuran (THF, η = 0.456 mPa.s at 25 ^{o}C), *N*,*N*-dimethyl formamide (DMF, η = 0.794 mPa.s at 25 ^{o}C), dioxane (η = 1.18 mPa.s at 25 ^{o}C), and dimethylsulfoxide (DMSO, η = 1.99 mPa.s at 25 ^{o}C), and their global MFA yielded the corresponding <*k*> values for each sample in the different solvents. Assuming that the pyrenyl terminal of each EG$_n$ side chain could probe a spherical volume, whose diameter was defined by

the $r_{EE,SC}$ (= $n^{0.5}\times l$, with n being the number of chemical bonds of length l (~ 0.125 nm)) of the side chain, allowed the calculation of a predicted value for $[Py]_{loc}$ which was found to correlate strongly with $\langle k \rangle$, as had been observed for the Py_x-G(N) dendrons.[17,18] The strong correlation between $\langle k \rangle$ obtained from PEF measurements and $[Py]_{loc}$ suggests that PEF provides an experimental means to probe the internal density of macromolecules in general, and the conformation adopted by the EG_y side chains of PEG_yMA samples in solution in particular. This application of PEF to probe the conformation of macromolecules, and specific parts of a macromolecule, in solution represents an important development in the use of PEF which should nicely complement scattering experiments.[3,4,15,16,23–35]

3.3 Experimental

Materials: Celite, chloroform (≥ 99.8%), dichloromethane (DCM, ≥ 99.8%), diethyl ether (≥ 99%), *N*,*N*-dimethylformamide (DMF, ≥ 99.8%), dimethylsulfoxide (DMSO, ≥ 99.9%), 4-(dimethylamino)pyridine (DMAP, ≥ 99%), 1,4-dioxane (< 99%), ethyl acetate (≥ 99.7%), methacrylic anhydride (94%), octa(ethylene glycol) (≥ 95%), 1-pyrenemethanol (98%), sodium chloride, sodium hydride (60% dispersion in mineral oil), sodium hydroxide (NaOH, pellets, ≥ 97%), sodium sulfate (anhydrous, ≥ 99%), tetrahydrofuran (≥ 99%), thionyl chloride (≥ 99%), triethylamine (≥ 99.5%), and tri(ethylene glycol) (99%) were obtained from Sigma (Oakville, ON, Canada). Diethylene glycol monomethyl ether (> 99%) was supplied by TCI (Portland, OR, USA). Dodeca(ethylene glycol) (≥ 97 %) was supplied by SiChem (Bremen, Germany). Penta(ethylene glycol) (≥ 95%) and tetrahydrofuran optima (≥ 99.9%) were purchased from Fisher Scientific (Ottawa, ON, Canada). All chemicals were used as received.

The radical initiator 2,2'-azobisisobutyronitrile (AIBN, Sigma, 98%) was recrystalized in ethanol three times.

p-Toluenesulfonyl chloride (Sigma, ≥ 98%) was dissolved in diethyl ether and washed with 2 M NaOH. The organic phase was extracted and dried with sodium sulfate.

Preparation of the 1-pyrenemethoxy diethylene glycol methyl ether (PyEG$_2$ME) model compound: The synthesis of the model compound 1-pyrenemethoxy diethylene glycol methyl ether follows the reaction scheme outlined in Scheme 3.1 and is described in more detail hereafter.

1-Pyrenemethanol (0.40 g, 1.7 mmol) was added to a round bottom flask (RBF) with 100 mL of chloroform. Thionyl chloride (0.63 mL, 8.6 mmol) was added dropwise, and the solution was brought to a gentle reflux for 2 hours. The solvent and excess thionyl chloride were evaporated using nitrogen. THF was dried by stirring with calcium hydride overnight before distilling off 50 mL into a second RBF. Diethylene glycol monomethyl ether (0.21 g, 1.7 mmol) was then added to the second RBF under a nitrogen atmosphere to which sodium hydride (0.08 g, 1.9 mmol) was added. The reaction was refluxed for 1 hour before adding 1-chloromethyl pyrene dissolved in a small amount of dried and distilled THF. The reaction was left stirring under nitrogen atmosphere overnight at 40 °C. The next day, the THF was removed using rotary evaporation and re-dissolved in dichloromethane (DCM). The solution was then washed with a saturated solution of sodium chloride. The organic phase was collected and dried with sodium sulfate and then purified by column chromatography using a 50:50 ethyl acetate : hexane mixture as the eluent. The product obtained was a yellow oil and its chemical composition was verified using ^{1}H NMR (Figure S3.1).

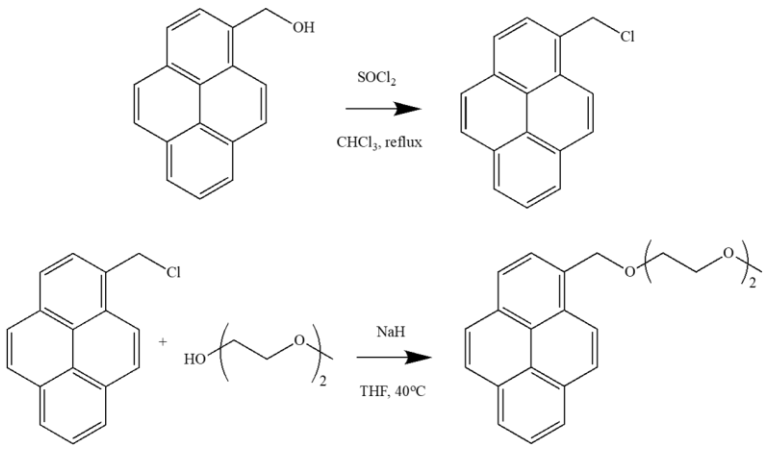

Scheme 3.1. Reaction scheme for the synthesis of the model compound 1-pyrenemethoxy diethylene glycol methyl ether.

Preparation of 1-pyrenemethyl ether oligo(ethylene glycol) (PyEG$_y$OH): The synthesis of 1-pyrenemethyl ether oligo(ethylene glycol) (PyEG$_y$OH, where *y*= 3, 5, 8, and 12) follows the reaction scheme outlined in Scheme 3.2. The same protocol was used to prepare PyEG$_3$OH, PyEG$_5$OH, PyEG$_8$OH, and PyEG$_{12}$OH. The synthesis of PyEG$_3$OH is described in more detail hereafter.

Tri(ethylene glycol) (3.00 g, 20.0 mmol) and *p*-toluenesulfonyl chloride (1.70 g, 22.0 mmol) were added to a round bottom flask (RBF) equipped with a magnetic stirrer and freshly distilled DCM. Triethylamine (TEA) (4.18 mL, 30 mmol) was added to the RBF dropwise and the reaction was left to stir overnight. The next day, the reaction was washed with a saturated solution of sodium chloride. The organic phase was extracted and dried with sodium sulfate. The product was a pale-yellow oil, that contained mostly mono-tosylated tri(ethylene glycol) (TosEG$_3$OH) and a small amount of doubly-tosylated tri(ethylene glycol) contaminant. The TosEG$_3$OH product was used in the next step without further purification. *N*,*N*-dimethylformamide (DMF) was dried using 4Å molecular sieves before distilling off 50 mL into a RBF to which 1-pyrenemethanol (2.29 g,

9.87 mmol) and sodium hydride (0.32 g, 7.89 mmol) were added under a nitrogen atmosphere. The reaction mixture was then allowed to stir for 1 hour as the colour of the solution changed from yellow to purple. TosEG_3OH (1.00 g, 3.29 mmol) was added to the RBF, which was placed in an oil bath at 50 ºC and left to stir overnight. The next day, 5 mL of MilliQ water was added to the RBF to quench any unreacted sodium hydride. The reaction solution was added to a separatory funnel along with 50 mL of MilliQ water and ethyl acetate. The organic phase was extracted and dried with sodium sulfate. Silica gel chromatography was used to purify the crude product using ethyl acetate as the eluent (acetone was added to the eluent for the higher molecular weight monomers). The final product was a pale-yellow oil. The chemical composition of $PyEG_3OH$ and the other $PyEG_yOH$ derivatives was verified using ^{1}H- NMR (Figure S3.2-S3.5 in the SI).

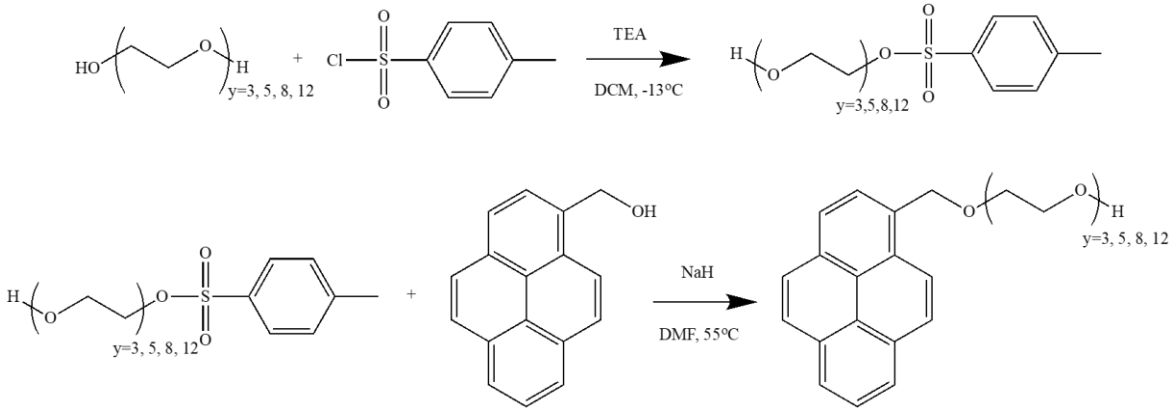

Scheme 3.2. Reaction scheme for the synthesis of 1-pyrenemethyl ether oligo(ethylene glycol) ($PyEG_yOH$, where *y*= 3, 5, 8, and 12).

Preparation of 1-pyrenemethyl ether oligo(ethylene glycol) methacrylate (PyEG$_y$MA): The synthesis of 1-pyrenemethyl ether oligo(ethylene glycol) methacrylate ($PyEG_yMA$, where *y*= 3, 5, 8, and 12) follows the reaction scheme outlined in Scheme 3.3. The same protocol was used to

prepare $PyEG_3MA$, $PyEG_5MA$, $PyEG_8MA$, and $PyEG_{12}MA$. The following discussion describes the preparation of $PyEG_3MA$ in more detail.

$PyEG_3OH$ (0.15 g, 0.41 mmol) and DMAP (5.0 mg, 0.04 mmol) were added to a RBF with 25 mL of freshly distilled DCM. The RBF was placed in an ice water bath and methacrylic anhydride (0.09 mL, 0.62 mmol) was added dropwise. The reaction was left to stir overnight at room temperature. The next day, the reaction mixture was washed with 2 M NaOH (aq) three times. The organic phase was dried with sodium sulfate and the product was purified by silica gel chromatography using ethyl acetate as the eluent. The chemical composition of the $PyEG_yMA$ monomers for y = 3, 5, 8, and 12 was confirmed by analysis of their ^1H NMR spectra shown in Figures S3.6-S3.9 in the SI, respectively.

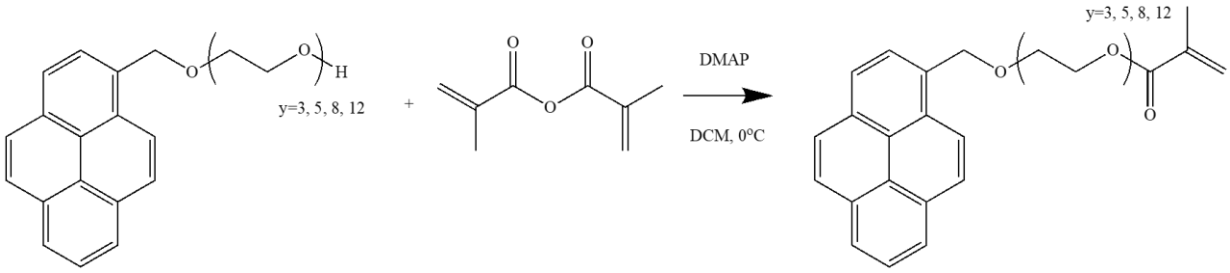

Scheme 3.3. Reaction scheme for the synthesis of 1-pyrenemethyl ether oligo(ethylene glycol) methacrylate ($PyEG_yMA$, y=3, 5, 8, and 12)

Preparation of poly(1-pyrenemethyl ether oligo(ethylene glycol) methacrylate) (P($PyEG_yMA$)): The synthesis of poly(1-pyrenemethyl ether oligo(ethylene glycol) methacrylate) (P($PyEG_yMA$), where y= 3, 5, 8, and 12) follows the reaction scheme outlined in Scheme 3.4. The same protocol was used to prepare P($PyEG_3MA$), P($PyEG_5MA$), P($PyEG_8MA$), and P($PyEG_{12}MA$). The polymerization of P($PyEG_3MA$) is presented hereafter.

$PyEG_3MA$ (150 mg, 0.35 mmol) was added to a Schlenk tube with 2 mL of THF optima. AIBN (0.28 mg, 1.73 mmol) was added from a 0.6 mg/mL stock solution and the solution was degassed with nitrogen (4.0, Praxair) for 30 mins. The tube was sealed and added to an oil bath at 65 °C. The solution mixture was left to react overnight. The next morning, the polymerization was terminated and the polymer was precipitated 5-6 times in diethyl ether. The chemical structure of each $P(PyEG_yMA)$ polymer is shown in Table 3.1 and they were characterized using ^1H NMR and GPC in Figures S3.10 and S3.11, respectively.

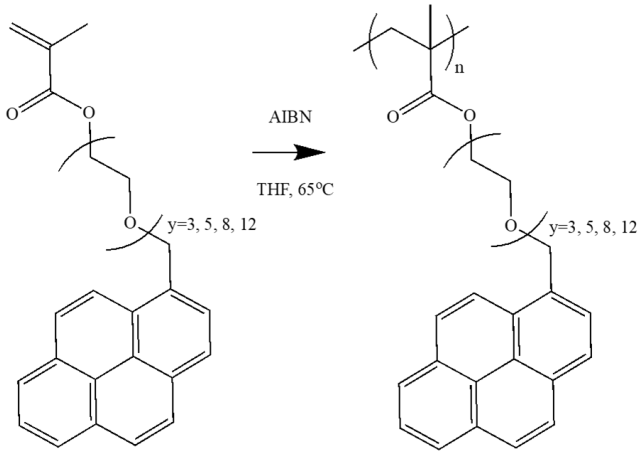

Scheme 3.4. Reaction scheme for the synthesis of poly(1-pyrenemethyl ether oligo(ethylene glycol) methacrylate) ($P(PyEG_yMA)$, y=3, 5, 8, and 12).

Gel permeation chromatography: Absolute molecular weights of the $P(PyEG_yMA)$ samples where y = 5, 8, and 12 were obtained by injecting 1 mg/mL polymer solutions in DMSO into a TOSOH EcoSEC High Temperature GPC instrument equipped with a triple detection system and two 300 × 7.8 mm^2 TOSOH TSKgel Alpha-M 13 μm columns. This detection system includes an in-line differential refractometer, a Wyatt Dawn Heleos8 MALLS detector (wavelength, λ= 660 nm), and

a viscometer. A flow rate of 0.6 mL/min of DMSO at 70 ºC was used. The system was calibrated with a 1 mg/mL solution of pullulan standard in DMSO with a weight-average molecular weight (M_w) and dispersity ($Đ$) of 47.1 × 10^3 g.mol^{-1} and 1.07, respectively.

PyPEG$_3$MA was found to be insoluble in DMSO at 1 mg/mL. Therefore, the absolute molecular weight of P(PyEG$_3$MA) was obtained by injecting a 1 mg/mL polymer solution in THF into a Malvern Viscotek GPC equipped with a differential refractometer, UV-Vis absorption detection, right angle light scattering (RALS), and low angle light scattering (LALS) detectors. This GPC system is equipped with three 300 × 8 mm^2 PolyAnalytik Superes linear mixed-bed columns. A flow rate of 1 mL/min of THF at 35 ºC was used. The system was calibrated with a 1 mg/mL THF solution of a polystyrene (PS) standard with peak molecular weight and $Đ$ of 90×10^3 g.mol^{-1} and 1.04, respectively. The P(PyEG$_y$MA) samples with y = 5, 8, and 12 were found to interact with the columns of the THF GPC and therefore were only characterized in DMSO.

The GPC traces for P(PyEG$_3$MA) in THF and P(PyEG$_5$MA), P(PyEG$_8$MA), and P(PyEG$_{12}$MA) in DMSO can be found in Figure S3.11 in the SI.

Chemical composition: The chemical composition of the PyPEG$_y$MA monomers and polymers were confirmed by the analysis of the ^{1}H NMR spectra acquired on a Bruker 300 MHz high resolution spectrometer in either DMSO-d_6 or $CDCl_3$.

UV-Vis spectroscopy: A Varian Cary 100 Bio spectrophotometer was used to acquire the absorption spectra and prepare solutions with a 0.1 absorbance at 344 nm of the polymers in tetrahydrofuran (THF), *N*,*N*-dimethylformamide (DMF), dioxane, and dimethylsulfoxide (DMSO). The solution of a pyrene-labeled polymer with an absorbance of 0.1 at 344 nm has a concentration in pyrenyl labels of approximately 2.5×10^{-6} M, low enough to prevent intermolecular pyrene excimer formation (PEF).

Steady-state fluorescence (SSF) measurements: All fluorescence spectra were acquired on a HORIBA QM-400 spectrofluorometer equipped with a xenon arc lamp. The SSF spectra were acquired for polymer solutions in degassed THF, DMF, dioxane, and DMSO with a 2.5×10^{-6} M pyrene concentration to avoid the inner filter effect. The solutions were excited at 344 nm and scanned from 350 to 600 nm using 1 nm slit widths for both the excitation and emission monochromators. Dividing the florescence intensity of the excimer (I_E) by the fluorescence intensity of the monomer (I_M), calculated by integrating the area underneath the spectrum from 500 to 530 nm and ± 4 nm from the wavelength of the first peak, I_1, in the monomer emission, respectively, yielded the I_E/I_M ratio which was used to quantify the efficiency of PEF.

Time Resolved Fluorescence (TRF) Measurements: All fluorescence decays were obtained with a HORIBA FluoroHub equipped with a DeltaDiode at 336 nm. The solutions were excited at 336 nm and the monomer and excimer fluorescence decays were acquired with 20,000 counts at the decay maximum over 1,024 channels at 375 and 510 nm using cut-off filters at 370 and 495 nm, respectively. A time-per-channel of either 0.0514 ns/ch or 0.102 ns/ch was employed for the decay acquisition. An aluminum reflective monolith was used to acquire the instrument response function (IRF), which was obtained by setting the emission monochromator to the excitation wavelength of 336 nm.

Model Free Analysis (MFA): The MFA was used to analyze the fluorescence decays of the P(PyEG$_y$MA) samples. The MFA makes no assumptions on the shape of the macromolecule and on whether the type of pyrene labeling is specific or random. It simply assumes that the fluorescence decays of the pyrenyl labels (Py_{diff}*) forming excimer by diffusion can be handled by a sum of exponentials with pre-exponential factors a_i and decay times τ_i. MFA of the decays yields the number-average lifetime $<\tau>$, whose expression is provided in Equation 3.1. In turn,

$<\tau>$ can be used in Equation 3.2 with the natural lifetime τ_M of the pyrene monomer to determine the average rate constant $<k>$ for PEF. Beside the pyrene species Py_{diff}*, the MFA also involves three other pyrenyl species. In particular, some pyrenyl labels are unable to form excimer while they remain excited. These pyrenyl groups emit as if they were free in solution with the lifetime τ_M and are referred to as Py_{free}*. The Py_{diff}* species forms an excimer $E0$* or D*, depending on whether it is obtained from two well or two poorly stacked pyrenyl labels, respectively. The species $E0$* and D* emit with their own lifetime τ_{E0} and τ_D and can also be generated from the direct excitation of a pyrene aggregate. Equation S3.1 in the SI retrieves the molar fractions f_{Mdiff} and f_{Mfree} of the pyrene species Py_{diff}* and Py_{free}*. Equation S3.2 in the SI retrieves the molar fractions $f_{EdiffE0}$, f_{EdiffD}, f_{EE0}, and f_{ED} for the pyrene species Py_{diff}* that form an excimer $E0$* or D* by diffusive encounters, or the pyrene species that form an excimer $E0$* and D* instantaneously upon direct excitation of a pyrene aggregate. The molar fractions f_{Mdiff}, f_{Mfree}, $f_{EdiffE0}$, f_{EdiffD}, f_{EE0}, and f_{ED} can be combined to yield the molar fractions f_{diff} (= f_{diffE0}+f_{diffD}), f_{free}, f_{E0}, and f_D of the pyrenyl species Py_{diff}*, Py_{free}*, $E0$*, and D*, respectively. The molar fraction f_{agg} of the aggregated pyrenes is taken as the sum $f_{E0} + f_D$. The TRF decays of the pyrene monomer and excimer were fit globally according to Equations S3.1 and S3.2 in the SI, respectively. A fit was deemed acceptable when the residuals and the autocorrelation of the residuals were randomly distributed around zero and the χ^2 was less than 1.3. All the parameters were optimized according to the Marquardt-Levenberg algorithm.[36] The MFA has been reviewed numerous times and the reader is referred to these documents for more in-depth information.[37–39]

$$<\tau>=\sum_{i=1}^{3} a_i \tau_i \qquad (3.1)$$

$$< k >= \frac{1}{< \tau >} - \frac{1}{\tau_M} \tag{3.2}$$

3.4 Results and Discussion

The side chain tips of four poly(oligo(ethylene glycol) methyl ether methacrylate) samples were end-labeled with a 1-pyrenemethoxy group to yield four P(PyEG$_y$MA) samples, where y = 3, 5, 8, and 12. The P(PyEG$_y$MA) samples were synthesized by the grafting through technique using conventional radical polymerization as described in the Experimental section. The chemical structure of the P(PyEG$_y$MA) samples is presented in Table 3.1 together with their absolute number-average molecular weight (M_n), number-average degree of polymerization (DP), dispersity ($Đ$), and the number N_S of non-hydrogen atoms in the side chains. N_S is related to the number y of ethylene glycol units by the relationship $N_S = 3 + 3 \times y$. Since the analysis of the $<k>$ values obtained from the MFA of the decays suggested that the side chains would adopt a Gaussian conformation, the EG$_y$ side chains used for the P(PyEG$_y$MA) samples would only spread over a maximum of 10 structural units for the longest side chains. Consequently, the DP of these polymers were deemed large enough to neglect chain end effects.

Dilute solutions of these polymers were prepared in tetrahydrofuran (THF), *N*,*N*-dimethylformamide (DMF), dioxane, and dimethylsulfoxide (DMSO) and their steady-state fluorescence (SSF) spectra were acquired. We note that the PEF experiments were conducted at a polymer concentration that was lower than 2 mg/L, 3 orders of magnitude lower than the 1 mg/mL solutions used for the GPC experiments, which explains why dissolution of the P(PyEG$_y$MA) samples was not an issue in DMSO.

Table 3.1. Chemical structure, M_n, *DP*, *Đ*, and N_S for the P(PyEG$_y$MA) samples.

Sample	P(PyEG$_3$MA)	P(PyEG$_5$MA)	P(PyEG$_8$MA)	P(PyEG$_{12}$MA)
				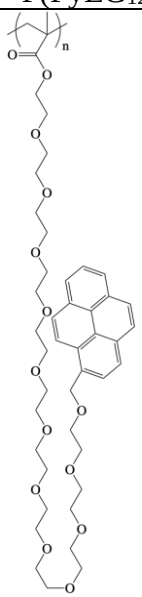
M_n (g/mol)	83 000[a]	58 000[b]	70 000 [b]	176 000 [b]
DP	205	118	112	220
Đ	1.5	1.4	1.6	2.7
N_S	12	18	27	39

[a] GPC in THF; [b] GPC in DMSO

The spectra obtained in THF and DMSO, which are the solvents with the lowest and highest viscosity, are presented in Figures 3.1A and 3.1B, respectively. The spectra obtained in DMF and dioxane showed similar features and are provided in Figure S3.12 in the SI. The spectra were normalized to the first peak of the pyrene monomer emission, I_1, which corresponds to the 0-0 transition of pyrene. The spectra shown in Figure 3.1 display the characteristic spectral features of a polymer labeled with the chromophore pyrene. The sharp peaks found between 375 and 410 nm were typical of the pyrene monomer fluorescence and the broad and structureless emission of the excimer was centered around 480 nm. The large $[Py]_{loc}$ generated by each pyrene end-labeled side chain of the P(PyEG$_y$MA) samples led to the formation of large amounts of excimer whose

fluorescence dwarfed that of the monomer, as shown in Figure 3.1A and B from the almost non-existent monomer emission peaks. Since DMSO is ~4 times more viscous than THF, excimer formation, which occurs through diffusive encounters between pyrenyl labels, was reduced in DMSO resulting in more pronounced monomer fluorescence peaks in DMSO, as shown in Figure 3.1B, compared to Figure 3.1A for the spectra acquired in less viscous THF. A clear trend was observed in all solvents, whereby PEF increased with decreasing side chain length of the P(PyEG$_y$MA) samples. This trend is reasonable, as a shorter oligo(ethylene glycol) linker holds the pyrenyl groups closer to the polymethacrylate backbone in a process that increases $[Py]_{loc}$ and promotes PEF.

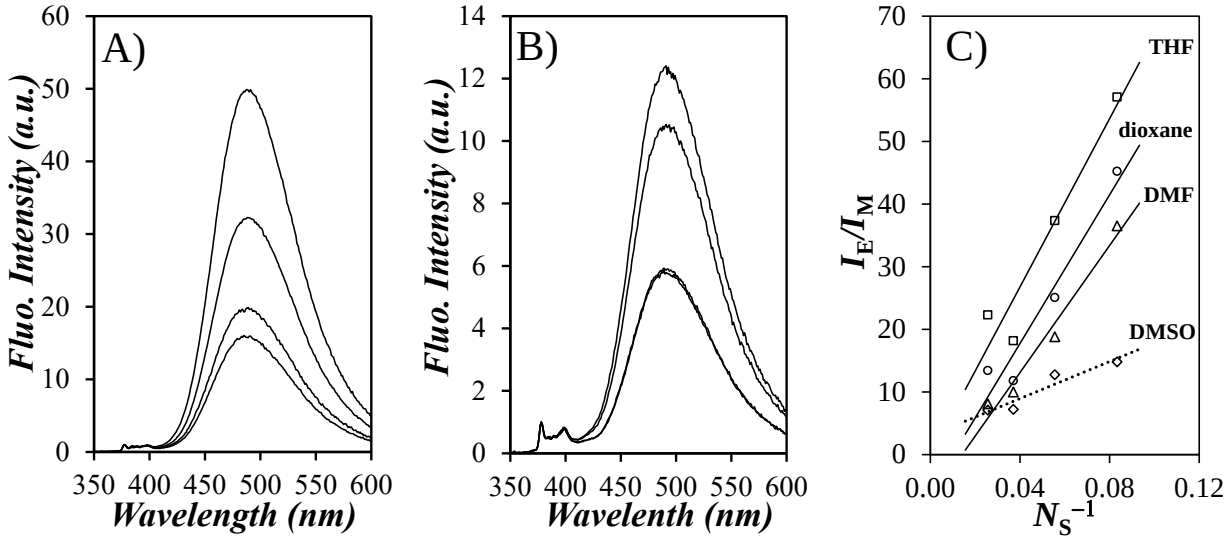

Figure 3.1. Normalized SSF spectra of the P(PyEG$_y$MA) samples in A) THF and B) DMSO (λ_{ex} = 344 nm; from top to bottom, P(PyEG$_y$MA) samples with y = 3, 5, 8, and 12). C) Plot of the I_E/I_M ratios obtained for the P(PyEG$_y$MA) samples in (□) THF, (△) DMF, (○) dioxane, and (◇) DMSO.

The efficiency of PEF could be better quantified by plotting the I_E/I_M ratio, obtained by taking the ratio of the fluorescence intensity of the excimer (I_E) over that of the monomer (I_M), as a function of the inverse of the number (N_S) of non-hydrogen atoms in the side chains of the P(PyEG$_y$MA) samples in Figure 3.1C. With some scatter, the trends indicated that I_E/I_M increased linearly with N_S^{-1}. The scatter in the data is mostly due to residual unattached pyrene that emits as free monomer, and has been shown to strongly affect the I_E/I_M ratio of macromolecules having a large pyrene content such as the P(PyEG$_y$MA) samples.[40,41] An expression for the I_E/I_M ratio, derived with the reasonable assumption that PEF is irreversible at room temperature, is given in Equation 3.3, where K, ϕ_E, ϕ_M, τ_M, and k_{diff} are an experimental constant characteristic of the steady-state fluorometer used for the fluorescence experiments, the quantum yield of the excimer and monomer, the monomer natural lifetime, and the rate constant for PEF by diffusive encounters, respectively.[42] The expression for k_{diff} is given in Equation 3.4, where N_A is Avogadro's number, R is the molecular diameter of pyrene, D is the diffusion coefficient experienced by the pyrenyl labels, and p is the probability of forming an excimer upon encounter between an excited and a ground-state pyrene.[43]

$$\frac{I_E}{I_M} = K \times \frac{\phi_E}{\phi_M} \tau_M \times k_{diff} [Py]_{loc} \tag{3.3}$$

$$k_{diff} = 4\pi N_A RDp \tag{3.4}$$

According to Equation 3.3, the linear relationship between I_E/I_M and N_S^{-1} in Figure 3.1C indicates that $[Py]_{loc}$ is inversely proportional to N_S, thus suggesting a fairly simple relationship for the location of the side chain ends of the P(PyEG$_y$MA) samples in solution. Based on Equations

3.3 and 3.4, the I_E/I_M ratio should also be inversely proportional to solvent viscosity as is the diffusion coefficient D used in the expression of k_{diff}. This trend is somewhat obeyed in Figure 3.1C, where THF and DMSO with the lowest and highest solvent viscosity showed the most and least steep trends, respectively. However, dioxane with a viscosity of 1.18 mPa.s yielded larger I_E/I_M ratios than DMF with a viscosity of 0.79 mPa.s. These conflicting results were most likely a consequence of the different effects that solvents have on the quantum yields (ϕ_E and ϕ_M), the monomer lifetime (τ_M), and the probability (p) of PEF.[43] Complications resulting from solvent-induced differences in quantum yields and lifetimes can be eliminated by determining the average rate constant $<k>$ for PEF from the model free analysis (MFA) of the fluorescence decays of the P(PyEG$_y$MA) samples acquired in the four solvents, since $<k>$ is directly equal to the product of k_{diff} and $[Py]_{loc}$, as shown in Equation 3.5.[37–39]

$$< k >= k_{\text{diff}} \times [Py]_{\text{loc}} \tag{3.5}$$

The fits of the fluorescence decays according to the MFA were good, as shown in Figure S3.15 in the SI. All parameters retrieved from the MFA of the decays are listed in Tables S3.3 – 3.5. In particular, the global MFA of the fluorescence decays yielded the molar fraction of aggregated pyrenyls (f_{agg}), which was always smaller than 0.2, indicating that PEF occurred mainly through diffusive encounters (see Table S3.5). To account for the residual level of pyrene aggregation, the quantity $<k>/f_{diff}$ was plotted as a function of N_S^{-1} in Figure 3.2A, where f_{diff} represents the molar fraction of pyrenyl labels forming excimer by diffusive encounters. The $<k>/f_{diff}$ values obtained in THF and DMSO were the largest and smallest, respectively, with DMF

and dioxane yielding intermediate $<k>/f_{diff}$ values, as had been observed for the I_E/I_M ratios plotted in Figure 3.1C.

Most interestingly, the $<k>/f_{diff}$-*vs*-N_S^{-1} plots were linear in all solvents. The rate constant k_{diff} for PEF by diffusive encounters was expected to remain constant, since all P(PyEG$_y$MA) samples were labeled with the same pyrene derivative. The fact that $<k>/f_{diff}$ increased linearly with N_S^{-1} suggested that $[Py]_{loc}$ was proportional to N_S^{-1}. Since $[Py]_{loc}$ equals the number of ground-state pyrene (n_{Py}) molecules located in the volume (V_{blob}) probed by an excited pyrene, typically referred to as a *blob*,[44,45] the linear relationship between $[Py]_{loc}$ and N_S^{-1} imposed that the ratio n_{Py}/V_{blob} should scale as N_S^{-1}. This condition could be accommodated by assuming that the radius (R) of a spherical *blob* could be represented by half the end-to-end distance $r_{EE,SC}$ of the EG$_y$ side chain ($R = r_{EE,SC}/2$) connecting the pyrenyl label to the polymethacrylate backbone of the P(PyEG$_y$MA) sample as shown in Figure 3.3, where $r_{EE,SC}$ is given by Equation 3.4. Equation 3.4 assumes as a first approximation that the EG$_y$ side chain is a Gaussian chain with an unknown bond length l. Consequently, the product $[Py]_{loc} \times l^3$ was considered throughout this report.

$$r_{EE,SC} = \sqrt{N_S} \times l \tag{3.4}$$

According to Equation 3.4, V_{blob} should scale as $N_S^{3/2}$. Taking into account that a pyrenyl label located $2\times R$ away in one direction from the excited pyrene could still result in a pyrene-pyrene encounter, n_{Py} should equal $4\times R/h$, where h is the length of one methacrylate unit (~$2\times l$). As such, n_{Py} would scale as $N_S^{0.5}$ so that $[Py]_{loc} = n_{Py}/V_{blob}$ would scale as N_S^{-1} as suggested by the $<k>/f_{diff}$-*vs*-N_S^{-1} found experimentally in Figure 3.2A.

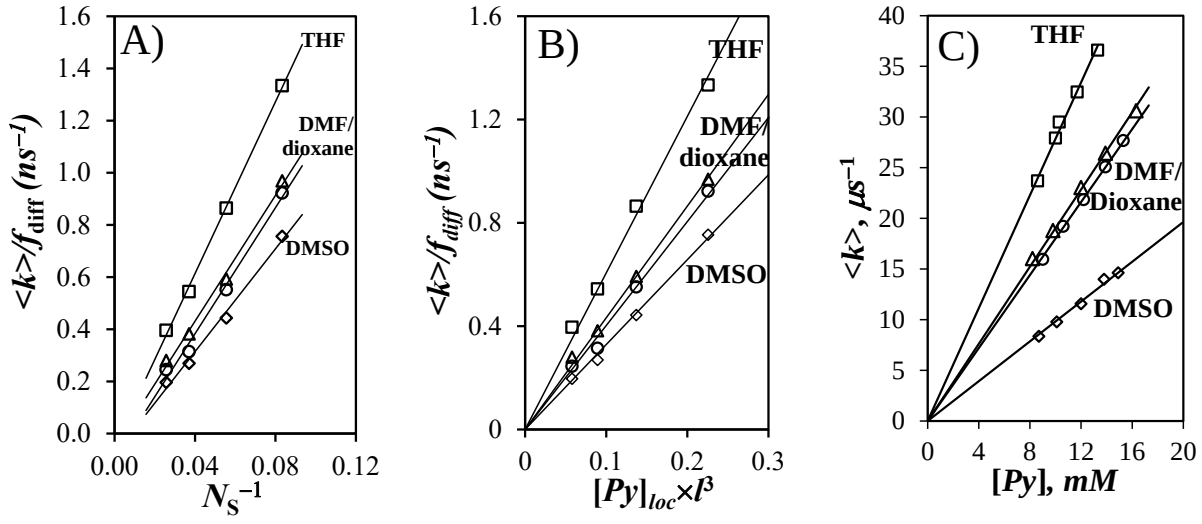

Figure 3.2. Plot of $\langle k \rangle / f_{\text{diff}}$ as a function of A) N_S^{-1} and B) $[Py]_{\text{loc}} \times l^3$ determined by Equation 3.5 for the P($PyEG_yMA$) samples. C) Plot of $\langle k \rangle$ as a function of concentration for the $PyEG_2ME$ model compound. Solvents: (□) THF, (△) DMF, (○) dioxane, and (◇) DMSO.

The good agreement obtained in Figure 3.2A between the ratio $\langle k \rangle / f_{\text{diff}}$ and N_S^{-1} assuming a Gaussian conformation for the side chains might appear surprising at first glance, as larger scaling exponents ranging between 0.57 and 0.75 have been proposed for the relationship between $R_{G,SC}$ or $r_{EE,SC}$ and N_{SC}.[26–34] However, it must also be stated that some reports in the literature have found good agreement between experimental scattering data and theory, while assuming Gaussian side chains.[23–25] Furthermore, the PBBs typically studied in the literature have much longer side chains than those involved in the P($PyEG_yMA$) samples. The short $PyEG_y$ side chains might explain why the assumption that they would adopt a Gaussian conformation, yields reasonable trends in Figure 3.2A.

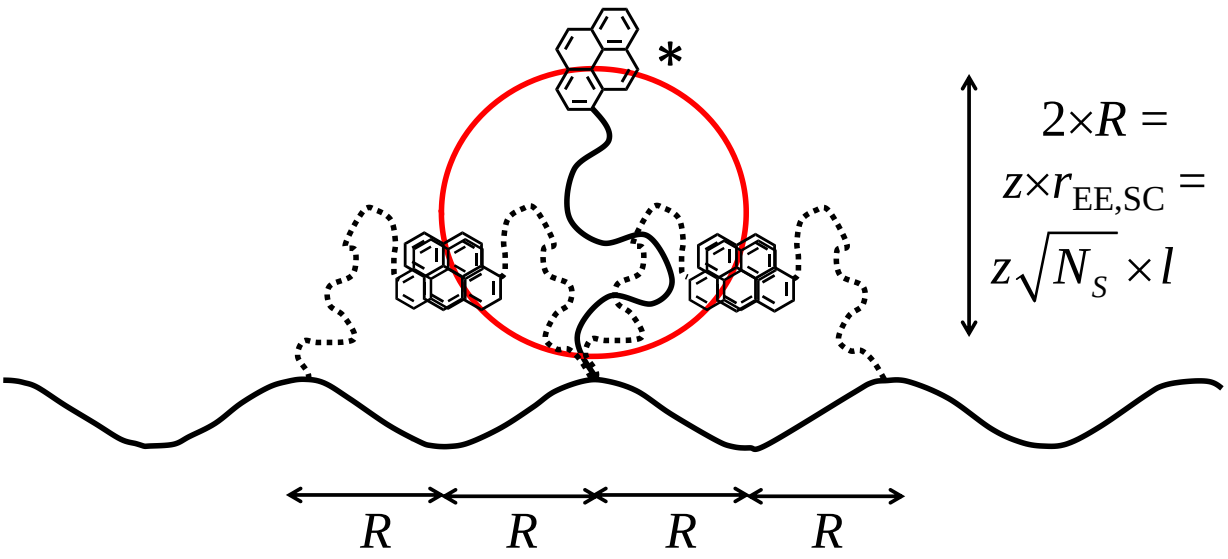

Figure 3.3. Schematic representation of the model used to calculate $[Py]_{loc}$.

Based on these considerations, Equation 3.5 was derived to estimate $[Py]_{loc}$. In Equation 3.5, $r_{EE,SC}$ was scaled by the factor z (< 1.0) to account for the fact that the side chains, which allow pyrene-pyrene encounters along the main chain, are oriented perpendicular to the main chain at the branching point, so that their effective length $r_{EE,SC}$ for PEF is reduced by an amount z. The parameter z was determined by conducting MMOs with HyperChem on a poly(methyl methacrylate) (PMMA) backbone, in a manner similar to what was done earlier with unstructured poly(*D*,*L*-glutamic acid)s.[46,47] The PMMA constructs were generated to ensure a random configuration of the MMA units by using the MS Excel random number generator, to decide the configuration of a given methyl carboxylate side group, depending on whether the generated random number was greater or smaller than 0.5. The PMMA construct was fully stretched before being allowed to relax and adopt an extended conformation. First, one methyl substituent located along the PMMA backbone was replaced by one $PyEG_y$ side chain, which was used as a reference.

A second methyl substituent located at the +5 position to the right of the reference was replaced with a second $PyEG_y$ side chain, referred to as the secondary side chain, and the two pyrenyl labels were induced to come within 0.34 nm from each other. The extent of overlap between the pyrene planes was determined from the number of carbons (n_C) in one pyrenyl label overlapping the frame of the other pyrenyl label. The secondary $PyEG_y$ side chain was then moved further to the next methacrylate along the PMMA backbone and the same procedure was repeated to determine n_C. n_C was found to decrease from an average value of 9 carbon atoms, a number that suggested good overlap between the two pyrenyl labels, for short separations between the primary and secondary $PyEG_y$ side chains, before dropping below a value of 7 carbon atoms. An n_C value of 7 marks the boundary between a good and poor overlap between two pyrenyl labels.[46,47] Consequently, an n_C value of less than 7 indicates that the pyrenyl labels were unable to generate a good overlap and thus could not form excimer, as shown in Figure S3.16. Figure S3.16 also nicely illustrates the purpose of the *z* value in Figure 3.3, as the $PyEG_y$ side chain is oriented perpendicularly to the main polymethacrylate backbone at the branching point, before making a sharp turn and proceeding parallel to the main chain. Since the PMMA backbone was atactic, this exercise was repeated three more times by moving the reference $PyEG_y$ side chain to another monomer unit to assess the effect that the configuration of the primary methacrylate unit onto which a $PyEG_y$ side chain had been attached, had on the trends shown in Figure S3.16. The distance separating the two branching points bearing the $PyEG_n$ side chains, that corresponded to an n_C value of 7, was taken as the maximum distance (d_{intra}^{o}) that would allow PEF to occur intramolecularly between two $PyEG_y$ side chains attached on a same PMMA backbone. The d_{intra}^{o} values obtained for each $PyEG_y$ side chain have been listed in Table S1 in SI.

To determine the maximum distance separating two methacrylate units bearing a $PyEG_y$ side chain and still allowing good overlap between the two pyrenyl labels, the PMMA chain bearing one $PyEG_y$ side chain was duplicated and the second construct was flipped by 180 ^{o} around the main chain, so that the two PMMA backbones be parallel to each other with their pyrenyl labels facing each other. The two extended PMMA chains were held at a distance d_{inter} between the two branching points bearing the $PyEG_n$ side chains and the pyrenyl labels were induced to overlap within 0.34 nm from each other. Here again, n_C was determined as a function of the distance d_{inter} separating the structural units bearing the $PyEG_y$ side chains. The distance d_{inter} between the two constructs was increased in 0.1 nm increments and n_C was determined for each d_{inter}. As shown in Figure S3.17, good overlap ($n_C > 7$) was observed between the two pyrenyl labels for short d_{inter}. But as d_{inter} increased, n_C was found to decrease below 7, indicating poor overlap between the pyrene labels, for a d_{inter} value which was referred to as d_{inter}^o, and was listed in Table S1 in SI. The ratio d_{intra}^o/d_{inter}^o was taken as the parameter z used in Figure 3.3 and Equation 3.5 and was found to equal 0.84, 0.89, 0.89, and 0.92 for the $PyEG_y$ side chains with y = 3, 5, 8, and 12, respectively. More details about the procedure used to determine z from the MMOs along with snapshots of the MMOs are provided in the SI.

$$[Py]_{loc} = \frac{n_{Py}}{V_{blob}} = \frac{\frac{4(z\sqrt{N_S}l/2)}{h}}{\frac{4}{3}\pi\left(\frac{z\sqrt{N_S}l}{2}\right)^3} = \frac{6}{\pi z^2 N_S l^3} \tag{3.5}$$

With z having been determined by MMOs, z could be introduced into Equation 3.5 to calculate $[Py]_{loc}\times l^3$, thus allowing a plot of $<k>/f_{diff}$ as a function of $[Py]_{loc}\times l^3$ in Figure 3.2B.

Interestingly, $\langle k \rangle / f_{diff}$ was found to increase linearly with $[Py]_{loc} \times l^3$ in Figure 3.2B, in the same manner as would be expected when plotting $\langle k \rangle$ as a function of $[Py]$ for a free pyrene derivative in solution.[18] The trends shown in Figure 3.2B showed the same solvent dependency for $\langle k \rangle / f_{diff}$ plotted as a function of $[Py]_{loc} \times l^3$, with THF and DMSO yielding the largest and smallest values, respectively, and with intermediate values being obtained in DMF and dioxane. Based on Equation 3.3, the slope of the $\langle k \rangle / f_{diff}$-*vs*-$[Py]_{loc} \times l^3$ trends was taken as k_{diff} for the P(PyEG$_y$MA) samples and plotted as a function of the inverse of viscosity in Figure 3.4A.

As inferred from Equations 3.2 and 3.3, the difference between the $\langle k \rangle / f_{diff}$-*vs*-$[Py]_{loc}$ trends in Figure 3.2B were most likely due to differences between the solvent viscosity (η), which is inversely proportional to D, and p. In an attempt to correct for η and p, the model compound 1-pyrenemethyl diethylene glycol methyl ether (PyEG$_2$ME) was synthesized. Concentrated solutions of PyEG$_2$ME were prepared in the four different solvents. The pyrene monomer and excimer fluorescence decays were acquired and fitted according to the MFA to yield $\langle k \rangle$. The parameters obtained from the fit of the monomer and excimer decays can be found in Table S3.2. As shown in Figure 3.2C, a plot of $\langle k \rangle$ as a function of PyEG$_2$ME concentration yielded a straight line in the four solvents, whose slope represented k_{diff}[inter] for PyEG$_2$ME in THF, DMF, dioxane, and DMSO, found to equal 2.8, 1.9, 1.8, and 1.0 $M^{-1}ns^{-1}$, respectively. A similar plot had been obtained earlier in Chapter 2 for another pyrene derivative, namely ethyl 4-(1-pyrene)butyrate in toluene, THF, DMF, and DMSO.[18] k_{diff}[inter] representing intermolecular PEF for PyEG$_2$ME was compared to k_{diff} for P(PyEG$_y$MA) in Figure 3.4A. Beside the difference in magnitude between the two quantities due to the unknown value of the bond length l, the two trends showed strikingly similar features, as would be expected since the solvents should affect PEF in the same manner for the PyEG$_2$ME and P(PyEG$_y$MA) samples prepared with a same pyrene derivative.

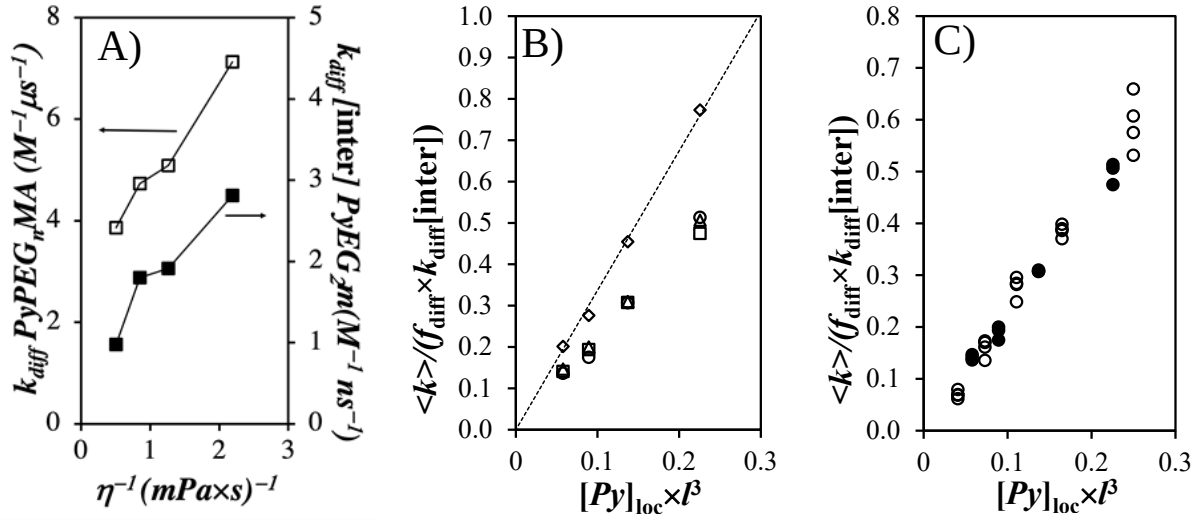

Figure 3.4. Plot of A) k_{diff} for the (□) P(PyEG$_y$MA) and k_{diff}[inter] for the (■) PyEG$_2$ME samples, B) <k>/($f_{diff}\times k_{diff}$[inter]) as a function of [Py]$_{loc}\times l^3$ for P(PyEG$_y$MA) in (□) THF, (△) DMF, (○) dioxane, and (◇) DMSO and C) <k>/($f_{diff}\times k_{diff}$[inter]) as a function of [Py]$_{loc}\times l^3$ for (●) the P(PyEG$_y$MA) samples in THF, DMF, and dioxane and (○) the pyrene-labeled dendrons studied earlier in toluene, THF, DMF, and DMSO.

The ratio <k>/($f_{diff}\times k_{diff}$[inter]), where <k> and k_{diff}[inter] were obtained for the P(PyEG$_y$MA) and PyEG$_2$ME samples, respectively, was plotted as a function of [Py]$_{loc}\times l^3$ in Figure 3.4B. The <k>/($f_{diff}\times k_{diff}$[inter]) ratios obtained in THF, DMF, and dioxane merged into a master line indicating that treatment of the data accounted satisfyingly for differences in the η and p values obtained in these three solvents. Yet, the <k>/($f_{diff}\times k_{diff}$[inter]) values obtained in DMSO did not align with this straight line. This exception was attributed to the high polarity of DMSO, which might have induced the pyrenyl labels to remain closer to the polymethacrylate backbone to reduce exposure to the solvent, thus increasing [Py]$_{loc}$ and resulting in <k>/($f_{diff}\times k_{diff}$[inter])

values that were higher than expected. As a matter of fact, $PyPEG_3MA$, which showed the largest deviation from the straight line was found to be insoluble at 1 mg/mL in DMSO. For this reason, the $<k>/(f_{diff}\times k_{diff}[inter])$ values obtained for the $P(PyEG_yMA)$ samples in THF, DMF, and dioxane were compared in Figure 3.4C to those obtained earlier for a series of Py_x-G(N) dendrons prepared with a 2,2-bis(hydroxymethyl) propionic acid backbone.[18] The generation number (N) of the dendrons ranged from 1 through 6, and x (= 2^N) represented the number of pyrenyl labels covalently attached to the terminal ends of a dendron of generation N. A good agreement was found in Figure 3.4C between the $<k>/(f_{diff}\times k_{diff}[inter])$ values obtained for the $P(PyEG_yMA)$ samples and the Py_x-G(N) dendrons.

The linear trends obtained between $<k>/(f_{diff}\times k_{diff}[inter])$ and $[Py]_{loc}$ for the Py_x-G(N) dendrimers and the $P(PyEG_yMA)$ PBBs in Figure 3.4C are the result of a procedure, whereby the features of a pyrene-labeled macromolecule were taken into account to predict a mathematical expression for $[Py]_{loc}$, whose value was then compared to $<k>$ obtained experimentally from the MFA of fluorescence decays. Because PEF can only occur between to pyrenyl labels covalently attached onto a same macromolecule that are within a few nanometers from each other (see Table S1), PEF only involves short oligomeric segments whose dimensions are minimally affected by excluded volume. This is probably the reason why the assumption that the oligomeric segments connecting every two pyrenyl labels in the Py_x-G(N) and $P(PyEG_yMA)$ samples adopt a Gaussian conformation, seems to yield the good correlations shown in Figure 3.4 between $<k>$ and $[Py]_{loc}$.

3.5 Conclusion

Polymeric bottle brushes were readily synthesized with a polymethacrylate backbone and oligo(ethylene glycol) side chains terminated with a 1-pyrenemethoxy group ($P(PyEG_yMA)$,

where y= 3, 5, 8, and 12). The PEF efficiency in the P($PyEG_yMA$) constructs was characterized by the average rate constant $<k>$ for PEF determined from the MFA of the pyrene monomer and excimer fluorescence decays. Assuming that the end-to-end distance of the oligo(ethylene glycol) side chain could be approximated by a Gaussian chain probing a spherical volume led to the quantitative determination of $[Py]_{loc}$. Accounting for changes in η and p associated with different solvents enabled the normalization of the $<k>/f_{diff}$ values obtained in THF, DMF, and dioxane. $<k>/(f_{diff} \times k_{diff}[inter])$ reported on the dynamics of the ethylene glycol side chains and was found to increase linearly with increasing $[Py]_{loc}$. The remarkable agreement found between the values obtained for the P($PyEG_yMA$) samples and the Py_x-G(N) dendrons supports the notion that the procedure developed in this series of experiments establishes a quantitative relationship between $<k>$ for PEF occurring in pyrene-labeled macromolecules and $[Py]_{loc}$. In turn, since the pyrenyl labels are covalently attached to the macromolecule, $[Py]_{loc}$ reflects the internal density of the macromolecule under study, thus enabling the characterization of its conformation in solution. The ability to relate PEF to the conformation of macromolecules in solution should nicely complement scattering techniques, which are currently the main analytical tool available for this purpose. This study represents another step toward the establishment that pyrene excimer formation/ fluorescence (PEF), between pyrenyl labels covalently attached to the ends of highly branched macromolecules is directly related to the conformation of the macromolecules under investigation.

Chapter 4

Persistence Length of PEGMA Bottle Brushes Determined by Pyrene Excimer Fluorescence

4.1 Abstract

Seven pyrene-labeled poly(oligo(ethylene glycol) methyl ether methacrylate)s ($PyEG_5$-PEG_nMAs) were prepared with n = 0, 3, 4, 5, 7, 9, and 19 ethylene glycol units by copolymerizing a small amount of penta(ethylene glycol) 1-pyrenemethyl ether methacrylate with an EG_nMA monomer. The conformation of the $PyEG_5$-PEG_nMA polymers evolved from a random coil for $PyEG_5$-PEG_0MA or poly(methyl methacrylate) to a polymeric bottle brush (PBB) architecture with increasing side chain length. These experiments took advantage of the dependency that exists between the efficiency of excimer formation between an excited and a ground-state pyrenyl label covalently attached to a macromolecule and the local pyrene concentration ($[Py]_{loc}$), which in turn depends on polymer conformation. The fluorescence decays of the $PyEG_5$-PEG_nMA samples were fitted according to the fluorescence blob model (FBM), whose parameters were used in combination with the Kratky-Porod worm like chain model, to calculate for the first time from fluorescence measurements the persistence length l_p(fluo) of these macromolecules. The average number of structural units per *blob* ($<N_{blob}>$) and l_p(fluo) were found to report on both the dynamics and conformation of the $PyEG_5$-PEG_nMA PBBs. Extrapolation of the $<N_{blob}>$ values obtained for different solvent viscosities to an infinitely high viscosity, to eliminate the contribution of dynamics, yielded N_{blob}^{o} and l_p^{o}, which was compared to the persistence length (l_p) determined by gel permeation chromatography (GPC) from conformation plots. l_p determined by GPC was almost twice larger than l_p^{o}. This difference in l_p was attributed to the different length scales probed by the two experiments. The FBM probes a polymer segment inside a *blob*, which is a sub-volume of the polymer coil, whereas the conformation plots generated from GPC analysis considered the entire polymer coil, which encompasses many *blobs*. These experiments open the path toward applying PEF to the determination of the l_p of polymers in solution.

4.2 Introduction

In 1974, Wilemski and Fixman published a seminal paper where they demonstrated mathematically that the process of end-to-end cyclization (EEC) of a monodisperse polymer chain terminated at one end with a luminophore and at the other end with a quencher could be well-described by a single cyclization rate constant (k_{cy}).[1,2] The simplicity of this result ushered in a flurry of studies aiming at characterizing the EEC of fluorescently end-labeled short chain alkanes,[3,4] rapidly followed by monodisperse synthetic oligomers,[5–11] and more recently oligopeptides,[12–16] to probe the kinetics of loop formation during protein folding. These early experiments were later complemented by new analytical developments based on the fluorescence blob model (FBM)[17] and the model free analysis (MFA),[18] that provided the means to obtain rate constants similar to k_{cy} but for any type of polymeric architecture or fluorescence labeling protocol.[19,20] As clearly stated by Wilemski and Fixman, the overarching goal of these experiments was to *provide useful information about the dynamical behavior of polymer chains*.[1,2] With this in mind, EEC experiments based on pyrene excimer fluorescence (PEF),[3–9] FRET,[12–14] or triplet-triplet annihilation[10,11,15,16] have been applied over the past 45 years to *convey detailed information about the shape and mobility of flexible polymers*.[9] As an example, for a similar polymer length, k_{cy} for a series of monodisperse pyrene end-labeled polystyrenes was ~10 times smaller than that for highly flexible polydimethylsiloxane.[6,7,9]

Yet, the focus placed on the study of polymer chain dynamics based on the determination of the rate constant k_Q for the quenching of an excited dye by a quencher covalently attached to a macromolecule, might have led the scientific community involved in fluorescence quenching studies to inadvertently overlook the more important relationship, shown in Equation 4.1 and Scheme 4.1, between k_Q and the local quencher concentration ($[Q]_{loc}$) experienced by an excited

dye (D^*) covalently attached to a macromolecule.[5,20] As suggested by Equation 4.1, the determination of $[Q]_{loc}$ from the experimentally determined k_Q should yield information about the local density of the macromolecule to which the quencher is covalently bound. In turn, information about the local macromolecular density can reveal the conformation of the macromolecule in solution. Unfortunately, the quantitative determination of $[Q]_{loc}$ has been challenging, so that all fluorescence quenching experiments conducted so far on fluorescently modified macromolecules have focused instead on the interpretation of k_Q with respect to the internal dynamics of the macromolecule.

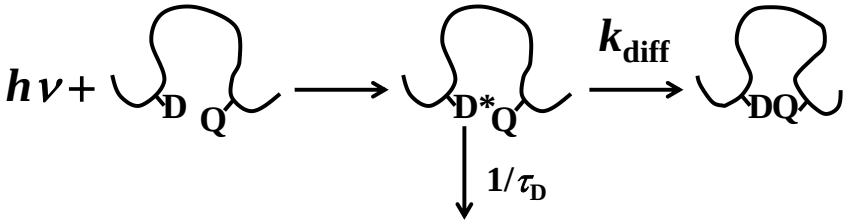

Scheme 4.1. Kinetic scheme for the quenching of an excited dye (D^*) and a quencher (Q) both covalently attached onto a macromolecule.

$$k_Q = k_{diff} \times [Q]_{loc} \tag{4.1}$$

Yet recent publications from this laboratory have proposed different methodologies based on the model free analysis (MFA) and fluorescence blob model (FBM) capable of extracting $[Q]_{loc}$ from k_Q values in a process that yields quantitative information about the conformation of macromolecules in solution. These experiments were conducted with pyrene-labeled macromolecules, where the dye pyrene plays the part of both dye and quencher during pyrene

excimer formation, have related $[Py]_{loc}$ to the conformation of polypeptides[21–24] and polysaccharide helices,[25] or the interhelical distance between oligo(*L*-glutamic acid) and oligosaccharide helical segments inside arborescent polymers[26] and amylopectin,[27] respectively. The application of the methodology based on the MFA to quantify the internal density of dendrimers or the conformation of the side chains of poly(oligo(ethylene glycol) methyl ether methacrylate)s (PEG_nMA, where *n* represents the number of ethylene glycol units in the side chains) has been described in Chapters 2 and 3 of this thesis. In contrast, this report applies the FBM to characterize the conformation of the main chain of a series of PEG_nMAs, as the length of the oligo(ethylene glycol) side chain is increased from 0 (for poly(methyl methacrylate)) to 19 ethylene glycol units.

More precisely, the present study aims to extract l_p from a careful analysis of the fluorescence data obtained with a series of pyrene labeled PEG_nMAs, which can be viewed as examples of polymeric bottle brushes (PBBs). PBBs have found many applications over the years. PBBs can serve as lubricants,[28,29] anti-fouling agents,[30,31] elastomers,[32,33] semiconductors,[34] and carriers for drug delivery.[35,36] The remarkable variety in the applications afforded by PBBs arises from the exquisite level of control that is now available for different architectural parameters such as the degree of polymerization (DP) of the side and main chain and the branching density, which define the final conformation of a PBB.[37–46] An increase in the side chain DP and degree of branching results in more steric hindrance between the side chains, which causes the polymer backbone to stiffen and extend locally. This stiffening is captured by the Kratky-Porod worm-like chain model (KPWLCM), which describes the local stiffness of polymers according to their persistence (l_p) and contour (L) length.[47] The vast knowledge which is now available about the conformation and stiffness of PBBs, which have been investigated through simulations,[37–46]

experiments,[48–58] or combinations of both,[59,60] thus provides an excellent background against which the l_p values determined from fluorescence experiments can be compared.

The proposed procedure uses pyrene excimer fluorescence/formation (PEF)[61] resulting from the encounter between an excited and a ground-state pyrene to determine l_p for a series of PBBs, by polymerizing different oligo(ethylene glycol) methyl ether methacrylate macromonomers to yield a series of PEG_nMA samples, where *n* ranges from 0 to 19. All PEG_nMA samples were randomly labeled by copolymerization of the EG_nMA macromonomers with different amounts of 1-pyrenemethyl ether penta(ethylene glycol) methacrylate to yield $PyEG_5$-PEG_nMA samples, that were all fluorescently labeled with the same pyrene derivative. Despite their widespread use,[62] no reference could be found where the l_p of PEG_nMAs had been determined. This absence of information on the l_p of PEG_nMAs might be due to the challenges associated with the preparation of high molecular weight PEG_nMA samples with a narrow molecular weight distribution (MWD),[63] that is required for studies by scattering techniques.[64] In comparison, PEF between pyrenyl labels attached onto a macromolecule occurs over a length scale that is much shorter than the overall macromolecular dimensions, so that the breadth of the MWD becomes irrelevant, an appealing feature when dealing with polydisperse samples. The PEF experiments take advantage of the fact that an excited pyrene covalently attached onto a macromolecule probes a finite and monodisperse volume referred to as a *blob*. The *blob* is used to compartmentalize the $PyEG_5$-PEG_nMA samples into strings of *blobs* composed of a number (N_{blob}) of structural units. N_{blob} could be determined quantitatively through the analysis of the fluorescence decays according to the fluorescence blob model (FBM).[19,20] In turn, application of the KPWLCM to the N_{blob} values retrieved from the FBM analysis yielded l_p(fluo) for the different PEG_nMA constructs. l_p(fluo) obtained by PEF measurements was found to be inversely proportional to the

solvent viscosity and to scale as the square of the number (N_S) of non hydrogen atoms in the flexible side chains of the PBBs, as would be expected theoretically.[37]

The dependency of l_p(fluo) with solvent viscosity reflected the dynamic nature of the PEF measurements and could be eliminated by extrapolating the $<N_{blob}>$ values to N_{blob}^o for an infinitely large viscosity, representative of a solvent where polymer dynamics were eliminated. This allowed for the calculation of l_p^o, which would reflect the conformation of the macromolecule. The l_p^o values of the $PyEG_5$-PEG_nMA samples were found to be smaller than the l_p values determined by building conformation plots based on the intrinsic viscosity ($[\eta]$) and molar mass (M) of the polymers obtained by GPC analysis.[65] The lower l_p^o values were attributed to the different length scales probed in PEF and GPC experiments. While GPC describes an entire polymer coil, whose dimension can be subject to excluded volumes which stiffen the main chain and increase l_p, PEF probes a much smaller sub volume of the polymer coil, that should be exempt of excluded volume, as required by the KPWLCM. Despite these discrepancies, the results obtained in this chapter suggest that the PEF methodology offers a new experimental means to determine the l_p of macromolecules in solution.

4.3 Experimental

Materials: Copper(II) bromide (Sigma, 99%), Celite (Sigma), dichloromethane (DCM, Sigma, ≥ 99.8%), diethylether (Sigma, ≥ 99%), *N,N*-dimethylformamide (DMF, Sigma, ≥ 99.8%), dimethylsulfoxide (DMSO, Sigma, ≥ 99.9%), 4-(dimethylamino)pyridine (DMAP, Sigma, ≥ 99%), ethyl acetate (Sigma, ≥ 99.7%), ethyl α-bromoisobutyrate (Sigma, 98%), tetra(ethylene glycol) methyl ether (EG_4, PurePEG, ≥ 97%), penta(ethylene glycol) (Fisher, ≥ 95%), penta(ethylene glycol) methyl ether (EG_5, PurePEG, ≥ 95%), hepta(ethylene glycol) methyl ether

(EG_7, TCI, ≥ 97%), 1,1,4,7,10,10-hexamethyl-triethylenetetramine (HMTETA, Sigma, ≥ 97%), methacrylic anhydride (Sigma, 94%), 1-pyrenemethanol (Sigma, 98%), sodium chloride (Sigma), sodium hydride (NaH, Sigma, 60% dispersion in mineral oil), sodium hydroxide (NaOH, Sigma, pellets, ≥ 97%), sodium sulfate (Sigma, anhydrous, ≥ 99%), tetrahydrofuran (Sigma, ≥ 99%), tetrahydrofuran optima (Fisher, ≥ 99.9%), and triethylamine (TEA, Sigma, ≥ 99.5%) were used as received.

Tri(ethylene glycol) methyl ether methacrylate (EG_3MA, Sigma, 93%) and two oligo(ethylene glycol) methyl ether methacrylates (EG_9MA with number average molecular weight (M_n) = 500 g/mol and $EG_{19}MA$ with M_n= 950 g/mol, Sigma) were dissolved in DCM, washed with 2 M NaOH, and dried with sodium sulfate before use.

The radical initiator 2,2'-azo-*bis*-isobutyronitrile (AIBN, Sigma, 98%) was recrystalized in ethanol three times.

p-Toluenesulfonyl chloride (Sigma, ≥ 98%) was dissolved in diethyl ether and washed with 2 M NaOH. The organic phase was extracted and dried with sodium sulfate. Unless otherwise specified, all other chemicals were purchased from commercially available sources and used as received.

Preparation of penta(ethylene glycol) mono p-toluenesulfonate (Tos_1-EG_5OH): The synthesis of penta(ethylene glycol) mono *p*-toluenesulfonate (Tos_1-EG_5OH) follows the reaction scheme outlined in Scheme 4.2 and is described in more detail hereafter.

Penta(ethylene glycol) (EG_5) (2.00 g, 8.39 mmol) was added to a round bottom flask (RBF) equipped with a magnetic stirrer with freshly distilled dichloromethane (DCM). Re-crystalized *p*-toluenesulfonyl chloride (1.76 g, 9.23 mmol) and triethyl amine (TEA) (1.74 mL, 12.6 mmol) were added to the RBF and left to stir overnight. The next day, the reaction mixture was washed three times with a saturated solution of aqueous sodium chloride. The organic layer was extracted and

dried with sodium sulfate. Silica gel chromatography was used to purify the singly tosylated EG_5 (Tos_1-EG_5OH) from the doubly tosylated EG_5 and unmodified EG_5 using ethyl acetate as the eluent. The Tos_1-EG_5OH fraction was dried *in vacuo* and its chemical composition was verified using ^1H NMR (Figure S4.1 in SI).

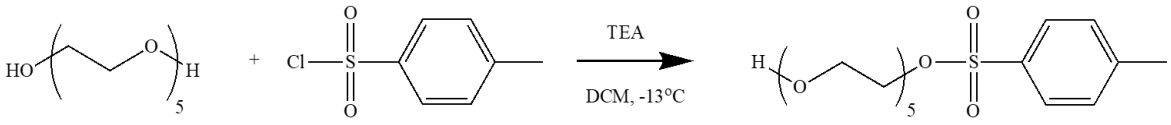

Scheme 4.2. Reaction scheme for the synthesis of penta(ethylene glycol) mono *p*-toluenesulfonate (Tos_1-EG_5OH).

Preparation of 1-pyrenemethyl ether penta(ethylene glycol) ($PyEG_5OH$): The synthesis of 1-pyrenemethyl ether penta(ethylene glycol) ($PyEG_5OH$) follows the reaction scheme outlined in Scheme 4.2 and is described in more detail hereafter.

1-Pyrenemethanol (1.18 g, 5.10 mmol) was added to a RBF with 50 mL of dried and distilled *N,N*-dimethylformamide (DMF). The solution was stirred and kept under a nitrogen atmosphere. Sodium hydride (NaH) (0.20 g, 5.10 mmol) was added to the RBF and the solution was allowed to stir for 1 hour, during which time the colour of the solution changed from yellow to dark red/purple. Tos_1-EG_5OH (1.00 g, 2.55 mmol) was then added. The RBF was placed in an oil bath at 55 ºC and left to stir overnight. After the RBF was removed from the oil bath and allowed to cool, 5 mL of Milli-Q water was added to the reaction solution to quench any unreacted NaH. Milli-Q water (50 mL) was then added to the reaction mixture, which was washed with 50 mL of ethyl acetate. The organic phase was collected and dried with sodium sulfate. The crude product

was purified by silica gel chromatography using ethyl acetate as eluent. The chemical composition of the purified $PyEG_5OH$ product was confirmed using ^1H NMR (Figure S4.2 in SI).

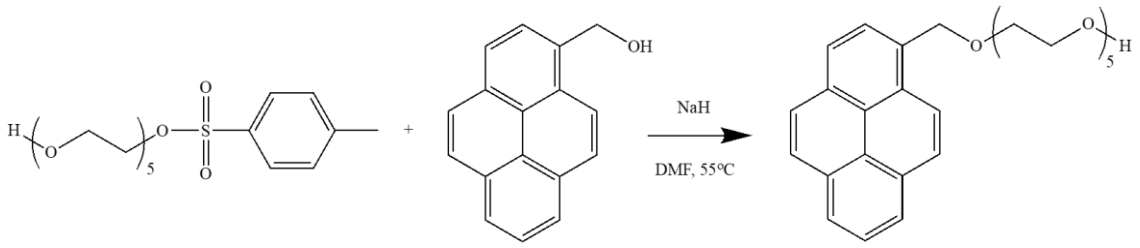

Scheme 4.3. Reaction scheme for the synthesis of 1-pyrenemethyl ether penta(ethylene glycol) ($PyEG_5OH$).

Methacrylation of oligo(ethylene glycol) methyl ethers (*EG_nOHs*) *and PyEG₅OH*: The same protocol was used to prepare the methacrylated oligo(ethylene glycol) methyl ethers (EG_nMAs, where n= 4, 5, 7) and $PyEG_5MA$. The synthesis of EG_5MA follows the reaction scheme outlined in Scheme 4.4 and is described in more detail hereafter.

EG_5OH (2.00 g, 7.93 mmol) and DMAP (0.0968 g, 0.793 mmol) were added to a RBF with 25 mL of freshly distilled DCM. The RBF was then placed in an ice water bath and the solution was stirred as methacrylic anhydride was added dropwise (1.18 mL, 7.93 mmol). The reaction was left to stir overnight. The reaction mixture was then washed three times with 2 M NaOH. The organic phase was extracted and dried with sodium sulfate. The crude product was purified by silica gel chromatography using ethyl acetate as the eluent. The chemical composition of the purified EG_5MA macromonomer was characterized by ^1H NMR (Figure S4.3 in SI).

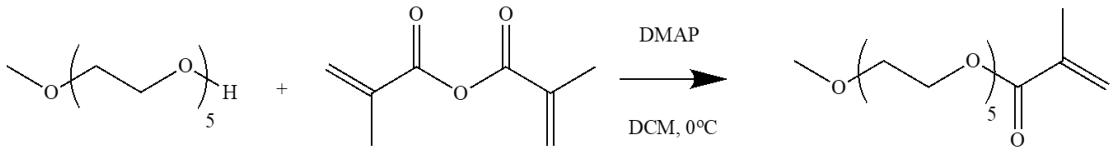

Scheme 4.4. Reaction scheme for the synthesis of EG_5MA.

Random copolymerization using conventional radical polymerization: The pyrene-labeled poly(oligo(ethylene glycol) methyl ether methacrylate)s ($PyEG_5$-PEG_nMAs) were prepared by conventional radical polymerization of methyl methacrylate (EG_0MA), tri(ethylene glycol) methyl ether methacrylate (EG_3MA), tetra(ethylene glycol) methyl ether methacrylate (EG_4MA), penta(ethylene glycol) methyl ether methacrylate (EG_5MA), hepta(ethylene glycol) methyl ether methacrylate (EG_7MA), and two oligo(ethylene glycol) methyl ether methacrylate (EG_9MA and $EG_{19}MA$) with $PyEG_5MA$. The chemical structure of the $PyEG_5$-PEG_nMA samples are shown in Table 1. The moles of $PyEG_5MA$ used in the polymerization were varied to obtain different molar percentages of pyrene-labeling, ranging from 1 to 10 mol% of $PyEG_5MA$, incorporated into the $PyEG_5$-PEG_nMA samples. The polymerization of $PyEG_5$-PEG_0MA labeled with 2 mol% of $PyEG_5MA$ is described in more detail hereafter.

$PyEG_5MA$ (0.02 g, 0.04 mmol) and methyl methacrylate (EG_0MA, 0.20 g, 2.00 mmol) were dissolved in 6.8 mL of THF such that the overall methacrylate concentration was approximately 0.3 M. The AIBN initiator (2.00 μg, 0.01 μmol) was added to the monomer solution from a stock solution and the mixture was placed in the polymerization tube. The tube was kept on ice before being degassed with nitrogen (Praxair, N4.0) for 30 minutes. After sealing the tube, it was left in an oil bath at 65 °C. The polymerization was terminated after a conversion of 20% or less was reached, as determined by ^1H NMR analysis, to minimize an eventual composition drift. The polymer was recovered by precipitating 5-6 times the polymer solution in THF into diethyl

ether to remove any unreacted monomer. The precipitated product was then dried in a vacuum oven overnight.

Table 4.1. Chemical structure of the $PyEG_5$-PEG_nMA samples with the number of atoms (N_S) in each side chain.

Sample	$PyEG_5$-PEG_0MA	$PyEG_5$-PEG_3MA	$PyEG_5$-PEG_4MA	$PyEG_5$-PEG_5MA	$PyEG_5$-PEG_7MA	$PyEG_5$-PEG_9MA	$PyEG_5$-$PEG_{19}MA$
Structure	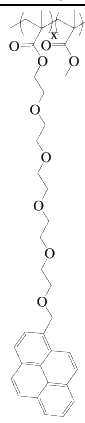	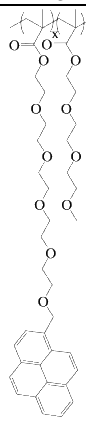		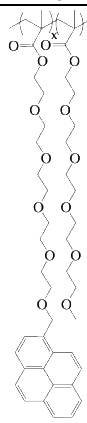	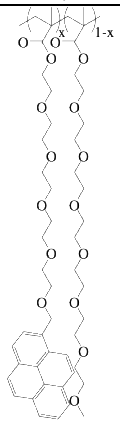	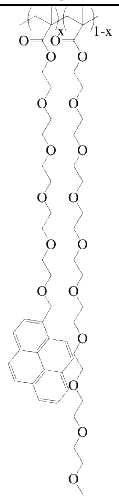	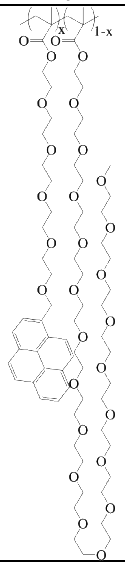
N_S	3	12	15	18	24	30	60

Random copolymerization using Initiators for Continuous Activator Regeneration Atom Transfer Radical Polymerization (ICAR-ATRP): Three of the $PyEG_5$-$PEG_{19}MA$ samples were prepared using ICAR-ATRP.[66] The protocol described for free radical copolymerization was applied to prepare $PyEG_5$-$PEG_{19}MA$ using ethyl α-bromoisobutyrate, Cu(II)Br/HMTETA, and AIBN as initiator, catalyst/ligand system, and radical source, respectively. An example of the ICAR-ATRP of $PyEG_5$-$PEG_{19}MA$ is provided in more detail hereafter.

A solution of $PyEG_5MA$ (0.02 g, 0.04 mmol) and $EG_{19}MA$ (1.00 g, 1.05 mmol) in 3.6 mL of THF, where the overall methacrylate concentration equaled 0.3 M, was transferred to the polymerization tube. A stock solution of Cu(II)Br (1.18 mg, 5.28 μmol) and HMTETA (4.3 μL,

15.8 μmol) was prepared in 10 mL of THF and then sonicated for 1 minute, from which 10 μL was added to the polymerization tube. Ethyl α-bromoisobutyrate (10.0 μL, 68.1 μmol) was added to 1 mL of THF from which 7.8 μL was added to the polymerization tube. AIBN (5.00 mg, 0.03 mmol) was added to 10 mL of THF to make a 3.05 mM stock solution. The solution was further diluted to 0.3 mM from which 0.2 mL was added to the polymerization tube, which was placed on ice and degassed for 30 min with nitrogen (Praxair, N4.0). The tube was then sealed and it was heated to 60 ^{o}C in an oil bath for 20 hours. Before the polymer was precipitated, the polymer solution in THF was filtered through a silica gel and Celite plug three times to remove copper. The polymer was further purified by 5-6 precipitations into diethyl ether.

Chemical composition and molecular weight distribution: The chemical composition of the $PyEG_5$-PEG_nMA polymers was confirmed by the analysis of the ^{1}H NMR spectra acquired on a Bruker 300 MHz high resolution spectrometer. A sample ^{1}H NMR spectrum of $PyEG_5$-PEG_5MA is provided as Figure S4.4 in the SI. The molecular weight distribution (MWD) of each $PyEG_5$-PEG_nMA sample was determined by GPC analysis using either THF or DMSO. The pyrene content (in mol%), M_n, and dispersity ($Đ$) of each sample are listed in Table 4.2.

Pyrene Content of $PyEG_5$-PEG_nMA samples: The pyrene content expressed as the molar fraction (x) of $PyEG_5MA$ monomer incorporated in the copolymers was calculated with Equation 4.2.

$$x = \frac{M}{\lambda_{Py}^{-1} + M - M_{Py}} \tag{4.2}$$

In Equation 4.2, λ_{Py}, M, and M_{Py} are the pyrene content of the polymer expressed in mol of pyrene per gram of polymer and the molar mass of the EG_nMA and $PyEG_5MA$ monomers, respectively.

Table 4.2. Pyrene content, absolute M_n, and dispersity of the $PyEG_5$-PEG_nMA samples.

$PyEG_5$-PEG_0MA			$PyEG_5$-PEG_3MA			$PyEG_5$-PEG_4MA		
Pyrene Content (mol %)	M_n (g/mol) [a]	$Đ$	Pyrene Content (mol %)	M_n (g/mol) [a]	$Đ$	Pyrene Content (mol %)	M_n (g/mol) [a]	$Đ$
0.9	40,000	1.6	0	293,000	2.9	1.2	105,000	1.5
2.0	45,000	1.3	0.5	153,000	2.7	1.9	84,000	1.6
2.6	24,000	1.3	1.6	118,000	1.9	2.2	88,000	1.5
3.3	43,000	1.8	2.0	128,000	2.8	2.4	83,000	1.4
3.3	46,000	1.5	2.0	149,000	3.0	3.1	89,000	1.3
-	-	-	3.0	200,000	1.7	-	-	-
-	-	-	3.4	91,000	2.1	-	-	-
-	-	-	3.8	150,000	1.6	-	-	-
$PyEG_5$-PEG_5MA			$PyEG_5$-PEG_7MA			$PyEG_5$-PEG_9MA		
Pyrene Content (mol %)	M_n (g/mol)[b]	$Đ$	Pyrene Content (mol %)	M_n (g/mol)[b]	$Đ$	Pyrene Content (mol %)	M_n (g/mol) [b]	$Đ$
0.4	121,000	2.1	2.2	232,200	3.8	0	152,000	1.5
2.2	55,000	1.6	3.0	222,000	3.7	0.8	420, 000	3.4
3.6	95,000	2.0	3.6	304,000	3.5	2.9	257,000	1.5
3.8	86,000	1.7	4.2	109,000	1.8	5.2	166,000	1.6
4.8	106,000	2.3	-	-	-	5.8	154,000	1.3
6.5	64,000	1.5	-	-	-	7.4	173,000	1.4
-	-	-	-	-	-	10.2	186,000	1.6
$PyEG_5$-$PEG_{19}MA$								
Pyrene Content (mol %)	M_n (g/mol) [b]	$Đ$						
0	134,000	1.4						
0.9	187, 000	1.2						
2.1	194,000	1.3						
3.2	683,000	2.8						
4.1	132,000	2.1						
5.2	85,300	1.3						
6.2	274,000	1.5						
6.6	92,000	1.3						

[a] GPC in THF.

[b] GPC in DMSO.

λ_{Py} was determined as follows. A polymer solution was prepared in THF with a known mass concentration (m) of a $PyEG_5$-PEG_nMA sample. The pyrene content of the polymer (λ_{Py}) was

calculated from the ratio $Abs/(m\times\varepsilon)$, where *Abs* is the absorption at 344 nm of the $PyEG_5$-PEG_nMA solution in THF and ε is the molar absorption coefficient of 1-pyrenemethanol in THF (ε(344 nm) = 42,700 $M^{-1}.cm^{-1}$).[67]

Gel Permeation Chromatography (GPC): Absolute molecular weights were obtained for $PyEG_5$-PEG_0MA, $PyEG_5$-PEG_3MA, and $PyEG_5$-PEG_5MA by injecting 1 mg/mL solutions of the samples dissolved in THF into a Viscotek GPC equipped with a differential refractive index, static light scattering (low and right angle), and UV-Vis absorption detector and three 300 × 8 mm^2 PolyAnalytik Superes linear mixed-bed columns. A flow rate of 1 mL/min of THF at 35 ºC was used. The system was calibrated with a 1 mg/mL THF solution of a polystyrene (PS) standard with $M = 90\times10^3$ $g.mol^{-1}$ and $Đ = 1.04$.

However, $PyEG_5$-PEG_7MA, $PyEG_5$-PEG_9MA, and $PyEG_5$-$PEG_{19}MA$ were found to interact with the column set of the GPC instrument in THF resulting in distorted GPC traces. As a result, the absolute molecular weights of these samples were obtained by injecting 2 mg/mL polymer solutions in DMSO into a TOSOH EcoSEC High Temperature GPC instrument equipped with a triple detection system and two 300 × 7.8 mm^2 TOSOH TSKgel Alpha-M 13 μm columns. This detection system includes an in-line differential refractometer, a Wyatt Dawn Heleos8 MALLS detector (wavelength λ= 660 nm), and a viscometer. A flow rate of 0.6 mL/min of DMSO at 70 ºC was used. The system was calibrated with a 1 mg/mL solution of pullulan standard in DMSO with $M_w = 47.1 \times 10^3$ $g.mol^{-1}$ and $Đ = 1.07$.

The specific refractive index increment (dn/dc) of each polymer in THF and DMSO was calculated using the differential refractometers of the GPC instruments. Sample GPC traces can be found in Figure S4.5 and S4.6 in the SI.

Persistence lengths (l_p's) were estimated from conformation plots based on the intrinsic viscosity ([η]) and molar mass (M) of the polymers obtained with the GPC in DMSO.[65] The resulting $(M^{1/2}/[\eta])^{1/3}$-*vs*-$M^{1/2}$ plots were linearized using the Bohdanecky approximation, where l_p was calculated from the slope of the conformation plots obtained with each polymer series. Some precautions were taken with the $PyEG_5$-PEG_9MA and $PyEG_5$-$PEG_{19}MA$ samples, which had rather small *d*n/*d*c values and scattered less. To minimize the error in the calculated l_p due to the error associated with the small *d*n/*d*c values determined from the GPC analysis, *d*n/*d*c was plotted as a function of pyrene content in Figure S4.7 and the line of best fit was used to predict the *d*n/*d*c value of the $PyEG_5$-PEG_9MA and $PyEG_5$-$PEG_{19}MA$ samples for a given pyrene content. Theoretically, l_p could also have been determined from conformation plots based on the scaling relationship between M and the radius of gyration (R_g) obtained from the MALLS detector. Unfortunately, this procedure turned out to be problematic in practice due to the low *d*n/*d*c values obtained for the polymers. Since the intrinsic viscosity covered a broader range of M values and yielded a stronger signal, this study focused solely on the $(M^{1/2}/[\eta])^{1/3}$-*vs*-$M^{1/2}$ plots.

Intrinsic Viscosity: Intrinsic viscosity measurements were conducted at 25 ºC using an ubbelohde viscometer in acetonitrile, THF, DMF, and DMSO. A circulating bath was used to maintain a steady temperature at 25 ºC. Three poly(oligo(ethylene glycol) methyl ether methacrylate)s (PEG_nMA, where n = 3, 9, and 19) were studied with M_w values equal to 845, 221, and 193 kg/mol for PEG_3MA, PEG_9MA, and $PEG_{19}MA$, respectively (Table 2). Both solvent and polymer solutions were filtered using 0.45 μm polytetrafluoroethylene prior to use to remove any dust. Stock solutions of 10 - 12 mg/mL were prepared and then diluted by 1 – 2 mL throughout the experiment.

Atomic Force Microscopy (AFM): AFM images were obtained with a Digital Instruments Dimension 3100 AFM at room temperature using a silicon cantilever in the tapping mode. The samples were prepared by spin coating a few drops of a dilute solution of polymer dissolved in tetrahydrofuran (THF) (10 mg/L) onto freshly cleaved mica surface at 2000 rpm.

UV-Vis Spectroscopy: A Varian Cary 100 Bio spectrophotometer was used to acquire the absorption spectra of the polymer solutions.

Steady-State Fluorescence (SSF) Measurements: All fluorescence spectra were acquired on a HORIBA QM-400 spectrofluorometer equipped with a xenon arc lamp. The SSF spectra were acquired for polymer solutions in aerated DMSO with a 2.5×10^{-6} M pyrene concentration, equivalent to an absorbance of ~0.1 at 344 nm. The solutions were excited at 344 nm and scanned from 350 to 600 nm using 1 nm slit widths for both the excitation and emission monochromator. Dividing the florescence intensity of the excimer (I_E) by the fluorescence intensity of the monomer (I_M), calculated by integrating the area underneath the spectrum from 500 to 510 nm and from 375 to 381 nm, respectively, yielded the I_E/I_M ratio, which was used to quantify the efficiency of pyrene excimer fluorescence/formation (PEF).

Time Resolved Fluorescence (TRF) Measurements: All fluorescence decays were obtained with an IBH time-resolved fluorometer. The solutions were excited at 344 nm and the monomer and excimer fluorescence decays were acquired with 20,000 counts at the decay maximum over 1,024 channels at 375 and 510 nm using cut-off filters at 370 and 495 nm, respectively. A time-per-channel of either 1.02 ns/ch or 2.04 ns/ch was employed for the decay acquisition. A Ludox solution was used for the instrument response function (IRF), which was obtained by setting the emission monochromator at 344 nm. The IRF was convoluted with the FBM equations shown as Equations S4.1 and S4.2 in SI and the convolution result was compared to the experimental decay.

Fluorescence Blob Model (FBM) Analysis: Each pair of monomer and excimer fluorescence decays acquired for a given $PyEG_5$-PEG_nMA sample was fit globally with Equations S4.1 and S4.2 according to the FBM.[19,20] The FBM compartmentalizes a polymer into equally sized *blobs*, where the volume of a *blob* is the volume probed by a pyrenyl label while it remains excited. The four pyrene species Py_{diff}*, Py_{k2}*, Py_{agg}*, and Py_{free}* are considered to represent PEF which occurs via dynamic and static pathways. Dynamic PEF takes place sequentially. Py_{diff}* represents an excited pyrenyl group, whose diffusion in solution is controlled by the polymer backbone and side chain dynamics. Py_{diff}* diffuses inside a *blob* populated by other ground-state pyrenes until Py_{diff}* becomes close enough to a ground-state pyrene molecule to turn into Py_{k2}*. The diffusive motions of two pyrenyl groups inside a *blob* are described by the rate constant k_{blob}. Rapid re-arrangement of Py_{k2}* and the nearby ground-state pyrene with the large rate constant k_2 ($k_2 \sim 10 \times k_{blob}$) results in the formation of an excimer made of two pyrenyl labels, that are well (*E*0*) or poorly (*D**) stacked and emit with their natural lifetimes τ_{E0} and τ_D, respectively. Static PEF occurs through direct excitation of a pyrene aggregate, resulting in the instantaneous formation of the *E*0* or *D** species. The species Py_{agg}* combines the two pyrenyl species *E*0* and *D** formed instantaneously from the direct excitation of a pyrene aggregate. Finally, those excited pyrenes that are isolated along the polymer backbone or do not form excimer will emit with their natural lifetime τ_M and are referred to as Py_{free}*. During the decay analysis the decays are fit twice, initially with a floating k_2 for all samples of a same $PyEG_5$-PEG_nMA series prepared with different pyrene contents. All k_2 values obtained for a same polymer series are then averaged and the averaged k_2 value is fixed in a second analysis. The parameters retrieved from the FBM analysis with a fixed k_2 have much lower error bars. The molar fractions f_{Mdiff}, f_{Mk2}, f_{Mfree}, where the index *M* indicates that they were derived from the monomer decays, and f_{Ek2}, $f_{EdiffE0}$, f_{EE0}, f_{EdiffD}, and f_{ED}, where the index *E* indicates

that they were derived from the excimer decays, were combined to yield the molar fractions f_{diff} ($=f_{diffE0} + f_{diffD}$), f_{k2}, f_{agg} ($=f_{E0} + f_{D}$), and f_{free} for the pyrene species Py_{diff}*, Py_{k2}*, Py_{agg}*, and Py_{free}*, respectively. The average number ($<n>$) of ground state pyrene molecules inside a *blob* and the rate constant (k_{blob}) describing the diffusive encounters of two structural units bearing a pyrenyl label inside a *blob* were also obtained from the FBM analysis. The number (N_{blob}) of structural units encompassed within a *blob* was calculated using f_{Mfree}, $<n>$, and x according to Equation 4.3.

$$N_{blob} = \frac{(1 - f_{M_{free}}) \times \langle n \rangle}{x} \tag{4.3}$$

The fluorescence decays of the pyrene monomer and excimer acquired for the $PyEG_5$-PEG_nMA samples were fitted globally according to Equations S4.1 and S4.2 in SI. The functions described by Equations S4.1 and S4.2 were convoluted with the IRF and the convolution product was compared to the experimental decays for optimization of the parameters with the Marquardt-Levenberg algorithm.[68] A fit was deemed acceptable when the χ^2 was lower than 1.3 and when both the residuals and autocorrelation of the residuals were randomly distributed around zero.

4.4 Results and Discussion

A series of pyrene-labeled poly(oligo(ethylene glycol) methyl ether methacrylate)s ($PyEG_5$-PEG_nMA with n = 0, 3, 4, 5, 7, 9, and 19) were synthesized using a grafting through technique by mainly free radical copolymerization of a same penta(ethylene glycol) 1-pyrenemethyl ether methacrylate ($PyEG_5MA$) and different oligo(ethylene glycol) methyl ether methacrylate (EG_nMA) macromonomers. Their chemical structure and the number (N_S) of non hydrogen atoms in each side chain were presented in Table 4.1. The design of the $PyEG_5$-PEG_nMA constructs was

carefully considered. An earlier study with pyrene-labeled poly(*n*-butyl methacrylate)s showed that the motion of the pyrenyl group became uncorrelated from the motion of the main chain when a 1-pyrenemethoxy derivative was connected to the main polymethacrylate backbone by a linker made of 2 or more ethylene glycol units.[69] The use of a penta(ethylene glycol) linker for the $PyEG_5$-PEG_nMA samples thus ensured that an excited pyrenyl label would probe a well-defined sub volume (V_{blob}) of the PBBs, referred to as a *blob* within the FBM framework, that would be unaffected by any main chain motion. In turn, this condition implied that each PBB was being probed over a same length scale defined by a same V_{blob} for all $PyEG_5$-PEG_nMA constructs considered in this study.

The SSF spectra for all pyrene contents of each $PyEG_5$-PEG_nMA series were acquired in acetonitrile, tetrahydrofuran (THF), *N,N*-dimethylformamide (DMF), and dimethylsulfoxide (DMSO) and are presented in Figures S4.8 – S4.11 in the SI. The spectra for all pyrene contents of the $PyEG_5$-PEG_4MA series in each solvent are shown in Figure 4.1.

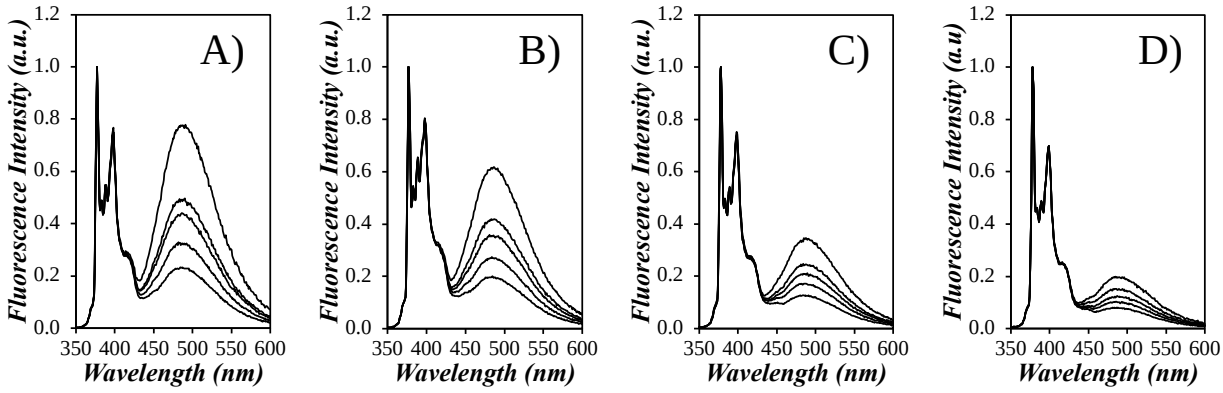

Figure 4.1. SSF spectra of $PyEG_5$-PEG_4MA in A) acetonitrile, B) THF, C) DMF, and D) DMSO with pyrene contents ranging from 1.2 to 3.1 mol% shown from bottom to top. $[Py] = 2.5\times10^{-6}$ M; λ_{ex}=344 nm.

The spectra were normalized at the first peak of the monomer emission, I_1, which is the 0-0 transition of pyrene. They showed the characteristic fluorescence peaks between 375 and 410 nm for the pyrene monomer and the broad and structureless excimer emission centered at 480 nm. It is apparent from Figure 4.1 that more excimer is produced in acetonitrile than in THF, DMF, and DMSO, with DMSO producing the least amount of excimer. The I_E/I_M ratio was calculated to quantify the efficiency of pyrene excimer formation (PEF) for the different constructs in different solvents. The I_E/I_M ratio is proportional to the local concentration of pyrene, $[Py]_{loc}$, and the rate constant for PEF through diffusive encounters, k_{diff}, as indicated by Equation 4.4.

$$\frac{I_E}{I_M} \sim k_{diff} \times [Py]_{loc} \tag{4.4}$$

The I_E/I_M ratios were plotted as a function of pyrene content for each $PyEG_5$-PEG_nMA sample in Figure S4.12. They yielded straight lines over a wide range of pyrene contents and the slope of these lines ($m(I_E/I_M)$) was plotted as a function of N_S in Figure 4.2. Based on the chemical structures shown in Table 4.1, N_S equals $3\times n+3$, where n is the number of EG units in the side chain of a PEG_nMA sample. In each solvent, the slope $m(I_E/I_M)$ decreased as N_S increased from 3 to 18 for the $PyEG_5$-PEG_nMA samples with n equal to 0, 3, 4, and 5, respectively. This decrease was attributed to an extension of the polymer backbone that resulted from increased crowding of the volume surrounding the main chain with increasing N_S. Main chain extension reduced the number of encounters between the pyrenyl terminals of the $PyEG_5$ side chains, which was associated with a decrease in $[Py]_{loc}$ in Equation 4.4. The decrease in $m(I_E/I_M)$ continued until an N_S of 24 for

PyEG$_5$-PEG$_7$MA was reached, after which $m(I_E/I_M)$ seemed to plateau for N_S values of 30 and 60 for PyEG$_5$-PEG$_9$MA and PyEG$_5$-PEG$_{19}$MA, respectively. The plateau region observed for N_S values larger than 25 indicated that a further increase in side chain length would not result in an increase in main chain extension, probably because the main chain was, or was close to being, fully extended on the length scale probed by an excited pyrene. The $m(I_E/I_M)$ vs. N_S trends shown in Figure 4.2 suggest that the steric hindrance generated by the side chains influences a region inside the PBB volume that is close to the main chain and where the shorter EG$_n$ side chains have the strongest effect. As the side chains become long enough to expand past the local region close to the main chain and into the mostly empty space away from the main chain, their effect on the main chain becomes less important resulting in the plateau observed for high side chain lengths in the $m(I_E/I_M)$ vs. N_S plot in Figure 4.2. Similar saturation effects with increasing side chain length have already been reported for PBBs.[70] The $m(I_E/I_M)$ ratios in Figure 4.2 were also found to be larger in acetonitrile, followed by THF, DMF, and DMSO. These observations are captured by Equations 4.5 and 4.6, which relate k_{diff} to the solvent viscosity, η.[71]

$$k_{diff} = 4\pi N_A RDp \tag{4.5}$$

$$D = \frac{k_B T}{6\pi\eta R_h} \tag{4.6}$$

In Equation 4.5, N_A, R, D, and p, are the Avogadro constant, the encounter radius between two pyrenyl derivatives, the diffusion coefficient of a pyrenyl dye, and the probability of forming an excimer upon encounter between an excited and a ground-state pyrene, respectively. In turn, D is related to η according to Equation 4.6, where k_B, T, and R_h are the Boltzmann constant, the

absolute temperature, and the hydrodynamic radius of a pyrenyl dye, respectively. The viscosity of acetonitrile, THF, DMF, and DMSO at 25 ºC equals 0.37, 0.46, 0.79, and 1.99 mPa·s, respectively.[72] Acetonitrile, with the lowest η, yielded the largest k_{diff} values and the largest $m(I_E/I_M)$ slopes in Figure 4.2A. Similarly, DMSO being the most viscous solvent yielded the lowest $m(I_E/I_M)$ slopes in Figure 4.2D. THF and DMF, with their intermediate η values, resulted in intermediate $m(I_E/I_M)$ slopes. As was pointed out in earlier reports,[26,73] solvent viscosity, while important, is not the only parameter affecting k_{diff}. The probability p, in Equation 4.5, depends also on the solvent and its value can offset the relationship expected from Equations 4.5 and 4.6 between k_{diff} and η^{-1}. Consequently, the interpretation of the parameter $m(I_E/I_M)$ obtained from the analysis of the steady-state fluorescence spectra offers only a qualitative description of the fluorescence results.

A more quantitative measure of polymer stiffness, such as the persistence length (l_p), could not be obtained from the $m(I_E/I_M)$ ratios. As a matter of fact, we are unaware of any procedure based on fluorescence quenching measurements capable of measuring l_p for polymers in solution. To address this apparent deficiency, the following discussion describes how a combination of PEF and FBM analysis could yield l_p for the $PyEG_5$-PEG_nMA samples. As mentioned earlier, the FBM compartmentalizes the PBBs into a string of identical *blobs* characterized by their number (N_{blob}) of structural units. The PBB segment inside a *blob* can be viewed as a worm-like chain (WLC), whose end-to-end distance ($<r_{EE}^2>_{blob}$) should obey the Kratky-Porod (KP) relationship given in Equation 4.7. In Equation 4.7, L would represent the contour length of the chain segment encompassed inside a *blob*, which would equal $N_{blob} \times b$, where b is the length of a monomer unit which was taken to equal 0.25 nm ($2 \times (0.154 \times \cos[(180\text{-}109)/2])$ nm), as is often assumed for an alkyl backbone in the all trans conformation.[57]

$$< r_{EE}^2 >_{KP} = 2l_p L - 2l_p^{\,2}\left[1 - \exp(-L/l_p)\right] \qquad (4.7)$$

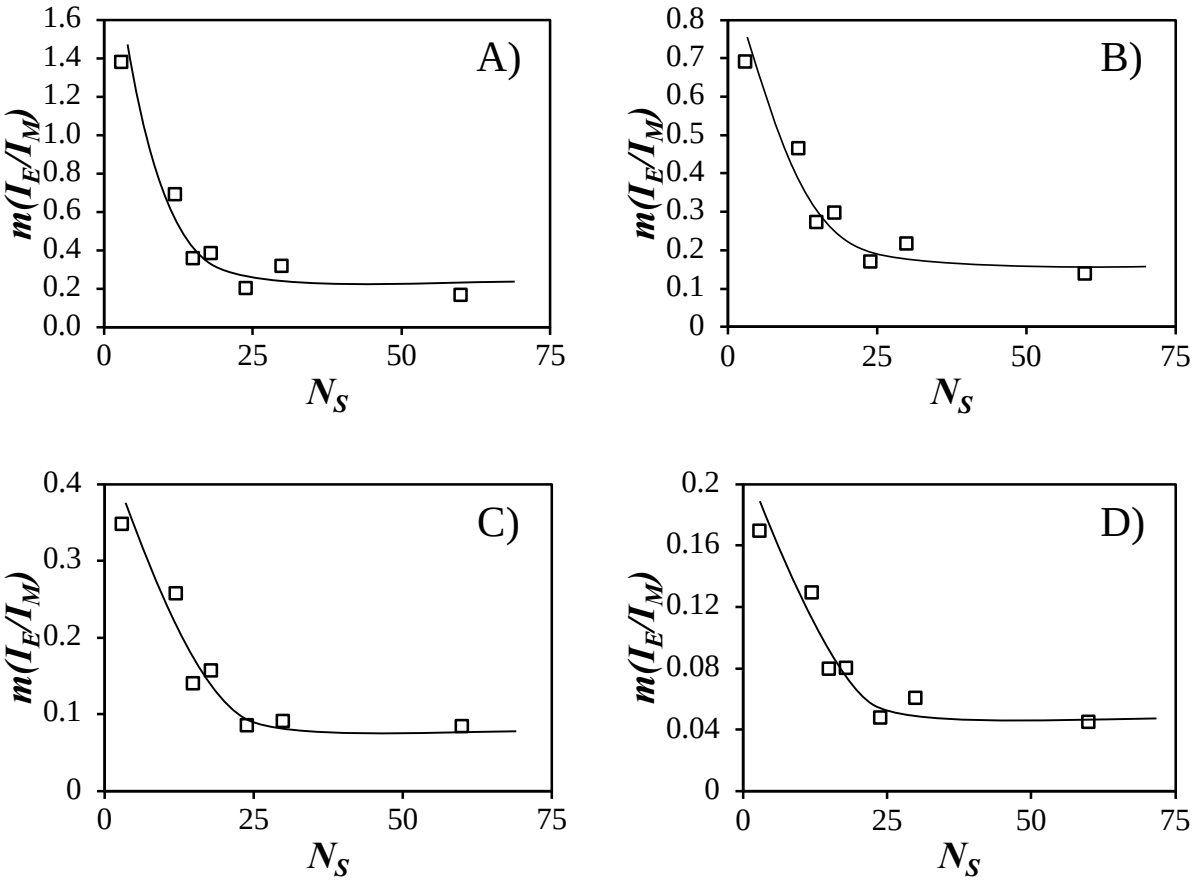

Figure 4.2. Plot of $m(I_E/I_M)$ versus N_S for the PyEG$_5$-PEG$_n$MA PBBs in A) acetonitrile, B) THF, C) DMF, and D) DMSO.

Since L is defined by the value of N_{blob} obtained experimentally from the FBM analysis of the fluorescence decays of the PyEG$_5$-PEG$_n$MA samples, $<r_{EE}^2>_{KP}$ in Equation 4.7 would be replaced by $<r_{EE}^2>_{blob}$, which would have to be determined independently to extract l_p. $<r_{EE}^2>_{blob}$ can be estimated from the rigid rod limit, which occurs when the polymer has reached a locally

extended conformation and equals $(N_{blob}(\infty)\times b)^2$, where $N_{blob}(\infty)$ represents N_{blob} for a polymer with infinitely long side chains. A plot of N_{blob} vs. N_S^{-2} happens to result in a straight line whose *y*-intercept, which would correspond to an infinitely long side chain, yields $N_{blob}(\infty)$. Furthermore, since all PyEG$_5$-PEG$_n$MA samples used the same pyrene derivative that described a same V_{blob} independent of the nature of the polymer studied, the condition $\langle r_{EE}^2\rangle_{blob} = [N_{blob}(\infty)\times b]^2$ should be obeyed by all PyEG$_5$-PEG$_n$MA samples. From the knowledge of $\langle r_{EE}^2\rangle_{blob}$, which is the same for all PyEG$_5$-PEG$_n$MA polymers, and $L = N_{blob}\times b$, which varies with polymer side chain length, the persistence length l_p could be extracted from Equation 4.7. The implementation of this strategy with the PyEG$_5$-PEG$_n$MA samples is described hereafter.

The monomer and excimer fluorescence decays of the PyEG$_5$-PEG$_n$MA samples were acquired in degassed solutions of acetonitrile, THF, DMF, and aerated DMSO and then globally analyzed using the fluorescence blob model (FBM) with Equations S4.1 and S4.2, respectively. A sample fit of the monomer and excimer fluorescence decays from PyEG$_5$-PEG$_0$MA is provided in Figure S4.13 to illustrate the quality of the fits. The fits of the fluorescence decays yielded $\langle n\rangle$ and f_{Mfree}, which were combined in Equation 4.3 with the molar fraction of structural units (x) bearing a pyrenyl label to yield N_{blob} for each polymer. Each polymer series was prepared with a minimum of four different pyrene contents ranging from 1 to 10 mol%. N_{blob} remained constant within error for each PyEG$_5$-PEG$_n$MA series, as displayed in Figure 4.3A, C, E, and G, demonstrating that the incorporation of pyrene pendants did not affect the conformation of the polymers in solution. The N_{blob} values were averaged for a given PyEG$_5$-PEG$_n$MA series to yield $\langle N_{blob}\rangle$, which was plotted as a function of N_S in Figure 4.3. Since PyEG$_5$-PEG$_0$MA had the smallest number of atoms in the side chain, it was expected to adopt the most flexible and coiled conformation and therefore, have the largest $\langle N_{blob}\rangle$, as was observed in Figure 4.3.

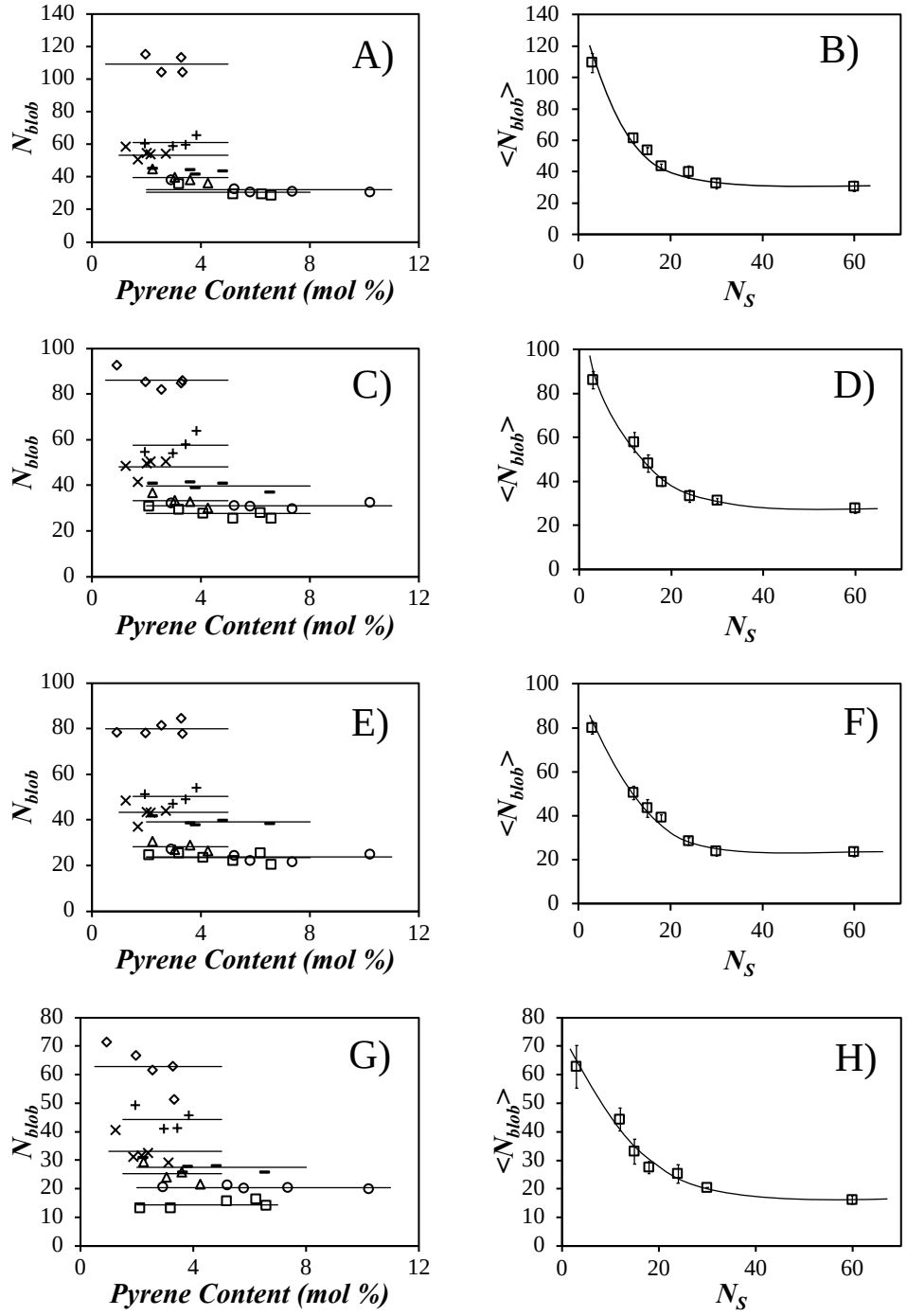

Figure 4.3. Plot of N_{blob} versus pyrene content and $<N_{blob}>$ versus N_S for the $PyEG_5$-PEG_nMA PBBs in A) + B) acetonitrile, C) + D) THF, E) + F) DMF, and G) + H) DMSO. (◆) $PyEG_5$-PEG_0MA, (+) $PyEG_5$-PEG_3MA, (×) $PyEG_5$-PEG_4MA, (━) $PyEG_5$-PEG_5MA, (▲) $PyEG_5$-PEG_7MA, (●) $PyEG_5$-PEG_9MA, and (■) $PyEG_5$-$PEG_{19}MA$.

Figure 4.3 also illustrated that a plot of $<N_{blob}>$ as a function of N_S showed a behavior similar to that of $m(I_E/I_M)$ in Figure 4.2, decreasing with increasing N_S before reaching a plateau for N_S values of 30 and higher. This similarity is reasonable since N_{blob} is directly related to $[Py]_{loc}$ through $<n>$ in Equation 4.3, which is the main parameter controlling the I_E/I_M behavior for the $PyEG_5$-PEG_nMA samples in a same solvent.

The results from both SSF and TRF measurements shown in, respectively, Figures 4.2 and 4.3 suggested that the $PyEG_5$-PEG_{19}MA backbone had reached an extended conformation on the length scale of a *blob* for N_S values greater than 30. To determine the end-to-end distance $<r_{EE}^2>_{blob}$ of a *blob*, N_{blob} for an infinitely long side chain length ($N_{blob}(\infty)$) was determined through a plot of $<N_{blob}>$ vs. N_S^{-2}, as shown in Figure 4.4A. PMMA was not considered in Figure 4.4A as the $<N_{blob}>$ values in each of the solvents did not scale as the other $PyEG_5$-PEG_nMA PBBs. A straight line was obtained for the $PyEG_5$-PEG_nMA PBBs with n = 3, 4, 5, 7, 9, and 19 in each solvent. Extrapolation of the line to the y-intercept yielded $N_{blob}(\infty)$, which was found to equal 29.3 ± 1.5 in acetonitrile, 25.9 ± 0.7 in THF, 21.7± 1.9 in DMF, and 15.3± 0.9 in DMSO.

The sequence of $N_{blob}(\infty)$ values obtained in different solvents led to the conclusion that $N_{blob}(\infty)$ decreased with increasing solvent viscosity. Since $N_{blob}(\infty)$ is the N_{blob} value assigned to a fully extended segment of the $PyEG_5$-PEG_nMA samples, its value was not expected to depend on viscosity. This observation suggested that increasing solvent viscosity reduced the number of main chain structural units probed by an excited pyrene inside a *blob* due to a decrease of the mobility experienced by the pyrene label and the polymer backbone, and perhaps more importantly, that $N_{blob}(\infty)$ represented the extended $PyEG_5$-PEG_nMA backbone over the length scale probed by an excited pyrene in a given solvent.

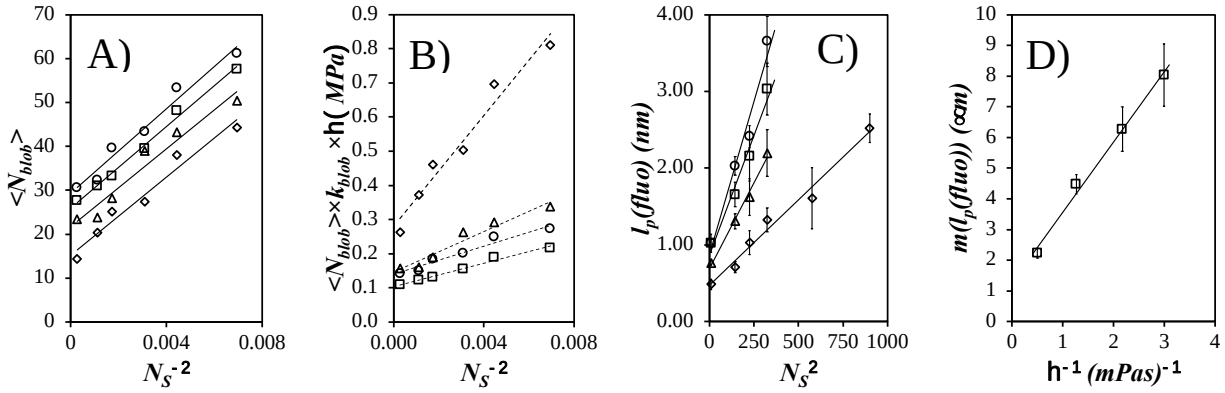

Figure 4.4. Plot of A) $<N_{blob}>$ versus N_S^{-2}, B) $<N_{blob}>\times k_{blob}\times \eta$, versus N_S^{-2} C) l_p(fluo) versus N_S^2, and D) m(l_p(fluo)) versus η^{-1} for the PyEG$_5$-PEG$_n$MA PBBs in (○) acetonitrile, (□) THF, (△) DMF, and (◇) DMSO.

The dependency of $N_{blob}(\infty)$ on solvent viscosity also indicated that the backbone, while extended, was still mobile over this length scale, and that the polymer mobility was dampened by the solvent. In essence, the polymer segment encompassed inside a *blob* can be viewed as a spring, similar to the springs used in the Rouse-Zimm model illustrated by Figure 4.5,[74,75] whose effective spring constant would increase with increasing solvent viscosity. Within this framework, a low viscosity solvent would result in a small effective spring constant, which would yield large displacements reflected by a large $N_{blob}(\infty)$ value. The pressure exerted by the polymer main chain in each of the four solvents could be investigated from the quantity $<N_{blob}>\times k_{blob}\times \eta$ expressed in MPa, in Figure 4.4B, to identify the differences in the polymer main chain dynamics with changing solvent viscosities. It is evident from the trends shown in Figure 4.4B that the polymer main chain must exert a greater pressure to displace itself when in DMSO compared to that same polymer in DMF, THF, or acetonitrile. A visual depiction of the pressure exerted by the main chain of a polymer coil during compression and extension is shown in Figure 4.5.

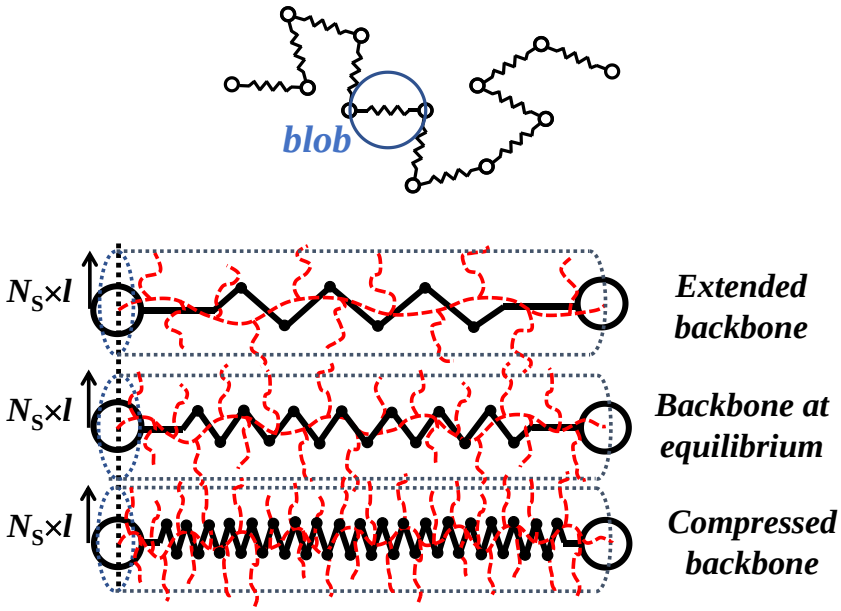

Figure 4.5. Figure of (top) bead and spring model based on the Rouse and Zimm theory with a *blob* and (bottom) compression and extension of the backbone located inside a *blob* to visualize the pressure exerted on the cross-section of the PBB with a diameter $2 \times N_S l$. The beads represent the monomers encompassed in a *blob*.

The dependency of $N_{blob}(\infty)$ on solvent viscosity also suggests that l_p determined through the use of $N_{blob}(\infty)$ in Equation 4.7 would also depend on solvent viscosity. Consequently, the l_p values determined from these fluorescence measurements will be referred to as l_p(fluo). $N_{blob}(\infty)$ was applied to determine $\langle r_{EE}^2 \rangle_{blob}$ in each solvent and with $\langle r_{EE}^2 \rangle_{blob}$ known, l_p(fluo) could be extracted from Equation 4.7. l_p(fluo) could not be determined for PyEG$_5$-PEG$_{19}$MA in all solvents, since the polymer backbone had reached a locally extended conformation and the contour length of a *blob* given by $N_{blob} \times b$ was approaching r_{EE} given by $N_{blob}(\infty) \times b$, resulting in an infinite l_p(fluo). Similarly, $\langle N_{blob} \rangle$ for PyEG$_5$-PEG$_n$MA with n equal to 7 and 9 were too close to $N_{blob}(\infty)$ in

acetonitrile, THF, and DMF and l_p(fluo) could not be determined for these constructs. For reasons that will be discussed later, l_p(fluo) was plotted as a function of N_S^2 in Figure 4.4C, where the solvent was shown to have a strong effect on the l_p(fluo) vs. N_S^2 trends. The interpretation of these trends is discussed hereafter.

In the case of PBBs, the effect of N_S on l_p is often discussed by considering that the main chain stiffness parameter (λ^{-1}), which can be the persistence length (l_p) or the Kuhn length ($l_K = 2\times l_p$), is the sum of two contributions as shown in Equation 4.8.[76] The first contribution (λ_0^{-1}) represents the intrinsic stiffness parameter reflecting local interactions near the main chain, while the second contribution (λ_b^{-1}) is a result of the resistance to bending induced by steric hindrance created by the flexible side chains. Theoretical studies predict that for flexible side chains, λ_b^{-1} scales as N_S^{α} where α takes a value of 15/8, close to 2.0.[37,38,76]

$$\lambda^{-1} = \lambda_0^{-1} + \lambda_b^{-1} \tag{4.8}$$

Plotting l_p(fluo) as a function of N_S^2 in Figure 4.4C yielded four different straight lines with non-zero intercepts. The linear relationship between l_p(fluo) and N_S^2 indicated that in a given solvent, l_p(fluo) behaved as predicted theoretically for PBBs prepared with flexible side chains.[37,38,76] In a manner similar to the trends obtained for $N_{blob}(\infty)$, l_p(fluo) decreased with increasing solvent viscosity in Figure 4.4C. The dependency of l_p(fluo) on solvent viscosity in Figure 4.4C could be either an intrinsic property of the PEG$_n$MA samples or a mere consequence of the dynamic nature of the PEF-based methodology applied to determine l_p(fluo). To assess whether the changes observed for l_p(fluo) with different solvents truly reflected the dimension of

the PEG_nMA samples, the intrinsic viscosity ([η]) of PEG_3MA, PEG_9MA, and $PEG_{19}MA$ homopolymers, that were not pyrene-labeled, were determined in acetonitrile, THF, DMF, and DMSO. Since l_p(fluo) increases from 0.7 in DMSO to 2.0 nm in acetonitrile for $PyEG_5$-PEG_3MA with a weight-average DP of 3,640, its r_{EE} calculated from Equation 4.7 should increase from 36 nm in acetonitrile to 60 nm in DMSO. Assuming that the hydrodynamic volume of the polymer coil scales as r_{EE}^3, [η] for PEG_3MA would be predicted to increase $(60/36)^3 = 4.6$-fold from DMSO to acetonitrile. Similarly large increases in [η] would be expected for the PEG_9MA and $PEG_{19}MA$ samples. To assess whether this was the case, Hugging-Kraemer plots were constructed by plotting the reduced and inherent viscosity versus polymer concentration in Figures S4.14 – S.4.17 in SI for the PEG_nMA samples with n = 3, 9, and 19 using polymer concentrations between 4 and 12 mg/mL, from which [η] was determined. The [η] values determined in acetonitrile, THF, DMF, and DMSO are summarized in Table 4.3.

Table 4.3. [η] of PEG_nMA homopolymers in acetonitrile, THF, DMF, and DMSO.

Sample	[η] in acetonitrile (mL/g)	[η] in THF (mL/g)	[η] in DMF (mL/g)	[η] in DMSO (mL/g)	<[η]> (mL/g)
PEG_3MA	53.4 ± 0.9	75.8 ± 1.5	78.5 ± 1.7	62.7 ± 1.3	67 ± 11
PEG_9MA	20.4 ± 0.1	24.2 ± 0.2	25.6 ± 0.2	25.3 ± 0.4	24 ± 2
$PEG_{19}MA$	6.4 ± 0.1	7.1 ± 0.1	8.5 ± 0.1	8.7 ± 0.0	7.7 ± 1.1

The [η] values reported in Table 4.3 were found to remain relatively constant in each of the four solvents, showing changes of less than 20% with respect to the average [η] obtained in

the four solvents for the PEG_3MA, PEG_9MA, and $PEG_{19}MA$ samples. These modest changes in $[\eta]$ were incompatible with the much larger changes in $[\eta]$ predicted from the l_p(fluo) values presented in Figure 4.4C. Consequently, the l_p(fluo) values reported in Figure 4.4C not only reflected polymer conformation based on their dependency on N_S^2, that matched theoretical predictions for PBBs with flexible side chains,[37,38,76] but also responded to the dynamics experienced by the polymers which were affected by the solvent viscosity. To confirm this relationship, the slope of the l_p(fluo) vs. N_S^2 trends ($m(l_p(\text{fluo}))$) were plotted against η^{-1} in Figure 4.4D. The linear relationship obtained between $m(l_p(\text{fluo}))$ and η^{-1} clearly illustrated that l_p(fluo) depended not only on the conformation of the macromolecules but also on their internal dynamics. This discussion suggested that the retrieval of l_p from the l_p(fluo) values obtained for the PEG_nMA samples required the elimination of the dynamic component inherently built into the l_p(fluo) values. To do this, the $<N_{blob}>$ values obtained for all the $PyEG_5$-PEG_nMA samples in the four solvents were plotted as a function of the inverse of the solvent viscosity in Figure 4.6A. The straight lines obtained for each $PyEG_5$-PEG_nMA series were extrapolated to a zero η^{-1} value yielding intercepts, with the y-axis corresponding to N_{blob}^{o} for a hypothetical solvent of infinitely large viscosity, for which polymer dynamics would be eliminated and that would only report on polymer conformation. N_{blob}^{o} was plotted as a function of N_S in Figure 4.6B. The N_{blob}^{o} vs. N_S plot in Figure 4.6B showed the same features as those observed in Figure 4.3 for different solvents. After a rapid decrease with increasing N_S, N_{blob}^{o} approached a plateau for N_S values greater than 30. Plotting N_{blob}^{o} as a function of N_S^{-2} in Figure 4.6C resulted in a straight line, which could be extrapolated to the y-intercept to yield $N_{blob}^{o}(\infty)$ found to equal 12.6 ± 1.1. In turn, $N_{blob}^{o}(\infty)$ could be used to calculate $<r_{EE}>_{blob}$ in Equation 4.7. Equation 4.7 was then applied to determine l_p^{o} for

the PEG_nMA samples in a solvent of infinite viscosity, which was plotted as a function of N_S^2 in Figure 4.6D. l_p^o was found to increase linearly with increasing N_S^2 as predicted theoretically.[37,38,76]

The l_p^o values obtained by fluorescence were then compared to l_p values obtained by gel permeation chromatography (GPC) [η]-conformation plots generated according to a procedure that was developed thanks to a simplification by Bohdanecky of the Yamakawa-Fujii (Y-F) equation.[77] These experiments are described in the SI and yielded the l_p values of PEG_0MA, PEG_3MA, PEG_7MA, and PEG_9MA in DMSO as shown in Figure 4.6D. The l_p^o values obtained by fluorescence were lower than the l_p values obtained from the GPC analysis, but both scaled as N_S^2 as predicted theoretically.

One of the factors which could contribute to the discrepancy between l_p and l_p^o shown in Figure 4.6D is the difference in length scale probed by both procedures. In the case of the $PyEG_5$-PEG_nMA samples, a fluorescence *blob* can be viewed as a spherical volume, where the short polymer segments involved in such *blobs* are not affected by excluded volume effects, as required for the application of the KPWLCM. In contrast, excluded volumes should be accounted for when considering the entire polymer coil, but are not for the analysis of the conformation plots. This conceptual difference might have led to the differences observed between the l_p and l_p^o values in Figure 4.6D.

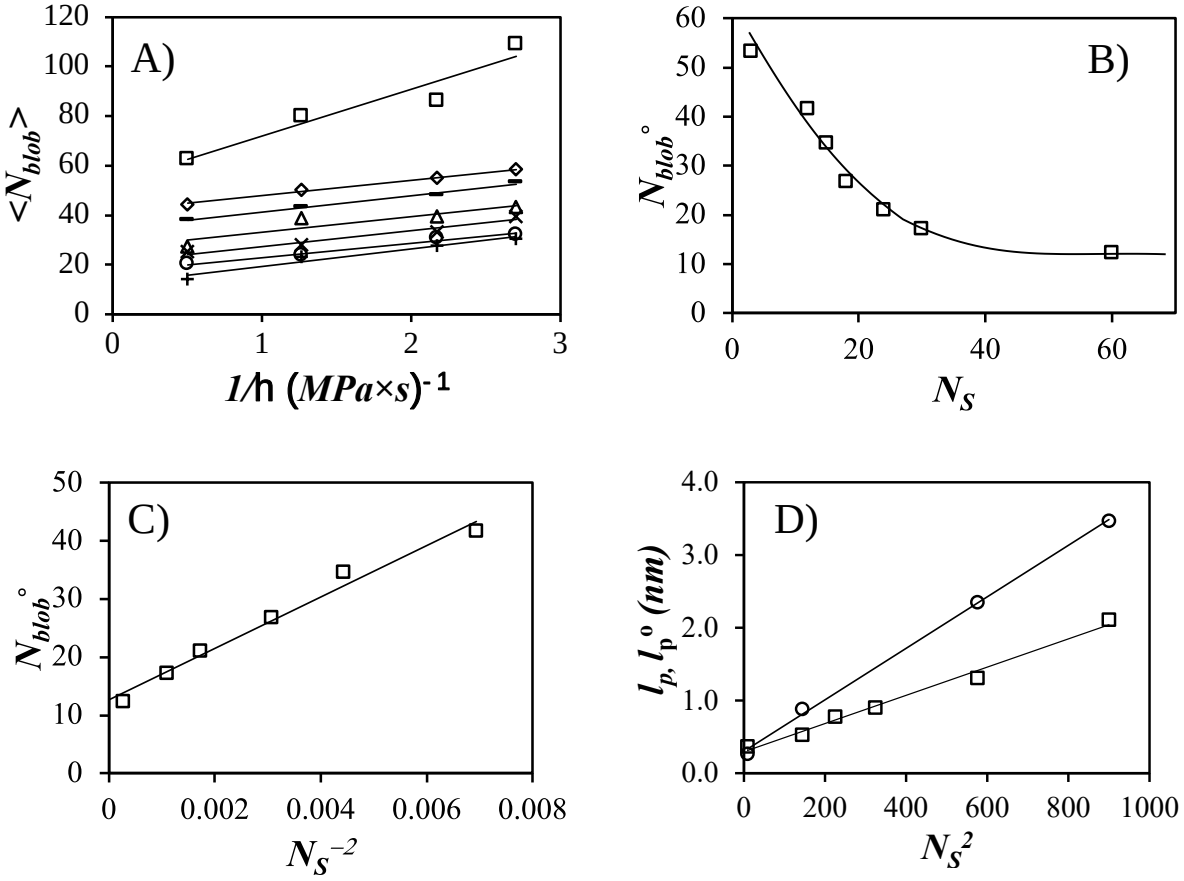

Figure 4.6. A) Plots of $<N_{blob}>$ as a function of η^{-1} for (□) $PyEG_5$-PEG_0MA, (◇) $PyEG_5$-PEG_3MA, (−) $PyEG_5$-PEG_4MA, (△) $PyEG_5$-PEG_5MA, (×) $PyEG_5$-PEG_7MA, (○) $PyEG_5$-PEG_9MA, and (+) $PyEG_5$-$PEG_{19}MA$. Plot of N_{blob}° as a function of B) N_S and C) N_S^{-2}. D) Plot of (□) l_p° obtained by PEF and (○) l_p obtained from GPC conformation plots as a function of N_S^2.

The backbone conformation of $PEG_{19}MA$ was further investigated by Lei Zhang from Prof. Tong Leung's laboratory, who used atomic force microscopy (AFM) to visualize individual $PEG_{19}MA$ macromolecules which were prepared without pyrene. This sample had number- (M_n) and weight- (M_w) average molecular weights of 134,000 and 193,000 $g.mol^{-1}$, respectively.

Individual polymer molecules were observed in Figure 4.7 ranging in length from 20 to 90 nm, in diameter from 10 to 20 nm, and in height from 0.5 to 1 nm. These results are consistent with the expected dimensions of these macromolecules, considering that a fully extended $PEG_{19}MA$ macromolecule would have a number average contour length of ~35 nm and an average width of ~16 nm. Furthermore, the AFM image shown in Figure 4.7 clearly demonstrates the presence of isolated macromolecules with no indication of aggregation. This observation eliminates the possibility that $PEG_{19}MA$ could aggregate, as has been found for PBBs prepared with longer poly(ethylene oxide) side chains which have been shown to crystalize, resulting in the formation of crystalsomes.[78] Figure 4.7 demonstrates that this is not the case for $PEG_{19}MA$. Although the chains observed in Figure 4.7 show some curvature, the steric hindrance generated by their side chains prevents them from adopting a fully coiled conformation, as would be expected from their l_p value of ~4.5 nm obtained through GPC analysis in DMSO (see Table S1).

The image shown in Figure 4.7 complements the conclusions drawn from the plateau reached for $m(I_E/I_M)$ in Figure 4.2 and for N_{blob}^{o} in Figure 4.6B, obtained by SSF and TRF, respectively. These plateaus were defined mostly by the $m(I_E/I_M)$ and N_{blob}^{o} values obtained with samples from the $PyEG_5$-$PEG_{19}MA$ series, and they were rationalized by evoking the stiffening and extension of the polymer backbone. Such a stiffening is clearly visible in the AFM picture, where the $PEG_{19}MA$ macromolecules appear as WLCs.

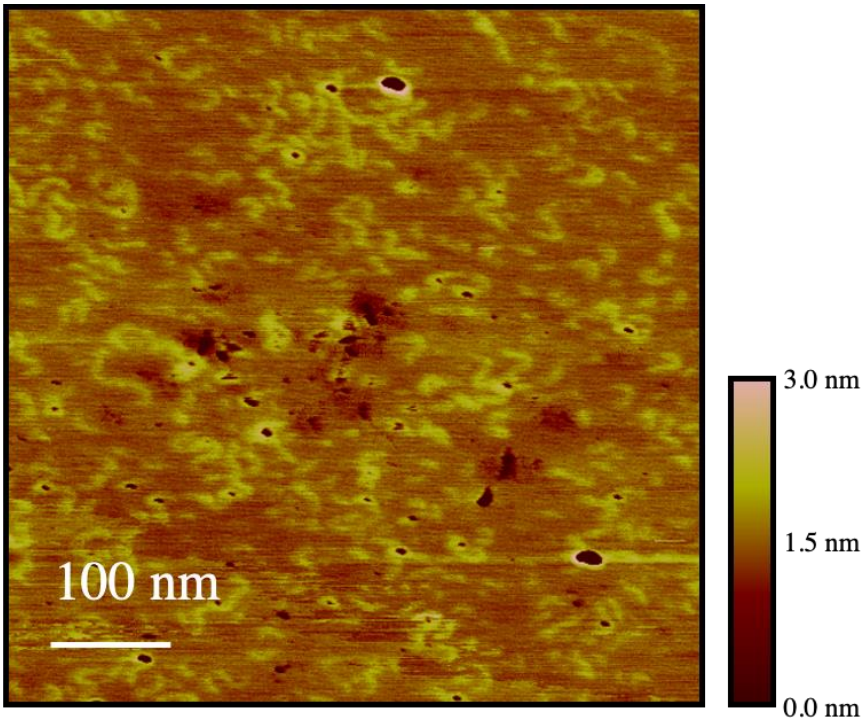

Figure 4.7. AFM topography image of $PEG_{19}MA$ spin-coated on a freshly cleaved mica surface from a 10 mg/L solution in THF.

4.5 Conclusion

A series of poly(oligo(ethylene glycol) methyl ether methacrylate)s (PEG_nMA, where n = 0, 3, 4, 5, 7, 9, and 19 ethylene glycol units) were synthesized and changes in their conformation were monitored as the length of their side chain, N_S, was increased from 3 to 60 atoms. The polymers were prepared with minimal amounts of a penta(ethylene glycol) 1-pyrenemethyl ether methacrylate monomer, which was copolymerized using a grafting-through approach along with the oligo(ethylene glycol) methyl ether methacrylate (EG_nMA) macromonomer. The seven pyrene-labeled PEG_nMA polymers ($PyEG_5$-PEG_nMA) were characterized in acetonitrile, THF, DMF, and DMSO. Analysis of the TRF decays using the FBM demonstrated that N_{blob} decreased

with increasing N_S and then approached a plateau for N_S values of 30 and 60. These results were consistent in each of the solvents studied and indicated that the FBM was responding to the stiffening of the polymer main chain. The FBM was then combined with the Kratky-Porod worm-like chain model (KPWLCM) to determine a persistence length l_p(fluo) for the PyEG$_5$-PEG$_n$MA PBBs using a *blob*-based approach. It was evident from the FBM analysis that the average number of structural units $<N_{blob}>$ encompassed within a *blob* was influenced by both the dynamics and conformation of the polymer main chain. The influence of main chain dynamics was removed from the FBM analysis through the extrapolation of $<N_{blob}>$ for each PyEG$_5$-PEG$_n$MA PBB to an infinitely high viscosity, N_{blob}^{o}. After re-calculating the persistence length l_p^{o} obtained using the FBM in the absence of main chain dynamics, l_p^{o} was found to increase linearly with the square of the number of atoms in the side chain N_S^2, as expected theoretically for flexible side chains. Gel permeation chromatography (GPC) was also applied to construct conformation plots based on [η], which were used to determine the l_p of the PyEG$_5$-PEG$_n$MA PBBs with n = 0, 3, 7, 9, and 19. While both l_p^{o} and l_p determined using GPC increased linearly with N_S^2, the slope obtained for l_p^{o} was almost half that for l_p. The difference in slope was attributed to the different length scales of the two experiments. A *blob* reflecting a localized volume unaffected by solvent quality represents a perfect application for the KPWLCM, which does not account for excluded volume effects. In contrast, all other measurements dealing with PBBs characterize the entire PBB volume and should thus use a modified version of the KPWLCM, that would account for excluded volume effects. The fact that the FBM-based results on macromolecules are little affected by excluded volume effects might turn out to be an important advantage of the FBM to study the conformation of macromolecules in solution.

Chapter 5

Location of a Hydrophobic Load in Poly(oligo(ethylene glycol) methyl ether methacrylate)s (PEGMAs) Dissolved in Water and Probed by Fluorescence

5.1 Abstract

The fluorescence of the dye pyrene was applied to probe the core of a series of pyrene-labeled poly(oligo(ethylene glycol) methyl ether methacrylate) ($PyEG_5$-PEG_nMA, where *n* equaled 3, 5, 9, and 19), prepared by copolymerizing different molar ratios of penta(ethylene glycol) 1-pyrenemethyl ether methacrylate ($PyEG_5MA$) with EG_nMA. These experiments took advantage of the ability of the 1-pyrenemethoxy derivative to report on the polarity of its surroundings and form an excimer upon encounter between an excited and a ground-state pyrene moiety. These fluorescence studies showed that, contrary to many other pyrene-labeled water-soluble polymers (Py-WSPs), the pyrene labels of the $PyEG_5$-PEG_nMA samples were not much aggregated in water. The origin of this effect could be traced back to the nature of the organic-like domain (OLD) generated around the polymethacrylate backbone by the high grafting density of the EG_n side chains radiating outward into the water. Fluorescence lifetime measurements suggested that this OLD was free of water and similar in nature to ethylene glycol, and that the OLD shielded the hydrophobic pyrenyl labels from exposure to the water phase. The OLD could be viewed as a cylinder centered around the polymethacrylate backbone, whose radius could be estimated by noting that the reach of the $PyEG_n$ derivative for the $PyEG_5$-PEG_nMA samples dissolved in water matched closely that obtained for a series of poly(alkyl methacrylate)s labeled with 1-pyrenebutanol studied in tetrahydrofuran. Using molecular mechanics optimization, the radius of the cylindrical OLD was estimated to equal 1.8 nm. The existence of the OLD was further demonstrated by showing that the PEG_nMA samples dissolved in water could be loaded with water-insoluble pyrene. This study suggests that PEG_nMAs generate a water-free OLD in water, which can be used to solubilize and protect a hydrophobic cargo like pyrene. This insight is expected to improve the design of future PEG_nMA-based drug delivery systems.

5.2 Introduction

Poly(ethylene glycol) (PEG) is a water-soluble and non-immunogenic polymer, which is commercially available in an assortment of molecular weights.[1] The covalent modification of a protein, peptide, or therapeutic drug with PEG, a process also known as PEGylation, was first introduced in 1977 and is commonly used to modify their pharmacokinetic properties.[1–4] The first medical treatment with a PEGylated protein approved by the food and drug administration (FDA) was for the enzyme adenosine deaminase in 1990[5] and since then, PEGylated enzymes, cytokines, antibiotics, and growth factors have been approved for commercial use.[4,6] The addition of a PEG chain to a biomacromolecule or drug increases the molecular weight of the macromolecule-polymer conjugate, which leads to reduced renal clearance and longer circulation lifetimes.[3,5] PEG is also known to offer 'stealth' to its conjugates by providing a steric shield preventing immune system recognition, which reduces blood clearance.[3,5] The improved pharmacokinetic properties associated with PEGylation allow for a decrease in dose frequency and the accumulation in more permeable tumor tissues.[4,5] As a result, PEG is the most commonly used polymer for drug delivery. Unfortunately, the increased use of PEGylation in the pharmaceutical industry has led to the realization that some patients become allergic to PEG, as demonstrated by the detection of anti-PEG antibodies, which lead to the interruption of the drug treatment in patients.[5,7]

It has been found that changing the PEG architecture, from a linear chain to a branched polymer with oligomeric PEG side chains, eliminated PEG antigenicity.[6] Branched structures have also been shown to increase blood circulation half-lives with respect to their linear analogues.[8,9] Branched architectures such as dendrimers and polymeric bottle brushes (PBBs) are desirable because they offer a large hydrodynamic volume with a precise molecular weight, and can be synthesized with a protected core which can be used to shuttle hydrophobic drugs. This study will

focus on PBBs, since they can be readily synthesized using either a living or radical polymerization technique and can reach large sizes hundreds of nanometers long.[6,10–13] The PBB architecture has been adopted in drug/peptide conjugates,[6,14–16] polymeric micelles,[9,17–20] and in unimolecular micelles[12,21–31] for drug delivery systems (DDSs).

PEG is typically introduced into PBB DDSs because it confers water solubility, is electrostatically neutral, and creates a hydration shell,[15] which shields the peptide or drug cargo from opsonization.[13] The polymer brush architecture, which has been applied for antimicrobial materials, has also been found to prevent the non-specific binding of proteins through a combination of surface hydration and steric shielding.[32] These features come handy for the design of drugamers,[33] prepared by copolymerizing a prodrug such as a methacrylate monomer, onto which a drug is covalently attached via a cleavable linker, with an oligo(ethylene glycol) methacrylate (EG_nMA with *n* being the number of ethylene glycol units in the side chains) to generate PEG_nMA PBBs.[34–39] While the protection afforded through steric shielding by PEG_nMAs to DDSs is well-accepted in the literature, [15,40,41] the exact origin of the protection induced by the PEG_nMA PBBs is not as well described. In particular, the nature of the medium generated by EG_n side chains close to the polymethacrylate backbone has never been carefully investigated in water.

To address this issue, different aspects of pyrene fluorescence are applied in this report to probe the local internal environment of a series of PEG_nMAs prepared with oligo(ethylene glycol) methyl ether side chains (EG_n) of increasing side chain length (*n*). Pyrene was chosen as the chromophore because of its sensitivity to the polarity of its local environment,[42] its hydrophobicity, and its long lifetime. These properties were employed to probe the local polarity experienced by a pyrenyl label covalently attached onto PEG_nMA via a penta(ethylene glycol) linker, investigate the effect of side chain length, and determine the solubility of pyrene inside the PEG_nMA samples.

The results suggest that PEG_nMAs generate a cylindrical core 3.6 nm in diameter and centered around the polymethacrylate backbone which is water-free and organic-like in nature, thus providing an ideal medium to host hydrophobic cargoes (like pyrene) and protect them from degradation by water-soluble agents. This insight into the different environments generated by PEG_nMA in aqueous solution, namely an organic-like core stabilized by a corona made of solvated EG_n side chains, should prove valuable when designing novel PEG_nMA-based DDSs.

5.3 Experimental

Materials: The preparation of the $PyEG_5$-PEG_nMA samples used in this study has been described in detail in Chapter 4 of this thesis and their chemical structure is shown in Table 5.1. Dichloromethane (DCM, ≥ 99.8%), diethylether (≥ 99%), *N,N*-dimethylformamide (DMF, ≥ 99.8%), dimethylsulfoxide (DMSO, ≥ 99.9%), 4-(dimethylamino)pyridine (DMAP, ≥ 99%), ethyl acetate (≥ 99.7%), ethylene glycol (> 99%), methacrylic anhydride (94%), 1-pyrenebutanol (99%), sodium chloride, sodium hydride (60% dispersion in mineral oil), sodium hydroxide (NaOH, pellets, ≥ 97%), sodium sulfate (anhydrous, ≥ 99%), triethylamine (≥ 99.5%), and tetrahydrofuran (≥ 99%) used for synthesis were purchased from Sigma. Tetrahydrofuran optima (≥ 99.9%) used for the fluorescence measurements and penta(ethylene glycol) methyl ether (EG_5OH, ≥ 95%) were obtained from Fisher and PurePEG, respectively. All these chemicals were used as received.

The oligo(ethylene glycol) methyl ether methacrylate monomers, namely EG_3MA (93%), EG_9MA with M_n= 500 g/mol, and $EG_{19}MA$ with M_n= 950 g/mol were supplied by Sigma. They were dissolved in dichloromethave (DCM) before being washed with 2 M NaOH (aq) and dried with sodium sulfate before use.

The radical initiator 2,2'-azobis(2-methylpropionitrile) (AIBN, Sigma, 98%) and molecular pyrene (Sigma, 98 %) were recrystalized in ethanol three times.

Unless otherwise specified all other chemicals were purchased from commercially available sources and used as received.

Methacrylation of 1-pyrenebutanol: 1-Pyrenebutanol (0.20 g, 0.73 mmol) and DMAP (8.91 mg, 0.07 mmol) were dissolved in 25 mL of freshly distilled DCM in a round bottom flask (RBF) equipped with a stir bar. The RBF was placed in an ice water bath and methacrylic anhydride (0.17 g, 1.09 mmol) was added dropwise. The solution was left to stir overnight. The next day, the reaction mixture was washed with an aqueous solution of 2 M NaOH three times. The organic phase was extracted and dried with sodium sulfate. The organic phase was then concentrated to 1 mL using a rotary evaporator. The product was purified by silica gel chromatography using DCM as the eluent. The chemical composition of the purified PyC_4MA product was verified using ^1H NMR (Figure S5.1 in SI).

Preparation of the PyC_4-$PEG_{19}MA$ series by conventional radical copolymerization: The random co-polymerization of PyC_4MA with oligo(ethylene glycol) methyl ether methacrylate ($EG_{19}MA$) was carried out to synthesize five PyC_4-$PEG_{19}MA$ samples using the protocol described hereafter. PyC_4MA (4.70 mg, 13.73 μmol) and $EG_{19}MA$ (0.25 g, 0.26 mmol) were dissolved in 1 mL THF such that the overall methacrylate concentration was approximately 0.3 M. The AIBN initiator (0.04 mg, 0.26 μmol) was added to the monomer solution from a 3 μM stock solution in 10 mL THF and the mixture was placed in the polymerization tube. The tube was kept on ice and degassed with nitrogen (Praxair, N4.0) for 30 minutes. After sealing the tube, it was left in an oil bath at 65 °C. The polymerization was terminated at a conversion of 20% or less was reached, as determined by ^1H NMR analysis, to minimize composition drift. The polymer was recovered by

precipitating the polymer solution in THF 5-6 times into diethyl ether to remove any unreacted monomer. The precipitated product was then dried in a vacuum oven overnight. The chemical structure of PyC_4-$PEG_{19}MA$ is shown in Table 5.1 and a sample ^1H NMR spectrum is shown in Figure S5.2 of the SI. The number average molecular weight, M_n, and dispersity, $Đ$, were characterized using gel permeation chromatography (GPC) and is shown in Table 5.2.

Table 5.1 Chemical structure and number, N_S, of atoms in each side chain for the pyrene-labeled PEG_nMA samples.

Sample	$PyEG_5$-PEG_3MA	$PyEG_5$-PEG_5MA	$PyEG_5$-PEG_9MA	$PyEG_5$-$PEG_{19}MA$	PyC_4-$PEG_{19}MA$
Structure	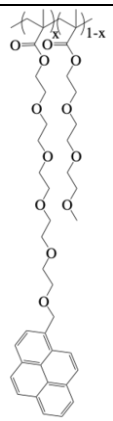	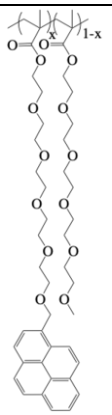	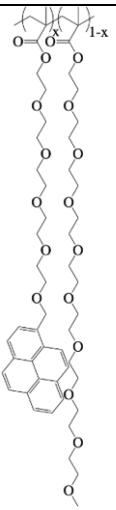	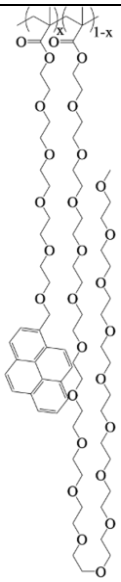	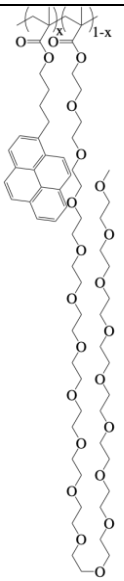
N_S	12	18	30	60	

Homopolymerization of EG_nMA using conventional radical polymerization: The homopolymerization of tri(ethylene glycol) methyl ether methacrylate (EG_3MA), penta(ethylene glycol) methyl ether methacrylate (EG_5MA), and the two oligo(ethylene glycol) methyl ether methacrylates (EG_9MA and $EG_{19}MA$) were conducted in a similar fashion. All EG_nMA monomers

were purchased from Sigma, except for EG_5MA, which was prepared from the methacrylation of penta(ethylene glycol) methyl ether conducted in the same manner as the methacrylation of 1-pyrenebutanol described earlier. The synthesis of PEG_5MA is described in more detail.

EG_5MA (0.8 g, 2.5 mmol) was dissolved in 8 mL of THF and the 0.3 M EG_5MA solution was then added to the polymerization tube followed by AIBN (0.4 mg, 2.5 μmol) obtained from a concentrated 3 mM AIBN stock solution in THF. The polymerization tube was set on ice before being degassed with nitrogen (Praxair, 4.0) for 30 min. The polymerization tube was placed in an oil bath at 65 °C and the reaction mixture was left to polymerize overnight for 20 hours. The next day, the polymer was precipitated in diethyl ether 4-5 times to remove any unreacted monomer. The chemical composition and molecular weight distribution of the PEG_nMA homopolymers were characterized using ^{1}H NMR (Figure S5.3 in the SI) and gel permeation chromatography (Table 5.3), respectively.

Pyrene content: Equation 5.1 was applied to calculate the molar fraction (x) of pyrene monomer incorporated into the copolymers $PyEG_5$-PEG_nMA and PyC_4-$PEG_{19}MA$. Equation 5.1 used the molar mass of the unlabeled monomer, M, the molar mass of the pyrene labeled monomer, M_{Py} (= 520.62 g/mol for $PyEG_5MA$ and 342 g/mol for PyC4MA), and the pyrene content, λ_{Py}, which is expressed in moles of pyrene per gram of polymer.

$$x = \frac{M}{\lambda_{Py}^{-1} + M - M_{Py}} \tag{5.1}$$

λ_{Py} was calculated for each pyrene-labeled polymer in tetrahydrofuran as follows. A polymer solution was prepared in THF with a known mass concentration (m in g/L). The absorbance of the

solution was determined with a 1.0 cm path length (b = 1.0 cm) quartz cuvette and the peak maximum at 344 nm was used in conjunction with the Beer-Lambert Law ($Abs=\varepsilon_{Py}\times c\times b$) to determine the concentration of pyrene ([Py] in mol/L) in the solution. The molar extinction coefficient, ε_{Py}, used for polymers labeled with 1-pyrenemethyl ether penta(ethylene glycol) and 1-pyrenebutyl derivatives in THF equaled 42,700 $M^{-1}.cm^{-1}$ and 42,250 $M^{-1}.cm^{-1}$ at 344 nm, respectively.[43,44] The ratio [Py]/m yielded the pyrene content (λ_{Py}) to be used in Equation 5.1.

Gel permeation chromatography (GPC): The absolute number-average molecular weight (M_n) and dispersity ($Đ$) were obtained by injecting 2 mg/mL polymer solutions in DMSO into a TOSOH EcoSEC High Temperature GPC instrument equipped with a triple detection system and two 300 × 7.8 mm^2 TOSOH TSKgel Alpha-M 13 μm columns. The detection system included an in-line differential refractometer, a Wyatt Dawn Heleos8 MALLS detector (wavelength, λ= 660 nm), and a viscometer. A flow rate of 0.5 mL/min of DMSO at 70 ºC was used. The system was calibrated with a 1 mg/mL solution of pullulan standard in DMSO with a weight average molecular weight (M_w) and $Đ$ of 47.1 × 10^3 $g.mol^{-1}$ and 1.07, respectively. GPC traces for the PyC_4-PEG_{19}MA series along with the PEG_nMA homopolymers are shown in Figure S5.4 in the SI.

Table 5.2. Pyrene content, absolute M_n, and $Đ$ for the PyC_4-PEG_{19}MA series.

Pyrene Content (mol %)	M_n (g/mol)	$Đ$
7.4	65,200	1.1
7.6	91,700	1.2
10.2	92,800	1.2
12.4	132,800	1.2
14.7	66,800	1.1

Table 5.3. Absolute M_n and $Đ$ for each PEG_nMA homopolymers.

PEG_3MA		PEG_5MA		PEG_9MA		$PEG_{19}MA$	
M_n (g/mol)	$Đ$	M_n (g/mol)	$Đ$	M_n (g/mol)	$Đ$	M_n (g/mol)	$Đ$
293,000	2.9	275,000	3.8	152,000	1.5	134,000	1.4

UV-Vis spectroscopy: A Varian Cary 100 Bio spectrophotometer was used to acquire the absorption spectra of the polymer solutions. Quartz cuvettes with a 1.0 mm and 10 mm pathlength were used, depending on the pyrene concentration. For the pyrene loading studies, the absorbance spectra were acquired in triplicate with a scan rate of 150 nm/min. The maximum absorbance observed at a wavelength of 338.5 nm was used to determine the absorbance for the loading studies.

Pyrene loading experiments: Pyrene (2 mg) was placed in a vial with 5 mL of PEG_nMA aqueous solution. The mixture was stirred and the absorbance at 338.5 nm of the supernatant was monitored over 7-14 days until a clear plateau was observed. This experiment was repeated using 6 – 7 different polymer concentrations ranging from 0.7 to 7.3 g/L for each PEG_nMA sample. The absorbance at the peak max, Abs_{total}, was then plotted versus the polymer concentration.

Steady-state fluorescence (SSF) measurements: A HORIBA QM-400 spectrofluorometer equipped with a xenon arc lamp was used to acquire the fluorescence spectra of the polymer solutions in degassed THF and in aerated water. To avoid the inner filter effect, the solutions were prepared with a 2.5×10^{-6} M pyrene concentration equivalent to an absorbance of ~0.1. All fluorescence spectra were acquired from 350 to 600 nm and with a 344 nm excitation wavelength. Slit widths of 1 nm were applied to both the excitation and emission monochromators. The I_E/I_M ratio was calculated by dividing the area under the excimer emission from 500 to 530 nm by the area under

the first peak of the monomer emission integrated over 4 nm before and 4 nm after the peak maximum, located at a wavelength ranging from 375 to 380 nm depending on the polymer concentration and composition.

A study on the effect of polymer concentration on the I_E/I_M ratio was conducted in water to ensure that the polymers were not aggregated, and that excimer formation occurred only intramolecularly for the range of pyrene contents of the $PyEG_5$-PEG_nMA samples studied. Three polymers were selected from the most ($PyEG_5$-PEG_3MA) and least ($PyEG_5$-$PEG_{19}MA$) hydrophobic polymer series with different pyrene contents. Their I_E/I_M ratio was determined with increasing polymer concentration for three different pyrene contents. The I_E/I_M ratio remained constant for each sample in Figure S5.6, indicating that no intermolecular excimer formation took place in these fluorescence experiments conducted with aqueous solutions of the $PyEG_5$-PEG_nMA samples.

Dividing the florescence intensity of the first peak (I_1) by that of the third peak (I_3) of the monomer emission found in the front part of the fluorescence spectra shown in Figures 5.1 and S5.5, corresponding to the pyrene monomer emission, yielded the I_1/I_3 ratio, which was used to assess the polarity of the medium probed by the pyrenyl label.

Time-resolved fluorescence (TRF) measurements: An IBH time-resolved fluorometer with a 340 nm nanoLED was used to acquire all fluorescence decays. The excitation wavelength was selected at 344 nm with the excitation monochromator, while the monomer and excimer fluorescence decays were obtained by monitoring their fluorescence at 375 and 510 nm with the emission monochromator, and using cut-off filters at 370 and 495 nm, respectively, to prevent stray light from reaching the detector. The decays had 20,000 counts at the maximum and were acquired over 1,024 channels with a time-per-channel of either 1.02 ns/ch or 2.04 ns/ch. The instrument response function (IRF) was obtained from the emission of a Ludox solution, by setting the emission

monochromator at the excitation wavelength of 344 nm. The IRF was convoluted to the mathematical decay function according to the fluorescence *blob* model (FBM) and the convolution product was compared to the experimental fluorescence decays.

Fluorescence decay analysis with the fluorescence blob model (FBM): The FBM is used to analyze the fluorescence decays of polymers, which have been randomly labeled with a chromophore, pyrene in this case. The FBM compartmentalizes the polymer backbone into individual monodisperse *blobs*. The volume, V_{blob}, of a *blob* is defined by the volume probed by a pyrene molecule, while it remains excited. Pyrene excimer formation (PEF) occurs when an excited pyrene encounters a ground-state pyrene. The FBM separates the pyrenyl labels attached onto a macromolecule into four different species. These include the pyrene species Py_{diff}* and Py_{k2}*, which are involved in a sequential process for excimer formation. Py_{diff}* diffuses in solution with a rate constant k_{blob} according to the dynamics experienced by the structural unit it is attached to until it comes within reach of a ground-state pyrene when it turns into the species Py_{k2}*, that re-arranges with a large rate constant k_2 ($k_2 \sim 10 \times k_{blob}$) to form one of two excimers $E0$* or D*. The pyrene species $E0$* or D* represent an excimer where the two pyrene labels are properly or poorly stacked and emit with their natural lifetimes τ_{E0} or τ_D, respectively. The excimer $E0$* and D* can also be formed instantaneously through direct excitation of pyrene aggregates (Py_{agg}*). Finally, the pyrene species Py_{free}* describes those pyrenyl labels, that are located in a pyrene-poor region of the macromolecule, cannot form excimer, and emit with their natural lifetime τ_M. Global analysis of the monomer and excimer fluorescence decays yields the molar fractions of the pyrene species contributing to the monomer and excimer decays. The molar fractions f_{Mk2}, f_{Mdiff}, and f_{Mfree} and the molar fractions f_{Ek2}, $f_{EdiffE0}$, f_{EdiffD}, f_{EE0}, and f_{ED} derived from, respectively, the monomer and excimer decays, can be combined to yield the molar fractions f_{diff} ($=f_{diffE0}+f_{diffD}$), f_{k2} ($=f_{k2E0}+$

f_{k2D}), f_{agg} (=f_{E0}+ f_D), and f_{free} which correspond to the pyrene species Py_{diff}*, Py_{k2}*, Py_{agg}*, and Py_{free}*, respectively. Fitting the fluorescence decays of the pyrene monomer and excimer according to the FBM yields the average number, <*n*>, of ground-state pyrene molecules within a *blob*, and the rate constant k_{blob}, representing the diffusive motions of two structural units bearing an excited and a ground-state pyrene inside a *blob*. The number of monomer units encompassed within a *blob*, N_{blob}, can then be calculated using Equation 5.2, where *x* is the molar fraction of structural units bearing a pyrenyl label as defined by Equation 5.1.

$$N_{blob} = \frac{\left(1 - f_{M_{free}}\right) \times < n >}{x} \tag{5.2}$$

Fluorescence decay acquisition and analysis: The fluorescence decays for the $PyEG_5$-PEG_nMA (with *n* = 3, 5, 9, and 19) and PyC_4-$EG_{19}MA$ samples were acquired in aerated Milli-Q water and both degassed tetrahydrofuran (THF) Optima and aerated Milli-Q water, respectively, before being fit globally according to the FBM with Equations S5.1 and S5.2 in the SI. The instrument response function (IRF) was convoluted with Equations S5.1 and S5.2 to generate a line of best fit, which was compared to the experimental decays. The parameters involved in the calculation of the convolution products were optimized with the Marquardt-Levenberg algorithm[45] and a fit was deemed acceptable when three criteria were satisfied. Those included that both the autocorrelation of the residuals and the residuals be randomly distributed around zero and that the χ^2 be lower than 1.3. A sample fit of the fluorescence decays is shown in Figure S5.6 in SI.

5.4 Results and Discussion

Penta(ethylene glycol) 1-pyrenemethyl ether methacrylate ($PyEG_5MA$) was randomly copolymerized with a series of oligo(ethylene glycol) methyl ether methacrylate monomers (EG_nMA, where n = 3, 5, 9, and 19) to prepare four series of pyrene-labeled poly(oligo(ethylene glycol) methyl ether methacrylate)s ($PyEG_5$-PEG_nMAs), whose synthesis and characterization was described in Chapter 4. While the PEG_nMA portion of the $PyEG_5$-PEG_nMA samples is fully water-soluble, the hydrophobic pyrenyl label has a reported solubility of 0.7 μmol/L for pyrene in water.[46,47] Consequently, the $PyEG_5$-PEG_nMA samples are expected to be fully soluble in an organic solvent like tetrahydrofuran (THF), whereas only the polymer substrate but not the pyrenyl labels should be soluble in water. Major differences are thus expected for the fluorescence response exhibited by the $PyEG_5$-PEG_nMA samples, depending on whether they were studied in an organic solvent or in water.

To this end, the steady-state fluorescence (SSF) spectra of each $PyEG_5$-PEG_nMA sample was acquired in THF, in Chapter 4 of this thesis, and water. A sample SSF spectrum of the $PyEG_5$-PEG_9MA series in THF and water is shown in Figure 5.1. The SSF spectra for the other polymers can be found in Figures S5.6 and S5.7 in the SI. All the spectra were normalized to unity at 377 nm, which is the 0-0 transition of pyrene. They displayed the characteristic pyrene monomer peaks between 370 and 410 nm, and the broad structureless emission of the pyrene excimer centered at 480 nm in THF and water.

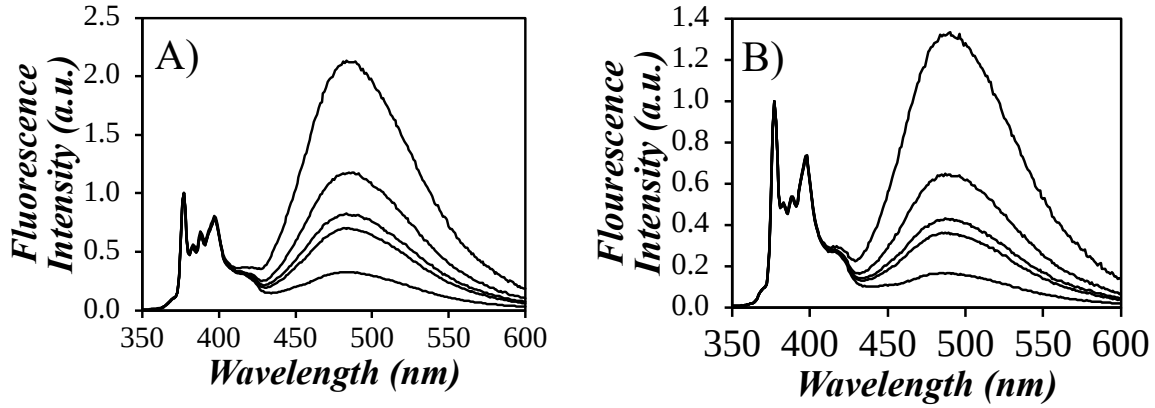

Figure 5.1. Steady state fluorescence spectra for the $PyEG_5$-PEG_9MA series in A) THF and B) water, ranging in pyrene content from 2.9 to 10.2 mol %. $[Py] = 2.5\times10^{-6}$ M and $\lambda_{ex} = 344$ nm.

Since the excimer fluorescence intensity in Figure 5.1 was much larger, relative to the fluorescence intensity of the pyrene monomer in THF than in water, it could be concluded that $PyEG_5$-PEG_9MA generated excimer much more efficiently in THF. This result was surprising, because pyrene excimer formation (PEF) depends on the local concentration ($[Py]_{loc}$) of ground-state pyrene experienced by an excited pyrene. Since $[Py]_{loc}$ would be expected to be much larger in water, due to aggregation of the hydrophobic pyrenyl labels, compared to an organic solvent where the pyrenyl labels are solvated, PEF for a pyrene-labeled water-soluble polymer (Py-WSP) is typically much more efficient in water than in an organic solvent, as has been reported numerous times in the literature.[48–52]

The PEF efficiency can be quantified from the monomer-to-excimer fluorescence intensity ratio, namely the I_E/I_M ratio, which was plotted in Figure 5.2 in THF and water as a function of the pyrene content of the different $PyEG_5$-PEG_nMA samples. The I_E/I_M ratio is proportional to the product of the bimolecular rate constant for PEF by diffusive encounters, k_{diff}, and $[Py]_{loc}$ as described in Equation 5.3.

$$\frac{I_E}{I_M} \propto k_{diff} \times [Py]_{loc} \tag{5.3}$$

When a Py-WSP is dissolved in water, aggregation of the insoluble pyrenyl labels leads to an increase in $[Py]_{loc}$, which results in an I_E/I_M ratio, that is typically much larger than the I_E/I_M ratio of the same polymer in an organic solvent, even if the viscosity of the organic solvent is much lower than that of water.[48–52]

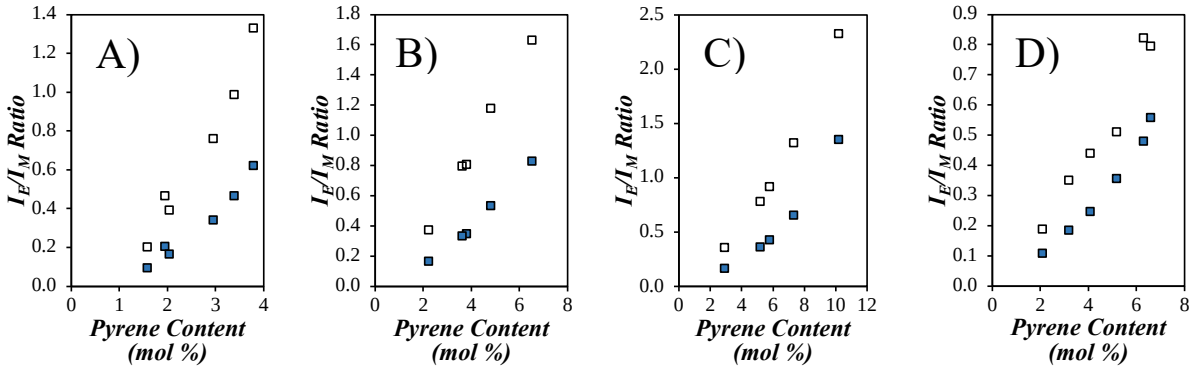

Figure 5.2. Plot of I_E/I_M ratio as a function of pyrene content for (A) $PyEG_5$-PEG_3MA, (B) $PyEG_5$-PEG_5MA, (C) $PyEG_5$-PEG_9MA, and (D) $PyEG_5$-$PEG_{19}MA$ in (□) THF and (■) water.

In fact, the hydrophobicity of pyrene is so strong that the formation of pyrene aggregates in water typically trumps variations in solvent viscosity, which affects k_{diff}. Despite these considerations, all the $PyEG_5$-PEG_nMA samples yielded a smaller I_E/I_M ratio in water than in THF, as can be seen in Figure 5.2. Each polymer was found to have a lower I_E/I_M ratio in water compared to THF regardless of the number of atoms, N_S, constituting the EG_n side chain. This is surprising,

considering that the $PyEG_5$-PEG_nMA samples were Py-WSPs. The implication of the I_E/I_M trends shown in Figure 5.2 is straightforward and indicates, namely, that the pyrenyl labels of the $PyEG_5$-PEG_nMA samples were not aggregated in water, despite their well-known hydrophobicity.

To support this statement, the excimer decays of four Py-WSPs acquired in water and in an organic solvent are shown in Table 5.5. The Py-WSPs were a pyrene-labeled hydrophobically modified alkali swellable emulsion polymer (Py(2.1)-HASE),[50] poly(*N*,*N*-dimethylacrylamide) (Py(5.2)-PDMA),[49] poly(*L*-glutamic acid) (Py(7.0)-PGA),[51] and a nanosized amylopectin fragment (Py(2.3)-NAF).[52] Their chemical structures are shown in Table 5.4 and the number in parenthesis represents the molar percentage of structural units labeled with pyrene. The fluorescence decays of the Py-WSPs were compared to those of $PyEG_5$-PEG_3MA in Table 5.5.

Table 5.4. Chemical structures of pyrene labeled polymers.

Py(2.1)-HASE	Py(5.2)-PDMA	Py(7.0)-PGA	Py(2.3)-NAF(57)
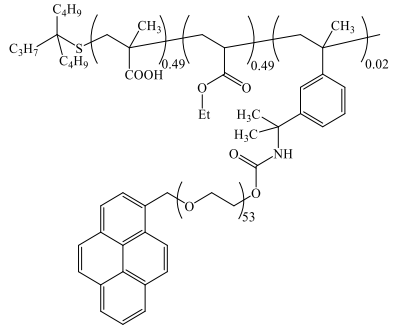	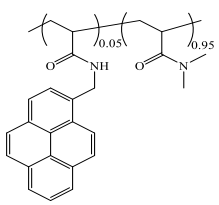	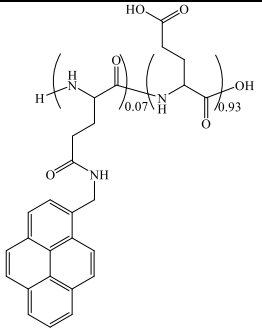	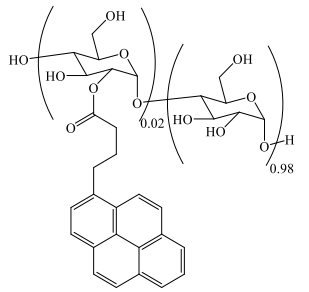

Upon visual inspection, the excimer fluorescence decays of all the Py-WSPs dissolved in an organic solvent exhibited a rise time before decaying. In aqueous solution, hardly any rise time could be detected for all Py-WSPs, with the exception of $PyEG_5$(3.7)-PEG_3MA, which had a well-defined rise time. The rise time was quantified by calculating the A_{E-}/A_{E+} ratio for each polymer.

The A_{E-}/A_{E+} ratio is obtained by fitting the excimer fluorescence decay with a sum of exponentials, and dividing the sum of the negative pre-exponential factors by the sum of the positive pre-exponential factors. An A_{E-}/A_{E+} ratio of zero indicates no rise time in the excimer fluorescence decay, with excimer being formed exclusively through direct excitation of pre-aggregated pyrenyl labels. In contrast, an A_{E-}/A_{E+} ratio equal to −1 indicates that PEF occurs solely through diffusive encounters between an excited and a ground-state pyrene. The A_{E-}/A_{E+} ratios ranged from −0.55 to −0.96 for all Py-WSPs in organic solvents. The less negative A_{E-}/A_{E+} ratios of −0.55 to −0.58 obtained for Py(7.0)-PGA and Py(2.3)-NAF in organic solvents are a consequence of the helical conformation adopted by the polypeptide and polysaccharide. The helical conformation resulted in a denser polymeric conformation, that brought the pyrenyl labels closer to each other, resulting in more pyrene aggregation and less negative A_{E-}/A_{E+} ratios.

The A_{E-}/A_{E+} ratios obtained for the Py-WSPs in aqueous solution ranged between 0.00 and −0.17, values that were much closer to 0 than the A_{E-}/A_{E+} ratios that were obtained for the same polymers in organic solvents, a clear result of pyrene aggregation induced by dissolution of the Py-WSP in water. The only exception was the A_{E-}/A_{E+} ratio of −0.63 for $PyEG_5$(3.7)-PEG_3MA in water. This A_{E-}/A_{E+} ratio was significantly more negative than the A_{E-}/A_{E+} ratio of the other Py-WSPs in aqueous solution listed in Table 5.5. In fact, it was even more negative than that of the Py(7.0)-PGA and Py(2.3)-NAF samples in organic solvents.

Table 5.5. TRF excimer decay and A_{E-}/A_{E+} values for pyrene labeled polymers in an organic solvent and aqueous solution.

	Py(2.1)-HASE	Py(5.2)-PDMA	Py(7.0)-PGA	Py(2.3)-NAF(57)	$PyEG_5(3.7)$-PEG_3MA
Organic solvent	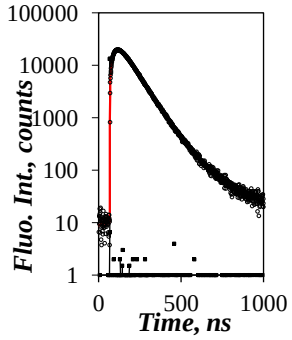	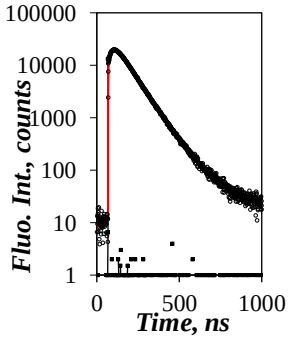	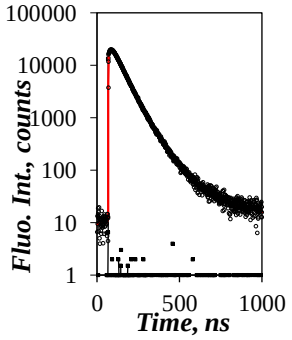	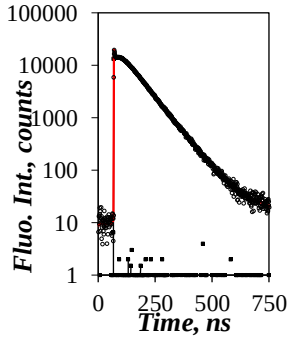	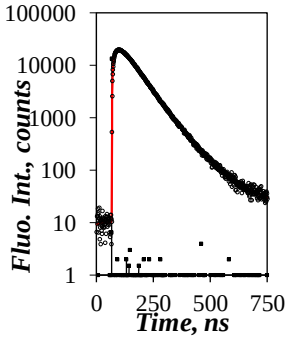
	THF [Poly] = 40 mg/L	DMF [Poly] = 6.3 mg/L	DMF [Poly] = 6.3 mg/L	DMSO [Poly] = 13.5 mg/L	THF [Poly] = 15.4 mg/L
A_{E-}/A_{E+}	–0.95	–0.80	–0.55	–0.58	–0.96
Aqueous solution	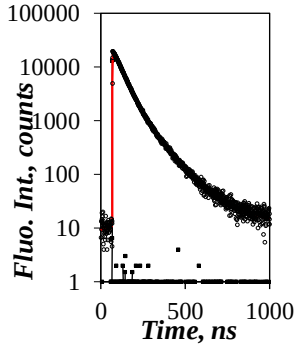	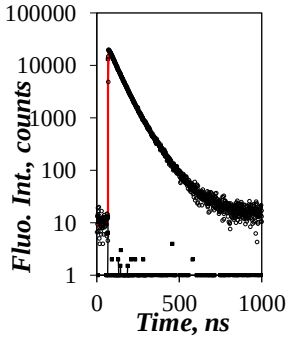	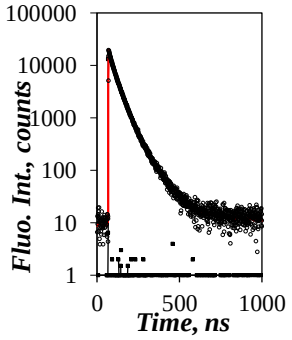	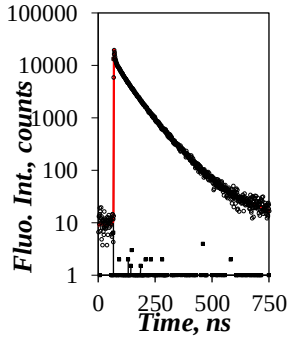	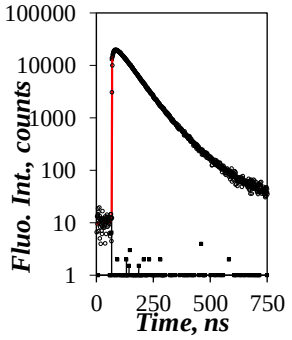
	Water pH 9 [Poly] = 30 mg/L	Water [Poly] = 6.3 mg/L	Water pH 9, 0.01 M Na_2CO_3, 0.05 M NaCl [Poly] = 6.3 mg/L	Water [Poly] = 13.5 mg/L	Water [Poly] = 15.4 mg/L
A_{E-}/A_{E+}	–0.17	–0.12	0.00	0.00	–0.63

While the extensive level of pyrene aggregation in the Py-HASE, Py-PDMA, Py-PGA, and Py-NAF samples dissolved in aqueous solution resulted in a large increase in the I_E/I_M ratio compared to its value for the same samples dissolved in an organic solvent, the much-reduced pyrene aggregation for the $PyEG_5$-PEG_nMA samples in water, demonstrated from the analysis of the excimer fluorescence decays, yielded much lower I_E/I_M ratios in water (see Figure 5.2).[49–52] These results suggest that the pyrenyl labels were not exposed to water when the $PyEG_5$-PEG_nMA samples were dissolved in water. Considering the architecture of the PEG_nMA samples, the pyrenyl labels must have located themselves close to the polymethacrylate backbone, where they experienced the crowded environment of the oligo(ethylene glycol) side chains.

Instead of being exposed to water, the pyrene labels of the $PyEG_5$-PEG_nMA samples must have experienced a medium similar to that of the ethylene glycol monomer used to prepare the EG_n side chains. To assess the validity of this hypothesis, $PyEG_5$-PEG_nMA samples were prepared with less than 1 mol % of pyrene (see exact pyrene content in Table 5.2) to generate isolated pyrenyl labels along the polymethacrylate backbone (the Py_{free}* species), that would not generate much excimer (small $[Py]_{loc}$ in Equation 5.3). The 1-pyrenemethoxy derivative was chosen to prepare the $PyEG_5$-PEG_nMA samples because of its sensitivity to the polarity of its local environment,[42] which is reflected in a change in the fluorescence intensity ratio (I_1/I_3) between the first (I_1) and the third (I_3) peak in the SSF spectrum of the pyrene monomer. The I_1/I_3 ratio of the 1-pyrenemethoxy derivative varies from 1.77 in water to 0.65 in hexane, taking a value of 1.47 in THF.[53] The I_1/I_3 ratios were calculated for each polymer in water and THF (Table 5.6) and were found to match those expected from the literature.[53] The I_1/I_3 ratios of the $PyEG_5$-PEG_nMA samples did not change much with N_S in both THF and

water, and they were similar to the I_1/I_3 ratio of $PyEG_5$-OH in the respective solvents (see Table 5.6). The similarity between the I_1/I_3 ratios of the $PyEG_5$-PEG_nMA and $PyEG_5$-OH samples in water demonstrates that the pyrenyl derivatives experienced an environment whose polarity was similar to that of water. It was also similar to the I_1/I_3 ratio of $PyEG_5$-OH in ethylene glycol, found to equal 1.9. Since the I_1/I_3 ratio of $PyEG_5$-OH took a same value in water and ethylene glycol, it provided no information about the environment experienced by the pyrenyl labels in the $PyEG_5$-PEG_nMA samples dissolved in water, beside the fact that this medium was polar.

Instead, time-resolved fluorescence (TRF) measurements were conducted for the $PyEG_5$-PEG_nMA samples prepared with a low pyrene content. The fluorescence decays of the pyrene monomer in these samples were dominated by a single exponential, with a contribution representing more than 60 % of the total pre-exponential weight, and whose decay time was attributed to the natural lifetime (τ_M) of the pyrenyl label. The τ_M values retrieved from the fit of the fluorescence decays with a sum of exponentials are listed in Table 5.6. With an average value of 212 ± 3 ns, the lifetime of the 1-pyrenemethoxy derivative bound to PEG_nMA dissolved in water was significantly larger than the lifetime of 137 ns for the $PyEG_5OH$ model compound in water. Since the lifetime of pyrene in polar solvents is typically controlled by the solubility of oxygen in the solvent, where oxygen is an efficient pyrene quencher, and the solvent viscosity, dramatic increases in the lifetime of pyrene have been observed when pyrene binds to a WSP, which hinders the accessibility of pyrene to oxygen dissolved in water.[54,55] The increase in τ_M from 137 ns for $PyEG_5$-OH free in water to 212 ns for $PyEG_5$-OH bound to

PEG_nMA dissolved in water is another example of this effect, where the pyrenyl derivative probes the ethylene glycol-rich environment generated by the side chains of the $PyEG_5$-PEG_nMA samples in water.

Table 5.6. I_1/I_3 value in water and THF and the natural lifetime, τ_M, in water for each $PyEG_5$-PEG_nMA sample and the $PyEG_5$-OH model compound.

Sample	I_1/I_3 in Water	I_1/I_3 in THF	τ_M (ns) in Water
$PyEG_5$-PEG_3MA	1.8 ± 0.017	1.5 ± 0.014	210
$PyEG_5$-PEG_5MA	1.8 ± 0.017	1.6 ± 0.024	215
$PyEG_5$-PEG_9MA	1.9 ± 0.0077	1.5 ± 0.042	213
$PyEG_5$-$PEG_{19}MA$	1.9 ± 0.015	1.6 ± 0.090	209
$PyEG_5$-OH	1.9	1.5	137

In an effort to assess the water content of the environment close to the polymethacrylate backbone probed by the pyrenyl labels, the lifetime of $PyEG_5$-OH was measured in mixtures of water and ethylene glycol. Plotting the lifetime of $PyEG_5$-OH as a function of the water content in the mixtures in Figure 5.3 showed that the lifetime increased with decreasing water content, reaching a value of 209 ns for $PyEG_5$-OH in pure ethylene glycol. Since the lifetime of $PyEG_5$-OH free in ethylene glycol (see Figure 5.3) or bound to PEG_nMA in water (see Table 5.6) were similar, it suggested that the environment probed by the pyrenyl derivatives in the $PyEG_5$-PEG_nMA samples seemed to be devoid of water and similar to that of ethylene glycol.

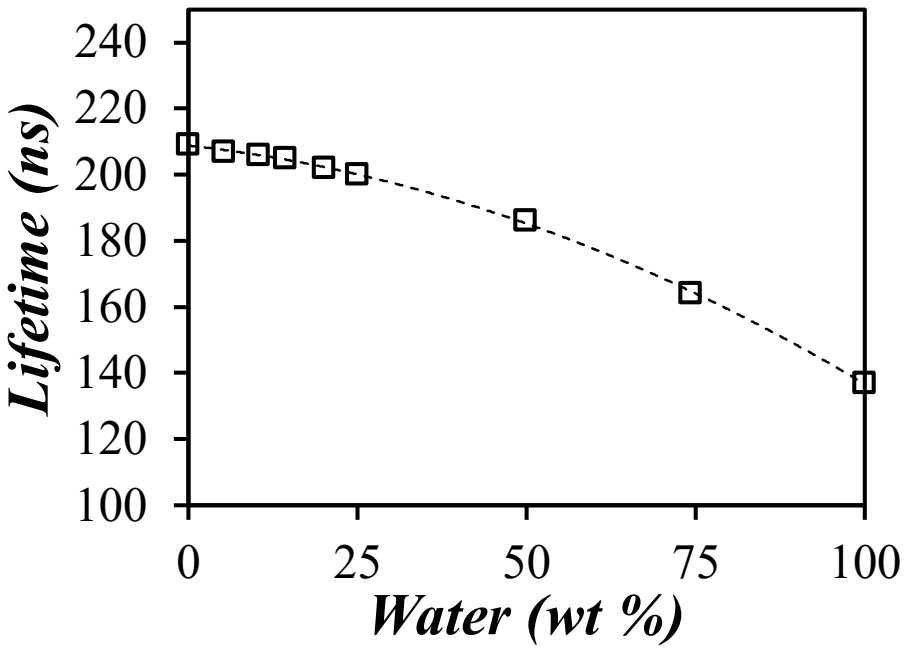

Figure 5.3. Lifetime of $PyEG_5$-OH model compound in mixtures of water and ethylene glycol solutions.

The conclusion reached at this point about the conformation adopted by the $PyEG_5$-PEG_nMA samples in water and THF was that the pyrene-terminated penta(ethylene glycol) side chain would stretch into THF to maximize its interactions with the solvent, but fold back in water to allow the hydrophobic pyrenyl label to probe the organic-like environment concentrated around the polymethacrylate backbone. These concepts were illustrated in Figure 5.4, which demonstrates the expected conformation of the $PyEG_5$ side chains of the $PyEG_5$-PEG_nMA samples in water and THF. In turn, the substantial differences in the conformation adopted by the $PyEG_5$ side chains should result in an excited pyrene probing a much smaller

volume in water than in THF. To assess the validity of this claim, the FBM was applied to the global analysis of the pyrene monomer and excimer fluorescence decays of the $PyEG_5$-PEG_nMA samples. The FBM compartmentalizes the pyrene-labeled macromolecules into sub-volumes called *blobs* whose size is characterized by N_{blob}, the number of structural units of the macromolecule found inside a *blob*.

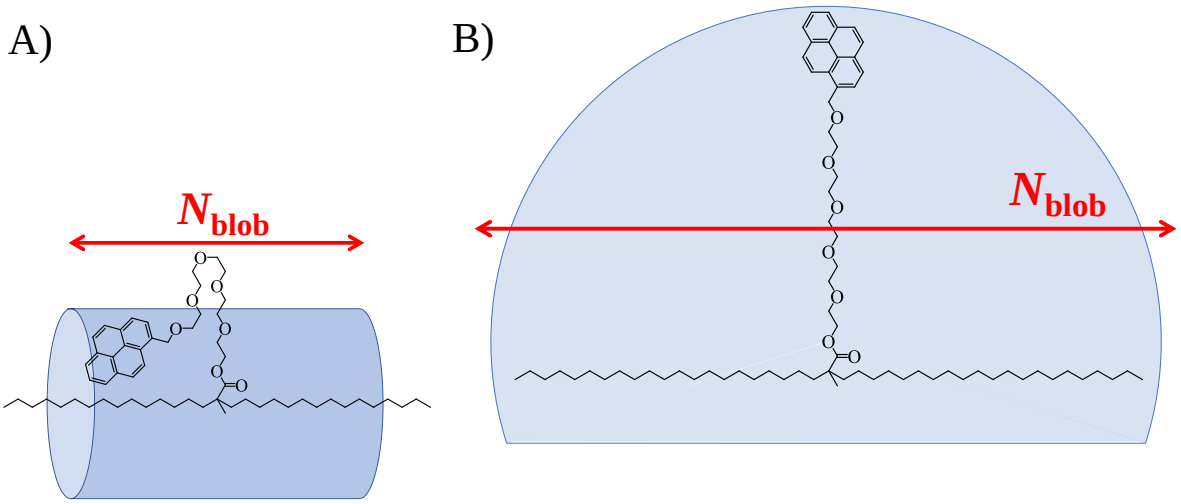

Figure 5.4. Schematic representation of the volume probed by a pyrenyl label bound to a PEG_nMA sample in A) water and B) THF.

The pyrene monomer and excimer TRF decays of the $PyEG_5$-PEG_nMA samples were acquired in water and THF and analyzed with the FBM to yield N_{blob} (see Equation 5.2). The N_{blob} values retrieved from this analysis were plotted in Figure 5.5A as a function of pyrene

content for the PyEG$_5$-PEG$_{19}$MA series in THF and water. The trend shown in Figure 5.5A indicates that N_{blob} did not change much with pyrene content, thus demonstrating that the presence of the pyrenyl labels did not affect the conformation and dynamics of the PyEG$_5$-PEG$_n$MA samples. N_{blob} took an average value of 28 ± 2 and 15 ± 1 structural units in THF and water, respectively. Since N_{blob} is a measure of the volume probed by an excited pyrenyl label, the decrease in N_{blob} from 28 in THF to 15 in water could be a result of either the increase in solvent viscosity from that of THF ($\eta_{25°C}$ = 0.46 mPa.s)[56] to that of water (($\eta_{25°C}$ = 0.89 mPa.s),[56] or the localization of pyrene in an environment close to the polymer backbone (see Figure 5.4).

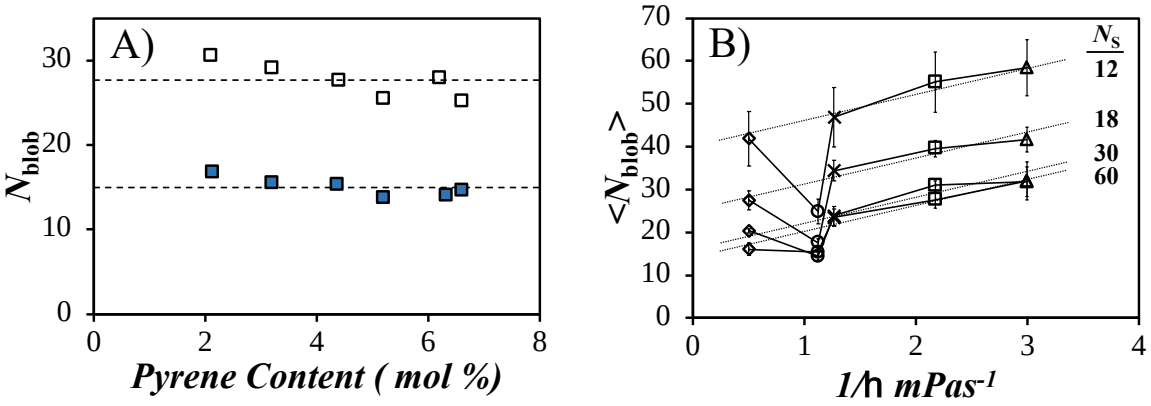

Figure 5.5. Plot of A) N_{blob} versus pyrene content for PyEG$_5$-PEG$_{19}$MA in (■) water and (□) THF and B) $<N_{blob}>$ versus η^{-1} for PyEG$_5$-PEG$_n$MA in (◆) DMSO, (○) water, (✖) DMF, (□) THF, and (▲) ACN, where the lines connecting data correspond top to bottom to PyEG$_5$-PEG$_3$MA, PyEG$_5$-PEG$_5$MA, PyEG$_5$-PEG$_9$MA, and PyEG$_5$-PEG$_{19}$MA, respectively.

To assess whether an increase in solvent viscosity would lead to a decrease in N_{blob} similar to that observed from THF to water, the average N_{blob} values, $\langle N_{blob} \rangle$, of $PyEG_5$-PEG_nMA in water were compared to those acquired in Chapter 4 in different organic solvents (acetonitrile (ACN, $\eta_{25°C}$ = 0.37 mPa.s), THF ($\eta_{25°C}$ = 0.46 mPa.s), *N*,*N*-dimethylformamide ($\eta_{25°C}$ = 0.79 mPa.s), and dimethyl sulfoxide (DMSO, $\eta_{25°C}$ = 1.99 mPa.s)).[56] $\langle N_{blob} \rangle$ was found to increase gently with the inverse of solvent viscosity in Figure 5.5B, indicating that a pyrene label would probe more monomer units with decreasing solvent viscosity. This trend was interrupted by a marked breakpoint corresponding to the $\langle N_{blob} \rangle$ obtained in water. Consequently, the anomalous decrease of $\langle N_{blob} \rangle$ in water shown in Figure 5.5B could not be due to an increase in solvent viscosity. Rather, the excited pyrenyl label is confined to a region close to the polymethacrylate backbone in water, which reduces its mobility and results in the smaller $\langle N_{blob} \rangle$ value, as depicted in Figure 5.4A.

N_{blob} is known to depend critically on the reach, and thus the linker length, of the excited pyrenyl label bound to a polymer. An increase in linker length always results in an increase in N_{blob}.[57–59] Consequently, the significant decrease in $\langle N_{blob} \rangle$ observed in Figure 5.5B for the $PyEG_5$-PEG_nMA samples in water suggests that the excited pyrenyl labels probe a volume equivalent to that described by a pyrenyl label bound to the polymethacrylate backbone via a shorter linker. To investigate the validity of this statement further, the $\langle N_{blob} \rangle$ values obtained for the $PyEG_5$-PEG_nMA samples in water and THF were compared in Figure 5.6A to those obtained earlier for a series of poly(alkyl methacrylate)s labeled with 1-pyrenebutanol (PyC4-PC_nMA with n = 1, 4, 6, 8, 12, and 18) in THF,[60] along with a PyC4-$PEG_{19}MA$ sample,

which was synthesized by copolymerizing 1-pyrenebutyl methacrylate with $EG_{19}MA$ (see chemical structure in Figure 5.1). The PyC4-PC_nMA samples, prepared with a shorter linker connecting the pyrenyl label to the polymethacrylate backbone, were insoluble in water. They yielded $<N_{blob}>$ values in THF that were consistently and substantially smaller than the $<N_{blob}>$ values obtained with the $PyEG_5$-PEG_nMA samples in THF, where the pyrenyl label was connected to the polymethacrylate backbone with a penta(ethylene glycol)-long linker. In contrast, the $<N_{blob}>$ vs. N_S trend in Figure 5.6A obtained for the $PyEG_5$-PEG_nMA samples in water lined up perfectly with that of the PyC4-PC_nMA samples in THF. This result suggested that in water, the pyrenyl label tethered to the polymethacrylate backbone via a penta(ethylene glycol) linker containing 18 atoms probed a volume similar to that of a 1-pyrenebutyl methacrylate linker in THF, containing 6 atoms. Molecular mechanics optimizations (MMOs) were conducted with HyperChem to measure the length between the α–carbon on the polymethacrylate backbone and the tip of the pyrene label. This distance, equal to 1.8 nm, can be viewed as the radius of the cylinder having the polymethacrylate backbone at its center, whose ethylene glycol-like environment enables the solubilization of hydrophobic pendants like pyrene. The consequence of this effect is that the pyrenyl label of the $PyEG_5$-PEG_nMA samples is held much closer to the polymethacrylate backbone than would be expected from the fairly long penta(ethylene glycol) linker.

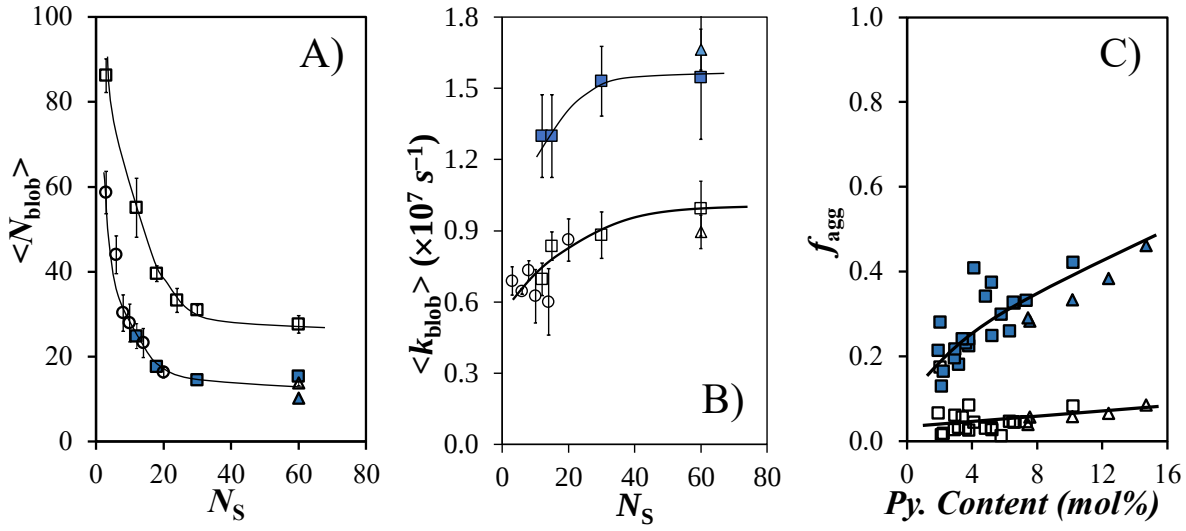

Figure 5.6. Plot of A) $<N_{blob}>$ and B) $<k_{blob}>$ versus N_S in (blue) water and (white) THF and C) f_{agg} versus pyrene content in (blue) water and (white) THF. (□) $PyEG_5$-PEG_nMA, (○) PyC_4-PC_nMA, and (△) PyC_4-$PEG_{19}MA$.

The rate constant of excimer formation within a *blob* averaged over all pyrene contents for a same polymer series, $<k_{blob}>$, was plotted as a function of N_S in Figure 5.6B for both the $PyEG_5$-PEG_nMA and PyC4-PC_nMA series in water and THF. Interestingly, all $<k_{blob}>$ values obtained in a given solvent clustered around two distinct master curves, which yielded much smaller $<k_{blob}>$ values in THF than in water. For the $PyEG_5$-PEG_nMA samples studied in water and THF, k_{blob} was found to be 1.7 (± 0.2) times larger in water than in THF. Unfortunately, these differences in k_{blob} resulting from a change in solvent are difficult to interpret due to the probability of forming an excimer upon encounter between an excited and a ground-state pyrene, which depends strongly on solvent. The similar $<k_{blob}>$ vs. N_S trends obtained for the

PyC4-PC_nMA and $PyEG_5$-PEG_nMA samples in THF was consistent with the observation made earlier, that $<k_{blob}>$ does not appear to depend much on the spacer length as long as the linker is constituted of at least 6 atoms, as is the case for the PyC4-PC_nMA series.

Finally, the molar fraction (f_{agg}) of aggregated pyrenyl labels could be determined from the FBM analysis of the fluorescence decays. In THF, f_{agg} was always lower than 0.09, thus reflecting the good solubility of pyrene in this solvent. Out of the 26 $PyEG_5$-PEG_nMA samples studied in water, 23 (i.e. 88%) had an f_{agg} value of less than 0.40 and all f_{agg} values were lower than 0.46. This range of f_{agg} values indicates that some pyrene aggregation took place, but that a majority of pyrenyl labels were solubilized in the aqueous $PyEG_5$-PEG_nMA solutions. This represents a rather low level of pyrene aggregation for aqueous solutions of Py-WSPs, which agrees with the conclusions drawn earlier from the A_{E-}/A_{E+} values reported in Table 5.5, which were much more negative than anticipated.

All the results thus far suggest that the polymethacrylate backbone is surrounded by an organic-like domain (OLD), which is able to solubilize the hydrophobic pyrenyl pendants. The pyrenyl terminal of the 18 atom-long penta(ethylene glycol) linker was found to be partly soluble in the medium close to the PEG_nMA backbone, where it probed a volume similar in size to that probed by a pyrenyl bound to the end of a much smaller 6 atom-long butyl ester linker. The fact that a pyrenyl group covalently bound to PEG_nMA would interact strongly with its core when dissolved in water led to the suggestion that free pyrene in water might actually bind to PEG_nMA. To this end, pyrene loading experiments were conducted with a series of PEG_nMA homopolymers, where n = 3, 5, 9, 19. As described in the Experimental

section, pyrene crystals were added to a vial containing an aqueous solution of PEG_nMA of known concentration. The supernatant was collected, and its absorbance measured at different time intervals until the absorbance reached a plateau, as shown in Figure 5.7A, before being returned to the vial. Similar experiments were conducted at different PEG_nMA concentrations and the pyrene absorbance at the plateau was plotted as a function of PEG_nMA concentration in Figure 5.7B. The linear increase in absorbance with increasing PEG_nMA concentration, observed in Figure 5.7B, could be rationalized by considering the equilibrium in Equation 5.4 leading to the relationship in Equation 5.5 between the polymer concentration and the concentration ratio ($[Py]_b/[Py]_f$) of pyrene bound to the polymer and free in water. Considering the law of mass conservation in Equation 5.6, and the fact that the solution absorbance in Equation 5.7 is equal to the sum of the absorbance of the different species in solution, Equation 5.8 could be derived that predicts a linear relationship between pyrene absorbance and PEG_nMA concentration.

$$Py_{free} + Poly \overset{K_{eq}}{\rightleftarrows} Py_{bound} \tag{5.4}$$

$$\frac{[Py]_b}{[Py]_f} = K_{eq} \times [Poly] \tag{5.5}$$

$$[Py] = [Py]_f + [Py]_b \tag{5.6}$$

$$Abs = \left(\varepsilon_b [Py]_b + \varepsilon_f [Py]_f\right) \times l \tag{5.7}$$

$$Abs = \left(\varepsilon_b l K_{eq} [Py]_f\right) \times [Poly] + \varepsilon_f l [Py]_f \qquad (5.8)$$

In Equations 5.5 – 5.8, $[Py]$, $[Py]_f$, $[Py]_b$, $[Poly]$, K_{eq}, ε_f, ε_b, and l are the total pyrene concentration, the concentrations of free pyrene in water and pyrene bound to the polymer, the polymer concentration, the constant for the equilibrium shown in Equation 5.4, the molar extinction coefficient of free and bound pyrene, and the path length of the absorbance cell, respectively. $[Py]_f$ represents the solubility limit of pyrene in water, known to equal 0.7 μM, and ε_f has been determined to equal 32,600 $M^{-1}cm^{-1}$ at 335 nm.[46,47] Based on Equation 5.8, the absorbance is expected to increase linearly with increasing polymer concentration with a slope (m) and intercept (p) equal to $\varepsilon_b l K_{eq}[Py]_f$ and $\varepsilon_f l[Py]_f$ (= 0.023, assuming a standard pathlength of 1.0 cm), respectively. This prediction is well-obeyed in Figure 5.7B.

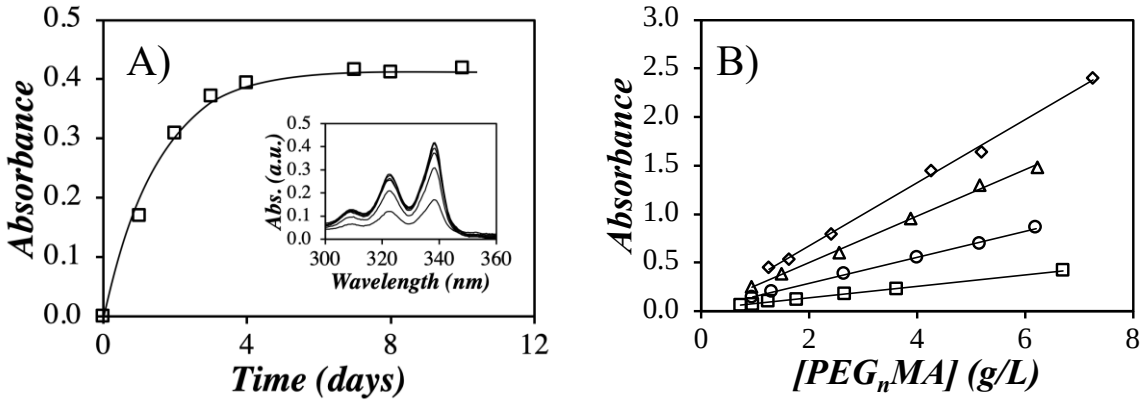

Figure 5.7. A) Plot of absorbance at 338.5 nm as a function of time for $PEG_{19}MA$ at 6.7 g/L. Insert: Absorbance spectra for a 6.7 g/L $PEG_{19}MA$ aqueous solution taken at 1, 2, 3, 4, 7, 8,

and 10 days. B) Plot of pyrene absorption as a function of (□) $PEG_{19}MA$, (○) PEG_9MA, (△) PEG_5MA, and (◇) PEG_3MA concentration after reaching equilibrium.

The y-intercepts of Figure 5.7B were expected to yield $[Py]_f$ based on Equation 5.8, which could then be used to determine K_{eq} from the slope of the straight lines. Unfortunately, the intercepts of the straight lines in Figure 5.7B yielded greater than 20% error, which prevented the determination of $[Py]_f$. Consequently, the known value of 0.7 μM was substituted for $[Py]_f$ to determine K_{eq} for each PEG_nMA sample.[46,47] ε_b was calculated and found to equal 33,500 ± 400 $M^{-1}cm^{-1}$ at 338.5 nm, as shown in Figure S5.6. K_{eq} was then calculated using the slopes obtained from Figure 5.7B and was found to equal 13.8 ± 0.1, 10.2 ± 0.1, 5.7 ± 0.0, and 2.5 ± 0.0 L/g for PEG_3MA, PEG_5MA, PEG_9MA, and $PEG_{19}MA$, respectively. All of the research conducted thus far has been indicative of an OLD, which surrounds the polymethacrylate main chain and is independent of the length of the EG_n side chain. Therefor, the binding of molecular pyrene should be less efficient at a given PEG_nMA concentration for a larger *n* value, as was indeed observed experimentally. Since pyrene is believed to bind to only a fraction of the polymer, close to the polymethacrylate main chain, the binding equilibrium described by Equation 5.4 could be refined with Equation 5.9, that reflected the binding of pyrene to the OLD. The concentration of polymer constituting the OLD, $[Poly]_{OLD}$, could be expressed by Equation 5.10 using the molar mass of the structural unit constituting the OLD (M_{OLD}) and the molar mass of the EG_nMA structural unit (M_0). The ratio $[Py]_b/[Py]_f$

could then be rewritten in Equation 5.11, which predicts that K_{eq} should be inversely proportional to M_0 of the PEG_nMA samples.

$$Py_{free} + Poly_{OLD} \overset{K'}{\rightleftarrows} Py_{bound} \tag{5.9}$$

$$[Poly]_{OLD} = [Poly] \times \frac{M_{OLD}}{M_0} \tag{5.10}$$

$$\frac{[Py]_b}{[Py]_f} = K' \times \frac{M_{OLD}}{M_0} \times [Poly] = K_{eq} \times [Poly] \tag{5.11}$$

Plotting K_{eq} as a function of M_0^{-1} yielded a straight line in Figure 5.8A, indicating that K_{eq} is proportional to M_0^{-1}, and that the binding of a hydrophobe to the PEG_nMA samples decreases with increasing M_0. This result is opposite to what would be expected, as an increase in the part of the polymer to which pyrene binds should lead to an increase in binding, and thus K_{eq}. This result further supports the notion of the existence of an OLD surrounding the polymethacrylate backbone of the PEG_nMA samples.

The loading capacities, taken as $[Py]_b/[Poly]$, were then calculated for each PEG_nMA sample. They were found to increase linearly with increasing M_0^{-1} and N_S^{-1} in Figures 5.8B and C, respectively. These trends indicated that the binding of the hydrophobic pyrene to PEG_nMA became less efficient with increasing n. This result is reasonable, as pyrene is believed to bind to the OLD generated around the polymethacrylate backbone of the PEG_nMA

samples. Past a certain critical side chain length, increasing the length of the EG_n side chain does not contribute to the OLD.

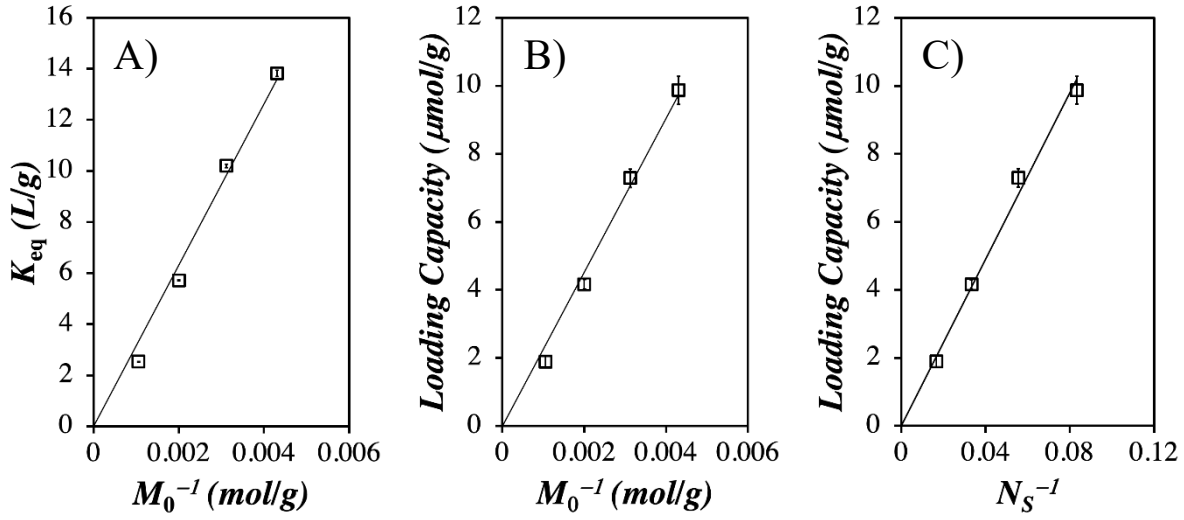

Figure 5.8. Plot of A) K_{eq} as a function of M_0^{-1}, B) loading capacity as a function of M_0^{-1}, and C) loading capacity as a function of N_S^{-1}.

5.5 Conclusion

The interior of a series of poly(oligo(ethylene glycol) methyl ether methacrylate) (PEG_nMA) samples was investigated using the chromophore pyrene and pyrene excimer fluorescence (PEF). The pyrene-labeled $PyEG_5$-PEG_nMA (with n = 3, 5, 9, 19) and PyC_4-$PEG_{19}MA$ samples, where the pyrene label was linked to the polymethacrylate backbone via a penta(ethylene glycol) and a butyl linker, respectively, were investigated in a good (THF) and poor (water) solvent for pyrene. Both solvents could properly solvate the PEG_nMA polymers.

All the results obtained from this pyrene fluorescence study demonstrate that the dense grafting density of the EG_n side chains stemming outward from the central polymethacrylate backbone of the PEG_nMA samples generates a water-free ethylene glycol-like environment in water, and that this environment can solvate organic molecules like pyrene. This organic-like domain (OLD) can be viewed as a cylinder with a 1.8 nm radius, based on the PEF measurements conducted with the PyC4-PC_nMA series in THF. As the EG_n side chains extend outward into the water phase and past the OLD, they become solvated with water molecules and no longer participate in the OLD close to the polymethacrylate backbone. Consequently, increasing the EG_n side chain length does not increase the volume of the OLD surrounding the polymethacrylate backbone resulting in the apparent reduction in K_{eq} and loading capacity reported in Figure 5.8 of pyrene to the PEG_nMA samples. Together, these data suggest that PEG_nMAs are a unique class of water-soluble polymers capable of solvating a hydrophobic pendant in water. The dense grafting density afforded by the PBB architecture allows the EG_n side chains to solvate hydrophobic organic molecules like pyrene, even when dissolved in aqueous solution. Consequently, this study demonstrates for the first time the existence of this OLD and should provide insight into the design of drug-polymer delivery systems and the establishment of drug release mechanisms.

Chapter 6

Concluding Remarks and Future Work

6.1 Summary of Accomplished work

Pyrene excimer fluorescence/formation (PEF) was used to characterize the conformation and internal dynamics of macromolecules with a complex architecture. The characterization of six generations of 2,2-bis(hydroxymethyl) propionic acid backbone dendrons and a series of poly(oligo(ethylene glycol) methyl ether methacrylate) (PEG_nMA with n = 0, 3, 4, 5, 7, 8, 9, 12, and 19) polymeric bottle brushes (PBBs) was conducted. The dendrons and PBBs were covalently labeled with a pyrenyl moiety, either homogenously or randomly, and then characterized by PEF-based techniques. Steady-state fluorescence (SSF) was applied to obtain qualitative information about the dynamics and conformations of the macromolecules in solution. These dynamics and conformations were then characterized in a quantitative manner through the analysis of the time-resolved fluorescence (TRF) decays using either the model free analysis (MFA) or the fluorescence blob model (FBM).

Chapter 2 focused on six generations of 2,2-bis(hydroxymethyl) propionic acid backbone dendrons, which were labeled at their terminal ends with 1-pyrenebutyric acid (Py_x-G(N)). The generation numbers N ranged from 1 to 6 and each dendron contained x (= 2^N) pyrene molecules. Dendrons, being monodisperse tree-like macromolecules, were used as spectroscopic standards to investigate the relationship between the concentration of the terminal ends versus their internal dynamics. Since the terminal ends were labeled with a pyrenyl moiety, the local concentration of pyrene, $[Py]_{loc}$, experienced by an excited pyrene reflected the concentration of terminal ends. $[Py]_{loc}$ was previously determined by calculating the average squared end-to-end distance between two pyrenyl groups, $\langle L_{Py}^2 \rangle$,[1] and the

dynamics of the terminal ends were studied in a variety of solvents including toluene, *N*,*N*-dimethylformamide (DMF), and dimethylsulfoxide (DMSO). The dynamics of the terminal ends were quantified by calculating the average rate constant, $\langle k \rangle$, for PEF using the MFA. $\langle k \rangle$ describes the formation of excimer between an excited and a ground-state pyrenyl molecule by diffusive encounters. However, PEF also occurred between pre-aggregated pyrenyl species. As dendrons reached the sixth generation, the fraction of aggregated pyrene, f_{agg}, increased to 20 – 35% in the different solvents. To account for the increase in aggregation with G(*N*), $\langle k \rangle$ was divided by the fraction f_{diff} of pyrenyl molecules forming excimer through diffusive encounters. Plots of $\langle k \rangle / f_{diff}$ – *vs* – $[Py]_{loc}$ yielded straight lines in each solvent, however, each with a different slope. The difference in slope was attributed to the influence on $\langle k \rangle$ of solvent viscosity, η, and the probability of PEF , *p*. To account for η and *p*, the model compound ethyl 4-(1-pyrene)butyrate (PyBE) was synthesized, and the average rate constant of excimer formed through diffusive intermolecular encounters, k_{diff}[inter], was determined in toluene, DMF, and DMSO and used to normalize the results obtained by the dendrons. A master plot of the Py_x-G(*N*) dendrons was constructed by plotting $\langle k \rangle / (f_{diff} \times k_{diff}[\text{inter}])$ vs. $[Py]_{loc}$, where all of the data in the three solvents, including the previously reported data in tetrahydrofuran (THF), collapsed onto a single straight line. The master straight line obtained experimentally for all six Py_x-G(*N*) dendrons in each of the four solvents demonstrated the linear relationship expected between $\langle k \rangle$ and $[Py]_{loc}$ and created a calibration curve independent of η and *p*, which could be used to compare the internal dynamics and conformation of other dendrons or branched macromolecules.

Following the successful establishment of a direct 1:1 correspondence between $<k>$ and $[Py]_{loc}$ for the pyrene-labeled dendrons in Chapter 2, Chapter 3 focused on using a similar approach to probe the conformation of the side chain ends of a series of PEG_nMA polymeric bottle brushes (PBBs). The conformation of the PBBs was probed in two studies. The first study, described in Chapter 3, involved the attachment of pyrenyl groups to each of the side chain ends of four PEG_nMA PBBs with n = 3, 5, 8, and 12 ethylene glycol units ($P(PyEG_nMA)$). Labeling of the terminal ends of the oligo(ethylene glycol) side chains enabled the specific study of the conformation and dynamics of the PBB side chains. The polymers were synthesized using a grafting-through technique and conventional radical polymerization. The macromonomers were monodisperse and prepared by labeling one end of the oligo(ethylene glycol) side chain with 1-pyrenemethanol. The singly end-labeled oligo(ethylene glycol) 1-pyrenemethyl ether derivative was then reacted with methacrylic anhydride to prepare the macromonomer with a methacrylate polymerizable end. $[Py]_{loc}$ was first calculated by determining the volume probed by the pyrene-labeled side chains. As a first approximation, pyrene was assumed to probe a spherical volume, whose diameter was defined by the linker length for a freely jointed chain, $n^{0.5} \times l$, which was assumed to adopt a Gaussian conformation. The MFA was used to calculate $<k>$ for the PBBs in THF, dioxane, DMF, and DMSO. To account for the differences in η and p, the model compound 1-pyrenemethoxy diethylene glycol methyl ether ($PyEG_2ME$) was synthesized and k_{diff}[inter] was calculated. A master plot of $<k>/(f_{diff} \times k_{diff}[\text{inter}])$ – *vs* – $[Py]_{loc}$ was then constructed for all $P(PyEG_nMA)$ samples in THF, dioxane, and DMF and it was compared to the master plot obtained in Chapter

2 for the pyrene-labeled dendrons. The trend for the PBBs was similar to that obtained for the dendrons, with the data showing good overlap. This study further demonstrated that the kinetics of PEF reflect $[Py]_{loc}$ and thus, the local density of the terminal ends of dendrons and PBBs, which can then be related to the conformation of the side chains of these macromolecules. For the P($PyEG_nMA$) samples, the results suggested that the side chains adopted a Gaussian conformation in solution.

Whereas the conformation of the side chain end groups of PBBs were investigated in Chapter 3, Chapter 4 focused on the conformation and dynamics experienced by the main chain of PBBs. To this end, penta(ethylene glycol) 1-pyrenemethyl ether methacrylate was copolymerized with seven oligo(ethylene glycol) methyl ether methacrylate macromonomers to prepare seven $PyEG_5$-PEG_nMAs with n = 0, 3, 4, 5, 7, 9, and 19 ethylene glycol units. PEF was applied to probe the PBB main chain conformation and stiffness as a function of increasing oligo(ethylene glycol) side chain length. The FBM was used to determine the average number of structural units encompassed within a *blob*, $<N_{blob}>$, for $PyEG_5$-PEG_nMA in acetonitrile, THF, DMF, and DMSO. A polymer which adopts a random coil conformation is expected to have a larger $<N_{blob}>$ compared to a polymer with a locally extended polymer backbone. $<N_{blob}>$ was monitored as a function of the number N_S of non-hydrogen atoms in the side chain of the $PyEG_5$-PEG_nMA ($N_S = n\times3+3$). $<N_{blob}>$ was found to decrease with increasing N_S for n = 0, 3, 4, 5, and 7 before plateauing for n = 9 and 19 in each of the four solvents. An increase in the side chain length caused increased steric repulsion between the side chains, which in turn caused the polymer main chain to locally extend. The extension of the polymer main chain

was reflected by the decrease of $<N_{blob}>$. The appearance of the plateau region for N_S values greater than 30 indicated that an increase in side chain length did not cause a further extension of the polymer main chain, leading to the conclusion that the main chain had reached a locally extended conformation. A plot of $<N_{blob}>$ versus N_S^{-2} produced straight lines with a *y*-intercept corresponding to an $<N_{blob}>$ equivalent to a PEG_nMA sample with an infinitely long side chain, $N_{blob}(\infty)$. However, the $N_{blob}(\infty)$ value calculated for the $PyEG_5$-PEG_nMA PBBs in each of the four solvents varied significantly and was found to be inversely proportional to solvent viscosity. This result was unexpected, since $N_{blob}(\infty)$ was expected to be independent of the solvent. An $N_{blob}(\infty)$ value that changes with solvent viscosity indicates that the FBM reported on both the conformation and the dynamics of the PBBs. If the polymer main chain was viewed as an ensemble of beads and springs similar to those used in the Rouse-Zimm model, the polymer in a more viscous solvent would have a larger effective spring constant, resulting in fewer monomeric units per unit time inside a *blob*. In contrast, a polymer in a less viscous solvent would have a smaller effective spring constant, resulting in more monomeric units per unit time being present inside a *blob*.

The $<N_{blob}>$ values obtained from the FBM analysis were then used in combination with the Kratky-Porod worm like chain (KPWLC) model to determine the persistence lengths, l_p, of each $PyEG_5$-PEG_nMA PBB. The l_p values calculated from the FBM analysis for each $PyEG_5$-PEG_nMA polymer were referred to as l_p(fluo) and were plotted against N_S^2. l_p(fluo) was found to increase linearly with increasing N_S^2, yielding a non-zero intercept as expected for a PBB with flexible side chains. Interestingly, l_p(fluo) was found to vary greatly with solvent

viscosity, with the l_p values in acetonitrile being 3 times larger than those calculated in DMSO. To confirm the validity of these results, intrinsic viscosity ($[\eta]$) measurements were conducted to monitor the changes in the hydrodynamic volume V_h of the PBBs with changing solvent. It was found that $[\eta]$ remained relatively constant within ± 20%, indicating that the changes in l_p(fluo) with solvent viscosity were due to the coupled response of polymer dynamics and conformation, when applying the FBM analysis to the fluorescence decays. In an attempt to separate the contribution of polymer conformation from that of polymer dynamics, all the $<N_{blob}>$ values were plotted as a function of η^{-1}, which produced straight lines for each $PyEG_5$-PEG_nMA polymer. The lines were extrapolated to the *y*-intercept to yield N_{blob}^o, which was the $<N_{blob}>$ value obtained in a hypothetical solvent of infinitely high viscosity and devoid of backbone dynamics. l_p^o values were calculated from N_{blob}^o, which corresponded to the persistence length of a polymer in an infinitely high viscosity solvent. Gel permeation chromatography (GPC) was also used to determine the l_p of the $PyEG_5$-PEG_nMA PBBs. The GPC was equipped with a multi-angle laser light scattering detector and a viscometer to generate conformation plots. The data were linearized using the Bohdanecky linearization method[2] and l_p was extracted from the slopes of the plots. l_p determined from the GPC analysis was found to be twice as large as l_p^o, a result which was attributed to the different length scales probed in the two experiments with PEF probing a small sub volume of the macromolecular volume and GPC probing the entire macromolecular volume generated by the PBBs.

In the final chapter, the $PyEG_5$-PEG_nMAs with n = 3, 5, 9, and 19 were characterized in an aqueous environment. Poly(ethylene glycol) is commonly used in drug delivery

applications to confer water solubility and stealth. While the PEG_nMA PBBs are fully water-soluble, the hydrophobic pyrenyl pendant is not. The ability of the oligo(ethylene glycol) side chains to shield the hydrophobe was investigated using the FBM. While higher f_{agg} values were obtained for the $PyEG_5$-PEG_nMAs in water compared to an organic solvent, f_{agg} remained lower than 50% for a polymer with 15 mol% pyrene labeling. These results led to the conclusion that the PBB architecture successfully shielded the hydrophobic load and kept the pyrene moieties isolated from one another. The volume probed by the pyrenyl moiety was also investigated by determining $<N_{blob}>$ for the $PyEG_5$-PEG_nMA PBBs in water. When compared to the results obtained in THF from Chapter 4, smaller $<N_{blob}>$ values were obtained in water. The results were then compared to an earlier study of a series of poly(alkyl methacrylates) (PAMAs), which had been labeled with a 1-pyrenebutyl derivative. The data obtained for the $PyEG_5$-PEG_nMA samples in water with the pyrenyl moiety attached to a 16 atom penta(ethylene glycol) linker were found to nicely overlap the data of the PAMAs studied in THF and labeled with a pyrenyl group separated from the main chain by a 4-atom linker. These results suggested that the hydrophobic pyrene pendant was probing a much smaller volume in water than in an organic solvent like THF and that the volume probed in water by pyrene attached to a 16-atom long linker was similar to the volume described by a pyrene group attached to a 4-atom linker in THF. This local volume probed by pyrene was generated by the EG_n side chains, which were densely packed around the main chain and afforded an organic-like domain (OLD), which solubilized the pyrenyl pendants. The length of the EG_n side chains did not seem to increase the volume of the OLD surrounding the polymethacrylate backbone.

The loading capacity of molecular pyrene in aqueous solutions of four unlabeled poly(ethylene glycol methyl ether methacrylate) (PEG_nMA, with n = 3, 5, 9, and 19) was then determined. Loading of molecular pyrene into the PEG_nMA homopolymers was monitored using UV-Vis spectroscopy, which allowed for the determination of the equilibrium constant, K_{eq}, for the binding of pyrene to the PBBs in water. K_{eq} was found to increase with the inverse of the molecular weight of the macromonomer M_0, indicating that the binding of the hydrophobe pyrene decreased with increasing M_0, as was expected if binding occurred solely to the OLD generated around the main chain. The loading capacities were determined and found to follow a similar trend of decreasing loading capacity with increasing M_0.

In summary, these studies conducted on pyrene-labeled dendrons and PBBs supported the notion, that PEF responds to $[Py]_{loc}$, which is itself proportional to the local macromolecular density and dynamics. This information was then applied to assess the conformation of the side chains of dendrons and PBBs, which were found to be well described by assuming Gaussian statistics, and how the l_p of PBBs varied with increasing side chain length. This body of experiments suggests that PEF represents an alternative experimental means to probe the internal conformation and dynamics of macromolecules in solution and should complement already well-established techniques based on scattering (static light, small angle X-ray, or small angle neutron scattering) or viscosity measurements.

6.2 Future Work

The studies conducted in Chapters 2 and 3 of this thesis open a new area of research relating the dynamics of the terminal ends of branched macromolecules to their local concentration. Using pyrene excimer fluorescence (PEF), the terminal ends of a macromolecule were chemically modified with a pyrene derivative and studied using the model free analysis (MFA). So far, a series of dendrons and polymeric bottle brushes have shown that the average rate constant $<k>$ of pyrene excimer fluorescence is proportional to the local concentration of pyrene, $[Py]_{loc}$. This relationship was used to generate a calibration curve, that can now be used to study a variety of branched macromolecules including star, comb, or hyperbranched/arborescent macromolecules to investigate their internal dynamics and conformation.[3,4]

Chapter 4 of this thesis focused on the conformation and dynamics of the main chain of PBBs. To further characterize the PBB architecture over a longer length scale, a follow up study with a pyrene derivative attached onto a longer oligo(ethylene glycol) linker would be of interest. As the linker length increases, the volume probed by the pyrene derivative will also increase. The decays can be acquired in a variety of solvents and analyzed with the FBM to determine the average number of monomer units encompassed within a *blob*, $<N_{blob}>$. The study of interest would be to monitor how the volume probed by an excited pyrene changes with increasing linker length. Using a longer linker for the pyrene labeled linker would give a third set of data for the PEG_nMA series. This thesis has utilized pyrene bound to a penta(ethylene glycol) linker and a master's student in the Duhamel laboratory is currently

using a 1-pyrenebutyl linker. Combining molecular mechanics optimization simulations, which are used to determine the theoretical N_{blob}^{theo} value, with the results from the FBM, which determines the experimental N_{blob}^{exp} value, the volume probed by the pyrene pendant can be investigated with respect to linker length. The densely grafted side chains are believed to have an influence on the volume probed by pyrene by hindering its diffusion. This study would further our understanding of the environment afforded by densely grafted PBBs.

Another interesting experiment would involve the co-polymerization of a lower molecular weight macromonomer, such as di(ethylene glycol) methyl ether methacrylate (EG_2MA), with a higher molecular weight side chain, such as $EG_{19}MA$, to quantify the changes in polymer main chain flexibility with changes in copolymer composition. Application of the *blob*-based approach to determine l_p^o would relate the change in main chain stiffness to the copolymer composition and it would be interesting to check if it follows theoretically expected trends.[5]

Chapter 5 demonstrated that PEG_nMA PBBs generate an organic-like domain centered around the polymer main chain. It was found that in water, a pyrenyl label attached to a 16 atom long penta(ethylene glycol) linker probed a volume that was smaller than expected, and which was similar to that probed by a pyrenyl group attached to a 4-atom linker. It would be interesting to study the changes in $<N_{blob}>$ for a series of PEG_nMA PBBs with a pyrene derivative attached onto a longer oligo(ethylene glycol) linker, to see if a similar conclusion could be reached. Such a study would solidify the conclusion that contrary to organic solvents, where a longer linker connecting pyrene to the polymethacrylate backbone results in a larger

N_{blob},[6] the same longer linker would not be expected to yield a larger *blob* in water since the hydrophobic pyrene would be probing the same organic-like environment surrounding the polymethacrylate backbone.

The overarching goal was to formulate the idea that PEF in pyrene-labeled macromolecules and $[Py]_{loc}$ provide information about the local internal density and dynamics of a polymer in solution. Scattering techniques have by far dominated the field of polymer characterization in solution, however, they require large concentrations of polymer sample prepared with a low dispersity. The major advantage of PEF is the ability to study polydisperse macromolecules at concentrations that are two-to-three orders of magnitude lower than those typically needed for any other type of techniques. The ability to apply PEF to study the conformation of polydisperse polymers, such as polynorbornene, or synthetic foldamers in solution at low concentrations represents an attractive alternative to scattering techniques.

References

Chapter 1

1. Jouenne, S.; Levache, B. Universal Viscosifying Behavior of Acrylamide-Based Polymers Used in Enhanced Oil-Recovery. *J. Rheol.* **2020**, *64*, 1295-1313.
2. Kazlauskas, R. Engineering more Stable Proteins. *Chem. Soc. Rev.* **2018**, *47*, 9026-9045.
3. Daniel, W. F. M.; Burdynska, J.; Vatankhah-Varnoosfaderani, M.; Mayjaszewski, K.; Paturej, J.; Rubinstein, M.; Dobrynin, A.; Sheiko, S. Solvent-Free, Supersoft and Superelastic Bottlebrush Melts and Networks. *Nat. Mater.* **2016**, *15*, 183-189.
4. Foster, M. P.; McElroy, C. A.; Amero, C. D. Solution NMR of Large Molecules and Assemblies. *Biochemistry* **2007**, *46*, 331-340.
5. Venditti, V.; Egner, T. K.; Clore, G. M. Hybrid Approaches to Structural Characterization of Conformational Ensembles of Complex Macromolecular Systems Combining NMR Residual Dipolar Coupling and Solution X-Ray Scattering. *Chem. Rev.* **2016**, *116*, 6305-6322.
6. Pelton, J. T.; McLean, L. R. Spectroscopic Methods for Analysis of Protein Secondary Structure. *Anal. Chem.* **2000**, *277*, 167-176.
7. Ortega, A.; Garcia de la Torre, J. Equivalent Radii and Ratios of Radii from Solution Properties as Indicators of Macromolecular Conformation, Shape, and Flexibility. *Biomacromolecules* **2007**, *8*, 2464-2475.

8. Morris, G. A.; Castile, J.; Smith, A.; Adams, G. G.; Harding, S. E. Macromolecular Conformation of Chitosan in Dilute Solution: A New Global Hydrodynamic Approach. *Carbohydr. Polym.* **2009**, *76*, 616-621.
9. Dutertre, F.; Bang, K.-T.; Loppinet, B. ; Choi, I.; Choi, T.-L.; Fystas, G. Structure and Dynamics of Dendronized Polymer Solutions: Gaussian Coil or Macromolecular Rod. *Macromolecules* **2016**, *49*, 2731-2740.
10. Boyle, B. M.; Heinz, O.; Miyake, G. M.; Ding, Y. Impact of the Pendant Group on the Chain Conformation and Bulk Properties of Norbornene Imide-Based Polymers. *Macromolecules* **2019**, *52*, 3426-3434.
11. Lakowicz, J. R. Principles of Fluorescence Spectroscopy, 3rd Ed. Springer, 2006.
12. Förster, T.; Kasper, K. Ein Konzentrationsumschlag der Fluoreszenz des Pyrens. *Z. Elektrochem.* **1955**, *59*, 976-980.
13. Birks, J. B.; Dyson, D. T.; Munro, I. H. "Excimer" Fluorescence. II. Lifetime Studies of Pyrene Solutions. *Proc. Roy. Soc. A* **1963**, *275*, 575-588.
14. Cuniberti, C.; Perico, A. Intramolecular Excimer Formation in Polymers. Pyrene-Labeled Poly(vinyl acetate). *Eur. Polym. J.* **1980**, *16*, 887-893.
15. Duhamel, J. New Insights in the Study of Pyrene Excimer Fluorescence to Characterize Macromolecules and their Supramolecular Assemblies in Solution. *Langmuir* **2012**, *28*, 6527-6538.

16. Li, L.; Duhamel, J. Conformation of Pyrene-Labeled Amylose in DMSO Characterized with the Fluorescence Blob Model. *Macromolecules* **2016**, *49*, 7965-7974.
17. Li, L.; Kim, D.; Zhai, X.; Duhamel, J. A Pyrene Excimer Fluoresce (PEF) Study of the Interior of Amylopectin in Dilute Solution. *Macromolecules* **2020**, *53*, 6850-6860.
18. Duhamel, J.; Kanagalingam, S.; O'Brien, T.; Ingratta, M. Side-Chain Dynamics of an α–Helical Polypeptide Monitored by Fluorescence. *J. Am. Chem. Soc.* **2003**, *125*, 12810-12822.
19. Casier, R.; Duhamel, J. The Effect of Amino Acid Size on the Internal Dynamics and Conformational Freedom of polypeptides. *Macromolecules* **2020**, *53*, 9811-9822.
20. Casier, R.; Duhamel, J. Effect of Structure on Polypeptide Blobs: A Model Study Using Poly(L-lysine). *Langmuir* **2020**, *36*, 7980-7990.
21. Casier, R.; Duhamel, J. Effect of Like Charges on the Conformation and Internal Dynamics of Polypeptides Probed by Pyrene Excimer Fluorescence. *Macromolecules* **2020**, *53*, 5147-5157.
22. Hirayama, F. Intramolecular Excimer Formation. I. Diphenyl and Triphenyl Alkanes. *J. Chem. Phys.* **1965**, *42*, 3163-3171.
23. Eisinger, J.; Guéron, M.; Shulman, R. G.; Yamane, T. Excimer Fluorescence of Dinucleotides, Polynucleotides, and DNA. *Proc. Natl. Acad. Sci.* **1966**. *55*, 1015-1020.
24. Chandros, E. A.; Dempster, C. J. Intramolecular Excimer Formation and Fluorescence Quenching in Dinaphthylalkanes. *J. Am. Chem. Soc.* **1970**, *92*, 3586-3593.

25. Wilemski, G.; Fixman, M. Diffusion-controlled Intrachain Reactions of Polymers. I Theory. *J. Chem. Phys.* **1974**, *60*, 866-877.

26. Wilemski, G.; Fixman, M. Diffusion-controlled Intrachain Reactions of Polymers. II Results for a Pair of Terminal Reactive Groups. *J. Chem. Phys.* **1974**, *60*, 878-890.

27. Zachariasse, K.; Kühnle, W. Intramolecular Excimers with α,ω–Diarylalkanes. *Z. Phys. Chem. Neue F.* **1976**, *101*, 267-276.

28. Yamamoto, M.; Goshiki, K.; Kanaya, T.; Nishijima, Y. Intramolecular Excimer of Di(1-pyrenemethyleneoxycarbonyl) Alkanes. *Chem. Phys. Lett.* **1978**, *56*, 333-335.

29. Cuniberti, C.; Perico, A. Intramolecular Excimers and Microbrownian Motion of Flexible Polymer Molecules in Solution. *J. Eur. Polym.* **1977**, *13*, 369–374.

30. Winnik, M. A.; Redpath, T.; Richards, D. H. The Dynamics of End-to-End Cyclization in Polystyrene Probed by Pyrene Excimer Formation. *Macromolecules* **1980**, *13*, 328-335.

31. Svirskaya, P.; Danhelka, J.; Redpath, A. E. C.; Winnik, M. A. Cyclization Dynamics of Polymers: 7. Applications of the Pyrene Excimer Technique to the Internal Dynamics of Polydimethylsiloxane Chains. *Polymer* **1983**, *24*, 319-322.

32. Ghiggino, K. P.; Snare, M. J.; Thistlethwaite, P. J. Cyclization Dynamics in Poly(ethylene oxide). Chain Length and Temperature Dependence. *Eur. Polym. J.* **1985**, *21*, 265-272.

33. Winnik, M. A. End-to-End Cyclization of Polymer Chains. *Acc. Chem. Res*. **1985**, *18*, 73−79.

34. Boileau, S.; Méchin, F.; Martinho, J.M.G.; Winnik, M.A. End-to-end cyclization of a pyrene end-capped poly(bisphenol A-diethylene glycol carbonate). *Macromolecules* **1989**, *22*, 215–220.
35. Slomkowski, S.; Winnik, M.A. fluorescence quenching in pyrene/benzil end-labeled poly(tetramethylene oxide). Cyclization dynamics in polymers 19. *Macromolecules* **1986**, *19*, 500– 501.
36. Duhamel, J. Internal Dynamics of Dendritic Molecules Probed by Pyrene Excimer Formation. *Polymers* **2012**, *4*, 211-239.
37. Chen, S.; Duhamel, J.; Winnik, M. A. Probing End-to-End Cyclization Beyond Wilemski and Fixmann. *J. Phys. Chem. B* **2011**, *115*, 3289-3302.
38. Farhangi, S.; Duhamel, J. Long Range Polymer Chain Dynamics Studied by Fluorescence Quenching. *Macromolecules* **2016**, *49*, 6149-6162.
39. Duhamel, J. Global Analysis of Fluorescence Decays to Probe the Internal Dynamics of Fluorescently Labeled Macromolecules. *Langmuir* **2014**, *30*, 2307-2324.
40. Mathew, A.; Siu, H.; Duhamel, J. A *Blob* Model to Study Chain Folding by Fluorescence. *Macromolecules* **1999**, *32*, 7100-7108.
41. Tachiya, M. Application of a Generating Function to Reaction Kinetics in Micelles. Kinetics of Luminescent Probes in Micelles. **1975**, *33*, 289-292.

42. Farhangi, S.; Weiss, H.; Duhamel, J. Effect of Side-Chain Length on the Polymer Chain Dynamics of Poly(alkyl methacrylate)s in Solution. *Macromolecules* **2013**, *46*, 9738-9747.
43. Siu, H.; Duhamel, J. Comparison of the Association Level of a Hydrophobically Modified Associative Polymer Obtained from an Analysis Based on Two Different Models. *J. Phys. Chem. B* **2005**, *109*, 1770−1780.
44. McNelles, S. A.; Thoma, J. L.; Adronov, A.; Duhamel, J. Quantitative Characterization of the Molecular Dimensions of Flexible Dendritic Macromolecules in Solution by Pyrene Excimer Fluorescence. *Macromolecules* **2018**, *51*, 1586−1590.
45. Thoma, J. L.; Duhamel, J.; Li, M-J.; Bertocchi, M. J.; Weiss, R. G. Long-Range, Polymer Chain Dynamics of a "Stiff" Polymer. Fluorescence from Poly(isobutylene-alt-maleic anhydride) with N-(1-Pyrenylmethyl)succinimide Groups. *Macromolecules* **2017**, *50*, 3396-3403.
46. Thoma, J. L.; Duhamel, J.; Bertocchi, M. J.; Weiss, R. G. Long Range Polymer Chain Dynamics of Highly Flexible Polysiloxane in Solution Probed by Pyrene Excimer Fluorescence. *Polymers* **2018**, *10*, 1-15.
47. Tomalia, D. A. Birth of a New Macromolecular Architecture: Dendrimers as Quantized Building Blocks for Nanoscale Synthetic Polymer Chemistry. *Prog. Polym. Sci.* **2005**, *30*, 294−324.

48. Buhleier, E.; Wehner, W.; Vögtle, F. Cascade and Nonskid-Chain-Like Syntheses of Molecular Cavity Topologies. *Synthesis* **1978**, *1978*, 155−158.

49. Denkewalter, R. G.; Kolc, J.; Lukasavage, W. J.; Corp, A. Macromolecular Highly Branched Homogeneous Compound Based on Lysine Units. U. S. Patent 4289872, September 15, 1981.

50. Tomalia, D. A.; Dewald, J. R. Dense Star Polymers Having Core, Core Branches, Terminal Groups. US Patent 4,507,466, March 26, 1985.

51. Tomalia, D. A.; Baker, H.; Dewald, J.; Hall, M.; Kallos, G.; Martin, S.; Roeck, J.; Ryder, J.; Smith, P. A New Class of Polymers: Starburst-Dendritic Macromolecules. *Polym. J.* **1985**, *17*, 117−132.

52. Newkome, G. R.; Yao, Z.; Baker, G. R.; Gupta, V. K. Cascade Molecules: A New Approach to Micelles. A [27]- Arborol. *J. Org. Chem.* **1985**, *50*, 2003−2004.

53. Yamamoto, K.; Imaoka, T.; Tanabe, M.; Kambe, T. New Horizon of Nanoparticle and Cluster Catalysis with Dendrimers. *Chem. Rev.* **2020**, *120*, 1397-1437.

54. Seo, S. E.; Hawker, C. J. The Beauty of Branching in Polymer Science. *Macromolecules* **2020**, *53*, 3257-3261.

55. Hawker,C.; Fréchet, J. M. J. Preparation of Polymers with Controlled Molecular Architecture. a New Convergent Approach to Dendritic Macromolecules. *J. Am. Chem. Soc.* **1990**, *112*, 7638−7647.

56. Miller, T. M.; Neenan, T. X. Convergent Synthesis of Monodisperse Dendrimers Based Upon 1,3,5-Trisubstituted Benzenes. *Chem. Mater.* **1990**, *2*, 346−349.

57. Zhang, X.; Zeng, Y.; Yu, T.; Chen, J.; Yang, G.; Li, Y. Advances in Photofunctional Dendrimers for Solar Energy Conversion.*J. Phys. Chem. Lett.* **2014**, *5*, 2340-2350.

58. Mignani, S.; Shi, X.; Rodrigues, J.; Roy, R.; Munoz-Fernandez, A.; Cena, V.; Majoral, J-P. Dendrimers Toward Translational Nanotherapeutics: Concise Key Step Analysis. *Bioconjugate Chem.* **2020**, *31*, 2060-2071.

59. Yang, J.; Zhang, Q.; Change, H.; Cheng, Y. Surface-Engineered Dendrimers in Gene Delivery. *Chem. Rev.* **2015**, *115*, 5274-5300.

60. Yamamoto, K.; Imaoka, T.; Tanabe, M.; Kambe, T. New Horizon of Nanoparticle and Cluster Catalysis with Dendrimers. *Chem. Rev.* **2020**, *120*, 1397-1437.

61. Kamil, Y. M.; Al-Rekabi, S. H.; Yaacob, M. H.; Syahir, A.; Chee, H.; Mahdi, M. A.; Bakar, M. H. A. Detection of Dengue Using PAMAM Dendrimer Integrated Tapered Optical Fiber Sensor. *Sci Rep* **2019**, *9*, 1-10.

62. De Gennes, P.G.; Hervet, H. Statistics of <<Starburst>> polymers. *J. Phys. Lett.* **1983**, *44*, 351–360.

63. Meléndez-Hevia, E.; Waddell, T. G.; Shelton, E. D. Optimization of Molecular Design in the Evolution of Metabolism: The Glycogen Molecule. *Biochem. J.* **1993**, *295*, 477-483.

64. Lescanec, R.L.; Muthukumar, M. Configurational Characteristics and Scaling Behavior of Starburst Molecules: A Computational Study. *Macromolecules* **1990**, *23*, 2280–2288.

65. Ballauff, M.; Likos, C. N. Dendrimers in Solution: Insight from Theory and Simulation. *Angew, Chem. Int. Ed.* **2004**, *43*, 2998-3020.

66. Tomalia, D. A.; Durst, H. D. Genealogically Directed Synthesis: Starburst/Cascade Dendrimers and Hyperbranched Structures. *Top. Curr. Chem*. **1993**, 165, 193-313.

67. Royer, C. A. Probing Protein Folding and Conformational Transitions with Fluorescence. *Chem. Rev.* **2006**, *106*, 1769-1784.

68. Raut, S.; Enciso, A. E.; Pavan, G, M.; Lee, C.; Yepremyan, A.; Tomalia, D. A.; Simanek, E. E.; Gryczynski, Z. Intrinsic Fluorescence of Triazine Dendrimers Provides a New Approach to Study Dendrimer Structure and Conformational Dynamics. *J. Phys. Chem. C* **2017**, *121*, 6946-6954.

69. Adronov, A.; Gilat, S. L.; Fréchet, J. M. J.; Ohta, K.; Neuwahl, F. V. R.; Flemming, G. R. Light Harvesting and Energy Transfer in Laser-Dye-Labeled Poly(aryl ether) Dendrimers. *J. Am. Chem. Soc.* **2000**, *122*, 1175-1185.

70. Zaragoza-Galan, G.; Fowler, M.; Rein, R.; Solladie, N.; Duhamel, J.; Rivera, E. Fluorescence Resonance Energy Transfer in Partially and Fully Labeled Pyrene Dendronized Porphyrins Studied with Model Free Analysis. *J. Phys. Chem. C* **2014**, *118*, 8280-8294.

71. Studzian, M.; Pulaski, L.; Tomalia, D. A.; Klajnert-Maculewicz, B. Non-Traditional Intrinsic Luminescence (NTIL): Dynamic Quenching Demonstrates the Presence of Two

Distinct Fluorophore Types Associated with NTIL Behavior in Pyrrolidone-Terminated PAMAM Dendrimers. *J. Phys. Chem. C* **2019**, *123*, 18007-18016.

72. Baker, L. A.; Crooks, R. M. Photophysical Properties of Pyrene-Functionalized Poly(propylene imine) Dendrimers. *Macromolecules* **2000**, *33*, 9034-9039.
73. Yip, J.; Duhamel, J.; Bahun, G. J.; Adronov, A. A Study of the Dynamics of the Branch Ends of a series of Pyrene-Labeled Dendrimers Based on Pyrene Excimer Formation. *J. Phys. Chem. B* **2010**, *114*, 10254-10265.
74. Farhangi, S.; Casier, R.; Li, L.; Thoma, J. L.; Duhamel, J. Characterization of the Long-Range Internal Dynamics of Pyrene Labeled Macromolecules by Pyrene Excimer Fluorescence. *Macromolecules* **2016**, *49*, 9597-9604.
75. Chen, S.; Duhamel, J.; Bahun, G.; Adronov, A. Effect of Fluorescent Impurities in the Study of Pyrene-Labeled Macromolecules by Fluorescence. *J. Phys. Chem. B* **2011**, *115*, 9921-9929.
76. Thoma, J.; McNelles, S. A.; Adronov, A.; Duhamel, J. Direct Measure of the Local Concentration of Pyrenyl Groups in Pyrene-Labeled Dendrons Derived from the Rate of Fluorescence Collisional Quenching. *Polymers* **2020**, *12*, 2919.
77. Yip, J.; Duhamel, J.; Bahun, G. J.; Adronov, A. A Study of the Dynamics of the Branch Ends of a Series of Pyrene-Labeled Dendrimers Based on Pyrene Excimer Formation. *J. Phys. Chem. B* **2010**, *114*, 10254-10265.

78. Fowler, M. A.; Duhamel, J.; Bahun, G. J.; Adronov, A.; Zaragoza-Galan, G.; Rivera, E. Studying Pyrene-Labeled Macromolecules with the Model-Free Analysis. *J. Phys. Chem. B* **2012**, *116*, 14689-14699.

79. Gruschwitz, F. V.; Klein, T.; Catrouillet, S.; Brendel, J. C. Supramolecular Polymer Bottlebrushes. *Chem. Commun.* **2020**, *56*, 5079-5110.

80. Xie, G.; Martinez, M. R.; Olszewski, M.; Sheiko, S.; Matyjaszewski, K. Molecular Bottlebrushes as Novel Materials. *Biomacromolecules* **2019**, *20*, 27-54.

81. Matyjaszewski, K.; Tsarevsky, N. V. Macromolecular Engineering by Atom Transfer Radical Polymerization. *J. Am. Chem. Soc.* **2014**, *136*, 6513-6533.

82. Cho, H. Y.; Krys, P.; Szczesniak, K.; Schroeder, H.; Park, S.; Jurga, S.; Buback, M.; Matyjaszewski. Synthesis of Poly(OEOMA) Using Macromonomers via "Grafting-Through" ATRP. *Macromolecules* **2015**, *48*, 6385-6395.

83. Stals, P. J. M.; Li, Y.; Burdyńska, J.; Nicolay, R.; Nese, A.; Palmans, A. R. A.; Meijer, E. W.; Matyjaszewski, K.; Sheiko, S. S. How Far Can We Push Polymer Architecture. *J. Am. Chem. Soc.* **2013**, *135*, 11421-11424.

84 Huang, K.; Jacobs, A.; Rzayev, J. De Novo Synthesis and Cellular Uptake of Organic Nanocapsules with Tunable Surface Chemistry. *Biomacromolecules* **2011**, *12*, 2327−2334.

85 Xie, G.; Krys, P.; Tilton, R. D.; Matyjaszewski, K. Heterografted Molecular Brushes as Stabilizers for Water-in-Oil Emulsions. *Macromolecules* **2017**, *50*, 2942−2950.

86. Grubbs, R. B.; Grubbs, R. H. 50th Anniversary Perspective: Living Polymerization – Emphasizing the Molecule in Macromolecules. *Macromolecules* **2017**, *50*, 6979-6997.

87. Kuhn, W. Über die Gestalt Fadenförmiger Moleküle in Lösungen. *Kolloid Z* **1934**, *68*, 2-15.

88. Flory, P. J. Chapters 1 and 2. *Statistical Mechanics of Chain Molecules*. Wiley, New York. **1969**, pp: 1-48.

89. Kratky, O.; Porod, G. Röntgenuntersuchung Gelöster Fadenmoleküle. *Rec. Trav. Chim.* **1949**, *68*, 1106-1122.

90. Fredrickson, G. H. Surfactant-Induced Lyotropic Behaviour of Flexible Polymer Solutions. *Macromolecules* **1993**, *26*, 2825-2831.

91. Subbotin, A.; Saariaho, M.; Ikkala, O.; Brinke, G. Elasticity of Comb Copolyerm Cylindrical Brushes. *Macromolecules* **2000**, *33*, 3447-3452.

92. Nakamura, Y.; Norisuye, T. Backbone Stiffness of Comb-Branched Polymers. *Polym. J.* **2001**, *11*, 874-878.

93. Hsu, H-P.; Paul, W.; Binder, K. Standard Definitions of Persistence Length Do Not Describe the Local "Intrinsic" Stiffness of Real Polymer Chains. *Macromolecules* **2010**, *43*, 3094-3102.

94. Hsu, H-P, Paul, W.; Rathgeber, S.; Binder, K. Characteristic Length Scales and Radial Monomer Density Profiles of Molecular Bottle Brushes: Simulation and Experiment. *Macromolecules* **2010**, *43*, 1592-1601.

95. Hsu, H-P.; Paul, W.; Binder, K. Estimation of Persistence Lengths of Semiflexible Polymers: Insight from Simulations. *Polym. Sci. Ser. C* **2013**, *55*, 39-59.

96. Binder, K.; Hsu, H-P.; Paul, W. Understanding the Stiffness of Macromolecules from Linear Chains to Bottle-Brushes. *Eur. Phys. J. Special Topics* **2016**, *225*, 1663-1671.

97. Rathgeber, S.; Pakula, T.; Wilk, A.; Matyjaszewski, K.; Beers, K. L. On the Shape of Bottle-Brush Macromolecules: Systematic Variation of Architectural Parameters. *J. Chem. Phys.* **2005**, *122*, 1-13.

98. Chatterjee, D.; Vilgis, T. A. Scaling Laws of Bottle-Brush Polymers in Dilute Solutions. *Macromol. Theory Simul.* **2016**, *25*, 518-523.

99. Altares, T., Jr.; Wyman, D. P.; Allen, V. R.; Meyersen, K. Preparation and Characterization of Some Star- and Comb-Type Branched Polystyrenes. *J. Polym. Sci. Part A: Polym. Chem.* **1965**, *3*, 4131-4151.

100. Berry, G. C.; Orofino, T. A. Branched Polymers. III. Dimensions of Chains with Small Excluded Volume. *J. Chem. Phys.* **1964**, *40*, 1614-1621.

101. Pannell, J. Polystyrenes of Known Structure: Part 2. Comb-Shaped Molecules. *Polymer* **1971**, *12*, 558–578.

102. Sierra-Vargas, J.; Franta, E.; Rempp, P. Macromers as Intermediates for the Synthesis of Graft Copolymers. *Makromol. Chem.* **1981**, *182*, 2603-2609.

103. Kawakami, Y.; Miki, Y.; Tsuda, T.; Murthy, R. A. N.; Yamashita, Y. Silicone Macromers for Graft Polymer Synthesis. *Polymer J.* **1982**, *14*, 913-917.

104. Rempp, P.; Lutz, P.; Masson, P.; Franta, E. Macromonomers- A New Class of Polymeric Intermediates in Macromolecular Synthesis. I- Synthesis and Characterization. *Makromol. Chem., Suppl.* **1984**, *8*, 3-15.

105. Wintermantel, M.; Schmidt, M. Rodlike Combs. *Macromol. Rapid. Commun.* **1994**, *15*, 279-284.

106. Wintermantel, M.; Gerle, M.; Fischer, K.; Schmidt, M.; Wataoka, I.; Urahawa, H.; Kajiwara, K.; Tsukahara, Y. Molecular Bottlebrushes. *Macromolecules* **1996**, *29*, 978-983.

107. Zhang, B.; Gröhn, F.; Pedersen, J. S.; Fischer, K.; Schmidt, M. Conformation of Cylindrical Brushes in Solution: Effect of Side Chain Length. *Macromolecules* **2006**, *39*, 8440-8450.

108. Terao, K.; Takeo, Y.; Tazaki, M.; Nakamura, Y.; Norisuye, T. Polymacromonomer Consisting of Polystyrene. Light Scattering Characterization in Cyclohexane. *Polym. J.* **1999**, *31*, 193-198.

109. Hokajo, T.; Terao, K.; Nakamura, Y.; Norisuye, T. Solution Properties of Polymacromonomers Consisting of Polystyrene V. Effect of Side Chain Length on Chain Stiffness. *Polym. J.* **2001**, *6*, 481-485.

110. Rathgeber, S.; Pakula, T.; Wilk, A.; Matyjaszewski, K.; Lee, G-I.; Beers, K. L. Bottle-Brush Macromolecules in Solution: Comparison Between Results Obtained from Scattering Experiments and Computer Simulations. *Polymer* **2006**, *47*, 7318-7327.

111. Kikuchi, M.; Lien, L. T. N.; Narumi, A.; Jinbo, Y.; Izumi, Y.; Nagai, K.; Kawaguchi, S. Conformational Properties of Cylindrical Rod Brushes Consisting of a Polystyrene Main Chain and Poly(*n*-hexyl isocyanate) Side Chain. *Macromolecules* **2008**, *41*, 6564-6572.

112. Holtzer, A. Interpretation of the angular distribution of the light scattered by a polydisperse system of rods. *J. Polym. Sci.* **1955**, *17*, 432-434.

113. Gerle, M.; Fischer, K.; Roos, S.; Müller, A. H. E.; Schmidt, M. Main Chain Conformation and Anomalous Elution Behaviour of Cylindrical Brushes as Revealed by GPC/MALLS, Light Scattering, and SFM. *Macromolecules* **1999**, *32*, 2629-2637.

114. Fischer, K.; Schmidt, M. Solvent-Induced Length Variation of Cylindrical Brushes. *Macromol. Rapid. Commun.* **2001**, *22*, 787-791.

115. Kikuchi, M.; Nakano, R.; Jinbo, Y.; Saito, Y.; Ohno, S.; Togashi, D.; Enomoto, K.; Narumi, A.; Haba, O.; Kawaguchi, S. Graft Density Dependence of Main Chain Stiffness in Molecular Rod Brushes. *Macromolecules* **2015**, *48*, 5878-5886.

116. Liang, H.; Cao, Z.; Wang, Z.; Sheiko, S.; Dobrynin, A. V. Combs and Bottlebrushes in a Melt. *Macromolecules* **2017**, *50*, 3430-3437.

117. Young, R. J.; Lovell, P. A. Scattering Methods. *Introduction to polymers*. 3rd ed.; CRC Press: Taylor & Francis Group.: Boca Raton, FL, U.S.A, 2011, pp:281-291.

118. Rudin, A. Light Scattering. *The Elements of Polymer Science and Engineering*. 2nd e.d; Elsevier Science & Technology, 1998, pp:80-89.

119. Benoit, H.; Doty, P. Light Scattering from Non-Gaussian Chains. *J. Phys. Chem.* **1953**, *57*, 958-963.

120. Konishi, T.; Yoshizaki, T.; Saito, T.; Einaga, Y.; Yamakawa., H. Mean Square Radius of Gyration of Oligo- and Polystyrenes in Dilute Solutions. *Macromolecules* **1990**, *23*, 290-297.

121. Shimada, J.; Yamakawa, H. Statistical Mechanics of Helical Worm-Like Chains. XV. Excluded-Volume Effects. *J. Chem. Phys.* **1986**, *85*, 591-600.

122. Yamakawa, H.; Stockmayer, W. H. Statistical Mechanics of Wormlike Chains. ll. Excluded Volume Effects. *J. Chem. Phys.* **1972**, *57*, 2843-2854.

123. Yamakawa, H.; Shimada, J. Stiffness and Excluded-Volume Effects in Polymer Chains. *J. Chem. Phys.* **1985**, *83*, 2607-2611.

124. Li, Y.; Zhang, M.; Mao, M.; Turner, R.; Moore, R. B.; Mourey, T. H.; Slater, L. A.; Hauenstein, J. R. Chain Stiffness of Stilbene Containing Alternating Copolymers by SAXS and SEC. *Macromolecules* **2012**, *45*, 1595-1601.

125. Pedersen, J. S.; Schurtenberger, P. Scattering Functions of Semiflexible Polymers with and without Excluded Volume Effects. *Macromolecules* **1996**, *29*, 7602-7612.

126. Mourey, T.; Le, K.; Bryan, T.; Zheng, S.; Bennett, G. Determining Persistence Length by Size Exclusion Chromatography. *Polymer* **2005**, *46*, 9033- 9042.

127. Yamakawa, H.; Fujii, M. Intrinsic Viscosity of Wormlike Chains. Determination of the Shift Factor. *Macromolecules* **1974**, *7*, 128-135.

128. Yamakawa, H.; Yoshizaki, T. Transport Coefficients of Helical Wormlike Chains. 3. Intrinsic Viscosity. *Macromolecules* **1980**, *13*, 633-643.

129. Bohdanecky, M. New Method for Estimating the Parameters of the Wormlike Chain Model from the Intrinsic Viscosity of Stiff-Chain Polymers. *Macromolecules* **1983**, *16*, 1483-1492.

130. Sheiko, S. S.; Borisov, O. V.; Prokhorova, S. A.; Moller, M. Cylindrical Molecular Brushes Under Poor Solvent Conditions: Microscopic Observation and Scaling Analysis. *Eur. Phys. J. E.* **2004**, *13*, 125-131.

131. Nese, A.; Li, Y.; Averick, S.; Kwak, Y.; Konkolewicz, D.; Sheiko, S. S.; Matyjaszewski, K. Synthesis of Amphiphilic Poly(*N*-vinylpyrrolidone)-*b*-poly(vinylacetate) Molecular Brushes. *ACS Macro Lett.* **2012**, *1*, 227-231.

132. Gunari, N.; Schmidt, M.; Janshoff, A. Persistence Length of Cylindrical Brush Molecules Measured by Atomic Force Microscopy. *Macromolecules* **2006**, *39*, 2219-2224.

133. Park, I.; Shirvanyants, D.; Nese, A.; Matyjaszewski, K.; Rubinstein, M.; Sheiko, S.S. Spontaneous and Specific Activation of Chemical Bonds in Macromolecular Fluids. *J. Am. Chem. Soc.* **2010**, *132*, 12487-12491.

134. Sheiko, S. S.; Sun, F.C.; Randall, A.; Shirvanyants, D.; Rubinstein, M.; Lee, H.; Matyjaszewski, K. Adsorption-Induced Scission of Carbon-Carbon Bonds. *Nature* **2006**, *440*, 191-194.

135. Li, Y.; Nese, A.; Matyjaszewski, K.; Sheiko, S. S. Molecular Tensile Machines: Anti-Arrhenius Cleavage of Disulfide Bonds. *Macromolecules* **2013**, *46*, 7196-7201.

136. Rivett, C.; Walker, C.; Bustamante, C. Polymer Chain Statistics and Conformational Analysis of DNA Molecules with Bends or Sections of Different Flexibility. *J. Mol. Biol.* **1998**, *280*, 41-59.

137. Zhao, C.; Wu, D.; Lian, X.; Zhang, Y.; Song, X.; Zhao, H. Amphiphilic Asymmetric Comb Copolymer with Pendant Pyrene Groups and PNIPAM Side Chains: Synthesis, Photophysical Properties, and Self-Assembly. *J. Phys. Chem. B* **2010**, *114*, 6300-6308.

138. Gadwal, I.; Rao, J.; Baettif, J.; Khan, A. Functionalized Molecular Brushes. *Macromolecules* **2014**, *47*, 35-40.

139. Kawaguchi, S.; Akaike, K.; Zhang, Z-M.; Matsumoto, H.; Ito, K. Water Soluble Bottlebrushes. *Polym. J.* **1998**, *30*, 1004-1007.

140. Mao, J.; Gan, Z. Amphiphilic PEG-co-PGL-g-PCL Copolymer Brushes: Synthesis, Micellization and Controlled Drug Delivery. *Macromol. Chem. Phys.* **2009**, *210*, 2078-2086.

141. Zeng, X.; Liu, D.; Liu, D. Poly(L-lysine)-based Cylindrical Copolypeptide Brushes as Potential Drug and Gene Carriers. *Colloid Polym. Sci.* **2016**, *294*, 1909-1920.

142. Chen, Y.; Zhou, H.; Sun, Z.; Li, H.; Huang, H.; Liu, L.; Chen, Y. Shell of Amphiphilic Molecular Bottlebrush Matters as Unimolecular Micelle. *Polymer* **2018**, *149*, 316-324.

143. Huang, Y-S.; Chen, J-K.; Kuo, S-W.; Hsieh, Y-A.; Yamamoto, S.; Nakanishi, J.; Huang, C-F. Synthesis of Poly(*N*-vinylpyrrolidone) Based Polymer Bottlebrushes by ATRP and RAFT Polymerization: Toward Drug Delivery Application. *Polymers* **2019**, *11*, 1-13.

144. Sivokhin, A. P.; Orekhov, D. V.; Kazantsev, O. A.; Gubanova, O. V.; Kamorin, D. M.; Zarubina, I. S.; Bolshakova, E. A.; Zaitsev, S. D. Amphiphilic Thermoresponsive Copolymer Bottlebrushes: Synthesis, Characterization, and Study of their Self-Assembly into Flower-Like Micelles. *Polym. J.* **2021**, *53*, 655-665.

Chapter 2

1. Brandrup, J.; Immergut, E. H.; Grulke, E. A. Eds. *In Polymer Handbook*, 4th ed.; Wiley: New York, NY, USA, 1999; pp 1-83.
2. Lakowicz, J. R. *In Principles of Fluorescence Spectroscopy*, 3rd ed.; Springer: New York, NY, USA, 2006; pp 277-330.
3. Duhamel, J. Global Analysis of Fluorescence Decays to Probe the Internal Dynamics of Fluorescently Labeled Macromolecules. *Langmuir* **2014**, *30*, 2307-2324.
4. Duhamel, J. Internal Dynamics of Dendritic Molecules Probed by Pyrene Excimer Formation. *Polymers* **2012**, *4*, 211 -239.
5. Duhamel, J. New Insights in the Study of Pyrene Excimer Fluorescence to Characterize Macromolecules and their Supramolecular Assemblies in Solution. *Langmuir* **2012**, *28*, 6527-6538.

6. Siu, H.; Duhamel, J. Comparison of the Association Level of a Hydrophobically Modified Associative Polymer Obtained from an Analysis Based on Two Different Models. *J. Phys. Chem. B* **2005**, *109*, 1770-1780.
7. Birks, J. B. *Photophysics of Aromatic Molecules*; Wiley: London, UK, 1970.
8. Winnik, M.A. End-to-end cyclization of polymer chains. *Accounts Chem. Res.* **1985**, *18*, 73–79.
9. Chen, S.; Duhamel, J.; Winnik, M.A. Probing End-to-End Cyclization Beyond Willemski and Fixmann. *J. Phys. Chem. B* **2011**, *115*, 3289–3302.
10. Cuniberti, C.; Perico, A. Intramolecular excimer formation in polymers. *Eur. Polym. J.* **1980**, *16*, 887–893.
11. Yip, J.; Duhamel, J.; Bahun, G.J.; Adronov, A. A Study of the Dynamics of the Branch Ends of a Series of Pyrene-Labeled Dendrimers Based on Pyrene Excimer Formation. *J. Phys. Chem. B* **2010**, *114*, 10254–10265.
12. Modrakowski, C.; Flores, S.C.; Beinhoff, M.; Schlüter, A.D. Synthesis of Pyrene Containing Building Blocks for Dendrimer Synthesis. *Synthese* **2001**, *2001*, 2143–2155.
13. Figueira-Duarte, T.M.; Simon, S.C.; Wagner, M.; Druzhinin, S.I.; Zachariasse, K.A.; Müllen, K. Polypyrene Dendrimers. *Angew. Chem. Int. Ed.* **2008**, *47*, 10175–10178.
14. Figueira-Duarte, T.M.; Müllen, K. Pyrene-Based Materials for Organic Electronics. *Chem. Rev.* **2011**, *111*, 7260–7314.

15. Stewart, G.M.; Fox, M.A. Fluorophore-labeled dendrons as light harvesting antennae. *J. Am. Chem. Soc.* **1996**, *118*, 4354–4360.
16. Giovanella, U.; Mróz, W.; Foggi, P.; Fabbrizzi, P.; Cicchi, S.; Botta, C. Multi-Colour Electroluminescence of Dendronic Antennae Containing Pyrenes as Light Harvesters. *ChemPhysChem* **2009**, *11*, 683–688.
17. Thomas, K.R.J.; Thompson, A.L.; Sivakumar, A.V.; Bardeen, C.J.; Thayumanavan, S. Energy and Electron Transfer in Bifunctional Non-Conjugated Dendrimers. *J. Am. Chem. Soc.* **2005**, *127*, 373–383.
18. Vanjinathan, M.; Lin, H.-C.; Nasar, A.S. Synthesis, Characterization and Photophysical Properties of DCM-Based Light-Harvesting Dendrimers. *Macromol. Chem. Phys.* **2011**, *212*, 849–859.
19. Gu, T.; Whitesell, J.K.; Fox, M.A. Intramolecular Charge Transfer in 1:1 Cu(II)/Pyrenylcyclam Dendrimer Complexes. *J. Phys. Chem. B* **2006**, *110*, 25149–25152.
20. Morales-Espinoza, E.G.; Lijanova, I.V.; Morales-Saavedra, O.G.; Torres-Zuñiga, V.; Hernández-Ortega, S.; Garcia, M.M. Synthesis of Porphyrin-Dendrimers with a Pyrene in the Periphery and Their Cubic Nonlinear Optical Properties. *Molecules* **2011**, *16*, 6950–6968.
21. Baker, L.A.; Crooks, R.M. Photophysical Properties of Pyrene-Functionalized Poly (propylene imine) Dendrimers. *Macromolecules* **2000**, *33*, 9034–9039.

22. Wang, B.-B.; Zhang, X.; Jia, X.-R.; Li, Z.-C.; Ji, Y.; Yang, L.; Wei, Y. Fluorescence and aggregation behaviour of poly(amidoamine) dendrimers peripherally modified with aromatic fluorophores: The effect of dendritic architecture. *J. Am. Chem. Soc.* **2004**, *126*, 15180–15194.
23. Wang, B.-B.; Zhang, X.; Yang, L.; Jia, X.-R.; Ji, Y.; Li, W.-S.; Wei, Y. Poly (amisoamine) dendrimers bearing electron-donating fluorophores: Fluorescence and electrochemical properties. *Polym. Bull.* **2006**, *56*, 63–74.
24. Brauge, L.; Caminade, A.-M.; Majoral, J.-P.; Slomkowski, S.; Wolszczak, M. Segmental Mobility in Phosphorus-Containing Dendrimers. Studies by Fluorescent Spectroscopy. *Macromolecules* **2001**, *34*, 5599–5606.
25. Brauge, L.; Veriot, G.; Franc, G.; Deloncle, R.; Caminade, A.-M.; Majoral, J.-P. Synthesis of phosphorus dendrimers bearing chromophoric end groups: Toward organic blue light-emitting diodes. *Tetrahedron* **2006**, *62*, 11891–11899.
26. Caminade, A.-M.; Hameau, A.; Turrin, C.-O.; Ianchuk, M.; Delavaux-Nicot, B.; Majoral, J.-P. Fluorescent Phosphorus Dendrimers and Their Role in Supramolecular Interactions. *Phosphorus Sulfur Silicon Relat. Elem.* **2011**, *186*, 860–868.
27. Lekha, P.K.; Prasad, E. Tunable Emission of Static Excimer in a Pyrene-Modified Polyamidoamine Dendrimer Aggregate through Positive Solvatochromism. *Chem. A Eur. J.* **2011**, *17*, 8609–8617.

28. Wilken, R.; Adams, J. End-group dynamics of fluorescently labeled dendrimers. *Macromol. Rapid Commun.* **1997**, *18*, 659–665.
29. McNelles, S. A.; Thoma, J. L.; Adronov, A.; Duhamel, J. Quantitative Characterization of the Molecular Dimensions of Flexible Dendritic Macromolecules in Solution by Pyrene Excimer Fluorescence. *Macromolecules* **2018**, *51*, 1586−1590.
30. Press, W. H.; Flanery, B. P.; Tenkolsky, S. A.; Vetterling, W. T. *Numerical Recipes in Fortran: The Art of Scientific Computing*; Cambridge University Press: Cambridge and New York, 1992; pp 523−528.
31. Farhangi, S.; Casier, R.; Li, L.; Thoma, J.; Duhamel, J. Characterization of the Long Range Internal Dynamics of Pyrene-Labeled Macromolecules by Pyrene Excimer Fluorescence. *Macromolecules* **2016**, *49*, 9597-9604.
32. Farhangi, S.; Duhamel, J. Long Range Polymer Chain Dynamics Studied by Fluorescence Quenching. *Macromolecules* **2016**, *49*, 6149–6162.
33. Lide, D. R. *CRC Handbook of Chemistry and Physics*, 77th ed.; CRC Press: Boca Raton, FL, USA, 1996.
34. Hall, T.; Whitton, G.; Casier, R.; Gauthier, M.; Duhamel, J. Arborescent Poly(*L*-glutamic acid)s as Standards to Study the Dense Interior of Polypeptide Mesoglobules by Pyrene Excimer Fluorescence. *Macromolecules* **2018**, *51*, 7914-7923

35. Casier, R.; Duhamel, J. Effect of Like Charges on the Conformation and Internal Dynamics of Polypeptides Probed by Pyrene Excimer Fluorescence. *Macromolecules* **2020**, *53*, 5147–5157.

Chapter 3

1. Flory, J. P. Principles of Polymer Chemistry. Cornell University Press, Ithaca, 1953, pp 399-431.
2. De Gennes, P.-G. Scaling Concepts in Polymer Physics. Cornell University Press, Ithaca, 1979, pp 29-53.
3. Dai, Z.; Ngai, T.; Wu, C. Internal Motions of Linear Chains and Spherical Microgels in Dilute Solution. *Soft Matter* **2011**, *7*, 4111-4121.
4. Boyle, B. M.; Heinz, O.; Miyake, G. M.; Ding, Y. Impact of the Pendant Group on the Chain Conformation and Bulk Properties of Norbornene Imide-Based Polymers. *Macromolecules* **2019**, *52*, 3426-3434.
5. Haas, E.; Katchalski-Katzir, E.; Steinberg, I. Brownian Motion of the Ends of Oligopeptide Chains in Solution as Estimated by Energy Transfer Between the Chain Ends. *Biopolymers* **1978**, *17*, 11 – 31.
6. Hudgins, R.R.; Huang, F.; Gramlich, G.; Nau, W.M. A Fluorescence-Based Method for Direct Measurement of Submicrosecond Intramolecular Contact Formation in

Biopolymers: An Exploratory Study with Polypeptides. *J. Am. Chem. Soc.* **2002**, *124*, 556–564.

7. Norouzy, A.; Assaf, K. I.; Zhang, S.; Jacob, M. H.; Nau, W. M. Coulomb Repulsion in Short Polypeptides. *J. Chem. Phys. B* **2015**, *119*, 33 – 43.
8. Krieger, F.; Fierz, B.; Bieri, O.; Drewello, M.; Kiefhaber, T. Dynamics of Unfolded Polypeptide Chains as Model for the Earliest Steps in Protein Folding. *J. Mol. Biol.* **2003**, *332*, 265 – 274.
9. Krieger, F.; Möglich, A.; Kiefhabler, T. Effect of Proline and Glycine Residues on Dynamics and Barriers of Loop Formation in Polypeptide Chains. *J. Am. Chem. Soc*. **2005**, *127*, 3346 – 3352.
10. Fierz, B.; Kiefhaber, T. End-to-End vs Interior Loop Formation Kinetics in Unfolded Polypeptide Chains. *J. Am. Chem. Soc.* **2007**, *129*, 672 – 679.
11. Shahabi, M.; Hajihosseini, R.; Nau, W. M.; Noghabi, K. A.; Norouzy, A. Augmenting Peptide Flexibility by Inserting Gamma-Aminobutyric Acid (GABA) in Their Sequence. *Int. J. Pept. Res. Ther.* **2020**, https://doi.org/10.1007/s10989-020-10054-2.
12. Zachariasse, K.; Kühnle, W. Intramolecular Excimers with a,w-diarylalkanes. *Zeit. Phys. Chem.* **1976**, *101*, 267-276.
13. Cuniberti, C.; Perico, A. Intramolecular Excimer and Microbrownian Motions of Flexible Polymer Molecules in Solution. *Eur. Polym. J.* **1977**, *13*, 369-374.

14. Winnik, M. A. End-to-End Cyclization of Polymer Chains. *Acc. Chem. Res.* **1985**, *18*, 73-79.
15. Wang. X.; Guerrand, L.; Wu, B. ; Li, X. ; Boldon, L. ; Chen, W.-R. ; Liu, L. Characterization of Polyamidoamine dendrimers with Scattering Techniques. *Polymers* **2012**, *4*, 600-616.
16. Kikuchi, M.; Nakano, R.; Jinbo, Y. ; Saito, Y. ; Ohno, S.; Togashi, D.; Enomoto, K.; Narumi, A.; Haba, O.; Kawaguchi, S. Graft Density Dependence of Main Chain Stiffness in Molecular Rod Brushes. *Macromolecules* **2015**, *48*, 5878-5886.
17. Quantitative Characterization of the Molecular Dimensions of Flexible Dendritic Macromolecules by Pyrene Excimer Fluorescence. McNelles, S.; Thoma, J.; Adronov, A.; Duhamel, J. *Macromolecules* **2018**, *51*, 1586-1590.
18. Thoma, J.; McNelles, S. A.; Adronov, A.; Duhamel, J. Direct Measure of the Local Concentration of Pyrenyl Groups in Pyrene-Labeled Dendrons Derived from the Rate of Fluorescence Collisional Quenching. *Polymers* **2020**, *12*, 2919.
19. Lutz, J.-F.; Akdemir, Ö. ; Hoth, A. Point by Point Comparison of Two Thermosensitive Polymers Exhibiting a Similar LCST: Is the Age of PNIPAM Over? *J. Am. Chem. Soc.* **2006**, *128*, 13046-13047.
20. Lutz, J.-F. Thermo-Switchable Materials Prepared using the OEGMA-Platform. *Adv. Mater.* **2011**, *23*, 2237-2243.

21. Binder, K.; Butt, H.-J.; Floudas, G.; Frey, H.; Hsu, H.-P,; Landfester, K.; Kolb, U.; Kühnle, A.; Maskos, M.; Müllen, K.; Paul W.; Schmidt, M.; Spiess, H. W.; Virnau, P. Structure Formation of Polymeric Building Blocks: Complex Polymer Architecture. *Adv. Polym. Sci.* **2014**, *260*, 115-210.
22. Li, Z.; Tang, M.; Liang, S. ; Zhang, M. ; Biesold, G. M. ; He, Y.; Hao, S.-M.; Choi, W.; Liu, Y.; Peng, J.; Lin, Z. Bottlebrush Polymers: From Controlled-Synthesis, Self-Assembly, Properties to Applications. *Prog. Polym. Sci.* **2021**, *116*, 101387.
23. Nakamura, Y.; Norisuye, T. Backbone Stiffness of Comb-Branched Polymers. *Polym. J.* **2001**, *33*, 874-878.
24. Kinose, Y.; Sakakibara, K.; Ogawa, H.; Tsujii, Y. Main-Chain Stiffness of Cellulosic Bottlebrushes with Polystyrene Side Chains Introduced Regioselectivity at the O-6 Position. *Macromolecules* **2019**, *52*, 8733-8740.
25. Nakamura, Y.; Sugiyama, M.; Amitani, K.; Norisuye, T. Synchrotron Small-Angle X-Ray Scattering from Polystyrene Polymacromonomers in Toluene. *Polym. J.* **2007**, *39*, 1098-1104.
26. Rathgeber, S.; Pakula, T.; Wilk, A.; Matyjaszewski, K.; Lee, H.-I.; Beers, K. L. Bottle-Brush Macromolecules in Solution: Comparison between Results Obtained from Scattering Experiments and Computer Simulations. *Polymer* **2006**, *47*, 7318-7327.
27. Dutta, S.; Wade, M. A.; Walsh, D. J.; Guironnet, D.; Rogers, S. A.; Sing, S. E. Dilute Solution Structure of Bottlebrush Polymers. *Soft Matter* **2019**, *15*, 2928-2941.

28. Zhang, B.; Gröhn, F.; Pedersen, J. S.; Fischer, K.; Schmidt, M. Conformation of Cylindrical Brushes in Solution: Effect of Side Chain Length. *Macromolecules* **2006**, *39*, 8440-8450.

29. Kikuchi, M.; Nakano, R.; Jinbo, Y.; Saito, Y.; Ohno, S.; Togashi, D.; Enomoto, K.; Narumi, A.; Haba, O.; Kawaguchi, S. Graft Density Dependence of Main Chain Stiffness in Molecular Rod Brushes. *Macromolecules* **2015**, *48*, 5878-5886.

30. Kikuchi, M.; Lien, L. T. N.; Narumi, A.; Jinbo, Y.; Izumi, Y.; Nagai, K.; Kawaguchi, S. Conformational Properties of Cylindrical Rod Brushes Consisting of a Polystyrene Main Chain and Poly(*n*-hexyl isocyanate) Side Chains. *Macromolecules* **2008**, *41*, 6564-6572.

31. Birshtein, T. M.; Borisov, O. V.; Zhulina, Y. B.; Khokhlov, A. R.; Yurasova, T. A. Conformations of Comb-Like Macromolecules *Polym. Sci.* **1987**, *29*, 1293-1300.

32. Fredrickson, G. H. Surfactant-Induced Lyotropic Behavior of Flexible Polymer Solutions. *Macromolecules* **1993**, *26*, 2825-2831.

33. Saariaho, M.; Ikkala, O.; Szleifer, I.; Erukhimovich, I.; Brinke, G. T. On Lyotropic Behavior of Molecular Bottle-Brushes: A Monte Carlo Computer Simulation Study. *J. Chem. Phys.* **1997**, *107*, 3267-3276.

34. Rathgeber, S.; Pakula, T.; Wilk, A.; Matyjaszewski, K.; Beers, K. L. On the Shape of Bottle-Brush Macromolecules: Systematic Variation of Architectural Parameters. *J. Chem. Phys.* **2005**, *122*, 124904.

35. Hsu, H.-P.; Paul, W.; Binder, K. Standard Definitions of Persistence Length Do not Describe the Local “Intrinsic” Stiffness of Real Polymer Chains. *Macromolecules* **2010**, *43*, 3094-3102.

36. Press, W.H.; Flanery, B.P.; Tenkolsky, S.A.; Vetterling, W.T. *Numerical Receipes in Fortran: The Art of Scientific Computing*; Cambridge University Press: New York, NY, USA, 1992; pp 523−528.

37. Duhamel, J. Internal Dynamics of Dendritic Molecules Probed by Pyrene Excimer Formation. *Polymers* **2012**, *4*, 211-239.

38. Duhamel, J. New Insights in the Study of Pyrene Excimer Fluorescence to Characterize Macromolecules and their Supramolecular Assemblies in Solution. *Langmuir* **2012**, *28*, 6527-6538.

39. Global Analysis of Fluorescence Decays to Probe the Internal Dynamics of Fluorescently Labeled Macromolecules. Duhamel, J. *Langmuir* **2014**, *30*, 2307-2324.

40. Yip, J.; Duhamel, J.; Bahun, G.; Adronov, A. A Study of the Branch Ends of a Series of Pyrene-Labeled Dendrimers Based on Pyrene Excimer Formation. *J. Phys. Chem. B* **2010**, *114*, 10254-10265

41. Chen, S.; Duhamel, J.; Bahun, G.; Adronov, A. Effect of Fluorescent Impurities in the Study of Pyrene-Labeled Macromolecules by Fluorescence. *J. Phys. Chem. B* **2011**, *115*, 9921-9929.

42. Cuniberti, C.; Perico, A. Intramolecular Excimer Formation in Polymers. Pyrene Labeled Poly(vinyl acetate). *Eur. Polym. J.* **1980**, *16*, 887-893.
43. Lakowicz, J. R. Principles of Fluorescence, 3rd Ed. Springer, NY, 2006, pp 56, 284-287.
44. Mathew, A.; Siu, H.; Duhamel, J. A *Blob* Model to Study Chain Folding by Fluorescence. *Macromolecules* **1999**, *32*, 7100-7108.
45. Duhamel, J. Polymer Chain Dynamics in Solution Probed with a Fluorescence Blob Model. *Acc. Chem. Res.* **2006**, *39*, 953-960.
46. Casier, R.; Duhamel, J. Pyrene Excimer Fluorescence as a Direct and Easy Experimental Means to Characterize the Length Scale and Dynamics of Polypeptide *Foldons*. *Macromolecules* **2018**, *51*, 3450-3457.
47. Casier, R.; Duhamel, J. Blob-Based Predictions of Protein Folding Times from the Amino Acid Dependent Conformation of Polypeptides in Solution. *Macromolecules* **2021**, *54*, 919-929.

Chapter 4

1. Wilemski, G.; Fixman, M. Diffusion-controlled Intrachain Reactions of Polymers. I Theory. *J. Chem. Phys.* **1974**, *60*, 866-877.
2. Wilemski, G.; Fixman, M. Diffusion-controlled Intrachain Reactions of Polymers. II Results for a Pair of Terminal Reactive Groups. *J. Chem. Phys.* **1974**, *60*, 878-890.

3. Zachariasse, K.; Kühnle, W. Intramolecular Excimers with α,ω–Diarylalkanes. *Z. Phys. Chem. Neue F.* **1976**, *101*, 267-276.
4. Yamamoto, M.; Goshiki, K.; Kanaya, T.; Nishijima, Y. Intramolecular Excimer of Di(1-pyrenemethyleneoxycarbonyl) Alkanes. *Chem. Phys. Lett.* **1978**, *56*, 333-335.
5. Cuniberti, C.; Perico, A. Intramolecular Excimers and Microbrownian Motion of Flexible Polymer Molecules in Solution. *J. Eur. Polym.* **1977**, *13*, 369–374.
6. Winnik, M. A.; Redpath, T.; Richards, D. H. The Dynamics of End-to-End Cyclization in Polystyrene Probed by Pyrene Excimer Formation. *Macromolecules* **1980**, *13*, 328-335.
7. Svirskaya, P.; Danhelka, J.; Redpath, A. E. C.; Winnik, M. A. Cyclization Dynamics of Polymers: 7. Applications of the Pyrene Excimer Technique to the Internal Dynamics of Polydimethylsiloxane Chains. *Polymer* **1983**, *24*, 319-322.
8. Ghiggino, K. P.; Snare, M. J.; Thistlethwaite, P. J. Cyclization Dynamics in Poly(ethylene oxide). Chain Length and Temperature Dependence. *Eur. Polym. J.* 1985, *21*, 265-272.
9. Winnik, M. A. End-to-End Cyclization of Polymer Chains. *Acc. Chem. Res.* **1985**, *18*, 73-79.
10. Ushiki, H.; Horie, K.; Okamoto, A.; Mita, I. Rate of Diffusion-Controlled Intramolecular Triplet-Triplet Annihilation between the Terminal Groups of α,ω–Dianthrylpolystyrene. *Polym. J.* **1981**, *13*, 191-200.
11. Horie, K.; Schnabel, W.; Mita, I.; Ushiki, H. Rates of Intramolecular Collision between Terminal Groups of α,ω–Dianthrylpolystyrene in Benzene and Cyclohexane Solutions as

Studied by Triplet-Triplet Absorption Measurements. *Macromolecules* **1981**, *14*, 1422-1428.

12. Roccatano, D.; Sahoo, H.; Zacharias, M.; Nau, W. M. Temperature Dependence of Looping Rates in a Short Peptide. *J. Phys. Chem. B* **2007**, *111*, 2639-2646.
13. Hudgins, R. R.; Huang, F.; Gramlich, G.; Nau, W. M. A Fluorescence-Based Method for Direct Measurement of Submicrosecond Intramolecular Contact Formation in Biopolymers: An Exploratory Study with Polypeptides. *J. Am. Chem. Soc.* **2002**, *124*, 556-564.
14. Shahabi, M.; Hajihosseini, R.; Nau, W. M.; Noghabi, K. A.; Norouzy, A. Augmenting Peptide Flexibility by Inserting Gamma-Aminobutyric Acid (GABA) in their Sequence. *Intl. J. Pept. Res. Ther. ASAP* **2020**.
15. Fierz, B.; Kiefhaber, T. End-to-End vs Interior Loop Formation Kinetics in Unfolded Polypeptide Chains. *J. Am. Chem. Soc.* **2007**, *129*, 672-679.
16. Neuweiler, H.; Schultz, A.; Böhmer, M.; Enderlein, J.; Sauer, M. Measurements of Submicrosecond Intramolecular Contact Formation in Peptides at the Single-Molecule Level. *J. Am. Chem. Soc.* **2007**, *125*, 5324-5330..
17. Mathew, A.; Siu, H.; Duhamel, J. A *Blob* Model to Study Chain Folding by Fluorescence. *Macromolecules* **1999**, *32*, 7100-7108.

18. Siu, H.; Duhamel, J. Comparison of the Association Level of a Hydrophobically Modified Associative Polymer Obtained from an Analysis Based on Two Different Models. *J. Phys. Chem. B* **2005**, *109*, 1770-1780.
19. Duhamel, J. New Insights in the Study of Pyrene Excimer Fluorescence to Characterize Macromolecules and their Supramolecular Assemblies in Solution. *Langmuir* **2012**, *28*, 6527-6538.
20. Duhamel, J. Global Analysis of Fluorescence Decays to Probe the Internal Dynamics of Fluorescently Labeled Macromolecules. *Langmuir* **2014**, *30*, 2307-2324.
21. Duhamel, J.; Kanagalingam, S.; O'Brien, T.; Ingratta, M. Side-Chain Dynamics of an α–Helical Polypeptide Monitored by Fluorescence. *J. Am. Chem. Soc.* **2003**, *125*, 12810-12822.
22. Casier, R.; Duhamel, J. Pyrene Excimer Fluorescence as a Direct and Easy Experimental Means to Characterize the Length Scale and Dynamics of Polypeptide *Foldons*. *Macromolecules* **2018**, *51*, 3450-3457.
23. Casier, R.; Duhamel, J. The Effect of Like-Charges on the Conformation and Internal Dynamics of Polypeptides Probed by Pyrene Excimer Fluorescence. *Macromolecules* **2020**, *53*, 5147-5157.
24. Casier, R.; Duhamel, J. The Effect of Structure on Polypeptide Blobs: A Model Study Using Poly(*L*-Lysine). *Langmuir* **2020**, *36*, 7980-7990.

25. Conformation of Pyrene-Labeled Amylose in DMSO Characterized with the Fluorescence Blob Model. Li, L.; Duhamel, J. *Macromolecules* **2016**, *49*, 7965-7974.

26. Hall, T.; Whitton, G.; Casier, R.; Gauthier, M.; Duhamel, J. Arborescent Poly(L-glutamic acid)s as Standards to Study the Dense Interior of Polypeptide Mesoglobules by Pyrene Excimer Fluorescence. *Macromolecules* **2018**, *51*, 7914-7923.

27. Li, L.; Kim, D.; Zhai, X.; Duhamel, J. A Pyrene Excimer Fluorescence (PEF) Study of the Interior of Amylopectin in Dilute Solution. *Macromolecules* **2020**, *53*, 6850-6860.

28. Banquy, X.; Burdynska, J.; Lee, D. W.; Matyjaszewski, K.; Israelachvili, J. Bioinspired Bottle-Brush Polymer Exhibits Low Friction and Amontons-like Behavior. *J. Am. Chem. Soc*. **2014**, *136*, 6199-6202.

29. Faivre, J.; Shrestha, B.R. Burdynska, J.; Xie, G.; Moldovan, F.; Delair, T.; Benayoun, S.; David, L.; Matyjaszewski, K.; Banquy, X. Wear Protection without Surface Modification Using a Synergistic Mixture of Molecular Brushes and Linear Polymers. *ACS Nano* **2017**, *11*, 1762- 1769.

30. Xia, Y.; Adibnia, V.; Huang, R.; Murschel, F.; Faivre, J.; Xie, G.; Olszewski, M.; De Crescenzo, G.; Qi, W.; He, Z.; Su, R.; Matyjaszewski, K.; Banquy, X. Biomimetic Bottlebrush Polymer Coatings for Fabrication of Ultralow Fouling Surfaces. *Angew, Chem. Int. Ed.* **2019**, *58*, 1308-1314.

31. Pereira, A.; Sheikh, S.; Blaszykowski,C.; Pop-Georgievski, O.; Fedorov, K.; Thompson, M.; Rodriguez-Emmenegger, C. Antifouling Polymer Brushes Displaying Antithrombogenic Surface Properties. *Biomacromolecules* **2016**, *17*, 1179-1185.
32. Daniel, W. F. M.; Burdynska, J.; Vatankhah-Varnoosfaderani, M.; Matyjaszewski, K.; Paturej, J.; Rubinstein, M.; Dobrynin, A.V.; Sheiko, S. S. Solvent-Free, Supersoft and Superelastic Bottlebrush Melts and Networks. *Nat. Mater.* **2015**, *15*, 183-189.
33. Pakula, T.; Zhang, Y.; Matyjaszewski, K.; Lee, H-I.; Boerner, H.; Qin, S.; Berry, G. C. Molecular Brushes as Super Soft Elastomers. *Polymer* **2016**, *47*, 7198-7206.
34. Tonge, C. M.; Sauve, E. R.; Cheng, S.; Howard, T. A.; Hudson, Z. M. Multiblock Bottlebrush Nanofibers from Organic Electronic Materials. *J. Am. Chem. Soc.* **2018**, *140*, 11599-11603.
35. Qi, Y.; Simakova, A.; Ganson, N. J.; Li, X.; Luginbuhl, K. M.; Ozer, I.; Liu, W.; Hershfield, M. S.; Matyjaszewski, K.; Chilkoti, A. A Brush-Polymer/Exendin-4 Conjugate Reduces Blood Glucose Levels for up to Five Days and Eliminates Poly(ethylene glycol) Antigenicity. *Nat. Biomed. Eng*. **2016**, *1*, 1-12.
36. Johnson, J. A.; Lu, Y. Y.; Burts, A. O.; Xia, Y.; Durrell, A. C.; Tirrell, D. A.; Grubbs, R. H. Drug-Loaded, Bivalent-Bottle-Brush Polymers by Graft-through ROMP. *Macromolecules* **2010**, *43*, 10326–10335.
37. Fredrickson, G. H. Surfactant-Induced Lyotropic Behavior of Flexible Polymer Solutions. *Macromolecules* **1993**, *26*, 2825-2831.

38. Subbotin, A.; Saariaho, M.; Stepanyan, R.; Ikkala, O.; Brinke, G. Cylindrical Brushes of Comb Copolymer Macromolecules Containing Rigid Side Chains. *Macromolecules* **2000**, *33*, 6168-6173.

39. Hsu, H-P.; Paul, W.; Binder, K. One- and Two-Components Bottle-Brush Polymers: Simulations Compared to Theoretical Predictions. *Macromol. Theory. Simul.* **2007**, *16*, 660-689.

40. Hsu, H-P.; Paul, W.; Binder, K. Estimation of Persistence Lengths of Semiflexible Polymers: Insight from Simulations. *Polym. Sci. Ser. C.* **2013**, *55***,** 39–59.

41. Zhang, J-Z.; Peng, X-Y.; Liu, S.; Jiang, B-P.; Ji, S-C, Shen, X-C. The Persistence Length of Semiflexible Polymers in Lattice Monte Carlo Simulations. *Polymers* **2019**, *11*, 1-12.

42. Dutta, S.; Pan, T.; Sing, C. E. Bridging Simulation Length Scales of Bottlebrush Polymers Using a Wormlike Cylinder Model. *Macromolecules* **2019**, *52*, 4858-4878.

43. Liang, H.; Cao, Z.; Wang, Z.; Sheiko, S.; Dobrynin, A. Combs and Bottlebrushes in a Melt. *Macromolecules* **2017**, *50*, 3420-3437.

44. Chatterjee, D.; Vilgis, T. A. Scaling Laws of Bottle- Brush Polymers in Dilute Solutions. *Macromol. Theory Simul.* **2016**, *25*, 518-523.

45. Binder, K.; Hsu, H. -P.; Paul, W. Understanding the Stiffness of Macromolecules: From Linear Chains to Bottlebrushes. *Eur. Phys. J. Special Topics* **2016**, *225*, 1663-1671.

46. Hsu, H. -P.; Paul, W.; Binder, K. Estimation of Persistence Length of Semiflexible Polymers: Insight from Simulations. *Polym. Sci. Ser. C* **2013**, *55*, 39-59.

47. Kratky, O.; Porod, G. Röntgenuntersuchung Gelöster Fadenmoleküle. *Rec. Trav. Chim.* **1949**, *68*, 1106-1122.

48. Wintermantel, M.; Gerle, M.; Fischer, K.; Schmidt, M. Molecular Bottlebrushes. *Macromolecules* **1996**, *29*, 978-983.

49. Nakamura, Y.; Wan, Y.; Mays, J. W.; Iatrou, H.; Hadjichristidis, N. Radius of Gyration of Polystyrene Combs and Centipedes in Solution. *Macromolecules* **2000**, *33*, 8323-8328.

50. Kikuchi, M.; Lien, L. T. N.; Narumi, A.; Jinbo, Y.; Izumi, Y.; Nagai, K.; Kawaguchi, S. Conformational Properties of Cylindrical Rod Brushes Consisting of a Polystyrene Main Chain and Poly(n-hexyl isocyanate) Side Chains. *Macromolecules* **2008**, *41*, 6564-6572.

51. Li, Y.; Zhang, M.; Mao, M.; Turner, S. R.; Moore, R. B.; Mourey, T. H.; Slater, L. A.; Hauenstain, J. R. Chain Stiffness of Stilbene Containing Alternating Copolymers by SAXS and SEC. *Macromolecules* **2012**, *45*, 1595-1601.

52. Kikuchi, M.; Nakano, R.; Jinbo, Y.; Saito, Y.; Ohno, S.; Togashi, D.; Enomoto, K.; Narumi, A.; Haba, O.; Kawaguchi, S. Graft Density Dependence of Main Chain Stiffness in Molecular Rob Brushes. *Macromolecules* **2015**, *48*, 5878-5886.

53. Terao, K.; Takeo, Y.; Tazaki, M.; Nakamura, Y.; Norisuye, T. Polymacromonomer Consisting of Polystyrene. Light Scattering Characterization in Cyclohexane. *Polym. J.* **1999**, *31*, 193-198.

54. Terao, K.; Nakamura, Y.; Norisuye, T. Solution Properties of Polymacromonomers Consisting of Polystyrene. 2. Chain Dimensions and Stiffness in Cyclohexane and Toluene. *Macromolecules* **1999**, *32*, 711-716.

55. Zhang, B.; Gröhn, F.; Pedersen, J. S.; Fischer, K.; Schmidt, M. Conformation of Cylindrical Brushes in Solution: Effect of Side Chain Length. *Macromolecules* **2006**, *39*, 8440-8450.

56. Bolisetty, S.; Airaud, C.; Xu, Y.; Müller, A. H. E.; Harnau, L.; Rosenfeldt, S.; Lindner, P.; Ballauff, M. Softening of the Stiffness of Bottle-Brush Polymers by Mutual Interaction. *Phys. Rev. E.* **2007**, *75*, 1-4.

57. Lecommandoux, S.; Checot, F.; Borsali, R.; Schappacher, M.; Deffieux, A. Effect of Dense Grafting on the Backbone Conformation of Bottlebrush Polymers: Determination of the Persistence Length in Solution. *Macromolecules* **2002**, *35*, 8878-8881.

58. Ramachandran, R.; Beaucage, G.; Kulkarni, A. S.; McFaddin, D.; Merrick-Mack, J.; Galiatsatos, V. Persistence Length of Short-Chain Branched Polyethylene. *Macromolecules*, **2008**, *41*, 9802-9806.

59. Rathgeber, S.; Pakula, T.; Wilk, A.; Matyjaszewski, K.; Beers, K. L. On the Shape of Bottle-Brush Macromolecules: Systematic Variation of Architectural Parameters. *J. Chem. Phys.* **2005**, *122,* 1-13.

60. Hsu, H.-P.; Paul, W.; Rathgeber, S.; Binder, K. Characteristic Length Scales and Radial Monomer Density Profiles of Molecular Bottle-Brushes: Simulation and Experiment. *Macromolecules* **2010**, *43*, 1592-1601.
61. Birks, J. B. *Photophysics of Aromatic Molecules*; Wiley: New York, 1970; p 301.
62. Lutz, J.-F. Thermoswitchable Materials Prepared Using the OEGMA-Platform. *Adv. Mater.* **2011**, *23*, 2237-2243.
63. Cho, H. Y.; Krys, P.; Szcesniak, K.; Schroeder, H.; Park, S.; Jurga, S.; Buback, M.; Matyjaszewski, K. Synthesis of Poly(OEOMA) Using Macromonomers via "Grafting Throug" ATRP. *Macromolecules* **2015**, *48*, 6385-6395.
64. Tuukkanen, A. T.; Spilotros, A.; Svergun, D. I. Progress in Small-Angle Scattering from Biological Solutions at High-Brilliance Synchrotron. *IUCrJ* **2017**, *4*, 518-528.
65. Mourey, T.; Le, K.; Bryan, T.; Zheng, S.; Bennett, G. Determining Persistence Length by Size-Exclusion Chromatography. *Polymer* **2005**, *46*, 9033-9042
66. Matyjaszewski, K.; Jakubowski, W.; Min, K.; Tang, W.; Huang, J.; Braunecker, W. A.; Tsarevsky, N. V. Diminishing catalyst concentration in atom transfer radical polymerization with reducing agents. *Proc. Natl. Acad. Sci. U.S.A.***2006**, *103*, 15309−15314.
67. Siu, H.; Duhamel, J. Molar Absorbance Coefficient of Pyrene Aggregates in Water Generated by a Poly(ethylene oxide) Capped at a Single End with Pyrene. *J. Phys. Chem. B.* **2012**, *116*, 1226-1233.

68. Press, W. H.; Flannery, B. P.; Teukolsky, S. A.; Vetterling, W. T. *Numerical Recipes. The Art of Scientific Computing (Fortran Version)*; Cambridge University Press: Cambridge, p 82, 1992.
69. Farhangi, S.; Duhamel, J. Probing Side Chain Dynamics of Branched Macromolecules by Pyrene Excimer Fluorescence. *Macromolecules* **2015**, *49*, 353-361.
70. Rathgeber, S.; Pakula, T.; Wilk, A.; Matyjaszewski, K.; Lee, H-L.; Beers, K. Bottle-Brush Macromolecules in Solution: Comparison between Results Obtained from Scattering Experiments and Computer Simulations. *Polymer* **2006**, *47*, 7318-7327.
71. Lakowicz, J. R. Principles of Fluorescence, 3rd Ed. Springer, NY, 2006, pp 56, 284-287.
72. Rumble, J. R. Viscosity of Liquids. In *CRC Handbook of Chemistry and Physics*, 101st ed.; (Electronic ed.). CRC Press: Taylor & Francis. 1978; p 239-242.
73. Thoma, J.; McNelles, S. A.; Adronov, A.; Duhamel, J. Direct Measure of the Local Concentration of Pyrenyl Groups in Pyrene-Labeled Dendrons Derived from the Rate of Fluorescence Collisional Quenching. *Polymers* **2020**, *12*, 2919.
74. Rouse, P. E. A Theory of the Linear Viscoelastic Properties of Dilute Solutions of Coiling Polymers. *J. Chem. Phys.* **1953**, *21*, 1272-1280.
75. Zimm, B. H. Dynamics of Polymer Molecules in Dilute Solution: Viscoelasticity, Flow Birefringence, and Dielectric Loss. *J. Chem. Phys.* **1956**, *24*, 269-278.
76. Nakamura, Y.; Norisuye, T. Backbone Stiffness of Comb-Branched Polymers. *Polym. J.* **2001**, *33*, 874-878.

77. Bohdanecky, M. New Method for Estimating the Parameters of the Wormlike Chain Model from the Intrinsic Viscosity of Stiff-Chain Polymers. *Macromolecules* **1983**, *16*, 1483-1492.

78. Qi, H.; Liu, X.; Henn, D. M.; Mei, S.; Staub, M. C.; Zhao, B.; Li, C. Y. Breaking Translational Symmetry via Polymer Chain Overcrowding in Molecular Bottlebrush Crystallization. *Nat. Commun*. **2020**, *11*,1-9.

Chapter 5

1. Abuchowski, A.; Van Es, T.; Palczuk, C.; Davis, F. F. Alteration of Immunological Properties of Bovine Serum Albumin by Covalent Attachment of Polyethylene Glycol. *J. Biol. Chem.* **1977**, *252*, 3578-3581.

2. Abuchowski, A.; McCoy, J. R.; Palczuk, N. C.; Van Es, T.; Davis, F. F. Effect of Covalent Attachment of Polyethylene Glycol on Immunogenicity and Circulating Life of Bovine Liver Catalase. *J. Biol. Chem.* **1977**, *252*, 3582-3586.

3. Caliceti, P.; Veronese, F. M. Pharmacokinetic and Biodistribution Properties of Poly(ethylene glycol)-Protein Conjugates. *Adv. Drug Deliv. Rev.* **2003**, *55*, 1261-1277.

4. Alconcel, S. N. S.; Baas, A. S.; Maynard, H. D. FDA-Approved Poly(ethylene glycol)-Protein Conjugate Drugs. *Polym. Chem.* **2011**, *2*, 1442-1448.

5. Hershfiel, M. S. PEG-ADA Replacewment Therapy for Adenosine Deaminase Deficiency: An Update after 8.5 Years. *Clin. Immunol. Immunopathol.* **1995**, *76*, S228-232.
6. Knop, K.; Hoogenboom, D.; Fischer, D. Schubert, U. S. Poly(ethylene glycol) in Drug Delivery: Pros and Cons as Well as Potential Alternatives. *Angew. Chem., Int. Ed.* **2010**, *49*, 6288-6308.
7. Qi, Y.; Simakova, A.; Ganson, N. J.; Li, X.; Luginbuhl, K. M.; Ozer, I.; Liu, W.; Hershfield, M. S.; Matyjaszewski, K.; Chilkoti, A. A Brush-Polymer/Exendin-4 Conjugate Reduces Blood Glucose Levels for up to Five Days and Eliminates Poly(ethylene glycol) Antigenicity. *Nat. Biomed. Eng.* **2016**, *1*, 1-12.
8. Fox, M. E.; Szoka, F. C.; Fréchet, J. M. J. Soluble Polymer Carriers for the Treatment of Cancer: The Importance of Molecular Architecture. *Acc. Chem. Res.* **2009**, *42*, 1141-1151.
9. Imran Ul-Haq, M.; Lai, B. F. L.; Chapanian, R.; Kizhakkedathu, J. N. Influence of Architecture of High Molecular Weight Linear and Branched Polyglycerols on their Biocompatibility and Biodistribution. *Biomaterials* **2012**, *33*, 9135-9147.
10. Bakkour, Y.; Darcos, V.; Coumes, F.; Li, S.; Coudance, J. Brush-like Amphiphilic Copolymers Based on Polylactide and Poly(ethylene glycol): Synthesis, Self-Assembly and Evaluation as Drug Carrier. *Polymer* **2013**, *54*, 1746-1754.
11. Jones, M-C.; Ranger, M.; Leroux, J-C. pH-Sensitive Unimolecular Polymeric Micelles: Synthesis of a Novel Drug Carrier. *Bioconjugate Chem.* **2003**, *14*, 774-781.

12. Hussain, H.; Mya, K. Y.; He, C. Self-Assembly of Brush-Like Poly[poly(ethylene glycol) methyl ether methacrylate] Synthesized via Aqueous Atom Transfer Radical Polymerization. *Langmuir* **2008**, *24*, 13279-13286.
13. Müllner, M.; Dodds, S. J.; Nguyen, T-H.; Senyschyn, D.; Porter, C. J. H.; Boyd, B. J.; Caruso, F. Size and Rigidity of Cylindrical Polymer Brushes Dictate Long Circulating Properties In Vivo. *ACS Nano* **2015**, *9*, 1294-1304.
14. Blum, A. P.; Kammeyer, J. K.; Yin, J.; Crystal, D. T.; Rush, A. M.; Gilson, M, K.; Gianneschi, N. C. Peptides Displayed as High Density Brush Polymers Resist Proteolysis and Retain Bioactivity. *J. Am. Chem. Soc.* **2014**, *136*, 15422-15437.
15. Wang, D.; Lin, J.; Jia, F.; Tan, X.; Wangm Y.; Sun, X.; Cao, X.; Che, F.; Lu, H.; Gao, X.; Shimkonis, J. C.; Nyoni, Z.; Lu, X.; Zhang, K. Bottlebrush-Architectured Poly(ethylene glycol) as an Efficient Vector for RNA Interference in Vivo. *Sci. Adv.* **2019**, *5*, 1-10.
16. Lu, X.; Tran, T-H.; Jia, F.; Tan, X.; Davis, S.; Krishnan, S.; Amiji, M. M.; Zhang, K. Providing Oligonucleotides with Steric Selectivity by Brush-Polymer Assisted Compaction. *J. Am. Chem. Soc.* **2015**, *137*, 12466-12469.
17. Zhang, Y.; Yin, Q.; Lu, H.; Xia, H.; Lin, Y.; Cheng, J. PEG-Polypeptide Dual Brush Block Copolymers: Synthesis and Application in Nanoparticle Surface PEGylation. *ACS Macro Lett.* **2013**, *2*, 809-813.

18. Yao, Q.; Gutierrez, D. C.; Hoang, N. H.; Kim, D.; Wang, R.; Hobbs, C.; Zhu, L. Efficient Codelivery of Paclitaxel and Curcumin by Novel Bottlebrush Copolymer-based Micelles. *Mol. Pharmaceutics* **2017**, *14*, 2378-2389.

19. Yu, Q.; Roberts, M. G.; Pearce, S.; Oliver, A. M.; Zhou, H.; Allen, C.; Manners, I.; Winnik, M. A. Rodlike Block Copolymer Micelles of Controlled Length in Water Designed for Biomedical Applications. *Macromolecules* **2019**, *52*, 5231-5244.

20. Tran, T-H.; Nguyen, C. T.; Gonzalez-Fajardo, L.; Hargrove, D.; Song, D.; Deshmukh, P.; Mahajan, L.; Ndaya, D.; Lai, L.; Kasi, R. M. Long Circulating Self-Assembled Nanoparticles from Cholesterol-Containing Brush-Like Block Copolymers for Improved Drug Delivery to Tumors. *Biomacromolecules* **2014**, *15*, 4363-4375.

21. Liao, L.; Liu, J.; Dreaden, E. C.; Morton, S. W.; Shopsowitz, K. E.; Hammond, P. T.; Johnson, J. A. A Convergent Synthetic Platform for Single-Nanoparticle Combination Cancer Therapy: Ratiometric Loading and Controlled Release of Cisplatin, Doxorubicin, and Camptothecin. *J. Am. Chem. Soc.* **2014**, *136*, 5896-5899.

22. Hörtz, C.; Birke, A.; Kaps, L.; Decker, S.; Wachtersbach, E.; Fischer, K.; Schuppan, D.; Barz, M.; Schmidt, M. Cylindrical Brush Polymers with Polysarcosine Side Chains: A Novel Biocompatible Carrier for Biomedical Applications. *Macromolecules* **2015**, *48*, 2074-2086.

23. Johnson, J. A.; Lu, Y. Y.; Burts, A. O.; Xia, Y.; Durrell, A. C.; Tirrell, D. A.; Grubbs, R. H. Drug-Loaded, Bivalent-Bottle-Brush Polymers by Graft-through ROMP. *Macromolecules* **2010**, *43*, 10326–10335.

24. Johnson, J. A.; Lu, Y. Y.; Burts, A. O.; Lim, Y-H.; Finn, M. G.; Koberstein, J.; Turro, N. J.; Tirrell, D. A.; Grubbs, R. H. Core-Clickable PEG-*Branch*-Azide Bivalent-Bottle-Brush Polymers by ROMP: Grafting-Through and Clicking-To. *J. Am. Chem. Soc.* **2011**, *133*, 559-566.

25. Li, H.; Liu, H.; Nie, T.; Chen, Y.; Wang, Z.; Huang, H.; Liu, L.; Chen, Y. Molecular Bottlebrush as a Unimolecular Vehicle with Tunable Shape for Photothermal Cancer Therapy. *Biomaterials* **2018**, *178*, 620-629.

26. Zou, J.; Jafr, G.; Themistou, E.; Yap, Y.; Wintrob, Z. A. P.; Alexandridis, P.; Ceacareanu, A. C.; Cheng, C. pH-Sensitive Brush Polymer-Drug Conjugates by Ring-Opening Metathesis Copolymerization. *Chem. Commun.* **2011**, *47*, 4493-4495.

27. Yu, Y.; Zou, J.; Yu, L.; Ji, W.; Li, Y.; Law, W-C.; Cheng, C. Functional Polylactide-g-Paclitaxel–(Poly(ethylene glycol) by Azide–Alkyne Click Chemistry. *Macromolecules* **2011**, *44*, 4793-4800.

28. Yu, Y.; Chen, C-K.; Law, W-C.; Mok, J.; Zou, J.; Prasad, P. N.; Cheng, C. Well-Defined Degradable Brush Polymer–Drug Conjugates for Sustained Delivery of Paclitaxel. *Mol. Pharmaceutics* **2013**, *10*, 867-874.

29. Zou, J.; Yu, Y.; Li, Y.; Ji, W.; Chen, C-K.; Law, W-C.; Prasad, P. N.; Cheng, C. Well-Defined Diblock Brush Polymer-Drug Conjugates for Sustained Delivery of Paclitaxel. *Biomater. Sci.* **2015**, *3*, 1078-1084.

30. Sowers, M. M.; McCombs, J. R.; Wang, Y.; Paletta, J. T.; Morton, S. W.; Dreaden, E. C.; Boska, M. D.; Ottaviani, F.; Hammond, P, T.; Rajca, A.; Johnson, J. A. Redox-Responsive Branched-Bottlebrush Polymers for *in vitro* MRI and Fluorescence Imaging. *Nature Commun.* **2014**, *5*, 1-9.

31. Yu, Y.; Chen, C-K.; Law, W-C.; Sun, H.; Prasad, P. N.; Cheng, C. A Degradable Brush Polymer-Drug Conjugate for pH-Responsive Release of Doxorubicin. *Poly. Chem.* **2015**, *6*, 953-961.

32. Chen, W.-L.; Cordero, R.; Tran, H.; Ober, C. K. 50th Anniversary Perspective: Polymer Brushes: Novel Surfaces for Future Materials. *Macromolecules* **2017**, *50*, 4089-4113.

33. Das, D.; Chen, J.; Srinivasan, S.; Kelly, A. M.; Lee, B.; Son, H.-N.; Radella, F.; West, T. E.; Ratner, D. M.; Convertine, A. J.; Skerrett, S. j.; Stayton, P., S. Synthetic Macromolecular Antibiotic Platform for Inhalable Therapy against Aerosolized Intracellular Alveolar Infections. *Mol. Pharmaceutics* **2017**, *14*, 1988-1997.

34. Das, D.; Srinivasan, S.; Kelly, A. M.; Chiu, D. Y.; Daugherty, B. K.; Ratner, D. M.; Stayton, P. S.; Convertine, A. J. RAFT Polymerization of Ciprofloxacin Prodrug Monomers, for the Controlled Intracellular Delivery of Antibiotics. *Polym. Chem.* **2016**, *7*, 826-837.

35. Zhang, J.; Muirhead, B.; Dodd, M.; Liu, L.; Xu, F.; Mangiacotte, N.; Hoare, T.; Sheardown, H. An Injectable Hydrogel Prepared Using a PEG/Vitamin E Copolymer Facilitating Aqueous-Driven Gelation. *Biomacromolecules* **2016**, *17*, 3648-3658.
36. Cai, T.; Chen, Y.; Wang, Y. ; Wang, H.; Liu, X.; Jin, Q.; Agarwal, S.; Ji, J. Functional 2-Methylene-1,3-Dioxepane Terpolymer: A Versatile Platform to Construct Biodegradable Polymeric Prodrugs for Intracellular Drug Delivery. *Polym. Chem.* **2014**, *5*, 4061-4068.
37. Li, L.; Song, Y.; Je, J. ; Zhang, M. ; Liu, J. ; Ni, P. Zwitterionic Shielded Polymeric Prodrug with Folate-Targeting and pH Responsiveness for Drug Delivery. *J. Mater. Chem. B* **2019**, *7*, 786-795.
38. Zhuang, Y.; Su, Y.; Peng, Y. ; Wang, D. ; Deng, H. ; Xi, X. ; Zhu, X. ; Lu, Y. Facile Fabrication of Redox-Responsive Thiol Containing Drug Delivery System via RAFT Polymerization. *Biomacromolecules* **2014**, *15*, 1408-1418.
39. Davaran, S.; Rashidi, M. R. ; Hashemi, M. Synthesis and Characterization of Methacrylic Derivatives of 5-Amino Salicylic Acid with pH-Sensitive Swelling Properties. *AAPS PharmSciTech* **2001**, *2*, 29, 1-6.
40. Krishnan, S.; Weinman, C. J.; Ober, C. K. Advances in Polymers for Anti-Biofouling Surfaces. *J. Mater. Chem.* **2008**, *18*, 3405-3413.
41. Chiag, Y.-C.; Chang, Y.; Chen, W.-Y.; Ruaan, R.-C. Biofouling Resistance of Ultrafiltration Membranes Controlled by Surface Self-Assembled Coating with PEGylated Copolymers. *Langmuir* **2012**, *28*, 1399-1407.

42. Kalyanasundaram, K.; Thomas, J. K. Environmental Effects on Vibronic Band Intensities in Pyrene Monomer Fluorescence and their Application in Studies of Micellar Systems. *J. Am. Chem. Soc.* **1977**, *99*, 2039–2044.
43. Siu, H.; Duhamel, J. Molar Absorbance Coefficient of Pyrene Aggregates in Water Generated by a Poly(ethylene oxide) Capped at a single end with Pyrene. *J. Phys. Chem. B.* **2012**, *116*, 1226-1233.
44. Zaragoza-Galán, G.; Fowler, M.; Rein, R.; Solladie, N.; Duhamel, J.; Rivera, E. Fluorescence Resonance Energy Transfer in Partially and Fully Labeled Pyrene Dendronized Porphyrins Studied with Model Free Analysis. *J. Phys. Chem. C* **2014**, *118*, 8280-8294.
45. Press, W. H.; Flannery, B. P.; Teukolsky, S. A.; Vetterling, W. T. *Numerical Recipies. The Art of Scientific Computing (Fortran Version)*; Cambridge University Press: Cambridge, p 82, 1992.
46. Yekta, A.; Duhamel, J.; Adiwidjaja, H.; Brochard, P.; Winnik, M. A. A Fluorescence Probe Study of Micelle Like Cluster Formation in Aqueous Solutions of Hydrophobically Modified Poly(ethylene oxide). *Macromolecules* **1993**, *26*, 1829-36.
47. Kim, D.; Amos, R. C.; Gauthier, M.; Duhamel, J. Assemblies of Hydrophobically Modified Starch Nanoparticles Probed by Surface Tension and Pyrene Fluorescence. *ACS Symposium Series-Molecular Assemblies: Characterization and Applications.* Ed. Nagarajan, R. **2020**, Chapter 5, pp 61-75.

48. Cheung, S-T.; Winnik, M. A.; Redpath, A. E. C. The Effects of Solvent on End-to-End Cyclization of Poly(ethylene oxide) Probed by Intramolecular Pyrene Excimer Formation. *Makromol. Chem.* **1982**, *183*, 1815-1824.

49. Kanagalingam, S.; Ngan, C. F.; Duhamel, J. Effect of Solvent Quality on the Level of Association and Encounter Kinetics of Hydrophobic Pendants Covalently Attached onto a Water-Soluble Polymer. *Macromolecules* **2002**, *35*, 8560- 8570.

50. Prazeres, T. J. V.; Beingessner, R.; Duhamel, J. Characterization of the Association Level of Pyrene-Labeled HASEs by Fluorescence. *Macromolecules* **2001**, *34*, 7876-7884.

51. Duhamel, J.; Kanagalingam, S.; O'Brien, T. J.; Ingratta, M, W. Side-Chain Dynamics of an a-Helical Polypeptide Monitored by Fluorescence. *J. Am. Chem. Soc.* **2003**, *125,* 12810-12822.

52. Zhang, Q.; Kim, D.; Li, L.; Patel, S.; Duhamel, J. Surfactant Structure-Dependent Interactions with Modified Starch Nanoparticles Probed by Fluorescence Spectroscopy. *Langmuir* **2019**, *35*, 3432-3444.

53. Farhangi, S.; Duhamel, J. Pyrenyl Derivative with a Four-Atom Linker that Can Probe the Local Polarity of Pyrene-Labeled Macromolecules. *J. Phys. Chem. B* **2016**, *120*, 834-842.

54. Claracq, J.; Santos, S. F. C. R.; Duhamel, J.; Dumousseaux, C. ; Corpart, J.-M. Rigid Interior of Styrene-Maleic Anhydride Copolymer Aggregates Probed by Fluorescence Spectroscopy. *Langmuir* **2002**, *18*, 3829-3835.

55. Kim, D.; Amos, R.; Gauthier, M. Duhamel, J. Applications of Pyrene Fluorescence to the Characterization of Hydrophobically Modified Starch Nanoparticles. *Langmuir* **2018**, *34*, 8611-8621.

56. *CRC Handbook of Chemistry and Physics* ,77th Ed.; Boca Raton, FL, 1996.

57. Effect of Side-chain Length on the Side-chain Dynamics of α–Helical Poly(L-glutamic acid) as Probed by a Fluorescence Blob Model. Ingratta, M.; Duhamel, J. *J. Phys. Chem. B* **2008**, *112*, 9209-9218.

Chapter 6

1. McNelles, S.; Thoma, J.; Adronov, A.; Duhamel, J. Quantitative Characterization of the Molecular Dimensions of Flexible Dendritic Macromolecules by Pyrene Excimer Fluorescence. *Macromolecules* **2018**, *51*, 1586-1590.
2. Bohdanecky, M. New Method for Estimating the Parameters of the Wormlike Chain Model from the Intrinsic Viscosity of Stiff-Chain Polymers. *Macromolecules* **1983**, *16*, 1483-1492.
3. Matyjaszewski, K.; Tsarevsky, N. V. Macromolecular Engineering by Atom Transfer Radical Polymerization. *J. Am. Chem. Soc.* **2014**, *136*, 6513-6533.
4. Gauthier, M. Arborescent Polymers and Other Dendrigraft Polymers: A Journey Into Structural Diversity. *J. Polym. Sci. Part A: Polym. Chem.* **2007**, *45*, 3803-3810.

5. Fredrickson, G. H. Surfactant-Induced Lyotropic Behavior of Flexible Polymer Solutions. *Macromolecules***1993**, *26*, 2825-2831.
6. Farhangi, S.; Duhamel, J. Probing the Side Chain Dynamics of Branched Macromolecules by Pyrene Excimer Fluorescence. *Macromolecules* **2016**, *49*, 353-361.

References: Appendix A

S4

1. Duhamel, J. New Insights in the Study of Pyrene Excimer Fluorescence to Characterize Macromolecules and their Supramolecular Assemblies in Solution. *Langmuir* **2012**, *28*, 6527-6538.
2. Duhamel, J. Global Analysis of Fluorescence Decays to Probe the Internal Dynamics of Fluorescently Labeled Macromolecules. *Langmuir* **2014**, *30*, 2307-2324.
3. Yamakawa, H.; Fujii, M. Intrinsic Viscosity of Wormlike Chains, Determination of the Shift Factor. *Macromolecules* **1974**, *7*, 128-135.
4. Bohdanecky, M. New Method for Estimating the Parameters of the Wormlike Chain Model from the Intrinsic Viscosity of Stiff-Chain Polymers. *Macromolecules* **1983**, *16*, 1483-1492.

Appendix A: Supporting Information (SI)

S2 - Supporting Information for Chapter 2

Global Model Free Analysis (MFA) of the monomer and excimer fluorescence decays

Equations S2.1 and S2.2 were used to fit the monomer and excimer fluorescence decays globally according to the model free analysis (MFA). As explained in the main text, pyrene excimer formation (PEF) is assumed to occur with a distribution of rate constants that results in a distribution of decay times (τ_i) that is handled by a sum of exponentials with decay times τ_i and pre-exponential factors (a_i). Three species are expected to be present in a solution of a pyrene derivative leading to PEF. These are the pyrenes that are isolated, cannot form excimer, and behave as if they free in solution (Py_{free}*), form excimer by diffusive encounters (Py_{diff}*), and are aggregated as *E0** and *EL**, where *E*0* and *EL** correspond to pyrene aggregates that are well- and poorly stacked and emit with their lifetime τ_{E0} and τ_{EL}, respectively. The pyrene species that generate an excimer *E*0* or *EL** by diffusion are referred to as Py_{diffE0}* and Py_{diffEL}*, respectively.

$$[Py^*]_{(t)} = ([Py^*_{diffE0}]_{(t=0)} + [Py^*_{diffD}]_{(t=0)}) \times \sum_{i=1}^{n} a_i \times \exp(-t/\tau_i) + [Py^*_{free}]_{(t=0)} \times \exp(-t/\tau_M) \quad \text{(S2.1)}$$

$$[E^*]_{(t)} = -[Py^*_{diffE0}]_{(t=0)} \times \sum_{i=1}^{n} a_i \frac{\frac{1}{\tau_i} - \frac{1}{\tau_M}}{\frac{1}{\tau_i} - \frac{1}{\tau_{E0}}} \exp(-t/\tau_i)$$

$$+\left([E0^*]_{(t=0)} + [Py^*_{diffE0}]_{(t=0)} \times \sum_{i=1}^{n} a_i \frac{\frac{1}{\tau_i} - \frac{1}{\tau_M}}{\frac{1}{\tau_i} - \frac{1}{\tau_{E0}}} \right) \times \exp(-t/\tau_{E0})$$

$$-[Py^*_{diffEL}]_{(t=0)} \times \sum_{i=1}^{n} a_i \frac{\frac{1}{\tau_i} - \frac{1}{\tau_M}}{\frac{1}{\tau_i} - \frac{1}{\tau_{EL}}} \exp(-t/\tau_i)$$

$$+\left([EL^*]_{(t=0)} + [Py^*_{diffEL}]_{(t=0)} \times \sum_{i=1}^{n} a_i \frac{\frac{1}{\tau_i} - \frac{1}{\tau_M}}{\frac{1}{\tau_i} - \frac{1}{\tau_{EL}}} \right) \times \exp(-t/\tau_{EL}) + [ES^*]_{(t=0)} \times \exp(-t/\tau_S) \quad \text{(S2.2)}$$

The MFA program retrieves parameters that yields the molar fractions f_{diffE0}, f_{diffEL}, f_{free}, f_{E0}, and f_{EL} of the species Py_{diffE0}*, Py_{diffEL}*, Py_{free}*, $E0$*, and EL*, respectively. The state of the different pyrene molecules, that are forming by diffusive encounters, isolated, and aggregated, is then represented by the molar fractions f_{diff} (= f_{diffE0} + f_{diffEL}), f_{free}, and f_{agg} (= f_{E0} + f_{EL}), respectively.

Global Birks Scheme Analysis of the monomer and excimer fluorescence decays

The kinetic scheme representing pyrene excimer formation according to the Birks scheme is described in Scheme S2.1.

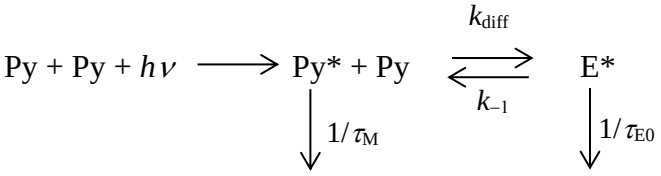

Scheme S2.1. Pyrene excimer formation according to the Birks scheme

Absorption of a photon by a ground-state pyrene in Scheme S2.1 results in an excited pyrene that can either fluoresce with its natural lifetime τ_M or diffusively encounter a ground-state pyrene to form an excimer ($E0^*$) with a rate constant k_{diff}. The excimer can either fluoresce with its lifetime τ_{E0} or dissociate with a rate constant k_{-1}. According to Scheme S2.1, the equations for the time-dependent concentrations of the pyrene monomer and excimer are presented in Equations S2.3 – S2.6, where $X = k_{diff} + \tau_M^{-1}$ and $Y = k_{-1} + \tau_{E0}^{-1}$.

$$[Py^*] = \frac{[Py^*]_o}{\sqrt{(X-Y)^2 + 4k_{diff}k_{-1}}}\left[\left(X - \tau_2^{-1}\right)\times\exp(-t/\tau_1) - (X - \tau_1^{-1})\times\exp(-t/\tau_2)\right] \quad \text{(S2.3)}$$

$$[E^*] = \frac{k_1[Py^*]_o}{\sqrt{(X-Y)^2 + 4k_{diff}k_{-1}}}\left[-\exp(-t/\tau_1) + \exp(-t/\tau_2)\right] \quad \text{(S2.4)}$$

$$\tau_1^{-1} = \frac{X + Y + \sqrt{(X-Y)^2 + 4k_{diff}k_{-1}}}{2} \quad \text{(S2.5)}$$

$$\tau_2^{-1} = \frac{X + Y - \sqrt{(X-Y)^2 + 4k_{diff}k_{-1}}}{2} \quad \text{(S2.6)}$$

[1]H-NMR Spectrum

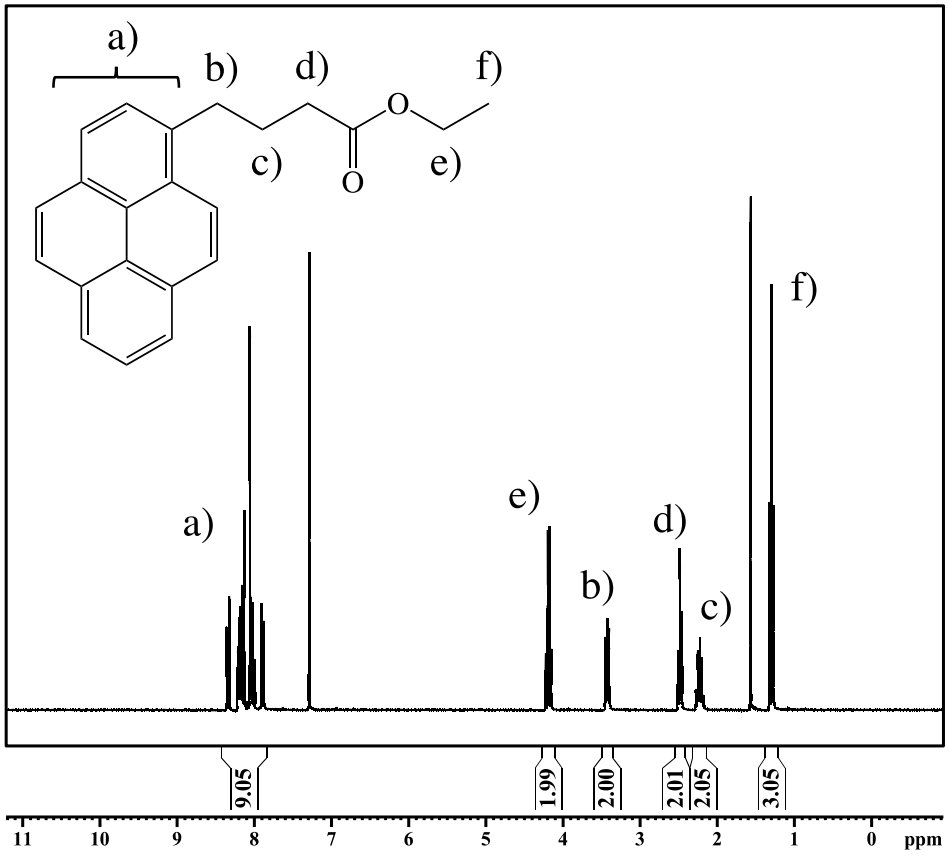

Figure S2.1. [1]H-NMR spectrum of ethyl 4-(1-pyrene)butyrate (PyBE). (300 MHz, $CDCl_3$): δ 1.30 (t, 3H), 2.23 (p, 2H), 2.48 (t, 2H), 3.42 (t, 2H), 4.18 (q, 2H), 7.82-8.41 (m, 9H).

Sample fit of the MFA

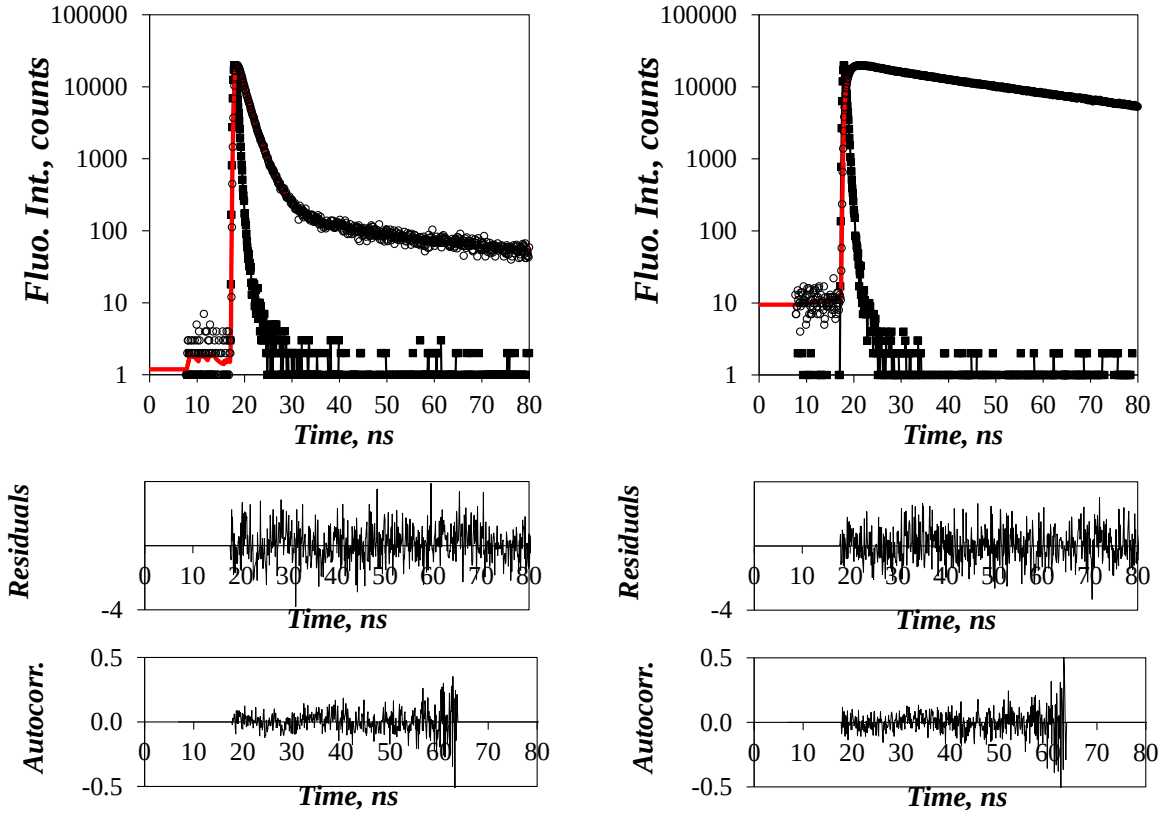

Figure S2.2. MFA of the (A) monomer (λ_{em} = 375 nm) and (B) excimer (λ_{em} = 510 nm) decay of Py_{32}-G(5) in degassed DMSO. χ^2 = 1.13, λ_{ex} = 344 nm.

SSF spectra of ethyl 4-(1-pyrene)butyrate (PyBE)

The SSF spectra for PyBE where acquired using the front face geometry to minimize reabsorption and the inner filter effect.

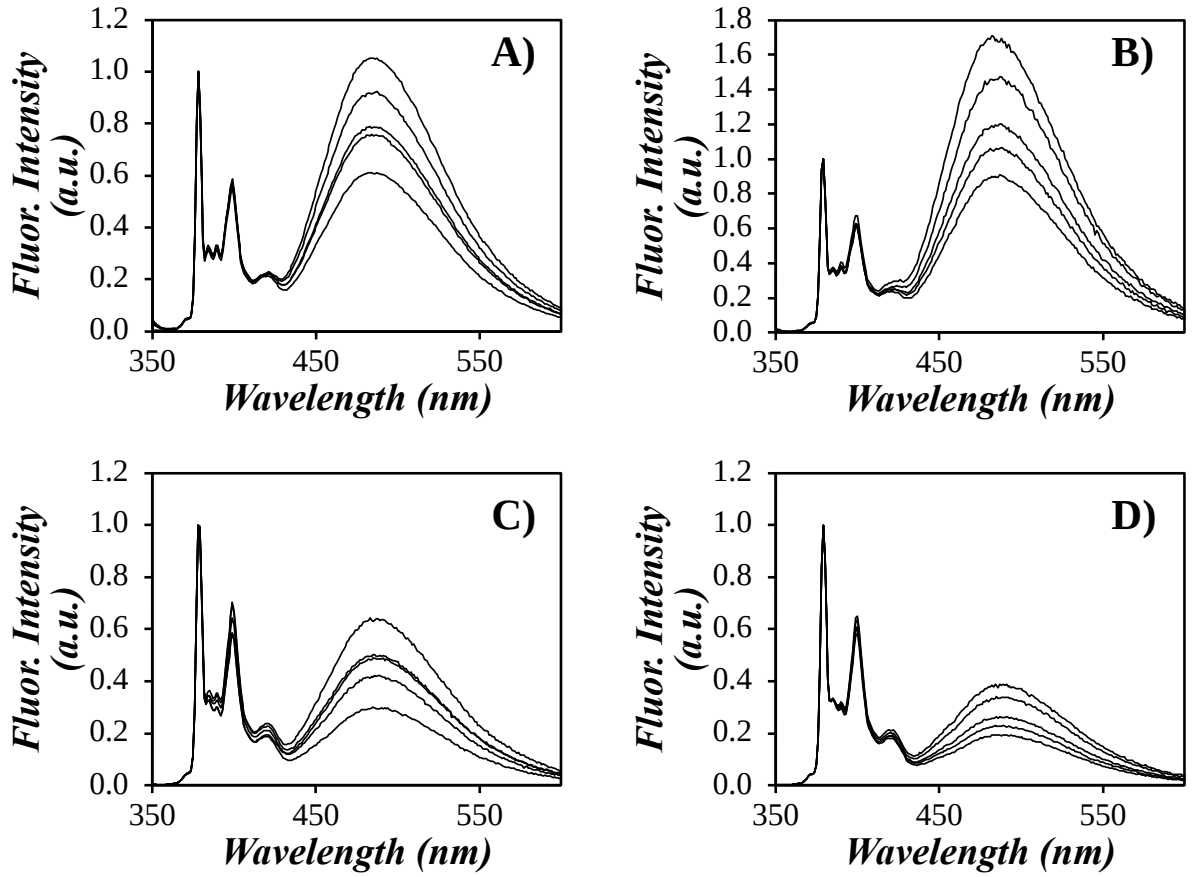

Figure S2.3. SSF spectrum of ethyl 4-pyrenylbutanoate in (A) THF, (B) toluene, (C) DMF, and (D) DMSO.

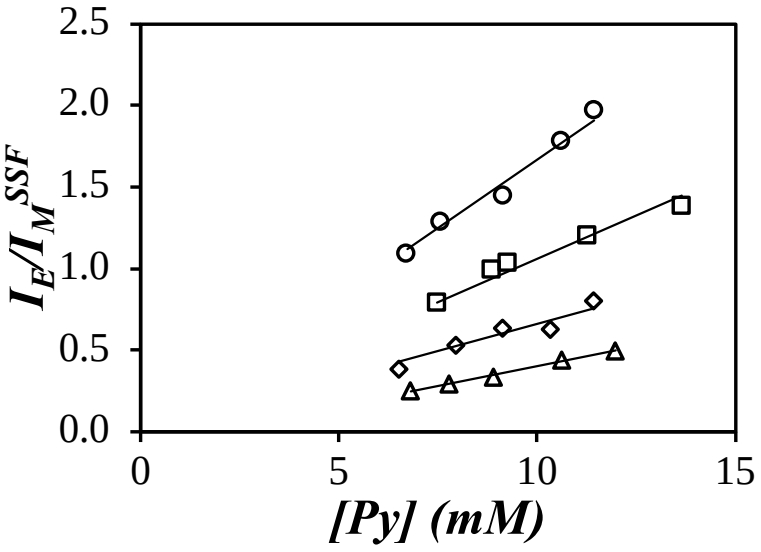

Figure S2.4. Plot of the I_E/I_M ratio versus concentration of PyBE in (○) toluene, (□) THF, (◇) DMF, and (△) DMSO.

Parameters retrieved from the Birks Scheme Analysis

Table S2.1. Parameters retrieved from the Birks scheme analysis of both the monomer and excimer decays of ethyl 4-(1-pyrene)butyrate in degassed toluene (Tol), *N*,*N*-dimethylformamide (DMF), dimethylsulfoxide (DMSO), and tetrahydrofuran (THF).

	Conc. (mM)	a_{M1}	τ_1 *(ns)*	a_{M2}	τ_2 *(ns)*	a_{E1}	a_{E2}	$k_{diff}\times[PyBE]$ (μs^{-1})	k_{-1} (μs^{-1})	τ_E *(ns)*	χ^2
Tol τ_M = 194 ns	6.7	0.67	31	0.33	61	2.27	2.29	22.0	2.7	53	1.07
	7.6	0.73	29	0.27	59	1.88	1.90	24.8	2.6	52	1.19
	9.1	0.80	25	0.20	58	1.65	1.66	30.3	2.7	52	1.16
	10.6	0.85	22	0.15	56	1.54	1.56	36.0	2.7	52	1.22
	11.4	0.85	21	0.15	55	1.49	1.50	38.1	3.0	51	1.21
DMF τ_M = 181 ns	6.5	0.28	42	0.72	81	1.95	1.96	10.0	2.7	56	1.21
	8.0	0.40	40	0.60	73	2.30	2.32	12.8	2.5	55	1.22
	9.1	0.45	38	0.55	68	2.43	2.45	14.5	2.3	53	1.19
	10.3	0.54	36	0.46	65	2.40	2.42	16.7	2.4	53	1.19
	11.4	0.59	34	0.41	63	2.30	2.31	18.2	2.4	52	1.14
DMSO τ_M = 145 ns	6.8	0.18	43	0.82	82	2.22	2.25	7.2	2.4	54	1.34
	7.8	0.20	43	0.80	75	2.54	2.58	8.3	1.9	52	1.33
	8.9	0.26	42	0.74	70	2.81	2.84	9.8	1.8	51	1.36
	10.6	0.36	42	0.64	64	3.35	3.39	11.7	1.3	51	1.36
	12.0	0.39	41	0.61	62	3.49	3.52	12.4	1.3	51	1.37
THF τ_M = 217 ns	7.5	0.50	31	0.50	76	1.61	1.62	18.0	5.1	57	1.11
	8.9	0.57	29	0.43	72	1.59	1.60	21.3	5.1	56	1.14
	9.3	0.60	29	0.40	70	1.81	1.82	22.1	4.5	56	1.11
	11.3	0.68	26	0.32	66	1.62	1.63	26.5	4.5	55	1.12
	13.7	0.75	23	0.25	63	1.40	1.41	32.6	4.8	55	1.12

Parameters retrieved from the MFA

Table S2.2. Parameters retrieved from the MFA (using program sumegs10bg) of both the monomer and excimer decays of ethyl 4-(1-pyrene)butyrate in degassed tetrahydrofuran (THF), degassed toluene (Tol), degassed dimethylformamide (DMF), and degassed dimethylsulfoxide (DMSO).

	Conc. (mM)	a_1	τ_1 *(ns)*	a_2	τ_2 *(ns)*	f_{Ediff}^{E0}	f_{EE0}	τ_{E0} *(ns)*	χ^2
THF	7.5	0.46	29	0.54	75	1.00	0.00	57	1.03
τ_M =	8.9	0.54	28	0.46	70	0.99	0.01	56	1.08
217 ns	9.3	0.58	28	0.42	68	0.99	0.01	56	1.05
	11.3	0.65	25	0.35	64	0.99	0.01	55	1.07
	13.7	0.72	22	0.28	61	0.99	0.01	55	1.02
Tol	6.7	0.64	30	0.36	60	0.99	0.01	53	1.02
τ_M =	7.6	0.67	27	0.33	57	0.99	0.01	52	1.10
194 ns	9.1	0.74	24	0.26	53	0.99	0.01	52	1.11
	10.6	0.82	21	0.18	53	0.99	0.01	52	1.16
	11.4	0.81	20	0.19	50	0.99	0.01	51	1.14
DMF	6.5	0.21	37	0.79	79	1.00	0.00	56	1.10
τ_M =	8.0	0.32	36	0.68	71	0.99	0.01	55	1.14
181 ns	9.1	0.31	32	0.69	64	0.99	0.01	53	1.07
	10.3	0.45	33	0.55	62	0.99	0.01	53	1.06
	11.4	0.45	31	0.55	58	0.99	0.01	52	1.05
DMSO	6.8	0.09	32	0.91	80	0.99	0.01	53	1.07
τ_M =	7.8	0.10	31	0.90	73	0.99	0.01	51	1.18
145 ns	8.9	0.11	29	0.89	67	0.99	0.01	51	1.16
	10.6	0.13	29	0.87	60	0.99	0.01	51	1.01
	12.0	0.13	28	0.87	58	0.99	0.01	50	1.13

Table S2.3. Parameters retrieved from the MFA of the monomer decays of the Py_x-G(*N*) dendrons in degassed toluene (Tol), degassed dimethylformamide (DMF), and degassed dimethylsulfoxide (DMSO).

	Generation (*N*)	a_1	τ_1 (ns)	a_2	τ_2 (ns)	a_3	τ_3 (ns)	*fMfree*	χ^2
Tol τ_M = 200 ns	1	0.16	1.6	0.79	5.7	0.04	17.2	0.010	1.05
	2	0.20	1.0	0.79	2.8	0.01	18.1	0.003	1.12
	3	0.25	0.4	0.73	1.7	0.01	7.5	0.004	1.02
	4	0.42	0.4	0.57	1.2	0.01	10.4	0.003	1.14
	5	0.57	0.3	0.42	1.0	0.01	6.9	0.003	1.17
	6	0.59	0.3	0.39	0.8	0.02	4.6	0.007	1.17
DMF τ_M = 180 ns	1	0.11	2.0	0.61	7.9	0.27	13.0	0.013	0.98
	2	0.24	2.0	0.74	4.3	0.01	32.9	0.004	1.01
	3	0.20	1.0	0.79	2.6	0.01	24.0	0.003	1.03
	4	0.50	1.2	0.50	2.1	0.01	30.1	0.002	1.04
	5	0.47	0.8	0.52	1.5	0.00	19.3	0.002	1.10
	6	0.87	0.8	0.12	1.8	0.01	15.9	0.003	1.09
DMSO τ_M = 145 ns	1	0.14	3.6	0.84	14.2	0.02	50.9	0.005	1.02
	2	0.19	2.0	0.79	6.3	0.01	26.8	0.003	1.01
	3	0.25	1.1	0.74	3.9	0.01	17.4	0.002	1.09
	4	0.40	1.3	0.59	3.1	0.01	22.0	0.002	1.07
	5	0.44	0.7	0.55	2.1	0.01	14.6	0.002	1.13
	6	0.61	0.6	0.38	1.6	0.01	14.8	0.002	1.13

Table S2.4. Parameters retrieved from the MFA of the excimer decays of the Py_x-G(*N*) dendrons in degassed toluene (Tol), degassed dimethylformamide (DMF), and degassed dimethylsulfoxide (DMSO).

	Generation (*N*)	f_{Ediff}^{E0}	f_{Ediff}^{D}	τ_{E0} *(ns)*	τ_{D} *(ns)*	τ_S *(ns)*	f_{EE0}	f_{ED}	f_{ES}^{*}	χ^2
Tol τ_M = 200 ns	1	0.95	-	49.4	-	4	0.00	-	0.05	1.05
	2	0.92	-	49.7	-	4	0.04	-	0.04	1.12
	3	0.88	-	49.0	-	4	0.04	-	0.08	1.02
	4	0.89	-	49.1	-	4	0.02	-	0.09	1.14
	5	0.89	-	49.6	-	4	0.01	-	0.09	1.17
	6	0.43	0.189	44.9	62.1	4	0.17	0.05	0.16	1.17
DMF τ_M = 180 ns	1	0.97	-	49.4	-	4	0.01	-	0.02	0.98
	2	0.95	-	49.4	-	4	0.01	-	0.05	1.01
	3	0.84	-	49.5	-	4	0.00	-	0.16	1.03
	4	0.79	-	49.4	-	4	0.00	-	0.21	1.04
	5	0.40	0.30	40.7	62.9	4	0.02	0.00	0.28	1.10
	6	0.44	0.08	42.5	116.0	4	0.16	0.00	0.32	1.09
DMSO τ_M = 145 ns	1	0.94	-	46.0	-	4	0.00	-	0.06	1.02
	2	0.93	-	45.9	-	4	0.02	-	0.05	1.01
	3	0.83	-	46.4	-	4	0.01	-	0.16	1.09
	4	0.77	-	46.4	-	4	0.00	-	0.23	1.07
	5	0.45	0.27	37.3	63.8	4	0.01	0.00	0.27	1.13
	6	0.35	0.25	33.2	60.3	4	0.00	0.13	0.28	1.13

Table S2.5 Molar fractions obtained from the MFA of the Py_x-G(*N*) dendrons in degassed toluene (Tol), degassed dimethylformamide (DMF), and degassed dimethylsulfoxide (DMSO).

	Generation (*N*)	f_{diff}^{E0}	f_{diff}^{D}	f_{diff}	f_{E0}	f_D	f_{agg}	f_{free}
Tol	1	0.99	-	0.99	0.00	-	0.00	0.01
τ_M = 200 ns	2	0.96	-	0.96	0.04	-	0.04	0.00
	3	0.95	-	0.95	0.05	-	0.05	0.00
	4	0.98	-	0.98	0.02	-	0.02	0.00
	5	0.98	-	0.98	0.01	-	0.01	0.00
	6	0.51	0.22	0.73	0.21	0.06	0.26	0.00
DMF	1	0.98	-	0.98	0.01	-	0.01	0.01
τ_M = 180 ns	2	0.99	-	0.99	0.01	-	0.01	0.00
	3	1.00	-	1.00	0.00	-	0.00	0.00
	4	1.00	-	1.00	0.00	-	0.00	0.00
	5	0.56	0.41	0.97	0.03	0.00	0.03	0.00
	6	0.64	0.12	0.76	0.23	0.01	0.24	0.00
DMSO	1	1.00	-	1.00	0.00	-	0.00	0.00
τ_M = 145 ns	2	0.98	-	0.98	0.02	-	0.02	0.00
	3	0.98	-	0.98	0.02	-	0.02	0.00
	4	1.00	-	1.00	0.00	-	0.00	0.00
	5	0.61	0.37	0.98	0.01	0.00	0.02	0.00
	6	0.48	0.34	0.82	0.00	0.17	0.17	0.00

S3 - Supporting Information for Chapter 3

Model free analysis (MFA) equations

$$[Py^*]_{(t)} = ([Py^*_{diffE0}]_{(t=0)} + [Py^*_{diffD}]_{(t=0)}) \times \sum_{i=1}^{n} a_i \times \exp(-t/\tau_i) + [Py^*_{free}]_{(t=0)} \times \exp(-t/\tau_M) \quad \text{(S3.1)}$$

$$[E^*]_{(t)} = -[Py^*_{diffE0}]_{(t=0)} \times \sum_{i=1}^{n} a_i \frac{\frac{1}{\tau_i} - \frac{1}{\tau_M}}{\frac{1}{\tau_i} - \frac{1}{\tau_{E0}}} \exp(-t/\tau_i)$$

$$+ \left([E0^*]_{(t=0)} + [Py^*_{diffE0}]_{(t=0)} \times \sum_{i=1}^{n} a_i \frac{\frac{1}{\tau_i} - \frac{1}{\tau_M}}{\frac{1}{\tau_i} - \frac{1}{\tau_{E0}}} \right) \times \exp(-t/\tau_{E0})$$

$$-[Py^*_{diffEL}]_{(t=0)} \times \sum_{i=1}^{n} a_i \frac{\frac{1}{\tau_i} - \frac{1}{\tau_M}}{\frac{1}{\tau_i} - \frac{1}{\tau_{EL}}} \exp(-t/\tau_i)$$

$$+ \left([EL^*]_{(t=0)} + [Py^*_{diffEL}]_{(t=0)} \times \sum_{i=1}^{n} a_i \frac{\frac{1}{\tau_i} - \frac{1}{\tau_M}}{\frac{1}{\tau_i} - \frac{1}{\tau_{EL}}} \right) \times \exp(-t/\tau_{EL}) + [ES^*]_{(t=0)} \times \exp(-t/\tau_S) \quad \text{(S3.2)}$$

[1]H NMR spectra

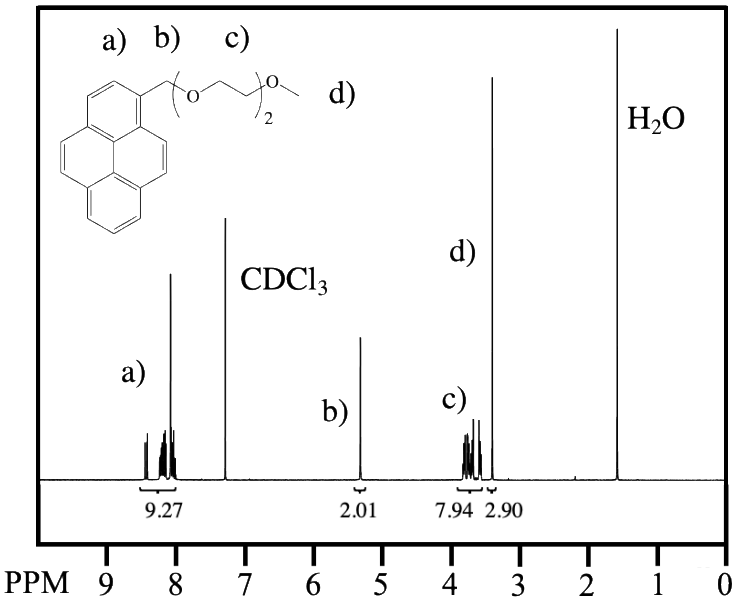

Figure S3.1. [1]H NMR spectrum of $PyEG_2ME$. ($CDCl_3$, 300 MHz). δ 3.40 (s, 3H), 3.58-3.84 (m, 8H), 5.32 (s, 2H), 7.99-8.48 (m, 9H).

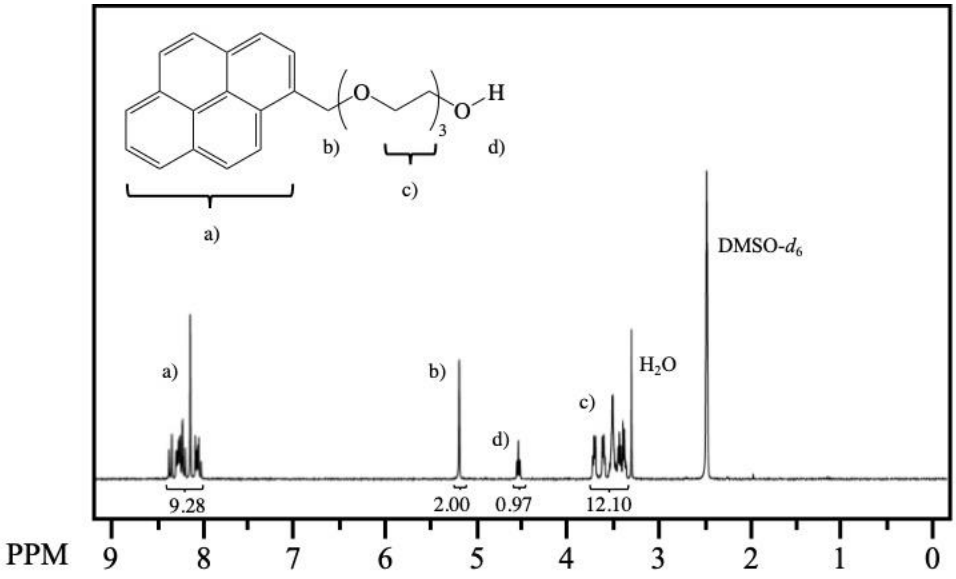

Figure S3.2. [1]H NMR spectrum of 1-pyrenemethyl ether tri(ethylene glycol) (DMSO-d_6, 300 MHz), δ 3.36-3.71 (m, 12H), 4.54 (t, 1H), 5.20 (s, 2H), 8.04-8.40 (m, 9H).

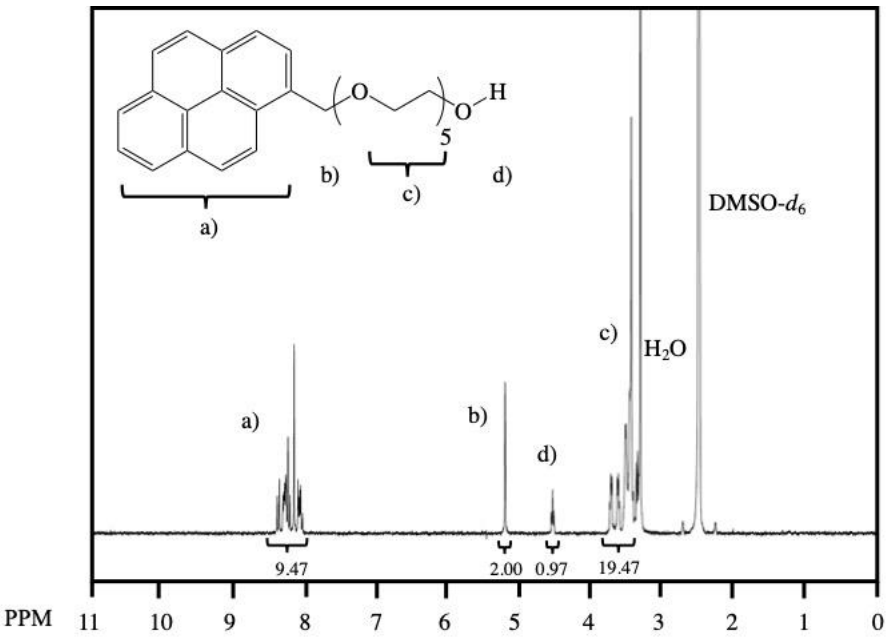

Figure S3.3. ^{1}H NMR spectrum of 1-pyrenemethyl ether penta(ethylene glycol) (DMSO-d_6, 300 MHz), δ 3.33-3.74 (m, 20H), 4.53 (t, 1H), 5.20 (s, 2H), 8.02-8.41 (m, 9H).

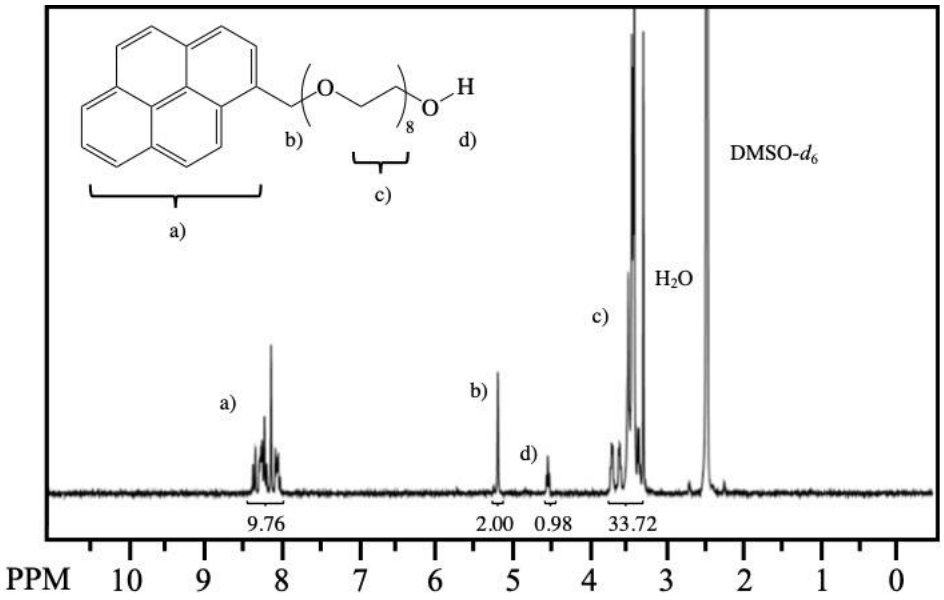

Figure S3.4. ^{1}H NMR spectrum of 1-pyrenemethyl ether octa(ethylene glycol) (DMSO-d_6, 300 MHz), δ 3.35-3.71 (m, 32H), 4.55 (t, 1H), 5.19 (s, 2H), 8.04-8.41 (m, 9H).

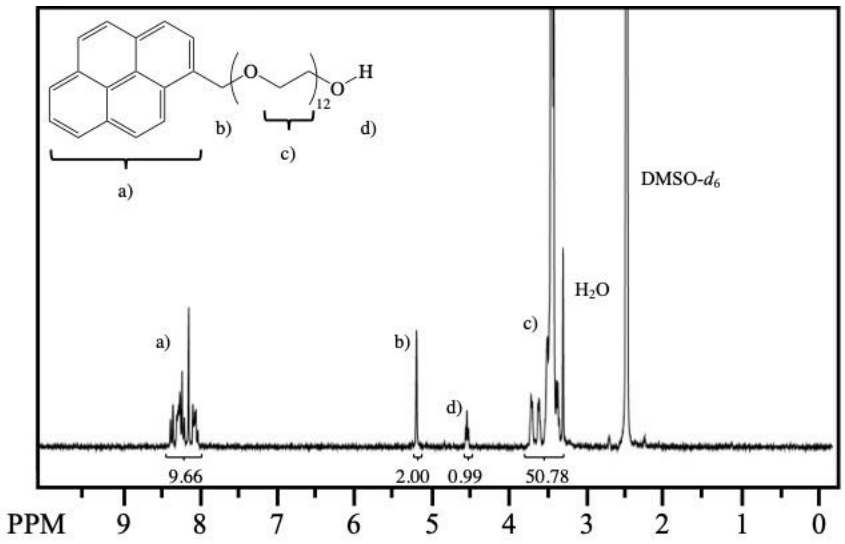

Figure S3.5. ^{1}H NMR spectrum of 1-pyrenemethyl ether dodeca(ethylene glycol) (DMSO-d_6, 300 MHz), δ 3.35-3.72 (m, 48H), 4.55 (t, 1H), 5.20 (s, 2H), 8.02-8.42 (m, 9H).

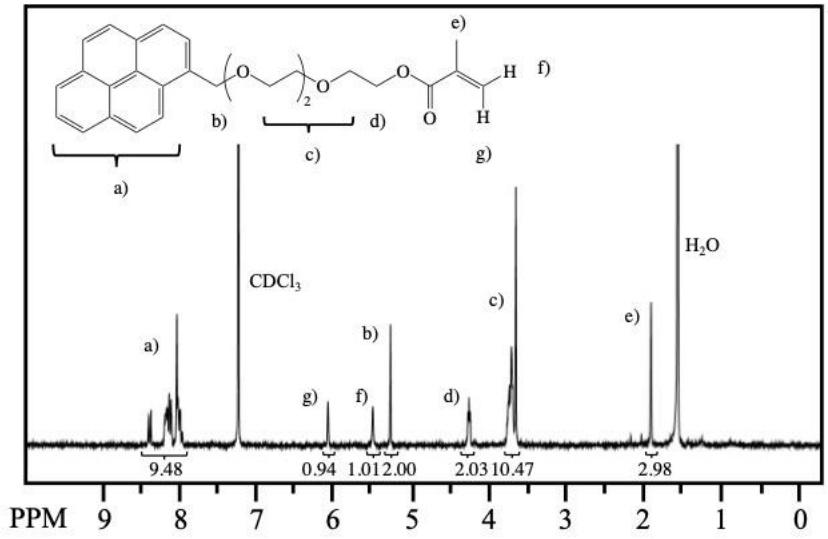

Figure S3.6. ^{1}H NMR spectrum of 1-pyrenemethyl ether tri(ethylene glycol) methacrylate ($CDCl_3$, 300 MHz), δ 1.91 (s, 3H), 3.63-3.78 (m, 10H), 4.27 (t, 2H), 5.23 (s, 2H), 5.52 (s, 1H), 6.09 (s,1H), 7.97-8.43 (m, 9H).

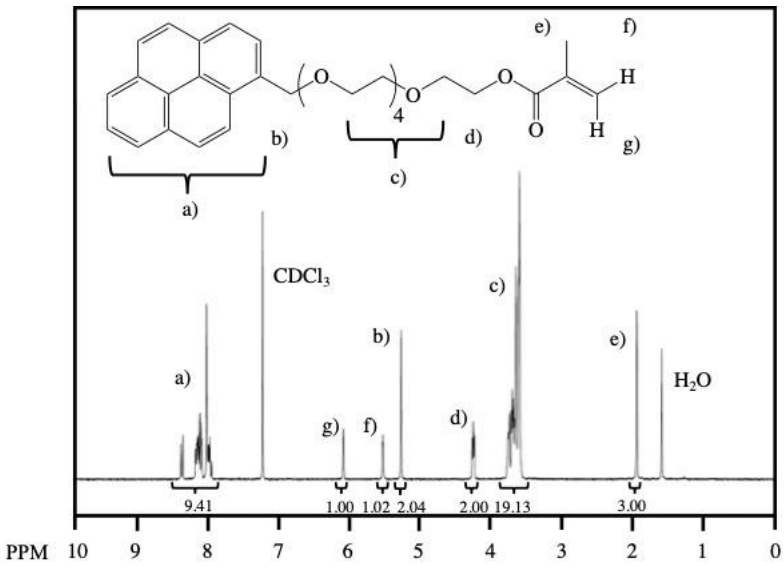

Figure S3.7. ^{1}H NMR spectrum of 1-pyrenemethyl ether penta(ethylene glycol) methacrylate ($CDCl_3$, 300 MHz), δ 1.92 (s, 3H), 3.56-3.79 (m, 18H), 4.26 (t, 2H), 5.28 (s, 2H), 5.54 (s, 1H), 6.10 (s,1H), 7.97-8.41 (m, 9H).

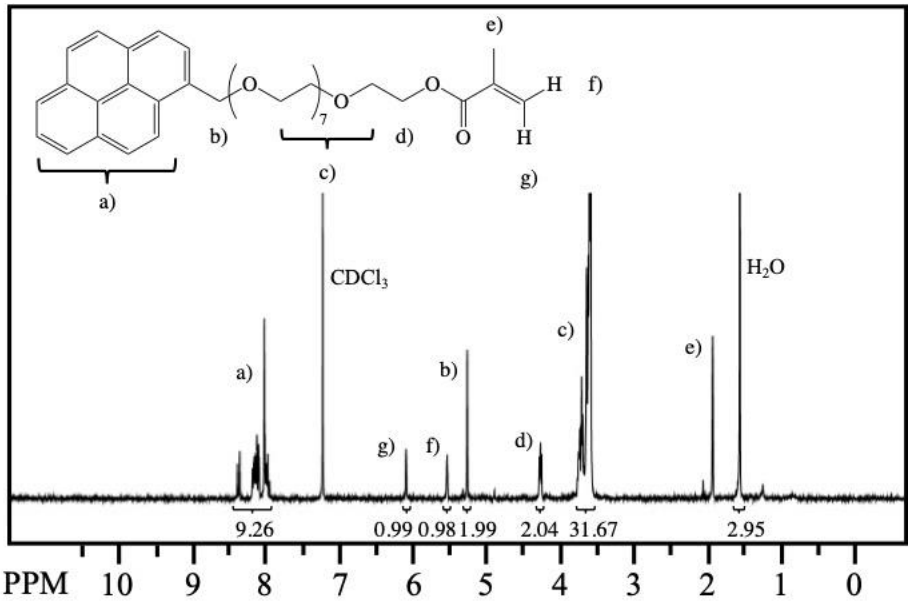

Figure S3.8. ^{1}H NMR spectrum of 1-pyrenemethyl ether octa(ethylene glycol) methacrylate ($CDCl_3$, 300 MHz), δ 1.94 (s, 3H), 3.55-3.77 (m, 30H), 4.28 (t, 2H), 5.28 (s, 2H), 5.55 (s, 1H), 6.10 (s,1H), 7.98-8.44 (m, 9H).

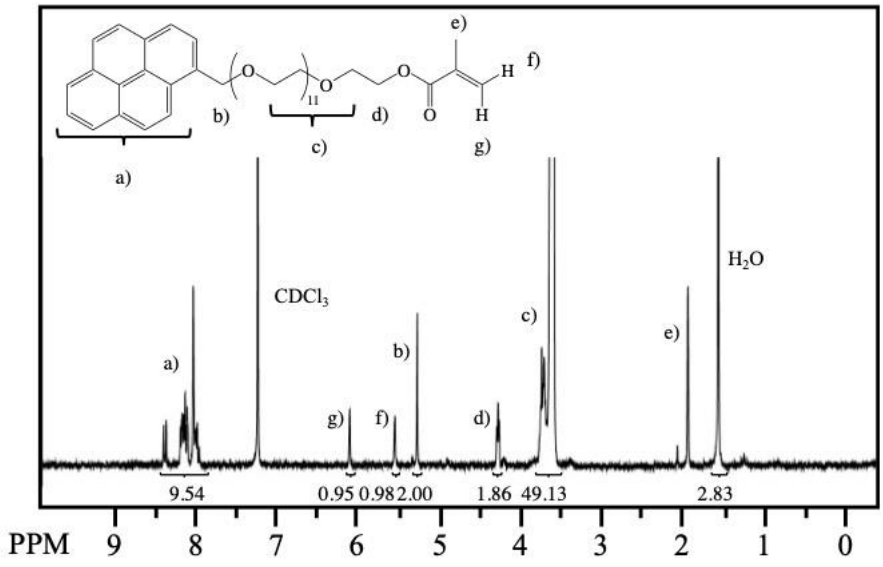

Figure S3.9. ^{1}H NMR spectrum of 1-pyrenemethyl ether dodeca(ethylene glycol) methacrylate ($CDCl_3$, 300 MHz), δ 1.94 (s, 3H), 3.55-3.79 (m, 46H), 4.29 (t, 2H), 5.29 (s, 2H), 5.55 (s, 1H), 6.12 (s,1H), 7.96-8.45 (m, 9H).

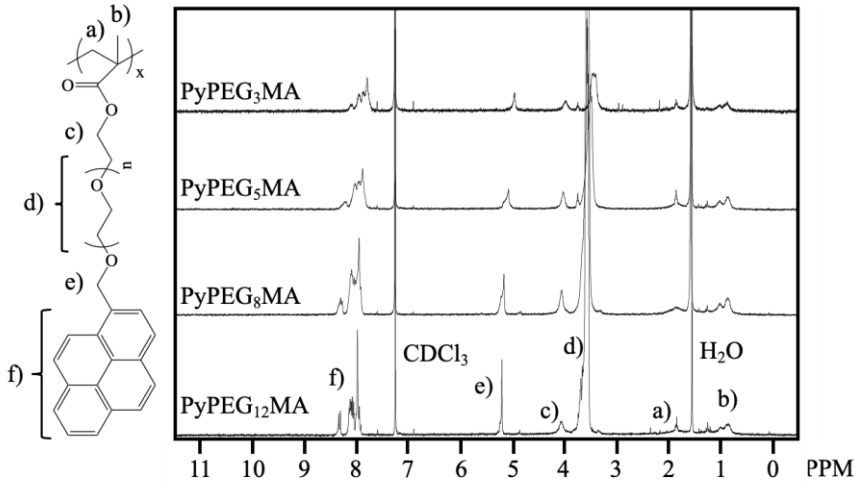

Figure S3.10. ^{1}H NMR spectrum of the $PyPEG_yMA$ samples. ($CDCl_3$, 300 MHz).

Gel permeation chromatography traces

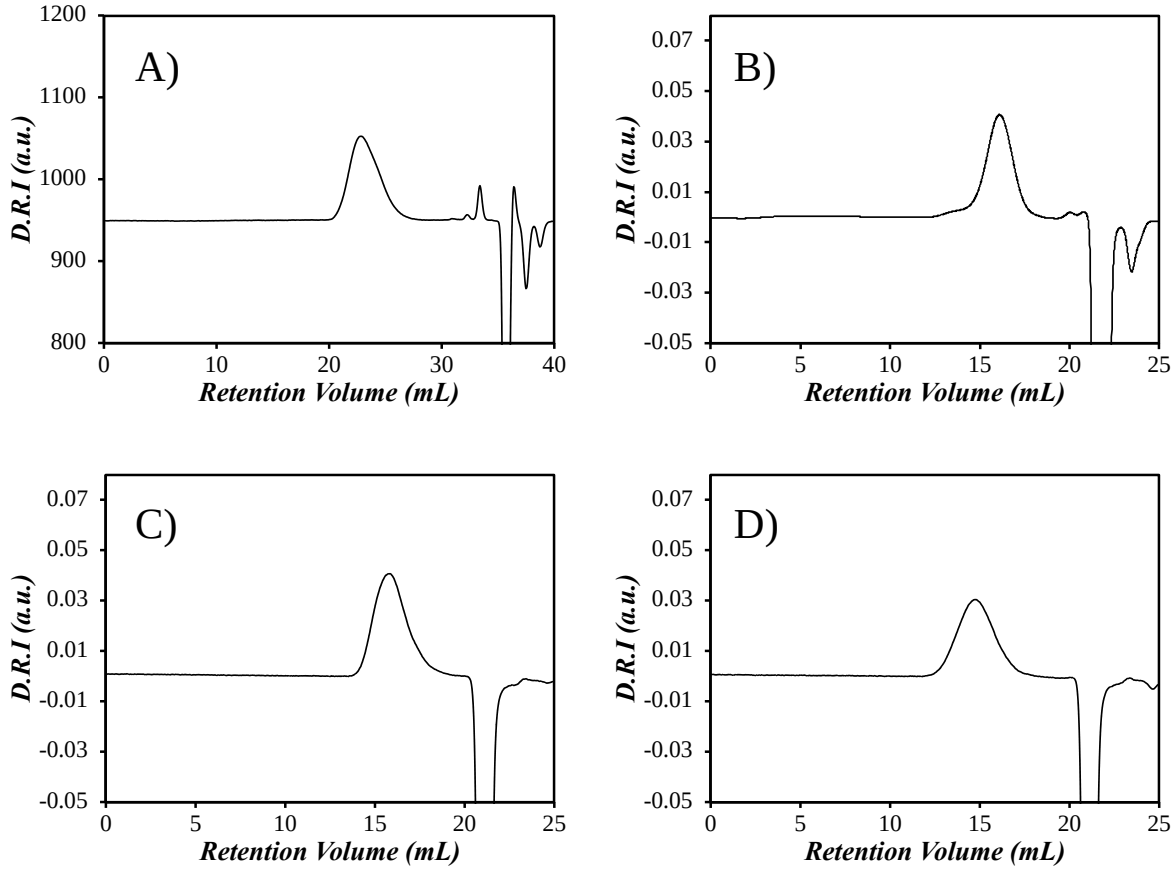

Figure S3.11. Gel permeation chromatograms obtained with the differential refractive index detector versus retention volume for (A) P($PyEG_3MA$) in THF and (B) P($PyEG_5MA$), (C) P($PyEG_8MA$), and (D) P($PyEG_{12}MA$) in DMSO.

SSF spectra of the P(PyEG$_y$MA) samples in DMF and dioxane

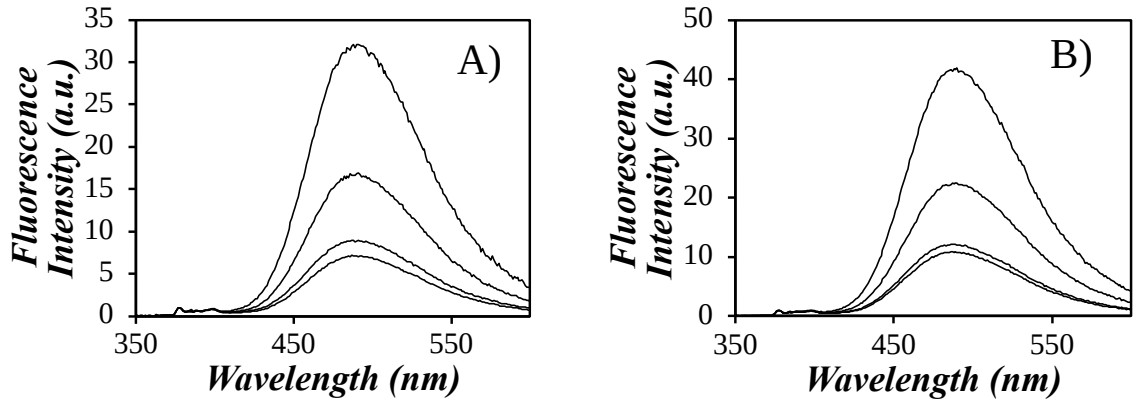

Figure S3.12. Normalized SSF spectra of P(PyEG$_y$MA) PBBs in A) DMF and B) dioxane (λ_{ex} = 344 nm; from top to bottom, P(PyEG$_y$MA) samples with y = 3, 5, 8, and 12).

SSF spectra of the PyEG$_2$ME model compound

All SSF spectra were acquired using front face geometry to minimize reabsorption.

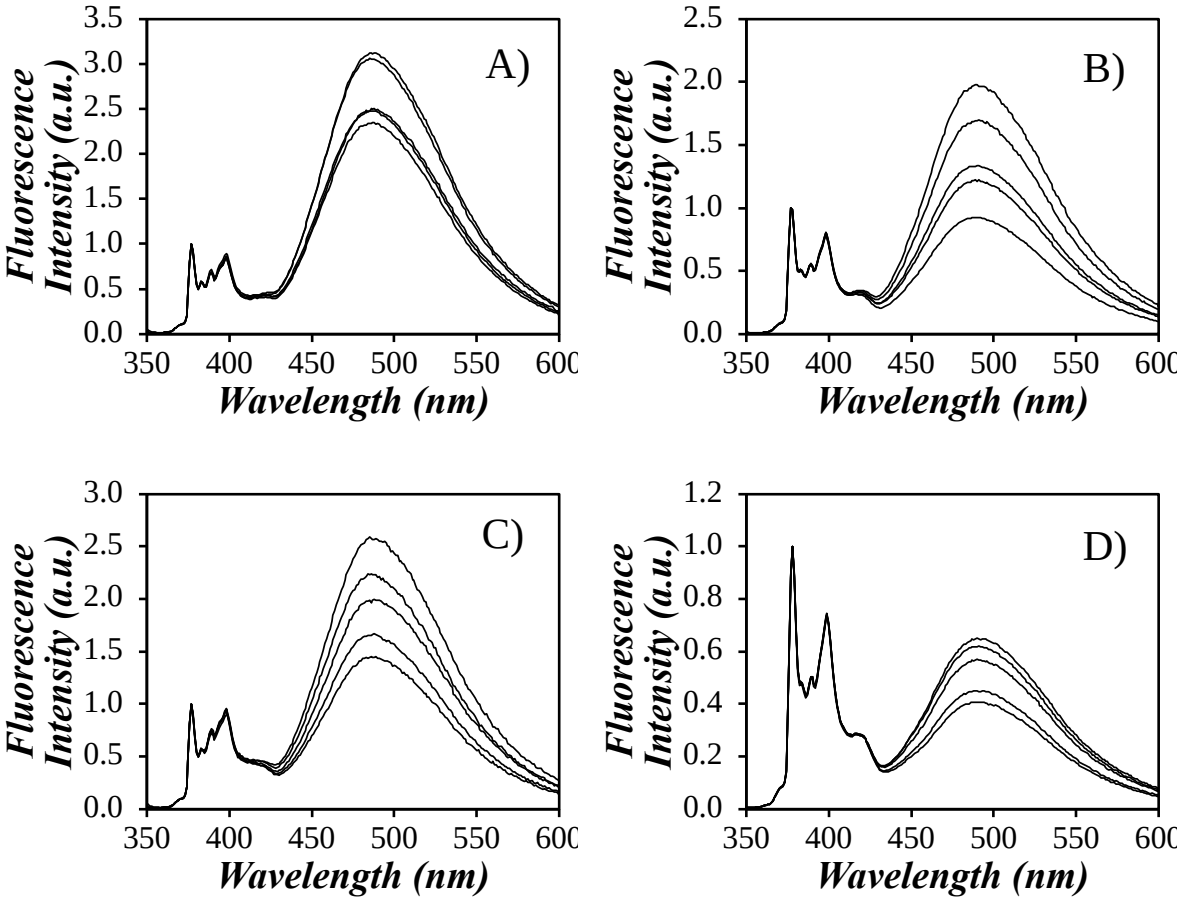

Figure S3.13. SSF spectra of PyEG$_2$ME in (A) THF, (B) DMF, (C) dioxane, and (D) DMSO. λ_{ex}=344 nm.

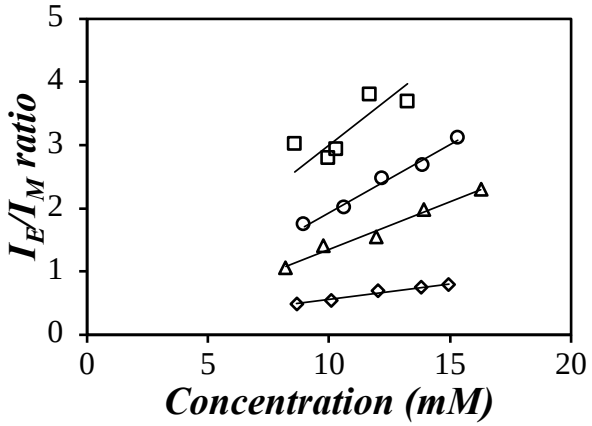

Figure S3.14. Plot of the I_E/I_M ratios versus the concentration of $PyEG_2EM$ in (□) THF, (○) DMF, (△) dioxane, and (◇) DMSO.

Sample fit of the global FBM analysis of the fluorescence decays

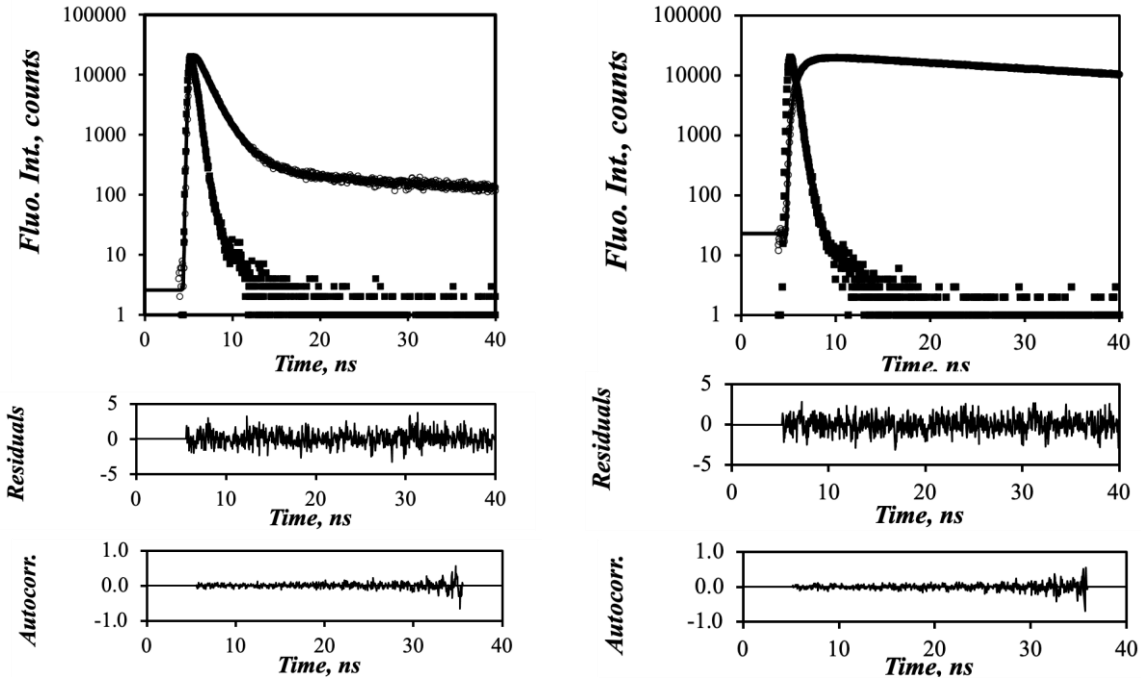

Figure S3.15. Global MFA of the (left) monomer (λ_{em} = 375 nm) and (right) excimer (λ_{em} = 510 nm) fluorescence decays of P(PyEG$_5$MA). χ^2 = 1.09, λ_{ex} = 336 nm.

Molecular mechanics optimization (MMO)

The MMOs were conducted with the program HyperChem using an AMBER molecular mechanics force field and the Polak-Ribiere molecular mechanics optimization. An atactic poly(methyl methacrylate) (PMMA) polymer backbone was generated by using the random number generator in MS excel to randomly select the configuration of each MMA unit. The PMMA chain was stretched by imposing the two ends of the chain to be held 1500 Å from each other before being allowed to relax. This PMMA backbone was then fixed when conducting the MMOs.

The influence of the PMMA backbone on the reach of each $PyEG_y$ side chain was determined by conducting a series of MMOs, whereby the methyl group of a MMA unit of the PMMA chain was replaced with a $PyEG_y$ side chain. This $PyEG_yMA$ unit was taken as reference. A secondary methacrylate unit, five units away from the reference unit, was labeled with a second $PyEG_y$ side chain. The two pyrene labels were induced to come within 0.34 nm from each other resulting in their π–π stacking (see Figure S3.16). The number of carbon atoms (n_C) of the reference pyrene overlapping the frame of the secondary pyrene was recorded. The secondary $PyEG_y$ side chain was sequentially moved further from the reference side chain along the PMMA chain and n_C was determined until the $PyEG_y$ side chains were too far apart and no overlap resulted between the two pyrenyl labels ($n_C \sim 0$). Since the PMMA backbone was atactic, this process was repeated three more times by changing the reference $PyEG_y$ side chain to another methacrylate unit. The number n_C was then plotted in Figure S3.17 as a

function of the number of MMA units separating the reference side chain from the secondary side chain.

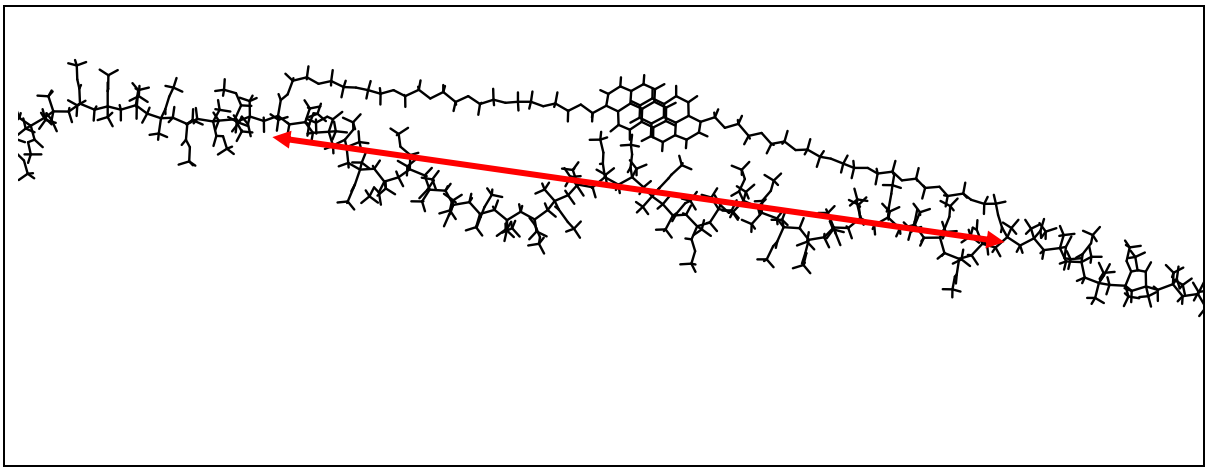

Figure S3.16. Snapshot of PMMA labeled with two $PyEG_8MA$ side chains.

These MMOs were repeated for each $PyEG_y$ side chain and the resulting plots of n_C as a function of the number of residues separating the primary from the secondary $PyEG_y$ side chains are shown in Figure S3.17. An n_C value lower than 7 marks the boundary between poor and good overlap between two pyrenyl labels. Consequently, the number of methacrylate structural units (N_o) and the distance d_{intra}^{o} corresponding to an n_C value equal to 7 were recorded as the maximum N_o and d_{intra} values separating two methacrylate units bearing a $PyEG_y$ side chain and still allowing good overlap between the two pyrenyl labels. The N_o and d_{intra}^{o} values are listed in Table S3.1.

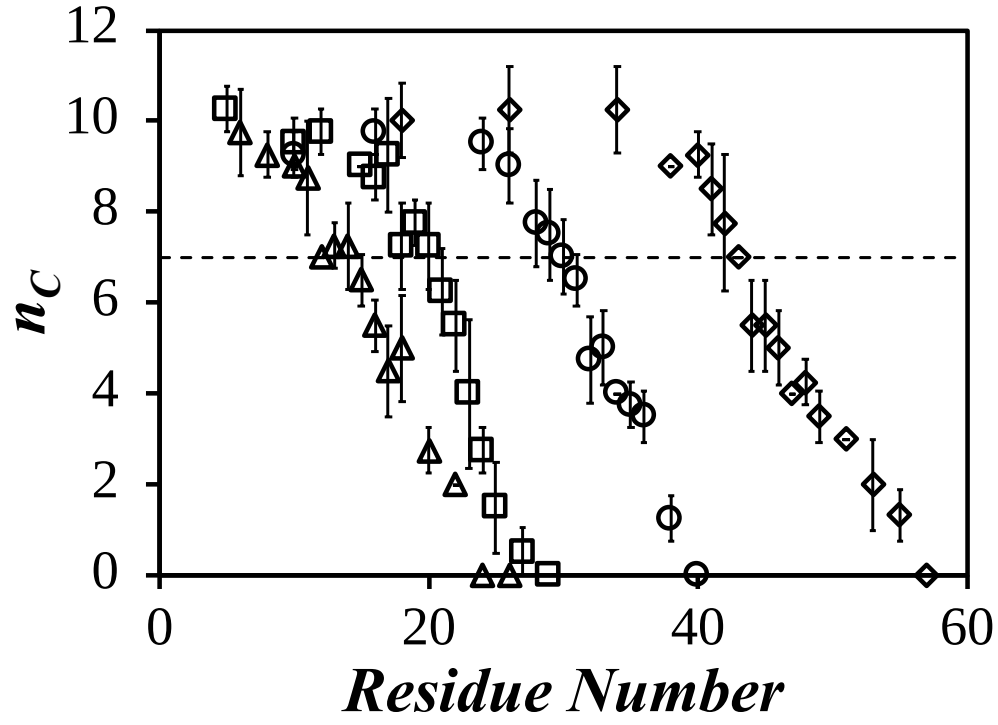

Figure S3.17. Plot of n_C versus residue number for the MMO simulations of (▲) $PyEG_3MA$, (□) $PyEG_5MA$, (○) $PyEG_8MA$, and (◇) $PyEG_{12}MA$. The dashed line represents a C–C overlap of 7 atoms which is considered a sufficient overlap to form excimer.

To measure the largest distance separating two methacrylate units bearing a $PyEG_y$ side chain, one PMMA chain labeled with a single $PyEG_y$ side chain was duplicated, and the duplicated chain was flipped by 180° around the polymethacrylate backbone. The two chains were then aligned parallel to one another with the $PyEG_y$ side chains facing each other. The polymers were brought closer to each other and the two pyrenyl labels were then induced to come within 0.34 nm from each other until the number n_C of carbons from one pyrene overlapping the frame of the other pyrene reached a value of 7, which was expected to provide

sufficient overlap between the two molecules to form an excimer. The distance d_{inter} between the two structural units bearing the $PyEG_y$ side chains of the two PMMA chains was then measured as illustrated in Figure S3.18 with the $PyEG_8$ side chain. The two chains were then brought closer to each other in 0.1 nm increments resulting in the plot of n_C as a function of d_{inter} shown in Figure S3.19. The value of d_{inter} where n_C equaled 7, representing the boundary between poor and good overlap between the pyrenyl labels, was recorded and listed in Table S3.1.

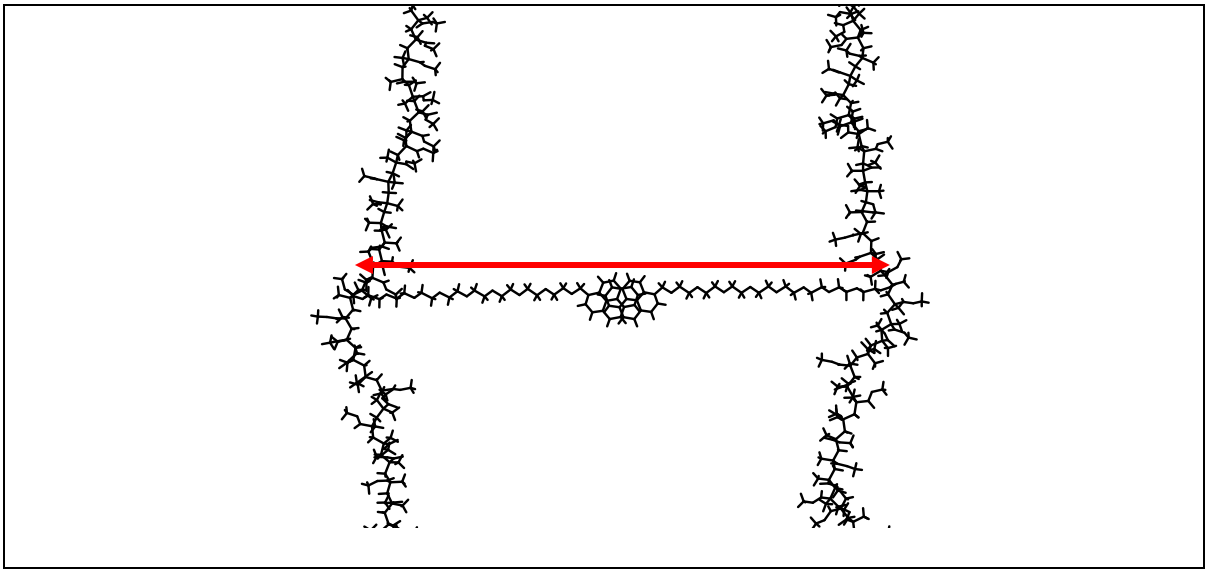

Figure S3.18. Snapshot of two PMMA polymers each labeled with a single $PyEG_8$ side chain.

The parameter z used to calculate $[Py]_{loc}$ in Equation S3.5 was then determined by taking the ratio $d_{intra}{}^{o}/d_{inter}{}^{o}$ for each $PyEG_y$ side chain reported in Table S3.1.

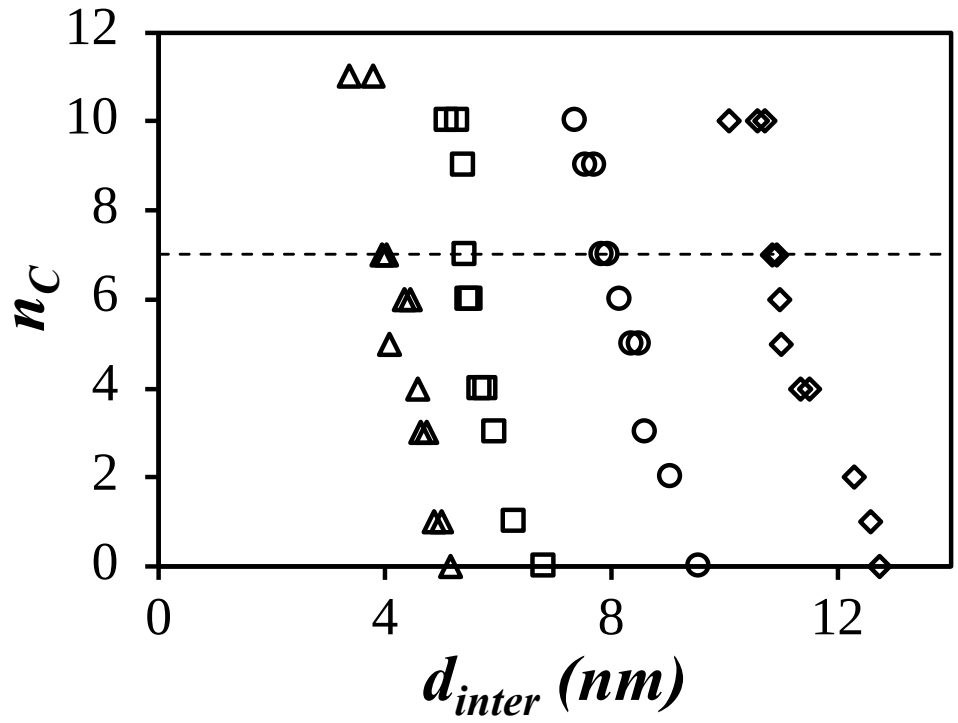

Figure S3.19. Plot of nc versus d_{inter} for the MMO simulations of (▲) $PyEG_3MA$, (■) $PyEG_5MA$, (●) $PyEG_8MA$, and (◆) $PyEG_{12}MA$. The dashed line represents a C–C overlap of 7 atoms which is considered a sufficient overlap to form excimer.

Table S3.1. N_o, d_{intra}^o, and d_{inter}^o values obtained for the $PyEG_y$ side chains

N_S	12	18	27	39
N_o	14	20	30	43
d_{intra}^o (nm)	3.4	4.8	7.1	10.1
d_{inter}^o (nm)	4.0	5.4	8.0	10.9
z	0.85	0.89	0.89	0.93

Parameters retrieved from the MFA analysis

Table S3.2. Parameters retrieved from the MFA (using program sumegs10bg) of both the monomer and excimer decays of 1-pyrenemethoxy diethylene glycol methyl ether self-quenching in degassed tetrahydrofuran (THF), degassed dimethylformamide (DMF), degassed dioxane, and degassed dimethylsulfoxide (DMSO).

	Conc. (mM)	a_1	τ_1 (ns)	a_2	τ_2 (ns)	f_{Ediff}^{E0}	f_{EE0}	τ_{E0} (ns)	χ^2
THF	8.6	0.56	27	0.44	49	0.98	0.02	49	1.0
τ_M =	10.0	0.76	26	0.24	50	0.97	0.03	49	1.1
280 ns	10.3	0.74	24	0.26	48	0.97	0.03	49	1.1
	11.7	0.81	23	0.19	48	0.97	0.03	48	1.2
	13.3	0.85	21	0.15	47	0.96	0.04	48	1.1
DMF	8.2	0.14	25	0.86	53	0.96	0.04	48	1.2
τ_M =	9.8	0.29	29	0.71	49	0.97	0.03	46	1.0
230 ns	12.0	0.44	27	0.56	44	0.96	0.04	46	1.1
	13.9	0.50	25	0.50	40	0.95	0.05	46	1.2
	16.3	0.60	23	0.40	37	0.97	0.03	45	1.2
dioxane	9.0	0.16	26	0.84	53	0.97	0.03	49	1.1
τ_M =	10.6	0.42	31	0.58	50	0.98	0.02	49	1.2
218 ns	12.2	0.48	29	0.52	46	0.98	0.03	49	1.2
	13.9	0.58	27	0.42	43	0.98	0.02	48	1.1
	15.3	0.60	25	0.40	40	0.97	0.03	48	1.2
DMSO	8.7	0.07	26	0.93	77	0.98	0.02	46	1.1
τ_M =	10.1	0.08	26	0.92	70	0.97	0.03	45	1.2
190 ns	12.0	0.12	33	0.88	63	0.97	0.03	44	1.1
	13.8	0.09	21	0.91	55	0.97	0.02	44	1.2
	14.9	0.08	19	0.92	53	0.97	0.03	43	1.1

Table S3.3. Parameters retrieved from the MFA analysis of the monomer decays for the P(PyEG$_n$MA) samples in deoxygenated THF, deoxygenated DMF, deoxygenated dioxane, and deoxygenated DMSO.

	Sample	τ_1 (ns)	a_1	τ_2 (ns)	a_2	τ_3 (ns)	a_3	f_{Mfree}	χ^2
THF τ_M=280 ns	PyPEG$_3$MA	0.5	0.54	1.1	0.45	11.5	0.01	0.00	1.0
	PyPEG$_5$MA	0.8	0.53	1.6	0.46	10.5	0.01	0.00	1.1
	PyPEG$_8$MA	1.2	0.47	2.3	0.49	9.3	0.03	0.01	1.0
	PyPEG$_{12}$MA	1.6	0.47	3.1	0.51	16.5	0.02	0.00	1.1
DMF τ_M=230 ns	PyPEG$_3$MA	1.5	0.50	0.6	0.48	7.5	0.01	0.00	1.0
	PyPEG$_5$MA	0.9	0.37	2.1	0.60	7.4	0.02	0.00	1.0
	PyPEG$_8$MA	1.7	0.47	3.5	0.50	15.1	0.02	0.01	1.0
	PyPEG$_{12}$MA	1.7	0.23	3.9	0.72	12.1	0.04	0.01	1.0
dioxane τ_M=218 ns	PyPEG$_3$MA	1.6	0.55	0.6	0.43	10.1	0.02	0.00	1.1
	PyPEG$_5$MA	0.9	0.31	2.3	0.65	7.2	0.03	0.01	1.0
	PyPEG$_8$MA	1.2	0.26	3.6	0.67	11.5	0.05	0.01	1.0
	PyPEG$_{12}$MA	1.2	0.17	4.2	0.77	11.8	0.06	0.00	1.0
DMSO τ_M=190 ns	PyPEG$_3$MA	0.7	0.44	2.0	0.50	7.4	0.04	0.01	1.1
	PyPEG$_5$MA	1.0	0.28	2.7	0.61	6.0	0.10	0.01	1.1
	PyPEG$_8$MA	1.5	0.29	4.4	0.64	12.6	0.06	0.01	1.1
	PyPEG$_{12}$MA	2.0	0.21	5.4	0.68	11.9	0.10	0.00	1.0

Table S3.4. Parameters retrieved from the MFA analysis of the excimer decays for the P(PyEG$_n$MA) samples in deoxygenated THF, deoxygenated DMF, deoxygenated dioxane, and deoxygenated DMSO.

	Sample	$f_{Ediff,E0}$	$f_{Ediff,D}$	τ_{E0} (ns)	τ_D (ns)	f_{EE0}	f_{ED}	χ^2
THF τ_M=280 ns	PyPEG$_3$MA	0.36	0.46	24	66	0.00	0.17	1.0
	PyPEG$_5$MA	0.42	0.48	27	64	0.00	0.09	1.1
	PyPEG$_8$MA	0.58	0.36	40	66	0.06	0.00	1.0
	PyPEG$_{12}$MA	0.53	0.42	47	47	0.01	0.04	1.1
DMF τ_M=230 ns	PyPEG$_3$MA	0.52	0.39	27	72	0.00	0.09	1.0
	PyPEG$_5$MA	0.55	0.41	33	57	0.00	0.05	1.0
	PyPEG$_8$MA	0.59	0.32	38	50	0.00	0.09	1.0
	PyPEG$_{12}$MA	0.57	0.39	37	51	0.00	0.04	1.0
dioxane τ_M= 218 ns	PyPEG$_3$MA	0.38	0.45	23	69	0.00	0.18	1.1
	PyPEG$_5$MA	0.39	0.52	35	61	0.08	0.00	1.0
	PyPEG$_8$MA	0.53	0.40	42	53	0.05	0.01	1.0
	PyPEG$_{12}$MA	0.54	0.41	47	47	0.00	0.04	1.0
DMSO τ_M=190 ns	PyPEG$_3$MA	0.30	0.50	20	53	0.00	0.21	1.1
	PyPEG$_5$MA	0.49	0.39	34	51	0.02	0.10	1.1
	PyPEG$_8$MA	0.50	0.40	41	41	0.04	0.05	1.1
	PyPEG$_{12}$MA	0.51	0.42	41	41	0.04	0.04	1.0

Table S3.5. Molar fractions retrieved from the MFA of the monomer and excimer decays for the P(PyEG$_n$MA) samples in deoxygenated THF, deoxygenated DMF, deoxygenated dioxane, and deoxygenated DMSO.

	Sample	f_{free}	$f_{diff,E0}$	$f_{diff,D}$	f_{diff}	f_{E0}	f_{D}	f_{agg}
THF τ_M=280 ns	PyPEG$_3$MA	0.00	0.36	0.46	0.82	0.00	0.17	0.17
	PyPEG$_5$MA	0.00	0.42	0.48	0.91	0.00	0.09	0.09
	PyPEG$_8$MA	0.01	0.57	0.36	0.93	0.06	0.00	0.06
	PyPEG$_{12}$MA	0.00	0.53	0.42	0.95	0.01	0.04	0.04
DMF τ_M=230 ns	PyPEG$_3$MA	0.00	0.52	0.39	0.91	0.00	0.09	0.09
	PyPEG$_5$MA	0.00	0.54	0.41	0.95	0.00	0.04	0.04
	PyPEG$_8$MA	0.01	0.58	0.32	0.90	0.00	0.09	0.09
	PyPEG$_{12}$MA	0.01	0.56	0.39	0.95	0.00	0.04	0.04
dioxane τ_M= 218 ns	PyPEG$_3$MA	0.00	0.37	0.44	0.82	0.00	0.18	0.18
	PyPEG$_5$MA	0.00	0.39	0.52	0.91	0.08	0.00	0.09
	PyPEG$_8$MA	0.01	0.53	0.40	0.93	0.05	0.01	0.06
	PyPEG$_{12}$MA	0.00	0.54	0.41	0.95	0.00	0.04	0.04
DMSO τ_M=190 ns	PyPEG$_3$MA	0.01	0.29	0.49	0.78	0.00	0.21	0.21
	PyPEG$_5$MA	0.01	0.49	0.38	0.87	0.02	0.10	0.12
	PyPEG$_8$MA	0.01	0.50	0.40	0.90	0.04	0.05	0.09
	PyPEG$_{12}$MA	0.00	0.50	0.42	0.92	0.04	0.04	0.08

S4 - Supporting Information for Chapter 4

Equations used to analyze the fluorescence decays of the PyEG$_5$-PEG$_n$MA samples

Equations S4.1 and S4.2 were employed to globally fit the monomer and excimer fluorescence decays of the PyEG$_5$-PEG$_n$MA samples, respectively.[1,2]

$$[Py^*]_{(t)} = [Py^*_{diff}]_{(t)} + [Py^*_{k2}]_{(t)} + [Py^*_{free}]_{(t)} = [Py_{diff}]_o \exp\left(-\left(A_2 + \frac{1}{\tau_M}\right)t - A_3\left(1-\exp(-A_4 t)\right)\right)$$

$$+\left([Py_{k2}]_o + [Py_{diff}]_o e^{-A_3}\sum_{i=0}^{\infty}\frac{A_3^i}{i!}\frac{A_2+iA_4}{A_2+iA_4-k_2}\right)\exp\left(-\left(k_2+\frac{1}{\tau_M}\right)t\right)$$

$$-[Py_{diff}]_o e^{-A_3}\sum_{i=0}^{\infty}\frac{A_3^i}{i!}\frac{A_2+iA_4}{A_2+iA_4-k_2}\exp\left(-\left(A_2+iA_4+\frac{1}{\tau_M}\right)t\right)$$

$$+[Py_{free}]_o \exp\left(-\frac{t}{\tau_M}\right)\Bigg] \qquad \text{(S4.1)}$$

$$[E^*]_{(t)} = [E0^*]_{(t)} + [D^*]_{(t)} = k_2\left(\left([Py_{k2}(E0)]_o + [Py_{diff}(E0)]_o e^{-A_3}\sum_{i=0}^{\infty}\frac{A_3^i}{i!}\frac{A_2+iA_4}{A_2+iA_4-k_2}\right)\right.$$

$$\times \frac{\exp\left(-\frac{t}{\tau_{E0}}\right)-\exp\left(-\left(k_2+\frac{1}{\tau_M}\right)t\right)}{k_2+\frac{1}{\tau_M}-\frac{1}{\tau_{E0}}}$$

$$+[Py_{diff}(E0)]_o e^{-A_3}\sum_{i=0}^{\infty}\frac{A_3^i}{i!}\frac{A_2+iA_4}{A_2+iA_4-k_2}\frac{\exp\left(-\left(A_2+iA_4+\frac{1}{\tau_M}\right)t\right)-\exp\left(-\frac{t}{\tau_{E0}}\right)}{A_2+iA_4+\frac{1}{\tau_M}-\frac{1}{\tau_{E0}}}\Bigg)$$

$$+k_2\Bigg(\Bigg([Py_{k2}(D)]_o+[Py_{diff}(D)]_o e^{-A_3}\sum_{i=0}^{\infty}\frac{A_3^i}{i!}\frac{A_2+iA_4}{A_2+iA_4-k_2}\Bigg)\times\frac{\exp\left(-\frac{t}{\tau_D}\right)-\exp\left(-\left(k_2+\frac{1}{\tau_M}\right)t\right)}{k_2+\frac{1}{\tau_M}-\frac{1}{\tau_D}}$$

$$+[Py_{diff}(D)]_o e^{-A_3}\sum_{i=0}^{\infty}\frac{A_3^i}{i!}\frac{A_2+iA_4}{A_2+iA_4-k_2}\frac{\exp\left(-\left(A_2+iA_4+\frac{1}{\tau_M}\right)t\right)-\exp\left(-\frac{t}{\tau_D}\right)}{A_2+iA_4+\frac{1}{\tau_M}-\frac{1}{\tau_D}}\Bigg)$$

$$+[E0]_o\times\exp\left(-\frac{t}{\tau_{E0}}\right)+[D]_o\times\exp\left(-\frac{t}{\tau_D}\right)\Bigg] \qquad \text{(S4.2)}$$

In Equations S1 and S2, the parameters A_2, A_3, and A_4 are given in Equations S3.a–c.

$$A_2 =< n > \times\frac{k_{blob}k_e[blob]}{k_{blob}+k_e[blob]} \qquad \text{(S4.3.a)}$$

$$A_3 =< n > \times\left(\frac{k_{blob}}{k_{blob}+k_e[blob]}\right)^2 \qquad \text{(S3.b)}$$

$$A_4 = k_{blob} + k_e [blob] \quad \text{(S4.3.c)}$$

B] ^{1}H NMR spectra

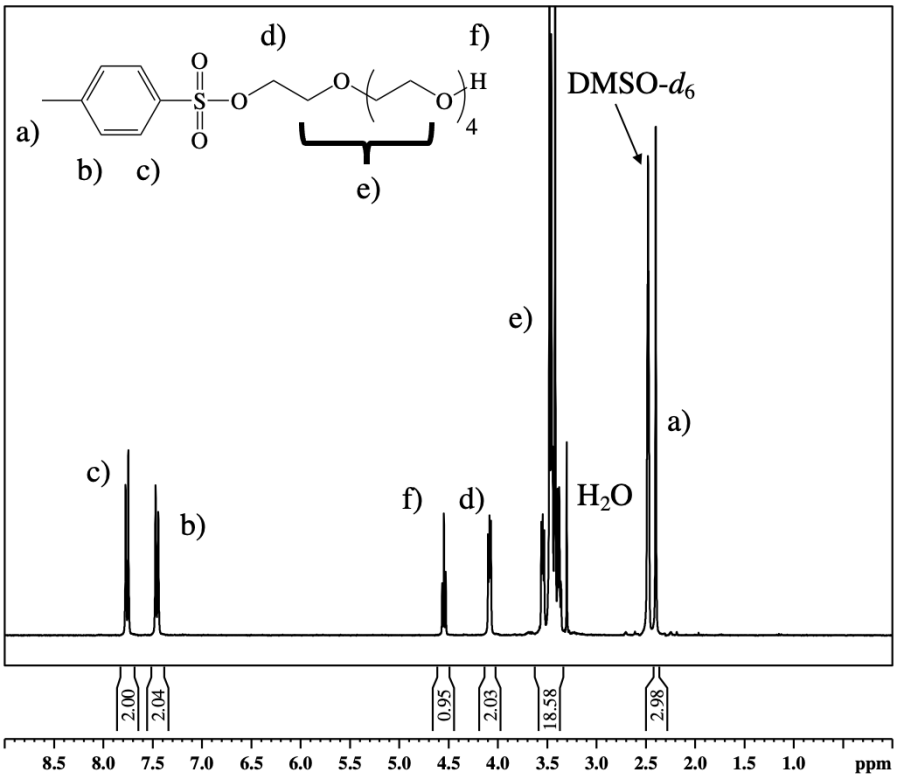

Figure S4.1. ^{1}H NMR spectrum of penta(ethylene glycol) mono *p*-toluene sulfonate. (DMSO-d_6, 300 MHz), δ 2.40 (s, 3H), 3.34-3.59 (m, 18H), 4.08 (t, 2H), 4.54 (t, 1H), 7,44 (d, 2H), 7.76 (d, 2H).

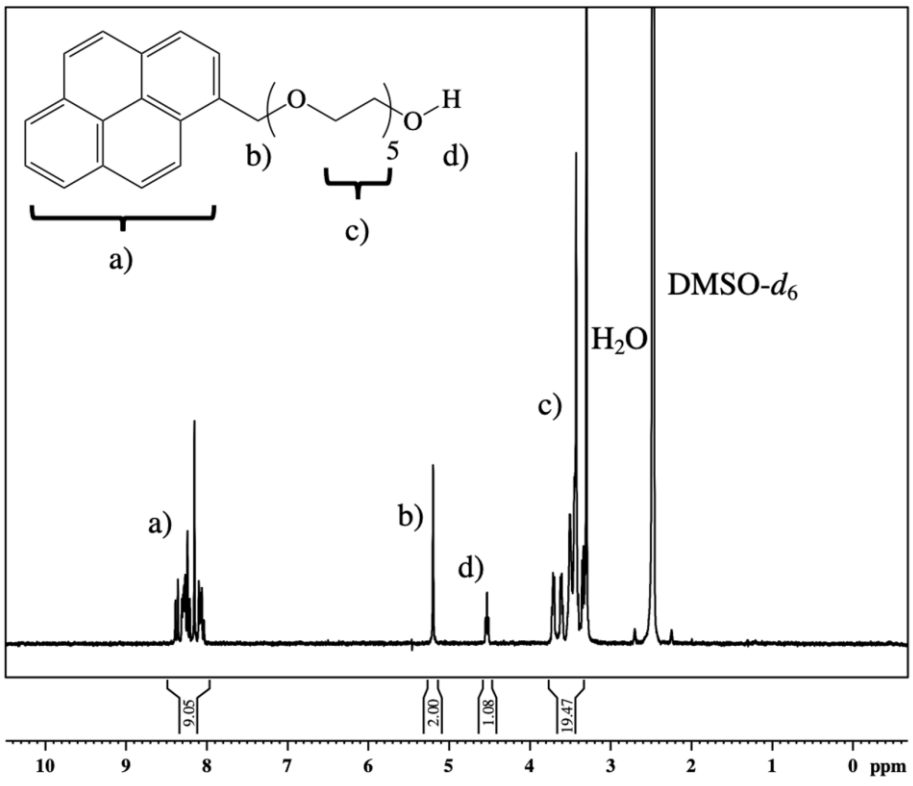

Figure S4.2. ^{1}H NMR spectrum of 1-pyrenemethyl ether penta(ethylene glycol) (DMSO-d_6, 300 MHz), δ 3.33-3.74 (m, 20H), 4.53 (t, 1H), 5.20 (s, 2H), 8.02-8.41 (m, 9H).

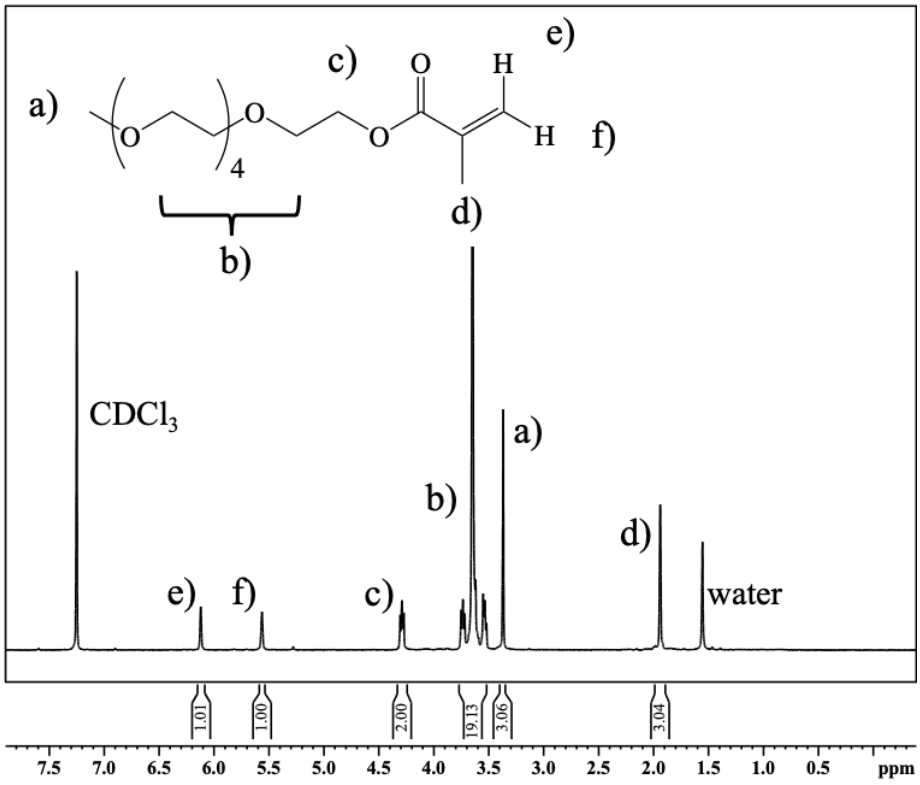

Figure S4.3. ^{1}H NMR spectrum of penta(ethylene glycol) methyl ether methacrylate ($CDCl_3$, 300 MHz), δ 1.94 (s, 3H), 3.37 (s, 3H), 3.51-3.77 (m, 18H), 4.29 (t, 2H), 5.57 (s, 1H), 6.13 (s,1H).

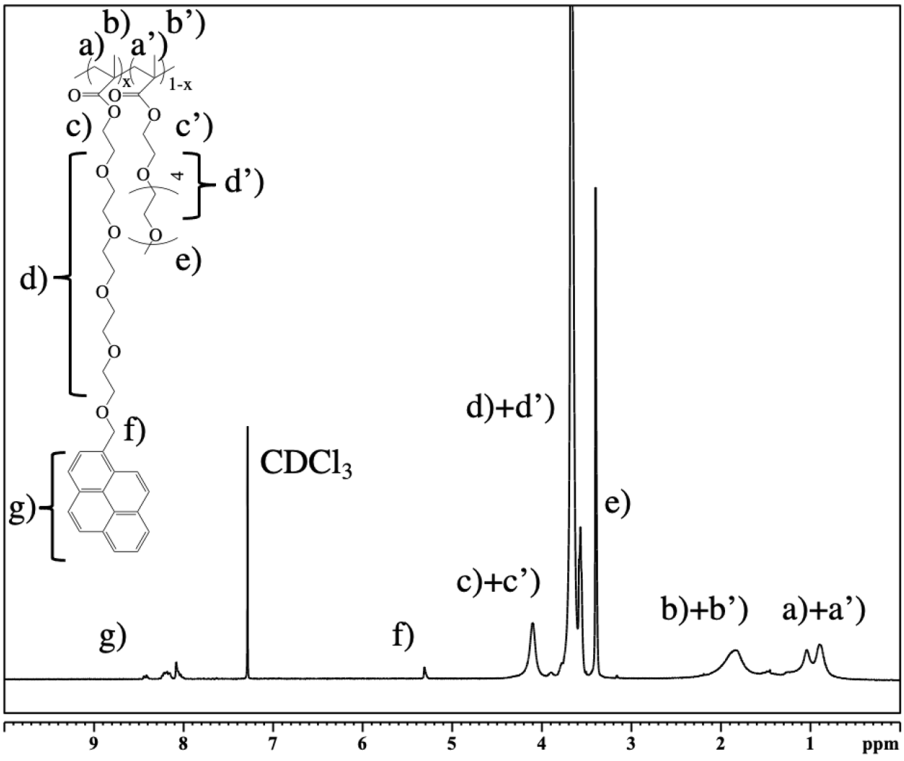

Figure S4.4. ^{1}H NMR spectrum of PyEG$_5$(3.6)-PEG$_5$MA. ($CDCl_3$, 300 MHz).

Gel permeation chromatography

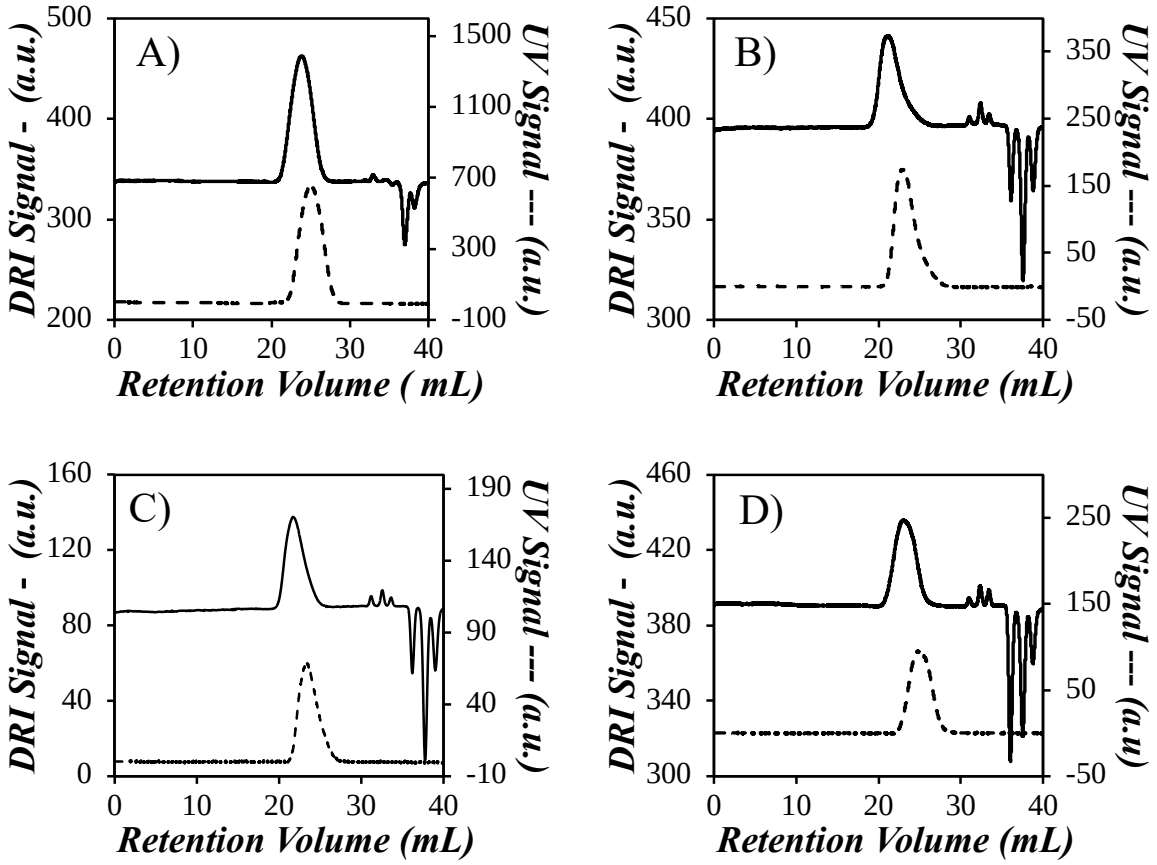

Figure S4.5. GPC traces in THF with (———) DRI and (- - - -) absorption detector for A) $PyEG_5(2.6)$-PEG_0MA, B) $PyEG_5(3.4)$-PEG_3MA, C) $PyEG_4(1.2)$-PEG_5MA and D) $PyEG_5(2.2)$-PEG_5MA. The number in parenthesis indicates the molar percentage of pyrene-labeled structural units.

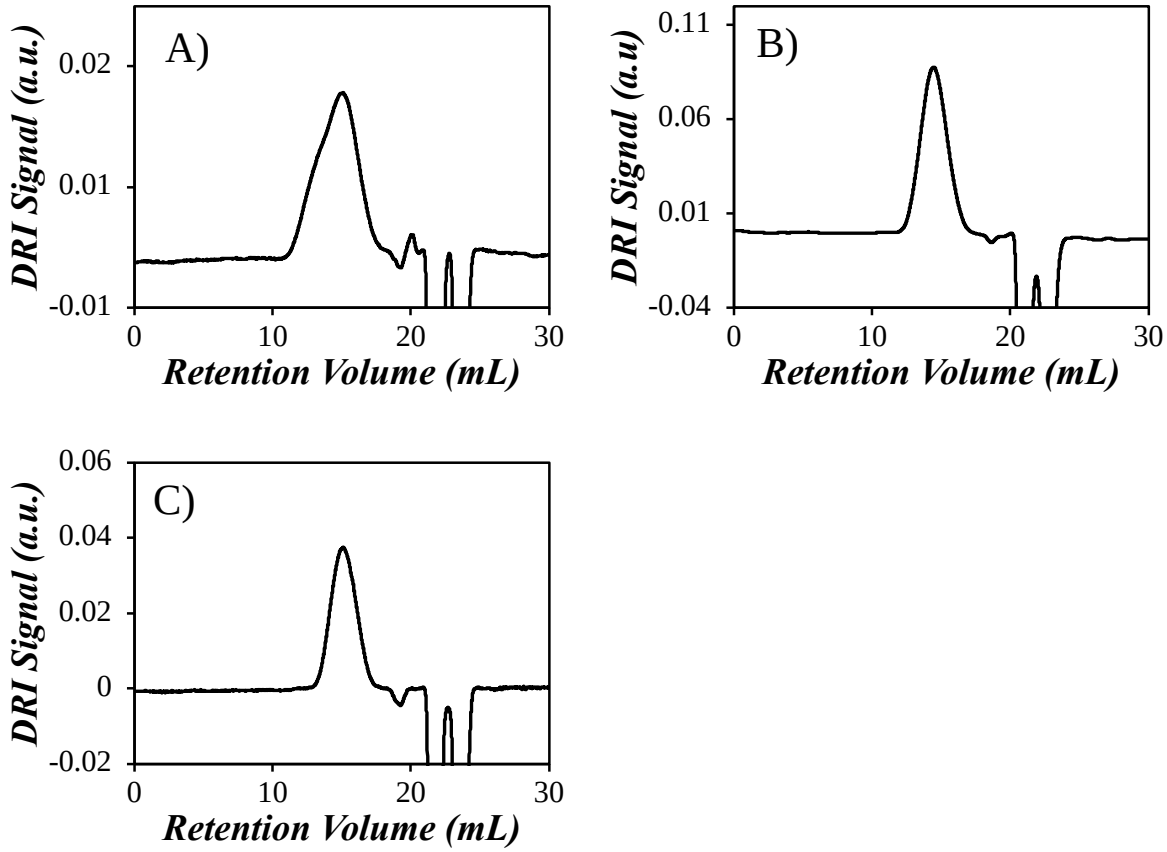

Figure S4.6. GPC traces in DMSO with DRI detector only for A) $PyEG_5$(3.6%)-PEG_7MA, B) $PyEG_5$(5.2)-PEG_9MA, and C) $PyEG_5$(2.1)-$PEG_{19}MA$. The number in parenthesis indicates the molar percentage of pyrene-labeled structural units.

All samples run in DMSO were first injected into a GPC instrument, that used *N*,*N*-dimethylformamide (DMF) with 0.1 wt% LiCl as eluent. The instrument was equipped with a DRI and UV detector. This was done to ensure that the polymers were free of any unreacted monomer or free pyrene derivative. Since the GPC system in DMF was not equipped with a

light scattering detector, the polymers were re-injected into the DMSO GPC for absolute molecular weight determination.

Plots of *d*n/*d*c versus pyrene content.

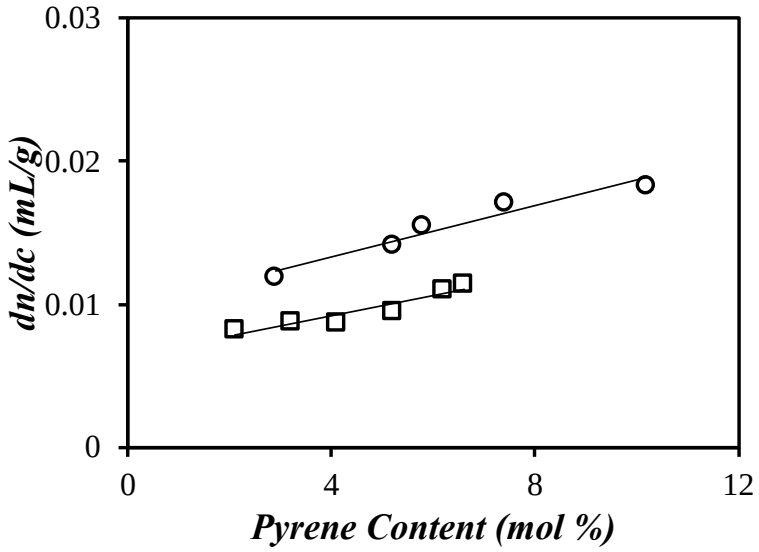

Figure S4.7. Plot of *d*n/*d*c versus pyrene content for (O) $PyEG_5$-PEG_9MA and (□) $PyEG_5$-$PEG_{19}MA$.

Steady-state fluorescence spectra

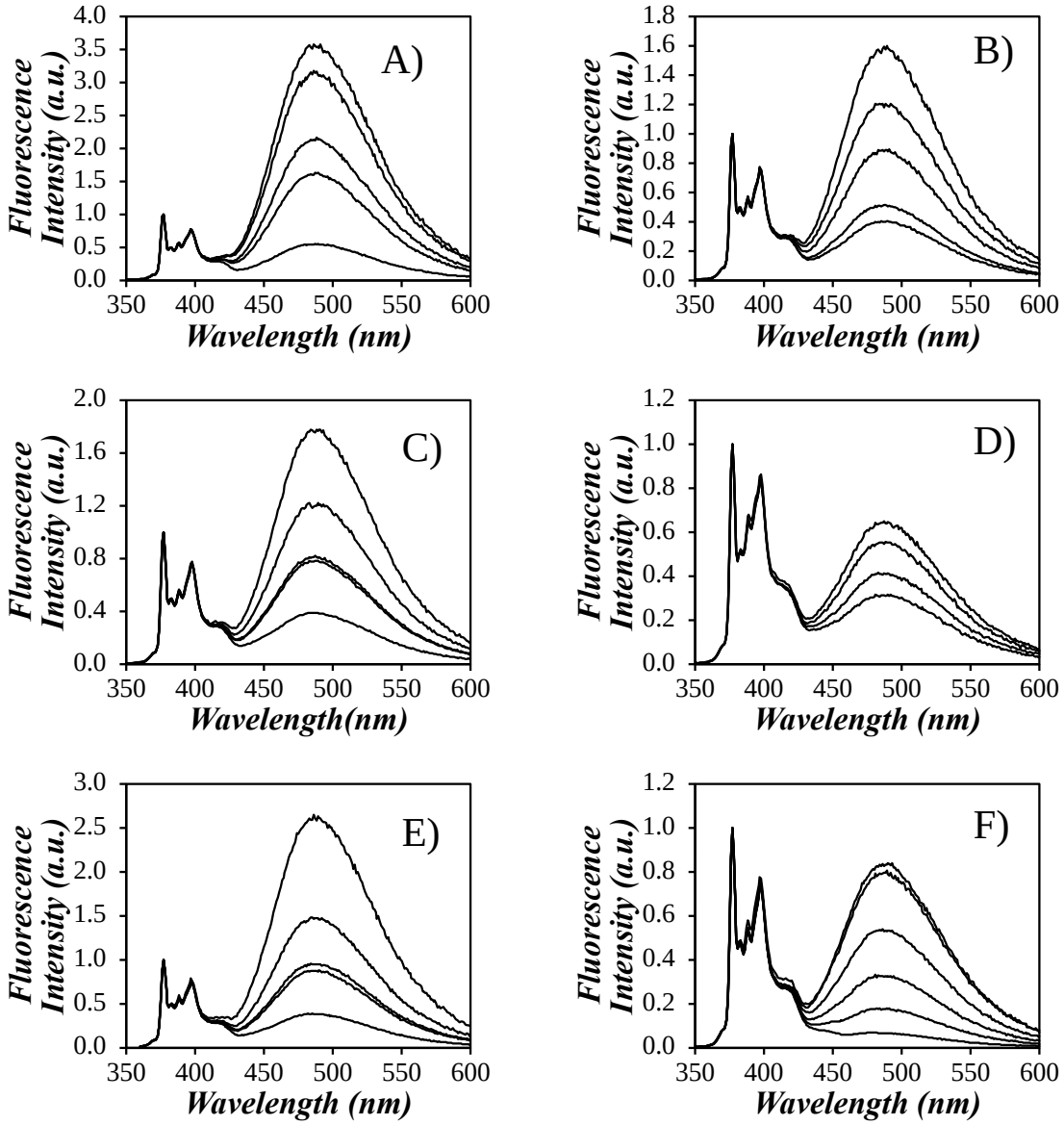

Figure S4.8. SSF spectra of A) $PyEG_5$-PEG_0MA, B) $PyEG_5$-PEG_3MA, C) $PyEG_5$-PEG_5MA, D) $PyEG_5$-PEG_7MA, E) $PyEG_5$-PEG_9MA, and F) $PyEG_5$-$PEG_{19}MA$ in acetonitrile. λ_{ex}=344 nm.

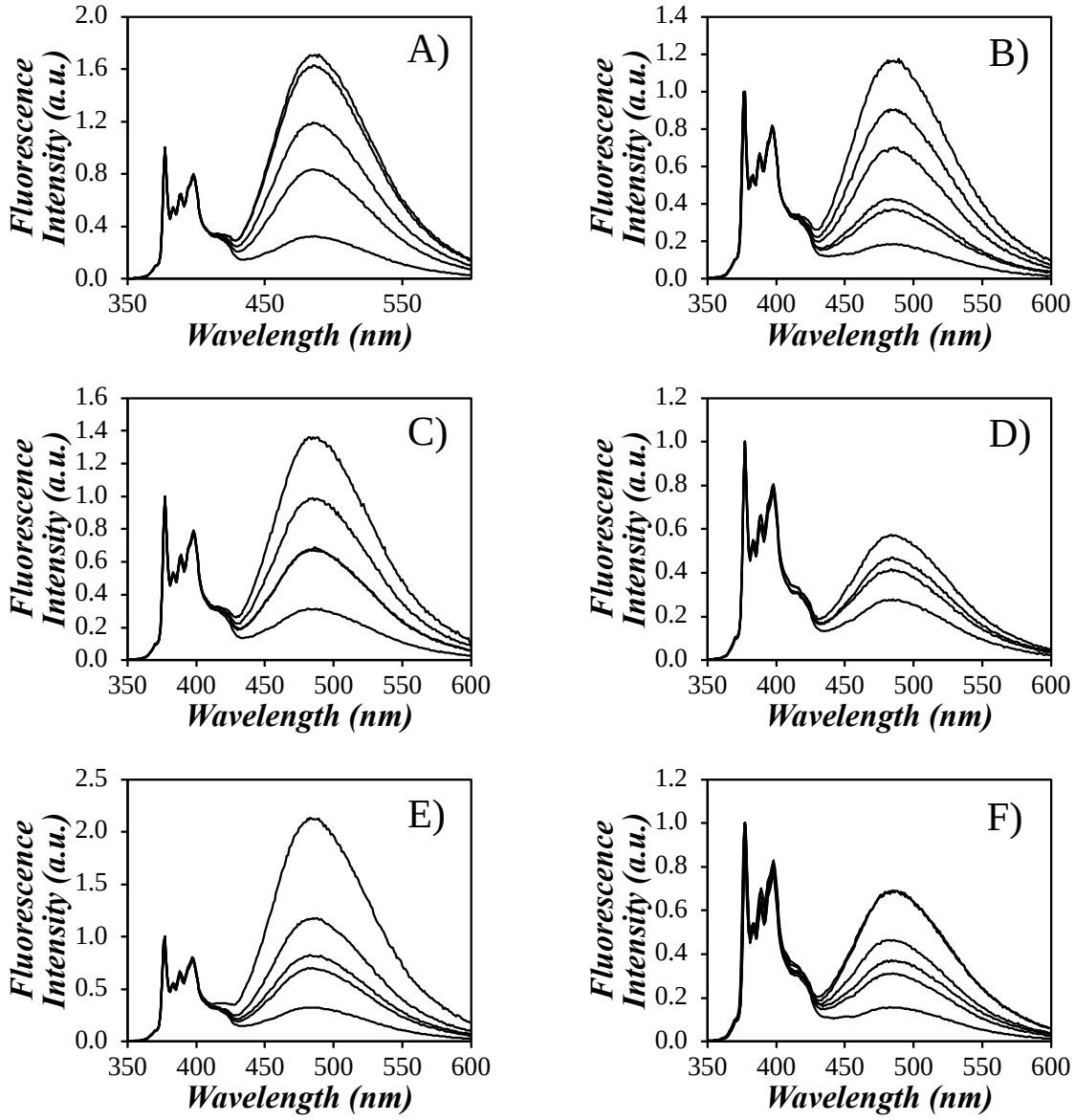

Figure S4.9. SSF spectra of A) $PyEG_5$-PEG_0MA, B) $PyEG_5$-PEG_3MA, C) $PyEG_5$-PEG_5MA, D) $PyEG_5$-PEG_7MA, E) $PyEG_5$-PEG_9MA, and F) $PyEG_5$-$PEG_{19}MA$ in THF. λ_{ex}=344 nm.

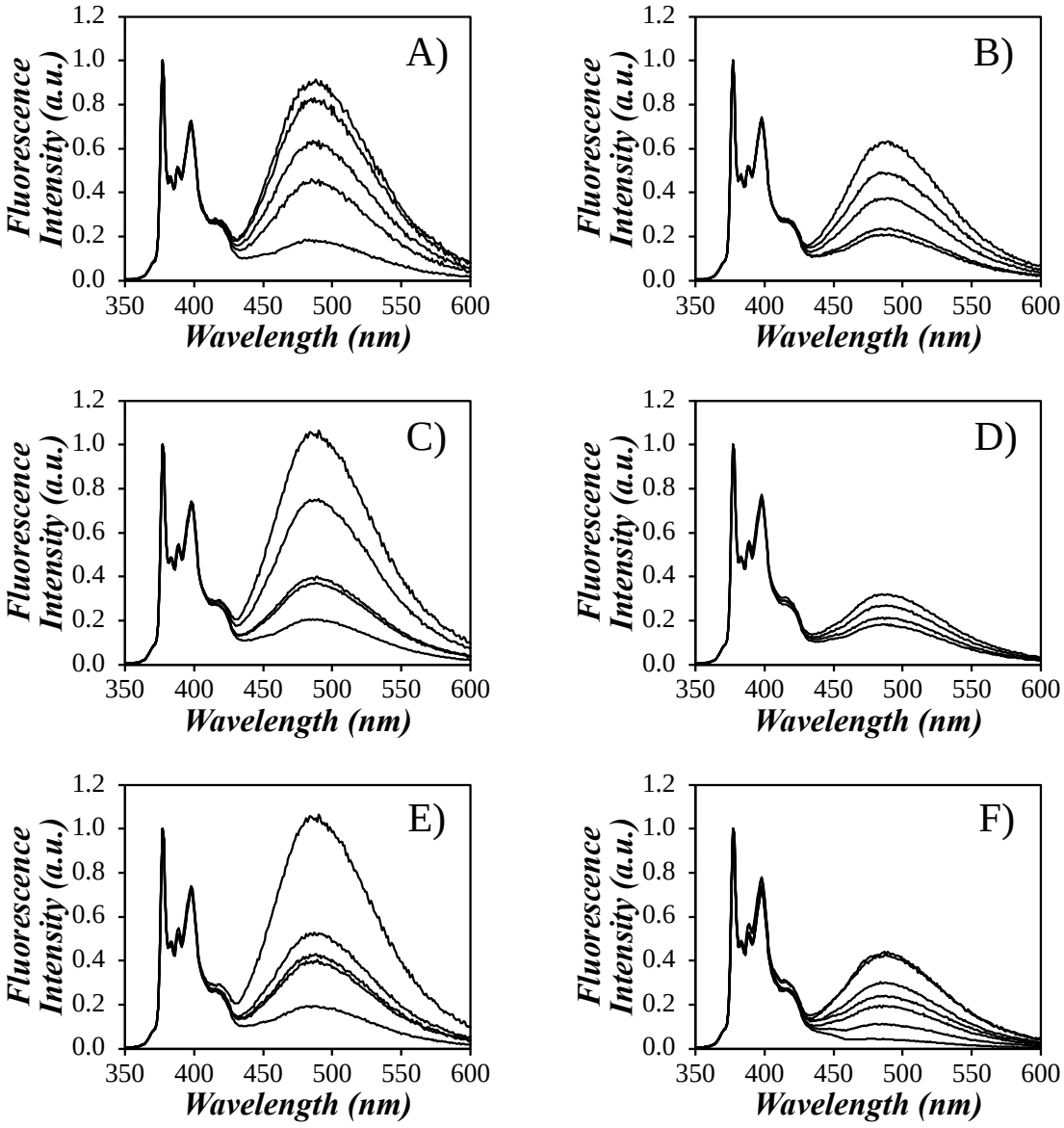

Figure S4.10. SSF spectra of A) $PyEG_5$-PEG_0MA, B) $PyEG_5$-PEG_3MA, C) $PyEG_5$-PEG_5MA, D) $PyEG_5$-PEG_7MA, E) $PyEG_5$-PEG_9MA, and F) $PyEG_5$-$PEG_{19}MA$ in DMF. λ_{ex}=344 nm.

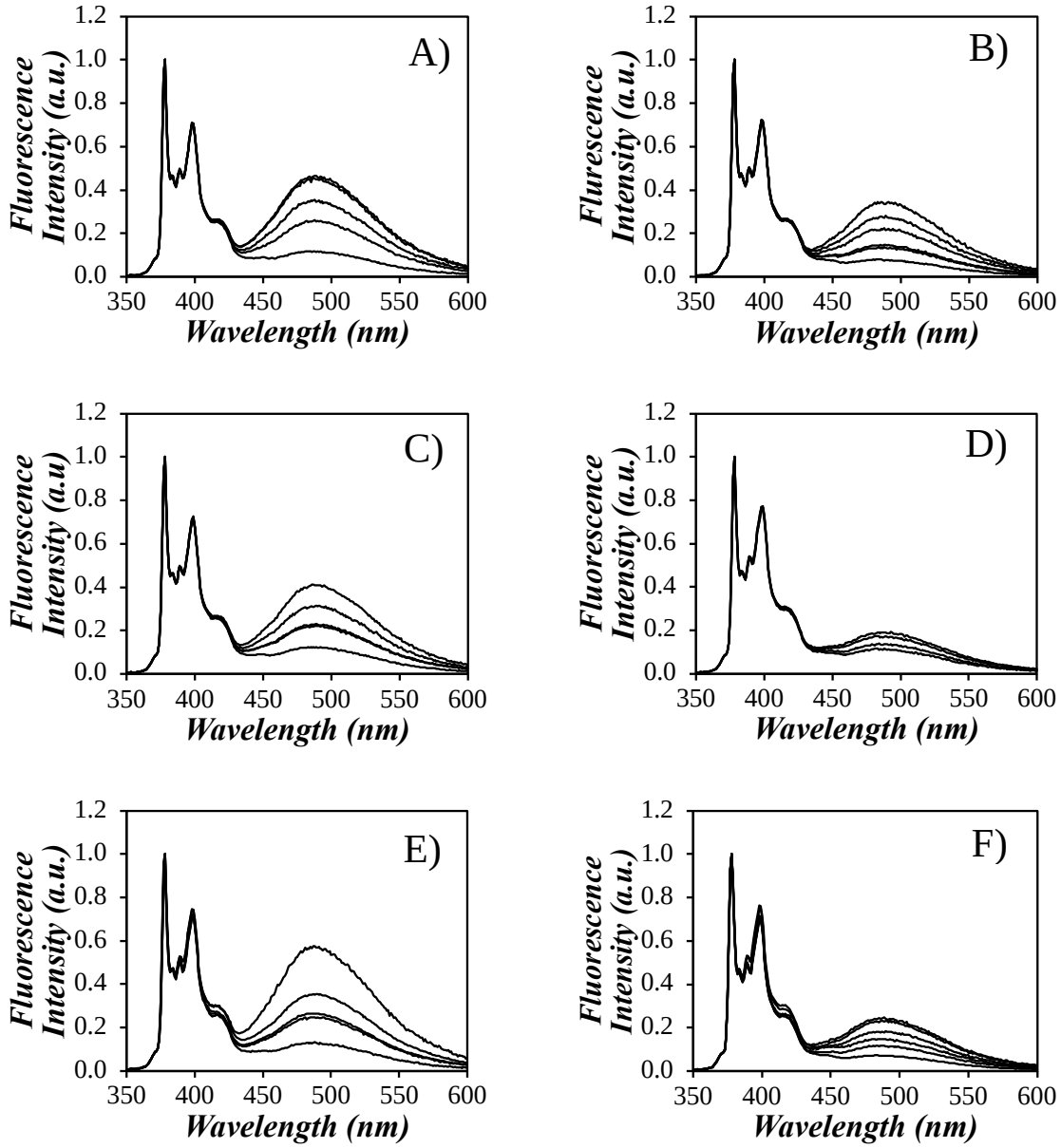

Figure S4.11. Steady-state fluorescence spectra of A) $PyEG_5$-PEG_0MA, B) $PyEG_5$-PEG_3MA, C) $PyEG_5$-PEG_5MA, D) $PyEG_5$-PEG_7MA, E) $PyEG_5$-PEG_9MA, and F) $PyEG_5$-$PEG_{19}MA$ in DMSO. [*Py*] = 2.5×10^{-6} M; λ_{ex} = 344 nm.

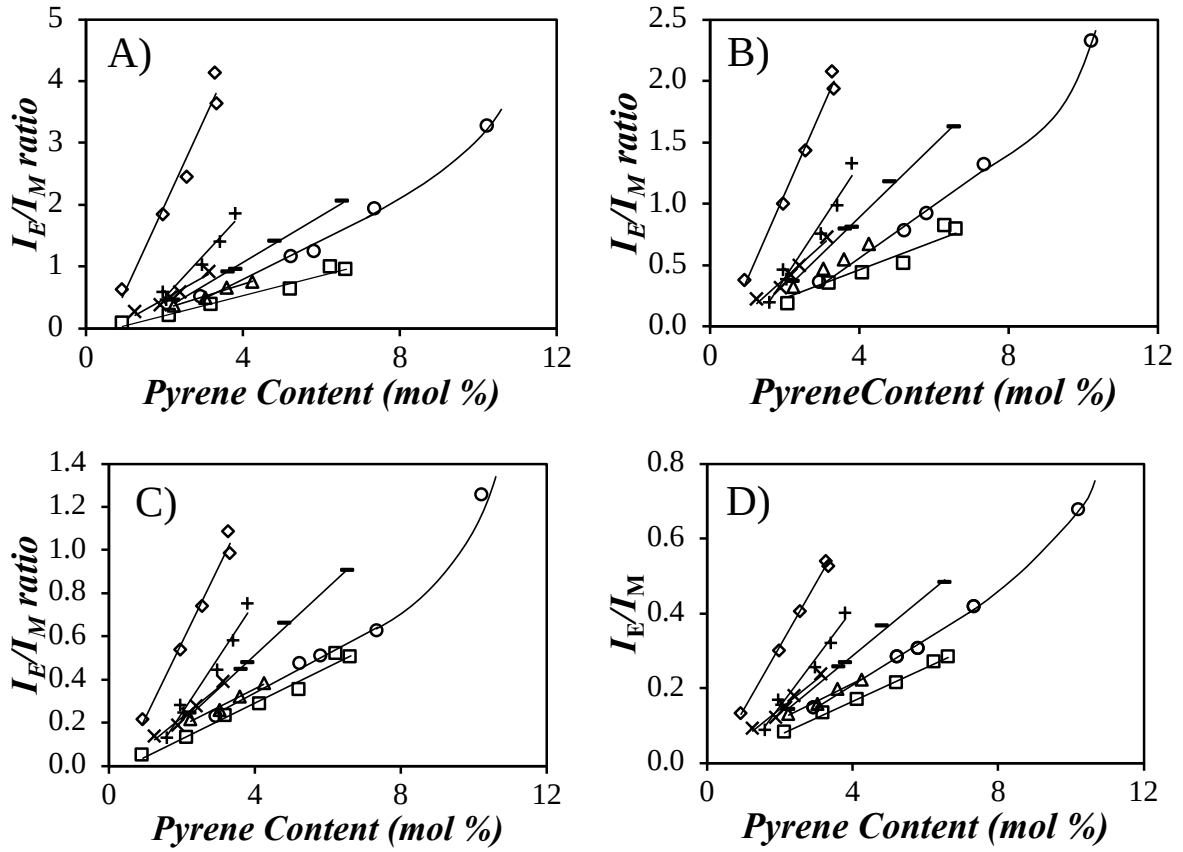

Figure S4.12. Plot of I_E/I_M ratio versus pyrene content for $PyEG_5$-PEG_nMA in A) acetonitrile, B) THF, C) DMF, and D) DMSO. (◆) $PyEG_5$-PEG_0MA, (+) $PyEG_5$-PEG_3MA, (×) $PyEG_5$-PEG_4MA, (−) $PyEG_5$-PEG_5MA, (▲) $PyEG_5$-PEG_7MA, (●) $PyEG_5$-PEG_9MA, and (■) $PyEG_5$-$PEG_{19}MA$.

Sample fit of the global FBM analysis of the fluorescence decays

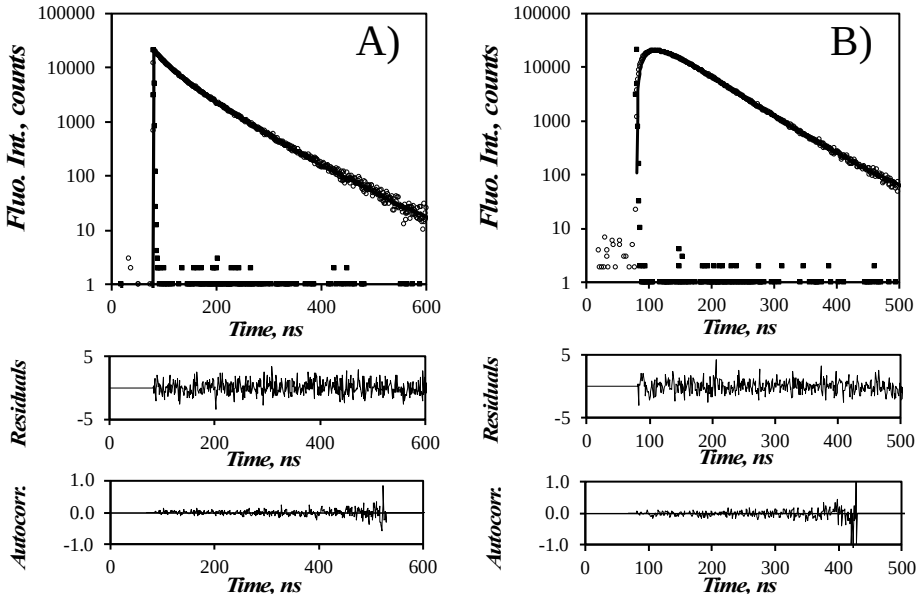

Figure S4.13. Global FBM analysis of the (A) monomer (λ_{em} = 375 nm) and (B) excimer (λ_{em} = 510 nm) fluorescence decays for $PyEG_5$-PEG_0MA with a pyrene content of 2.6 mol %. χ^2 = 1.15, λ_{ex} = 344 nm.

Huggins-Kraemer plots

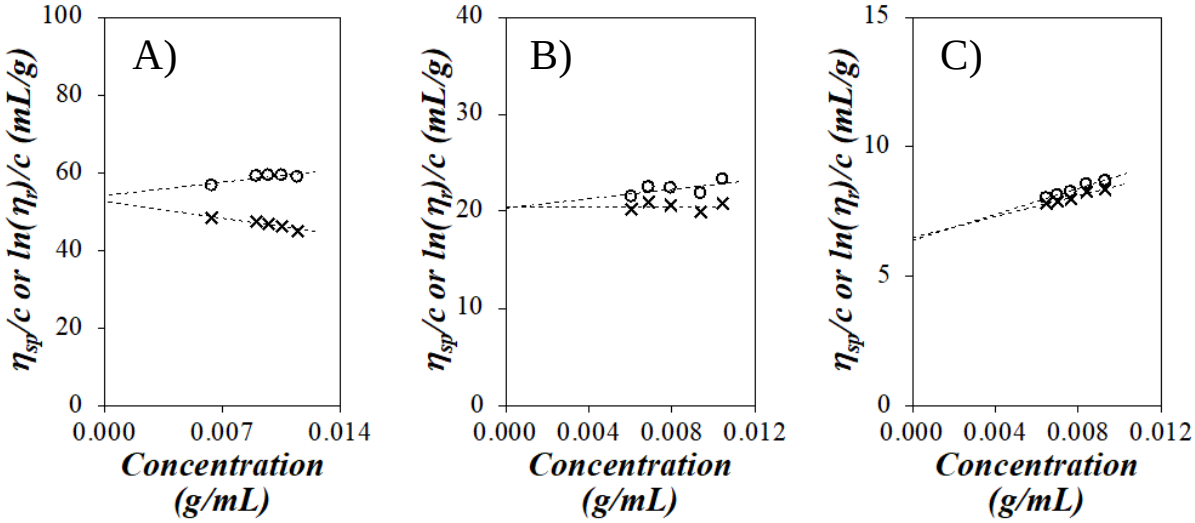

Figure S4.14. Plots of (O) η_{sp}/c and (×) $\ln(\eta_r)/c$ versus polymer concentration of A) PEG_3MA, B) PEG_9MA, and C) $PEG_{19}MA$ in acetonitrile.

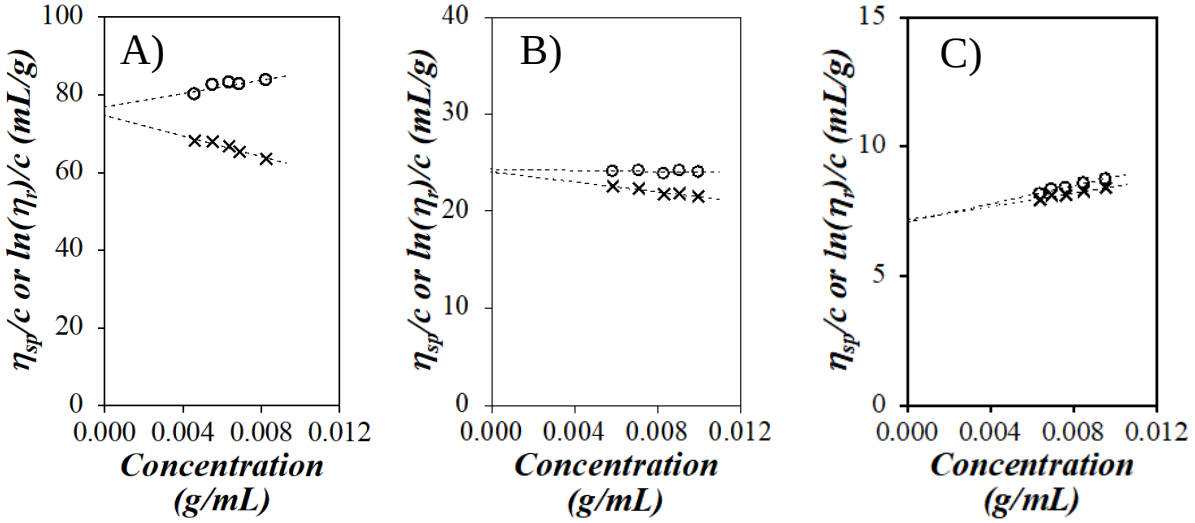

Figure S4.15. Plots of (O) η_{sp}/c and (×) $\ln(\eta_r)/c$ versus polymer concentration of A) PEG_3MA, B) PEG_9MA, and C) $PEG_{19}MA$ in THF.

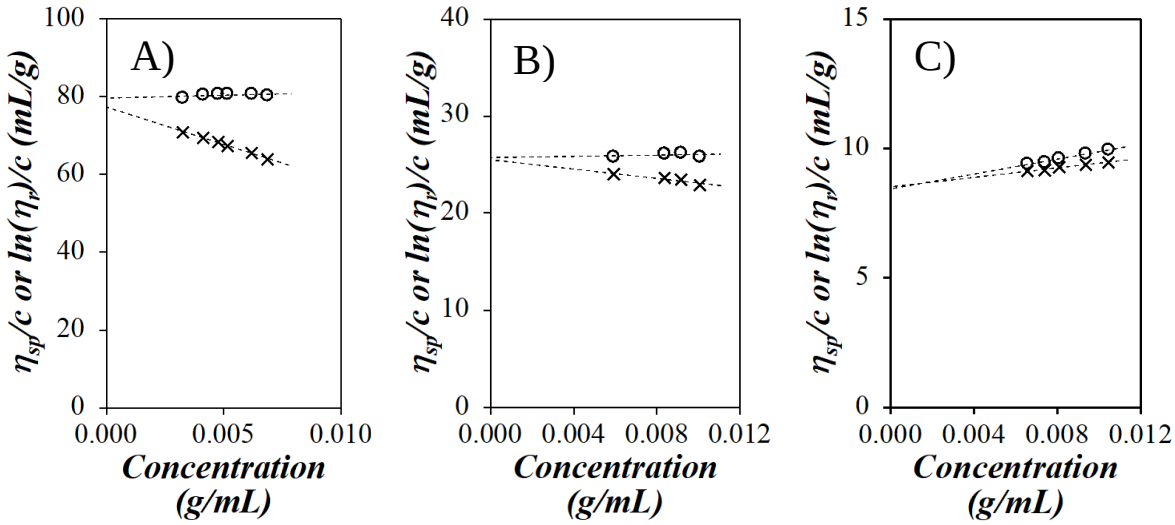

Figure S4.16. Plots of (O) η_{sp}/c and (×) $\ln(\eta_r)/c$ versus polymer concentration of A) PEG_3MA, B) PEG_9MA, and C) $PEG_{19}MA$ in DMF.

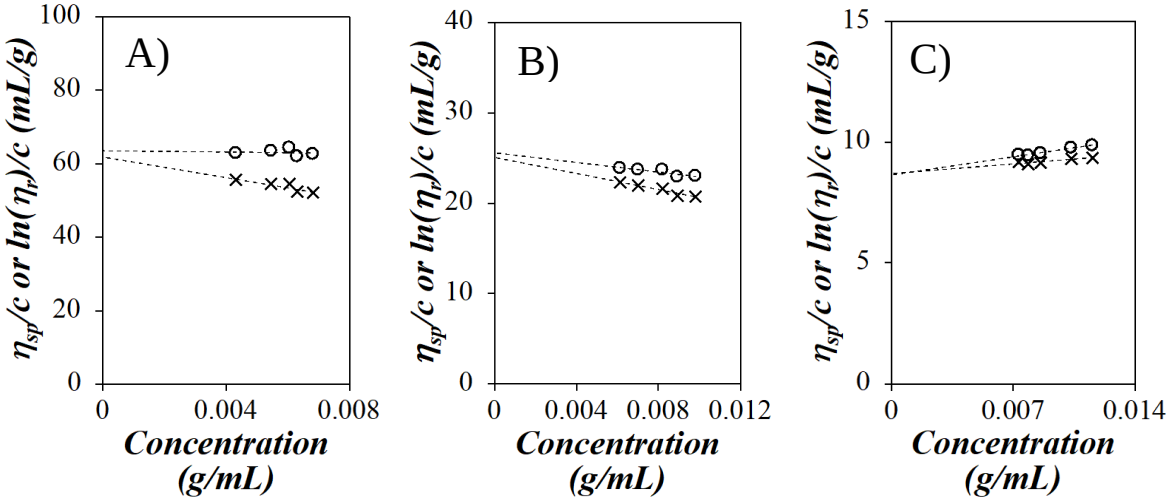

Figure S4.17. Plots of (O) η_{sp}/c and (×) $\ln(\eta_r)/c$ versus polymer concentration of A) PEG_3MA, B) PEG_9MA, and C) $PEG_{19}MA$ in DMSO.

Analysis of GPC [η] conformation plots

Since this study is the first of its kind, the validity of the PEF-based methodology to determine l_p^o needed to be assessed by comparing the l_p^o values with the l_p values determined by another technique. To this end, GPC experiments were also conducted with a combination of DRI, MALLS, and pressure detectors that yielded, respectively, the mass concentration, the absolute molar mass (M), and the intrinsic viscosity ($[\eta]$) for thin slices representing different fractions of the entire MWD of the polymer samples, where macromolecules with a same molecular weight would elute. In turn, conformation plots were obtained in Figure S4.15 by representing the quantity $(M^2/[\eta])^{1/3}$ as a function of $M^{1/2}$. The conformation plots showed the linear relationship expected from Equation S4.4, which is a simplification by Bohdanecky of the Yamakawa-Fujii (Y-F) equation[3] which has been found to apply over a broad range of L values.[4] The expressions of A_η and B_η used in Equation S4.4 are given in Equations S4.5 and S4.6, respectively.

$$\left(\frac{M^2}{[\eta]}\right)^{1/3} = A_\eta + B_\eta M^{1/2} \tag{S4.4}$$

$$A_\eta = \frac{A_0 M_L}{\Phi_{0,\infty}^{1/3}} \tag{S4.5}$$

$$B_\eta = \frac{B_0}{\Phi_{0,\infty}^{1/3}}\left(\frac{2l_p}{M_L}\right)^{-1/2} \tag{S4.6}$$

In Equations S5 and S6, A_o, M_L, $\Phi_{o,\infty}$, and B_o equal $0.46 - 0.53\times log(d/2l_p)$ where d is the hydrodynamic diameter of the PBB, M_o/b where M_o and b (=0.25 nm) are the molar mass and length of the structural unit, 2.87×10^{23} mol^{-1} which is the theoretical Flory constant for infinitely large molecular weights, and 1.05 for $M/(2l_pM_L)$ values ranging from 0.4 to 300, respectively. Conformation plots for the $PyEG_5$-PEG_0MA, $PyEG_5$-PEG_3MA, $PyEG_5$-PEG_7MA, $PyEG_5$-PEG_9MA, and $PyEG_5$-$PEG_{19}MA$ series were generated with 1, 1, 2, 2, and 5 polymer samples for each series, respectively. The linear conformation plots shown in Figure S4.15 were fit with straight lines whose slopes yielded B_η in Equation S4.6 which was used to determine l_p for the different $PyEG_5$-PEG_nMA series.

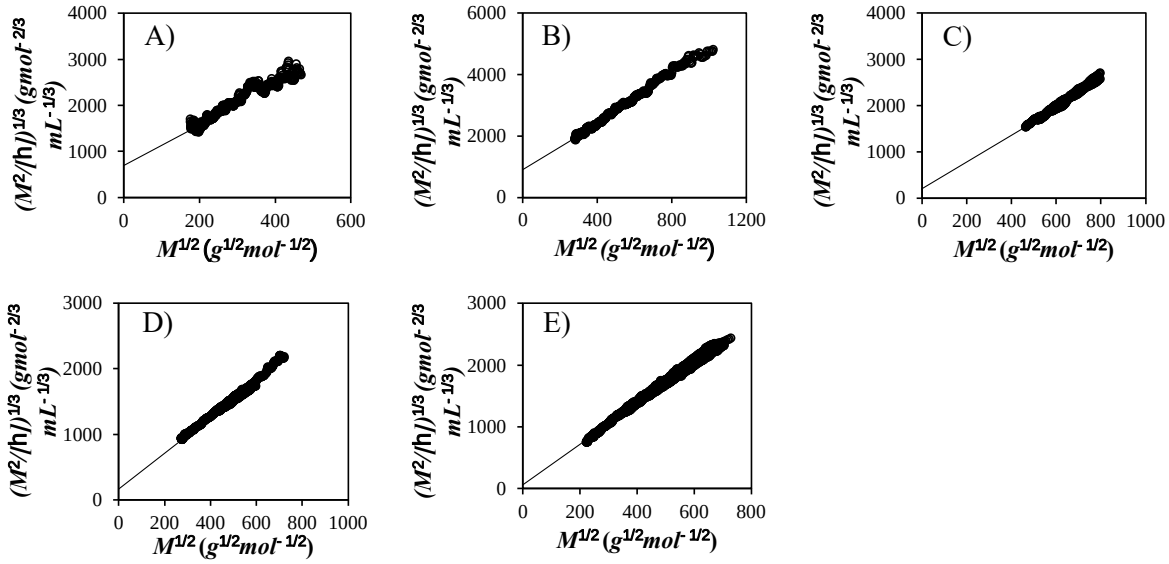

Figure S4.15. Bohdanecky linearization plots for the A) $PyEG_5$-PEG_0MA, B) $PyEG_5$-PEG_3MA, C) $PyEG_5$-PEG_7MA, D) $PyEG_5$-PEG_9MA, and E) $PyEG_5$-$PEG_{19}MA$ samples.

The l_p values retrieved from the $(M^2/[\eta])^{1/3}$-*vs*-$M^{1/2}$ conformation plots were listed in Table S4.1 along with the A_η, B_η, and M_L values used in Equations S4.4 – S4.6. The l_p values obtained by fluorescence were lower than those obtained from the GPC analysis however, both scaled as N_S^2.

Table S4.1. Bohdanecky Parameters and Persistence Lengths Obtained from GPC and FBM Analysis.

Sample	A_η ($gmol^{-2/3}mL^{-1/3}$)	B_η ($g^{1/2}mol^{-1/6}mL^{-1/3}$)	M_L ($gmol^{-1}nm^{-1}$)	l_p from GPC (nm)	l_p from FBM (nm)
$PyEG_5$-PEG_0MA	697	4.4	400	0.27 ± 0.03	0.38
$PyEG_5$-PEG_3MA	909	3.7	929	0.88 ± 0.04	0.50
$PyEG_5$-PEG_4MA	N/A	N/A	1105	N/A	0.61
$PyEG_5$-PEG_5MA	N/A	N/A	1282	N/A	0.85
$PyEG_5$-PEG_7MA	195 ± 21	2.97 ± 0.10	1634	2.35 ± 0.16	1.21
$PyEG_5$-PEG_9MA	173 ± 70	2.72 ± 0.26	2000	3.47 ± 0.66	1.89
$PyEG_5$-$PEG_{19}MA$	63.6 ± 59	3.29 ± 0.16	3800	4.49 ± 0.44	N/A

Parameters retrieved from the FBM analysis

Table S4.2. Parameters retrieved from the FBM analysis of the monomer decays for the $PyEG_5$-PEG_nMA samples in degassed acetonitrile.

Sample	Mol%	k_{blob} ($10^6 s^{-1}$)	<n>	$k_e[blob]$ ($10^6 s^{-1}$)	f_{Mdiff}	f_{k2}	f_{Mfree}	f_{MS}	χ^2
$PyEG_5$-PEG_0MA $k_2 = 1.49\times10^8$ s^{-1} τ_M = 270 ns	0.9	11.4	1.39	4.34	0.68	0.24	0.08	-	1.0
	2.0	11.8	2.30	3.50	0.57	0.42	0.02	-	1.2
	2.6	12.0	2.70	3.65	0.46	0.53	0.01	-	1.1
	3.3	10.7	3.71	2.42	0.37	0.62	0.00	-	1.2
	3.3	10.8	3.47	2.37	0.38	0.61	0.00	-	1.1
$PyEG_5$-PEG_3MA $k_2 = 1.11\times10^8$ s^{-1} τ_M = 270 ns	2.0	12.2	1.28	4.33	0.63	0.29	0.08	-	1.0
	2.1	12.3	1.09	3.70	0.65	0.24	0.11	-	1.1
	3.0	10.3	1.78	3.12	0.58	0.40	0.02	-	1.1
	3.4	10.6	2.08	3.39	0.51	0.48	0.02	-	1.1
	3.8	10.0	2.54	2.29	0.46	0.53	0.01	-	1.0
$PyEG_5$-PEG_4MA $k_2 = 0.91\times10^8$ s^{-1} τ_M = 270 ns	1.2	10.5	0.89	3.30	0.61	0.20	0.18	-	1.2
	1.9	11.0	1.08	3.00	0.64	0.24	0.12	-	1.1
	2.2	9.2	1.30	2.59	0.61	0.30	0.09	-	1.0
	2.4	8.9	1.39	2.75	0.59	0.33	0.07	-	1.2
	3.1	9.0	1.76	2.78	0.57	0.40	0.04	-	1.0
$PyEG_5$-PEG_5MA $k_2 = 1.43\times10^8$ s^{-1} τ_M = 270 ns	2.2	13.4	1.15	4.60	0.65	0.23	0.13	-	1.1
	3.6	12.2	1.65	3.19	0.63	0.34	0.03	-	1.2
	3.8	13.1	1.62	3.64	0.61	0.36	0.03	-	1.1
	4.8	11.6	2.13	3.21	0.56	0.43	0.02	-	1.2
	6.5	11.9	2.47	2.94	0.49	0.50	0.01	-	1.1
$PyEG_5$-PEG_7MA $k_2 = 1.49\times10^8$ s^{-1} τ_M = 270 ns τ_S = 4 ns	2.2	18.1	1.10	3.82	0.43	0.16	0.09	0.33	1.2
	3.0	17.7	1.26	3.06	0.42	0.21	0.04	0.33	1.1
	3.6	15.1	1.42	2.97	0.44	0.23	0.04	0.30	1.2
	4.2	17.0	1.59	2.76	0.43	0.28	0.03	0.26	1.2
$PyEG_5$-PEG_9MA $k_2 = 1.40\times10^8$ s^{-1} τ_M = 270 ns	2.9	12.3	1.31	2.88	0.64	0.21	0.15	-	1.1
	5.2	13.8	1.76	3.23	0.61	0.35	0.04	-	1.1
	5.8	14.2	1.82	3.16	0.55	0.41	0.04	-	1.2
	7.4	13.0	2.30	2.68	0.51	0.48	0.02	-	1.1
	10.2	12.2	3.12	1.98	0.36	0.63	0.01	-	1.1
$PyEG_5$-$PEG_{19}MA$ $k_2 = 1.33\times10^8$ s^{-1} τ_M = 270 ns	2.1	13.8	1.24	2.97	0.50	0.15	0.35	-	1.1
	3.2	12.7	1.39	2.97	0.59	0.22	0.19	-	1.2
	5.2	13.9	1.76	2.71	0.53	0.34	0.13	-	1.1
	6.2	12.4	1.93	2.51	0.57	0.38	0.06	-	1.1
	6.6	14.6	2.01	2.26	0.51	0.42	0.07	-	1.1

Table S4.3. Parameters retrieved from the FBM analysis of the monomer decays for the $PyEG_5$-PEG_nMA samples in degassed THF.

Sample	Mol%	k_{blob} ($10^6 s^{-1}$)	<n>	$k_e[blob]$ ($10^6 s^{-1}$)	f_{Mdiff}	f_{k2}	f_{Mfree}	χ^2
$PyEG_5$-PEG_0MA $k_2 = 1.02\times10^8$ s^{-1} τ_M = 270 ns	0.9	9.1	1.01	3.40	0.71	0.14	0.15	1.2
	2.0	9.5	1.74	3.84	0.69	0.27	0.04	1.1
	2.6	9.8	2.15	4.33	0.63	0.35	0.02	1.1
	3.3	9.1	2.79	4.10	0.57	0.43	0.00	1.1
	3.3	7.9	2.86	2.04	0.58	0.41	0.00	1.2
$PyEG_5$-PEG_3MA $k_2 = 0.71\times10^8$ s^{-1} τ_M = 270 ns	2.0	7.8	1.17	3.88	0.64	0.26	0.09	1.1
	2.1	7.5	1.00	3.47	0.66	0.25	0.09	1.1
	3.0	6.8	1.66	3.06	0.61	0.35	0.03	1.1
	3.4	6.5	2.01	2.74	0.56	0.43	0.01	1.1
	3.8	6.2	2.47	2.89	0.51	0.48	0.01	1.1
$PyEG_5$-PEG_4MA $k_2 = 0.68\times10^8$ s^{-1} τ_M = 270 ns	1.2	9.6	0.76	2.94	0.63	0.16	0.21	1.2
	1.9	8.1	0.99	2.69	0.65	0.21	0.21	1.1
	2.2	6.7	1.22	2.66	0.65	0.23	0.12	1.1
	2.4	6.5	1.33	2.48	0.65	0.26	0.09	1.0
	3.1	6.2	1.65	2.28	0.60	0.36	0.04	1.1
$PyEG_5$-PEG_5MA $k_2 = 0.88\times10^8$ s^{-1} τ_M = 270 ns	2.2	9.2	1.05	3.80	0.65	0.22	0.13	1.2
	3.6	8.3	1.57	3.26	0.62	0.33	0.05	1.1
	3.8	8.7	1.53	3.22	0.63	0.33	0.04	1.1
	4.8	7.9	2.01	3.25	0.57	0.41	0.02	1.1
	6.5	7.7	2.43	2.81	0.49	0.50	0.01	1.0
$PyEG_5$-PEG_7MA $k_2 = 0.80\times10^8$ s^{-1} τ_M = 270 ns	2.2	9.4	1.02	3.99	0.58	0.23	0.20	1.1
	3.0	9.9	1.13	3.55	0.61	0.29	0.10	1.1
	3.6	8.9	1.27	3.57	0.62	0.30	0.08	1.1
	4.2	9.7	1.36	3.50	0.57	0.37	0.06	1.1
$PyEG_5$-PEG_9MA $k_2 = 0.91\times10^8$ s^{-1} τ_M = 270 ns	2.9	10.1	1.12	3.64	0.62	0.22	0.16	1.1
	5.2	8.9	1.67	2.90	0.61	0.36	0.04	1.1
	5.8	9.0	1.83	2.81	0.57	0.40	0.03	1.1
	7.4	8.6	2.21	2.78	0.53	0.46	0.02	1.1
	10.2	7.4	3.31	2.86	0.40	0.60	0.00	1.1
$PyEG_5$-$PEG_{19}MA$ $k_2 = 0.86\times10^8$ s^{-1} τ_M = 270 ns	2.1	10.7	1.03	4.73	0.48	0.15	0.37	1.2
	3.2	11.3	1.13	3.84	0.59	0.24	0.17	1.2
	4.4	8.8	1.44	3.96	0.60	0.23	0.16	1.1
	5.2	10.4	1.53	3.42	0.53	0.33	0.13	1.2
	6.2	8.3	1.83	2.48	0.60	0.35	0.05	1.2
	6.6	10.0	1.77	2.69	0.53	0.41	0.06	1.2

Table S4.4. Parameters retrieved from the FBM analysis of the monomer decays for the $PyEG_5$-PEG_nMA samples in degassed DMF.

Sample	Mol%	k_{blob} ($10^6 s^{-1}$)	<n>	$k_e[blob]$ ($10^6 s^{-1}$)	f_{Mdiff}	f_{k2}	f_{Mfree}	χ^2
$PyEG_5$-PEG_0MA $k_2 = 0.80\times10^8$ s^{-1} τ_M = 230 ns	0.9	9.3	0.87	4.64	0.69	0.08	0.17	1.1
	2.0	8.3	1.59	3.99	0.70	0.08	0.04	1.1
	2.6	7.2	2.14	3.13	0.65	0.08	0.02	1.1
	3.3	6.9	2.76	2.20	0.59	0.08	0.00	1.1
	3.3	7.1	2.59	2.67	0.60	0.08	0.01	1.1
$PyEG_5$-PEG_3MA $k_2 = 0.73\times10^8$ s^{-1} τ_M = 230 ns	2.0	6.9	1.15	3.34	0.68	0.19	0.13	1.2
	2.1	7.7	0.91	4.16	0.60	0.20	0.20	1.2
	3.0	6.7	1.48	3.67	0.68	0.26	0.06	1.1
	3.4	6.8	1.74	3.03	0.65	0.31	0.03	1.1
	3.8	6.2	2.10	2.83	0.62	0.37	0.01	1.1
$PyEG_5$-PEG_4MA $k_2 = 0.62\times10^8$ s^{-1} τ_M = 230 ns	1.2	7.3	0.81	3.24	0.60	0.14	0.26	1.1
	1.9	7.9	0.87	3.75	0.62	0.18	0.20	1.1
	2.2	6.3	1.10	2.52	0.68	0.17	0.14	1.1
	2.4	6.2	1.18	2.67	0.67	0.21	0.12	1.1
	3.1	6.1	1.46	2.53	0.66	0.28	0.06	1.1
$PyEG_5$-PEG_5MA $k_2 = 0.69\times10^8$ s^{-1} τ_M = 230 ns	2.2	7.2	1.09	3.38	0.64	0.21	0.15	1.0
	3.6	6.8	1.48	2.78	0.63	0.31	0.06	1.0
	3.8	6.9	1.51	3.32	0.63	0.31	0.05	1.0
	4.8	6.3	1.96	2.51	0.58	0.39	0.03	1.1
	6.5	5.3	2.53	1.43	0.51	0.48	0.01	1.2
$PyEG_5$-PEG_7MA $k_2 = 0.58\times10^8$ s^{-1} τ_M = 230 ns	2.2	10.3	0.87	4.56	0.58	0.20	0.21	1.1
	3.0	8.8	0.97	4.84	0.55	0.30	0.15	1.1
	3.6	7.6	1.14	3.37	0.60	0.31	0.09	1.2
	4.2	8.1	1.22	3.87	0.54	0.39	0.08	1.1
$PyEG_5$-PEG_9MA $k_2 = 1.03\times10^8$ s^{-1} τ_M = 230 ns	2.9	10.30	0.97	4.76	0.68	0.14	0.18	1.0
	5.2	10.12	1.34	3.91	0.71	0.23	0.06	1.1
	5.8	11.52	1.37	3.96	0.69	0.25	0.06	1.1
	7.4	10.57	1.71	3.81	0.64	0.29	0.07	1.1
	10.2	9.22	2.55	3.27	0.56	0.43	0.01	1.2
$PyEG_5$-$PEG_{19}MA$ $k_2 = 0.83\times10^8$ s^{-1} τ_M = 230 ns	2.1	11.6	0.87	4.64	0.47	0.12	0.40	1.1
	3.2	10.0	1.05	4.14	0.60	0.18	0.23	1.1
	4.4	11.5	1.15	3.72	0.61	0.23	0.16	1.2
	5.2	10.4	1.35	3.70	0.57	0.26	0.16	1.1
	6.2	8.0	1.70	3.17	0.64	0.28	0.07	1.0
	6.6	11.5	1.45	3.06	0.57	0.36	0.07	1.2

Table S4.5. Parameters retrieved from the FBM analysis of the monomer decays for the $PyEG_5$-PEG_nMA samples in aerated DMSO.

Sample	Mol%	k_{blob} ($10^6 s^{-1}$)	<n>	$k_e[blob]$ ($10^6 s^{-1}$)	f_{Mdiff}	f_{k2}	f_{Mfree}	f_{MS}	χ^2
$PyEG_5$-PEG_0MA $k_2 = 1.43\times10^8$ s^{-1} τ_M = 120 ns	0.9	9.4	0.81	6.91	0.74	0.07	0.19	-	1.1
	2.0	8.6	1.38	5.73	0.82	0.13	0.05	-	1.1
	2.6	9.2	1.63	6.18	0.80	0.16	0.03	-	1.2
	3.3	8.2	2.08	4.68	0.79	0.20	0.01	-	1.1
	3.3	10.0	1.74	4.93	0.76	0.21	0.02	-	1.2
$PyEG_5$-PEG_3MA $k_2 = 0.87\times10^8$ s^{-1} τ_M = 120 ns	1.6	9.7	0.69	8.16	0.69	0.08	0.25	-	1.2
	2.0	7.1	1.06	6.01	0.77	0.14	0.09	-	1.1
	3.0	7.5	1.30	6.15	0.76	0.17	0.06	-	1.1
	3.4	7.9	1.49	6.51	0.74	0.21	0.05	-	1.1
	3.8	7.1	1.81	5.33	0.73	0.24	0.03	-	1.0
$PyEG_5$-PEG_4MA $k_2 = 0.83\times10^8$ s^{-1} τ_M = 120 ns	1.2	8.1	0.73	7.07	0.69	0.08	0.22	-	1.1
	1.9	8.1	0.84	6.64	0.70	0.10	0.20	-	1.1
	2.2	7.5	0.98	7.22	0.70	0.10	0.20	-	1.1
	2.4	6.9	1.06	5.47	0.75	0.13	0.12	-	1.2
	3.1	8.4	1.17	7.88	0.74	0.16	0.10	-	1.1
$PyEG_5$-PEG_5MA $k_2 = 0.76\times10^8$ s^{-1} τ_M = 120 ns	2.2	8.3	0.85	5.62	0.68	0.13	0.19	-	1.1
	3.6	8. 9	1.01	5.18	0.73	0.18	0.09	-	1.1
	3.8	8.0	1.13	4.89	0.73	0.20	0.07	-	1.1
	4.8	7.8	1.38	4.16	0.74	0.24	0.02	-	1.1
	6.5	7.3	1.72	4.62	0.68	0.29	0.03	-	1.2
$PyEG_5$-PEG_7MA $k_2 = 0.83\times10^8$ s^{-1} τ_M = 120 ns τ_S = 4 ns	2.2	13.6	0.72	5.48	0.35	0.09	0.08	0.48	1.0
	3.0	12.9	0.77	5.22	0.38	0.11	0.06	0.46	1.0
	3.6	9.9	1.00	5.90	0.49	0.13	0.07	0.31	1.1
	4.2	12.1	0.96	5.88	0.41	0.13	0.04	0.41	1.1
$PyEG_5$-PEG_9MA $k_2 = 1.05\times10^8$ s^{-1} τ_M = 120 ns	2.9	11.1	0.78	6.53	0.67	0.10	0.23	-	1.1
	5.2	9.4	1.20	5.20	0.75	0.17	0.08	-	1.1
	5.8	9.7	1.26	5.25	0.75	0.18	0.07	-	1.1
	7.4	9.3	1.53	4.98	0.75	0.22	0.02	-	1.1
	10.2	9.2	2.02	3.93	0.69	0.31	0.00	-	1.2
$PyEG_5$-$PEG_{19}MA$ $k_2 = 1.09\times10^8$ s^{-1} τ_M = 120 ns	2.1	17.5	0.54	3.71	0.45	0.07	0.48	-	1.0
	3.2	15.5	0.65	4.11	0.55	0.09	0.36	-	1.1
	5.2	12.6	0.99	4.48	0.67	0.15	0.18	-	1.0
	6.2	9.0	1.18	4.74	0.71	0.14	0.14	-	1.2
	6.6	13.5	0.95	3.62	0.78	0.20	0.03	-	1.2

Table S4.6. Parameters retrieved from the FBM analysis of the excimer decays for the $PyEG_5$-PEG_nMA samples in degassed acetonitrile.

Sample	Mol %	f_{Ek2}	τ_{E0} (ns)	$f_{EdiffE0}$	f_{EE0}	τ_D (ns)	f_{EdiffD}	f_{ED}	f_{ES}	χ^2
$PyEG_5$-PEG_0MA	0.9	0.25	49	0.47	0.00	59	0.24	0.03	-	1.0
	2.0	0.39	47	0.23	0.00	55	0.31	0.08	-	1.2
	2.6	0.49	47	0.21	0.00	52	0.22	0.08	-	1.1
	3.3	0.55	46	0.15	0.00	54	0.18	0.12	-	1.2
	3.3	0.55	46	0.18	0.01	54	0.17	0.09	-	1.1
$PyEG_5$-PEG_3MA	2.0	0.29	34	0.00	0.07	53	0.64	0.00	-	1.0
	2.1	0.31	47	0.29	0.17	66	0.31	0.01	-	1.1
	3.0	0.38	46	0.25	0.00	54	0.31	0.06	-	1.1
	3.4	0.44	50	0.39	0.00	54	0.08	0.08	-	1.1
	3.8	0.48	46	0.29	0.00	55	0.13	0.11	-	1.0
$PyEG_5$-PEG_4MA	1.2	0.24	27	0.04	0.03	55	0.69	0.00	-	1.2
	1.9	0.27	27	0.14	0.03	56	0.56	0.00	-	1.1
	2.2	0.32	25	0.01	0.04	61	0.64	0.00		1.0
	2.4	0.34	48	0.35	0.05	56	0.26	0.00	-	1.2
	3.1	0.39	46	0.49	0.01	70	0.06	0.05	-	1.0
$PyEG_5$-PEG_5MA	2.2	0.25	53	0.72	0.03	-	-	-	-	1.1
	3.2	0.56	53	0.61	0.05	-	-	-	-	1.2
	3.6	0.35	54	0.60	0.05	-	-	-	-	1.1
	4.8	0.41	52	0.53	0.06	-	-	-	-	1.2
	6.5	0.46	52	0.46	0.08	-	-	-	-	1.1
$PyEG_5$-PEG_7MA τ_S = 4 ns	2.2	0.25	26	0.02	0.05	59	0.68	0.00	0.00	1.2
	3.0	0.32	49	0.29	0.04	68	0.34	0.00	0.01	1.1
	3.6	0.32	43	0.27	0.02	63	0.36	0.00	0.03	1.2
	4.2	0.36	48	0.33	0.05	67	0.23	0.00	0.02	1.2
$PyEG_5$-PEG_9MA	2.9	0.24	42	0.48	0.00	66	0.25	0.03	-	1.1
	5.2	0.35	44	0.24	0.00	55	0.36	0.06	-	1.1
	5.8	0.40	49	0.33	0.00	55	0.21	0.05		1.2
	7.4	0.45	45	0.26	0.00	55	0.21	0.08	-	1.1
	10.2	0.57	45	0.15	0.10	54	0.18	0.00	-	1.1
$PyEG_5$-$PEG_{19}MA$	2.1	0.22	44	0.42	0.00	67	0.32	0.03	-	1.1
	3.2	0.27	47	0.51	0.00	64	0.19	0.04	-	1.2
	5.2	0.37	41	0.11	0.00	54	0.47	0.05	-	1.1
	6.2	0.38	43	0.22	0.00	54	0.35	0.05	-	1.1
	6.6	0.42	46	0.33	0.03	62	0.18	0.04	-	1.1

Table S4.7. Parameters retrieved from the FBM analysis of the excimer decays for the $PyEG_5$-PEG_nMA samples in degassed THF.

Sample	Mol %	f_{Ek2}	τ_{E0} (ns)	$f_{EdiffE0}$	f_{EE0}	τ_D (ns)	f_{EdiffD}	f_{ED}	χ^2
$PyEG_5$-PEG_0MA	0.9	0.17	56	0.82	0.01	-	-	-	1.2
	2.0	0.28	53	0.71	0.01	-	-	-	1.1
	2.6	0.35	52	0.63	0.02	-	-	-	1.1
	3.3	0.42	51	0.56	0.02	-	-	-	1.1
	3.3	0.41	51	0.57	0.02	-	-	-	1.2
$PyEG_5$-PEG_3MA	2.0	0.27	52	0.53	0.04	70	0.13	0.03	1.1
	2.1	0.23	55	0.52	0.17	83	0.07	0.02	1.1
	3.0	0.34	48	0.32	0.00	59	0.28	0.06	1.1
	3.4	0.41	52	0.33	0.00	55	0.20	0.06	1.1
	3.8	0.45	49	0.33	0.00	57	0.14	0.09	1.1
$PyEG_5$-PEG_4MA	1.2	0.20	42	0.41	0.04	73	0.35	0.00	1.2
	1.9	0.24	51	0.61	0.04	90	0.11	0.00	1.1
	2.2	0.26	42	0.47	0.01	65	0.26	0.01	1.1
	2.4	0.27	44	0.45	0.05	66	0.22	0.01	1.0
	3.1	0.37	46	0.37	0.01	60	0.25	0.01	1.1
$PyEG_5$-PEG_5MA	2.2	0.25	47	0.42	0.00	64	0.32	0.02	1.2
	3.2	0.34	49	0.51	0.00	68	0.12	0.03	1.1
	3.6	0.34	47	0.42	0.00	62	0.22	0.03	1.1
	4.8	0.41	34	0.02	0.03	52	0.54	0.00	1.1
	6.5	0.48	50	0.32	0.05	54	0.16	0.00	1.0
$PyEG_5$-PEG_7MA	2.2	0.27	49	0.47	0.02	67	0.23	0.02	1.1
	3.0	0.31	51	0.53	0.00	78	0.13	0.00	1.1
	3.6	0.32	51	0.58	0.01	74	0.07	0.01	1.1
	4.2	0.38	54	0.54	0.02	80	0.04	0.02	1.1
$PyEG_5$-PEG_9MA	2.9	0.25	51	0.57	0.00	75	0.15	0.03	1.1
	5.2	0.36	49	0.42	0.00	61	0.20	0.03	1.1
	5.8	0.41	50	0.50	0.00	69	0.08	0.01	1.1
	7.4	0.44	51	0.50	0.00	70	0.01	0.05	1.1
	10.2	0.55	48	0.27	0.00	55	0.10	0.08	1.1
$PyEG_5$-$PEG_{19}MA$	2.1	0.23	58	0.75	0.02	-	-	-	1.2
	3.2	0.27	59	0.69	0.04	-	-	-	1.2
	4.4	0.27	54	0.69	0.05	-	-	-	1.1
	5.2	0.37	56	0.60	0.03	-	-	-	1.2
	6.2	0.35	52	0.60	0.05	-	-	-	1.2
	6.6	0.42	54	0.53	0.05	-	-	-	1.2

Table S4.8. Parameters retrieved from the FBM analysis of the excimer decays for the $PyEG_5$-PEG_nMA samples in degassed DMF.

Sample	Mol %	f_{Ek2}	τ_{E0} (ns)	$f_{EdiffE0}$	f_{EE0}	τ_D (ns)	f_{EdiffD}	f_{ED}	χ^2
$PyEG_5$-PEG_0MA	0.9	0.17	55	0.81	0.02	-	-	-	1.1
	2.0	0.27	50	0.71	0.02	-	-	-	1.1
	2.6	0.32	48	0.65	0.03	-	-	-	1.1
	3.3	0.40	49	0.57	0.03	-	-	-	1.1
	3.3	0.39	49	0.59	0.03	-	-	-	1.1
$PyEG_5$-PEG_3MA	2.0	0.20	46	0.64	0.02	83	0.10	0.04	1.2
	2.1	0.20	55	0.49	0.20	99	0.08	0.03	1.2
	3.0	0.26	49	0.64	0.04	73	0.05	0.01	1.1
	3.4	0.31	46	0.45	0.04	61	0.20	0.00	1.1
	3.8	0.36	48	0.41	0.02	52	0.21	0.00	1.1
$PyEG_5$-PEG_4MA	1.2	0.19	44	0.51	0.01	70	0.28	0.00	1.1
	1.9	0.23	48	0.52	0.02	69	0.24	0.00	1.1
	2.2	0.20	38	0.55	0.01	65	0.24	0.01	1.1
	2.4	0.23	41	0.48	0.04	62	0.25	0.00	1.1
	3.1	0.29	42	0.44	0.02	60	0.25	0.00	1.1
$PyEG_5$-PEG_5MA	2.2	0.24	45	0.51	0.00	62	0.23	0.02	1.0
	3.2	0.32	50	0.65	0.02	128	0.00	0.01	1.0
	3.6	0.32	47	0.47	0.03	57	0.18	0.00	1.0
	4.8	0.39	45	0.45	0.00	61	0.13	0.03	1.1
	6.5	0.47	49	0.30	0.01	49	0.20	0.02	1.2
$PyEG_5$-PEG_7MA	2.2	0.25	18	0.20	0.02	57	0.53	0.00	1.1
	3.0	0.34	54	0.43	0.04	64	0.20	0.00	1.1
	3.6	0.33	49	0.46	0.04	66	0.18	0.00	1.2
	4.2	0.40	51	0.31	0.04	61	0.25	0.00	1.1
$PyEG_5$-PEG_9MA	2.9	0.17	53	0.82	0.01	-	-	-	1.0
	5.2	0.24	53	0.75	0.02	-	-	-	1.1
	5.8	0.26	54	0.72	0.02	-	-	-	1.1
	7.4	0.30	52	0.68	0.02	-	-	-	1.1
	10.2	0.42	51	0.55	0.02	-	-	-	1.2
$PyEG_5$-$PEG_{19}MA$	2.1	0.20	61	0.78	0.02	-	-	-	1.1
	3.2	0.22	56	0.76	0.02	-	-	-	1.1
	4.4	0.27	61	0.71	0.02	-	-	-	1.2
	5.2	0.31	54	0.67	0.03	-	-	-	1.1
	6.2	0.30	49	0.68	0.02	-	-	-	1.0
	6.6	0.37	55	0.60	0.03	-	-	-	1.2

Table S4.9. Parameters retrieved from the FBM analysis of the excimer decays for the $PyEG_5$-PEG_nMA samples in aerated DMSO.

Sample	Mol %	f_{Ek2}	τ_{E0} (ns)	$f_{EdiffE0}$	f_{EE0}	τ_D (ns)	f_{EdiffD}	f_{ED}	f_{ES}	χ^2
$PyEG_5$-PEG_0MA	0.9	0.08	40	0.90	0.02	-	-	-	-	1.1
	2.0	0.14	39	0.84	0.02	-	-	-	-	1.1
	2.6	0.17	38	0.81	0.03	-	-	-	-	1.2
	3.3	0.19	39	0.78	0.03	-	-	-	-	1.1
	3.3	0.21	41	0.76	0.03	-	-	-	-	1.2
$PyEG_5$-PEG_3MA	1.6	0.10	41	0.81	0.09	-	-	-	-	1.2
	2.0	0.14	39	0.80	0.05	-	-	-	-	1.1
	3.0	0.18	39	0.78	0.05	-	-	-	-	1.1
	3.4	0.21	39	0.75	0.04	-	-	-	-	1.1
	3.8	0.24	38	0.73	0.03	-	-	-	-	1.0
$PyEG_5$-PEG_4MA	1.2	0.10	40	0.88	0.02	-	-	-	-	1.1
	1.9	0.13	40	0.85	0.03	-	-	-	-	1.1
	2.2	0.13	38	0.85	0.02	-	-	-	-	1.1
	2.4	0.14	39	0.81	0.05	-	-	-	-	1.2
	3.1	0.17	39	0.81	0.02	-	-	-	-	1.1
$PyEG_5$-PEG_5MA	2.2	0.15	43	0.82	0.02	-	-	-	-	1.1
	3.2	0.19	44	0.77	0.03	-	-	-	-	1.1
	3.6	0.21	43	0.76	0.03				-	1.1
	4.8	0.24	42	0.73	0.03	-	-	-	-	1.1
	6.5	0.29	42	0.67	0.03	-	-	-	-	1.2
$PyEG_5$-PEG_7MA τ_S = 4 ns	2.2	0.19	49	0.74	0.04	-	-	-	0.03	1.0
	3.0	0.21	48	0.72	0.03	-	-	-	0.04	1.0
	3.6	0.21	43	0.75	0.03	-	-	-	0.01	1.1
	4.2	0.23	45	0.71	0.04	-	-	-	0.02	1.1
$PyEG_5$-PEG_9MA	2.9	0.12	44	0.85	0.02	-	-	-	-	1.1
	5.2	0.18	42	0.80	0.02	-	-	-	-	1.1
	5.8	0.19	42	0.79	0.02	-	-	-	-	1.1
	7.4	0.22	41	0.75	0.03	-	-	-	-	1.1
	10.2	0.30	41	0.67	0.04	-	-	-	-	1.2
$PyEG_5$-$PEG_{19}MA$	2.1	0.12	60	0.85	0.03	-	-	-	-	1.1
	3.2	0.13	57	0.83	0.03	-	-	-	-	1.2
	5.2	0.18	49	0.79	0.03	-	-	-	-	1.0
	6.2	0.17	44	0.81	0.02	-	-	-	-	1.1
	6.6	0.19	48	0.77	0.03	-	-	-	-	1.2

Table S4.10. Molar fractions retrieved from the FBM analysis of the monomer and excimer decays for the $PyEG_5$-PEG_nMA samples in degassed acetonitrile.

Sample	Mol %	f_{free}	f_{agg}	f_{diff}	f_{k2}	χ^2
$PyEG_5$-PEG_0MA	0.9	0.06	0.03	0.68	0.24	1.0
	2.0	0.01	0.08	0.53	0.39	1.2
	3.0	0.01	0.08	0.43	0.49	1.1
	3.4	0.00	0.12	0.33	0.55	1.2
	3.8	0.00	0.10	0.34	0.55	1.1
$PyEG_5$-PEG_3MA	2.0	0.05	0.06	0.61	0.28	1.0
	2.1	0.06	0.15	0.51	0.27	1.1
	3.0	0.01	0.06	0.55	0.38	1.1
	3.4	0.01	0.08	0.47	0.44	1.1
	3.8	0.01	0.11	0.41	0.47	1.0
$PyEG_5$-PEG_4MA	1.2	0.14	0.02	0.63	0.21	1.2
	1.9	0.09	0.03	0.64	0.24	1.1
	2.2	0.06	0.03	0.61	0.30	1.0
	2.4	0.05	0.05	0.58	0.33	1.2
	3.1	0.02	0.06	0.54	0.38	1.0
$PyEG_5$-PEG_5MA	2.2	0.09	0.03	0.65	0.23	1.1
	3.2	0.02	0.04	0.50	0.45	1.2
	3.6	0.02	0.05	0.59	0.34	1.1
	4.8	0.01	0.06	0.53	0.40	1.2
	6.5	0.01	0.08	0.66	0.29	1.1
$PyEG_5$-PEG_7MA	2.2	0.06	0.05	0.65	0.24	1.2
	3.0	0.03	0.04	0.62	0.31	1.1
	3.6	0.02	0.02	0.63	0.33	1.2
	4.2	0.02	0.05	0.57	0.37	1.2
$PyEG_5$-PEG_9MA	2.9	0.11	0.03	0.65	0.21	1.1
	5.2	0.02	0.06	0.58	0.34	1.1
	5.8	0.02	0.05	0.53	0.40	1.2
	7.4	0.01	0.07	0.47	0.44	1.1
	10.2	0.00	0.10	0.33	0.57	1.1
$PyEG_5$-$PEG_{19}MA$	2.1	0.28	0.02	0.53	0.16	1.1
	3.2	0.14	0.03	0.60	0.23	1.2
	5.2	0.08	0.05	0.53	0.34	1.1
	6.2	0.03	0.05	0.55	0.37	1.1
	6.6	0.04	0.06	0.49	0.41	1.1

Table S4.11. Molar fractions retrieved from the FBM analysis of the monomer and excimer decays for the $PyEG_5$-PEG_nMA samples in degassed THF.

Sample	Mol %	f_{free}	f_{agg}	f_{diff}	f_{k2}	χ^2
$PyEG_5$-PEG_0MA	0.9	0.13	0.01	0.72	0.14	1.2
	2.0	0.03	0.01	0.69	0.27	1.1
	2.6	0.02	0.02	0.62	0.34	1.1
	3.3	0.00	0.02	0.56	0.42	1.1
	3.3	0.00	0.02	0.57	0.41	1.2
$PyEG_5$-PEG_3MA	2.0	0.06	0.07	0.62	0.25	1.1
	2.1	0.05	0.17	0.56	0.21	1.1
	3.0	0.02	0.06	0.58	0.34	1.1
	3.4	0.01	0.06	0.53	0.41	1.1
	3.8	0.00	0.08	0.47	0.44	1.1
$PyEG_5$-PEG_4MA	1.2	0.17	0.03	0.64	0.16	1.2
	1.9	0.16	0.03	0.60	0.20	1.1
	2.2	0.09	0.02	0.66	0.23	1.1
	2.4	0.06	0.05	0.63	0.26	1.0
	3.1	0.02	0.02	0.60	0.36	1.1
$PyEG_5$-PEG_5MA	2.2	0.10	0.02	0.66	0.22	1.2
	3.2	0.03	0.03	0.61	0.33	1.1
	3.6	0.03	0.03	0.62	0.33	1.1
	4.8	0.01	0.03	0.55	0.41	1.1
	6.5	0.00	0.05	0.47	0.48	1.0
$PyEG_5$-PEG_7MA	2.2	0.15	0.02	0.60	0.23	1.1
	3.0	0.07	0.03	0.61	0.29	1.1
	3.6	0.05	0.03	0.62	0.30	1.1
	4.2	0.04	0.04	0.56	0.37	1.1
$PyEG_5$-PEG_9MA	2.9	0.12	0.03	0.63	0.22	1.1
	5.2	0.02	0.03	0.60	0.35	1.1
	5.8	0.02	0.01	0.57	0.40	1.1
	7.4	0.01	0.05	0.51	0.44	1.1
	10.2	0.00	0.08	0.37	0.55	1.1
$PyEG_5$-$PEG_{19}MA$	2.1	0.30	0.01	0.52	0.16	1.2
	3.2	0.13	0.03	0.60	0.24	1.2
	4.4	0.12	0.04	0.61	0.23	1.1
	5.2	0.08	0.03	0.54	0.34	1.2
	6.2	0.03	0.05	0.58	0.34	1.2
	6.6	0.03	0.04	0.52	0.41	1.2

Table S4.12. Molar fractions retrieved from the FBM analysis of the monomer and excimer decays for the $PyEG_5$-PEG_nMA samples in degassed DMF.

Sample	Mol %	f_{free}	f_{agg}	f_{diff}	f_{k2}	□□
$PyEG_5$-PEG_0MA	0.9	0.16	0.02	0.75	0.16	1.1
	2.0	0.03	0.02	0.85	0.32	1.1
	2.6	0.02	0.03	0.84	0.42	1.1
	3.3	0.00	0.04	0.84	0.59	1.1
	3.3	0.00	0.04	0.84	0.56	1.1
$PyEG_5$-PEG_3MA	2.0	0.10	0.05	0.66	0.18	1.2
	2.1	0.12	0.20	0.50	0.17	1.2
	3.0	0.04	0.05	0.66	0.25	1.1
	3.4	0.02	0.04	0.64	0.31	1.1
	3.8	0.01	0.02	0.61	0.36	1.1
$PyEG_5$-PEG_4MA	1.2	0.21	0.01	0.62	0.15	1.1
	1.9	0.16	0.02	0.64	0.19	1.1
	2.2	0.12	0.01	0.70	0.18	1.1
	2.4	0.09	0.04	0.66	0.20	1.1
	3.1	0.04	0.02	0.66	0.28	1.1
$PyEG_5$-PEG_5MA	2.2	0.11	0.02	0.66	0.21	1.0
	3.2	0.04	0.02	0.63	0.31	1.0
	3.6	0.04	0.03	0.63	0.31	1.0
	4.8	0.02	0.03	0.57	0.38	1.1
	6.5	0.00	0.03	0.50	0.47	1.2
$PyEG_5$-PEG_7MA	2.2	0.17	0.02	0.61	0.21	1.1
	3.0	0.10	0.03	0.56	0.30	1.1
	3.6	0.06	0.03	0.60	0.31	1.2
	4.2	0.04	0.04	0.53	0.38	1.1
$PyEG_5$-PEG_9MA	2.9	0.16	0.01	0.69	0.14	1.0
	5.2	0.05	0.01	0.71	0.23	1.1
	5.8	0.05	0.02	0.68	0.25	1.1
	7.4	0.05	0.02	0.64	0.29	1.1
	10.2	0.01	0.02	0.55	0.42	1.2
$PyEG_5$-$PEG_{19}MA$	2.1	0.35	0.02	0.51	0.13	1.1
	3.2	0.18	0.02	0.62	0.18	1.1
	4.4	0.12	0.02	0.62	0.24	1.2
	5.2	0.11	0.02	0.59	0.27	1.1
	6.2	0.05	0.02	0.64	0.28	1.0
	6.6	0.04	0.03	0.57	0.36	1.2

Table S4.13. Molar fractions retrieved from the FBM analysis of the monomer and excimer decays for the $PyEG_5$-PEG_nMA samples in aerated DMSO.

Sample	Mol %	f_{free}	f_{agg}	f_{diff}	f_{k2}	χ^2
$PyEG_5$-PEG_0MA	0.9	0.18	0.02	0.74	0.07	1.1
	2.0	0.04	0.02	0.81	0.13	1.1
	2.6	0.03	0.03	0.79	0.16	1.2
	3.3	0.01	0.03	0.77	0.19	1.1
	3.3	0.01	0.03	0.77	0.21	1.2
$PyEG_5$-PEG_3MA	1.6	0.22	0.07	0.63	0.08	1.2
	2.0	0.07	0.05	0.74	0.13	1.1
	3.0	0.05	0.04	0.74	0.17	1.1
	3.4	0.04	0.04	0.72	0.21	1.1
	3.8	0.02	0.03	0.71	0.23	1.0
$PyEG_5$-PEG_4MA	1.2	0.20	0.02	0.70	0.08	1.1
	1.9	0.17	0.02	0.70	0.10	1.1
	2.2	0.17	0.02	0.70	0.10	1.1
	2.4	0.10	0.04	0.73	0.13	1.2
	3.1	0.09	0.02	0.74	0.16	1.1
$PyEG_5$-PEG_5MA	2.2	0.16	0.02	0.69	0.13	1.1
	3.2	0.07	0.03	0.72	0.18	1.1
	3.6	0.05	0.03	0.72	0.20	1.1
	4.8	0.02	0.03	0.72	0.23	1.1
	6.5	0.02	0.03	0.66	0.29	1.2
$PyEG_5$-PEG_7MA	2.2	0.04	0.03	0.71	0.18	1.0
	3.0	0.04	0.03	0.72	0.20	1.0
	3.6	0.04	0.02	0.72	0.20	1.1
	4.2	0.03	0.04	0.70	0.23	1.1
$PyEG_5$-PEG_9MA	2.9	0.20	0.02	0.68	0.10	1.1
	5.2	0.07	0.02	0.75	0.16	1.1
	5.8	0.06	0.02	0.74	0.18	1.1
	7.4	0.02	0.03	0.74	0.22	1.1
	10.2	0.00	0.04	0.67	0.30	1.2
$PyEG_5$-$PEG_{19}MA$	2.1	0.44	0.02	0.47	0.07	1.1
	3.2	0.32	0.02	0.57	0.09	1.2
	5.2	0.15	0.03	0.67	0.15	1.0
	6.2	0.12	0.02	0.71	0.15	1.1
	6.6	0.02	0.03	0.76	0.19	1.2

S5 - Supporting Information for Chapter 5

Fluorescence blob model (FBM) equations

Equations S5.1 and S5.2 were used to globally fit the monomer and excimer decays of $PyEG_5$-PEG_nMA in water and PyC4-PEG_nMA in both water and THF. The parameters obtained from the fits are listed in Tables S5.1-S5.6 and a sample fit of the monomer and excimer decay is shown in Figure S5.8.

$$[Py^*]_{(t)} = [Py^*_{diff}]_{(t)} + [Py^*_{k2}]_{(t)} + [Py^*_{free}]_{(t)} = [Py_{diff}]_o \exp\left(-\left(A_2 + \frac{1}{\tau_M}\right)t - A_3\left(1-\exp(-A_4 t)\right)\right)$$

$$+\left([Py_{k2}]_o + [Py_{diff}]_o e^{-A_3}\sum_{i=0}^{\infty}\frac{A_3^i}{i!}\frac{A_2+iA_4}{A_2+iA_4-k_2}\right)\exp\left(-\left(k_2+\frac{1}{\tau_M}\right)t\right)$$

$$-[Py_{diff}]_o e^{-A_3}\sum_{i=0}^{\infty}\frac{A_3^i}{i!}\frac{A_2+iA_4}{A_2+iA_4-k_2}\exp\left(-\left(A_2+iA_4+\frac{1}{\tau_M}\right)t\right)$$

$$+[Py_{free}]_o \exp\left(-\frac{t}{\tau_M}\right)\Bigg] \qquad \text{(S5.1)}$$

$$[E^*]_{(t)} = [E0^*]_{(t)} + [D^*]_{(t)} = k_2\left(\left([Py_{k2}(E0)]_o + [Py_{diff}(E0)]_o e^{-A_3}\sum_{i=0}^{\infty}\frac{A_3^i}{i!}\frac{A_2+iA_4}{A_2+iA_4-k_2}\right)\right.$$

$$\times \frac{\exp\left(-\frac{t}{\tau_{E0}}\right)-\exp\left(-\left(k_2+\frac{1}{\tau_M}\right)t\right)}{k_2+\frac{1}{\tau_M}-\frac{1}{\tau_{E0}}}$$

$$+[Py_{diff}(E0)]_o e^{-A_3}\sum_{i=0}^{\infty}\frac{A_3^i}{i!}\frac{A_2+iA_4}{A_2+iA_4-k_2}\frac{\exp\left(-\left(A_2+iA_4+\frac{1}{\tau_M}\right)t\right)-\exp\left(-\frac{t}{\tau_{E0}}\right)}{A_2+iA_4+\frac{1}{\tau_M}-\frac{1}{\tau_{E0}}}\Bigg)$$

$$+k_2\Bigg(\Bigg([Py_{k2}(D)]_o+[Py_{diff}(D)]_o e^{-A_3}\sum_{i=0}^{\infty}\frac{A_3^i}{i!}\frac{A_2+iA_4}{A_2+iA_4-k_2}\Bigg)\times\frac{\exp\left(-\frac{t}{\tau_D}\right)-\exp\left(-\left(k_2+\frac{1}{\tau_M}\right)t\right)}{k_2+\frac{1}{\tau_M}-\frac{1}{\tau_D}}$$

$$+[Py_{diff}(D)]_o e^{-A_3}\sum_{i=0}^{\infty}\frac{A_3^i}{i!}\frac{A_2+iA_4}{A_2+iA_4-k_2}\frac{\exp\left(-\left(A_2+iA_4+\frac{1}{\tau_M}\right)t\right)-\exp\left(-\frac{t}{\tau_D}\right)}{A_2+iA_4+\frac{1}{\tau_M}-\frac{1}{\tau_D}}\Bigg)$$

$$+[E0]_o\times\exp\left(-\frac{t}{\tau_{E0}}\right)+[D]_o\times\exp\left(-\frac{t}{\tau_D}\right)\Bigg] \qquad \text{(S5.2)}$$

The expression of the parameters A_2, A_3, and A_4 used in Equations S1 and S2 are given in Equations S3.a–c.

$$A_2 =< n > \times\frac{k_{blob}k_e[blob]}{k_{blob}+k_e[blob]} \qquad \text{(S5.3.a)}$$

$$A_3 = < n > \times \left(\frac{k_{blob}}{k_{blob} + k_e[blob]} \right)^2 \qquad \text{(S5.3b)}$$

$$A_4 = k_{blob} + k_e[blob] \qquad \text{(S5.3.c)}$$

^{1}H NMR spectra

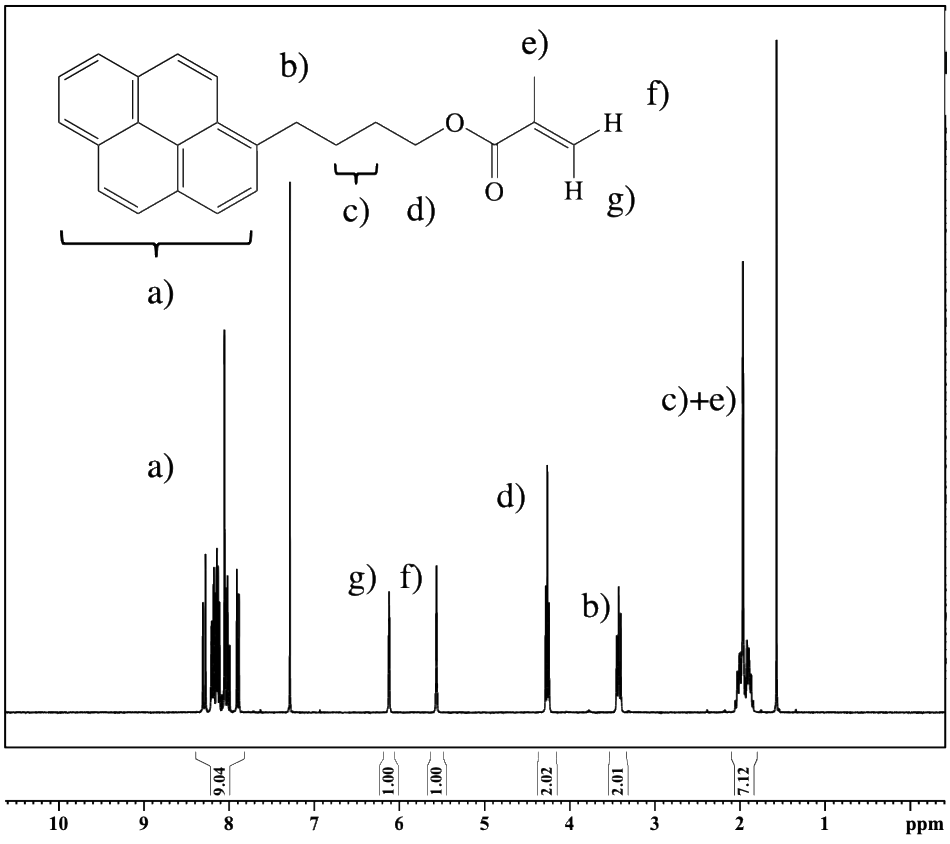

Figure S5.1. ^{1}H NMR spectrum of 1-pyrenebutyl methacrylate (PyC_4MA). (300 MHz, $CDCl_3$): δ 1.83-2.07 (m, 7H), 3.43 (t, 2H), 4.27 (t, 2H), 5.57 (d, 1H), 6.12 (d, 1H), 7.86-8.34 (m, 9H).

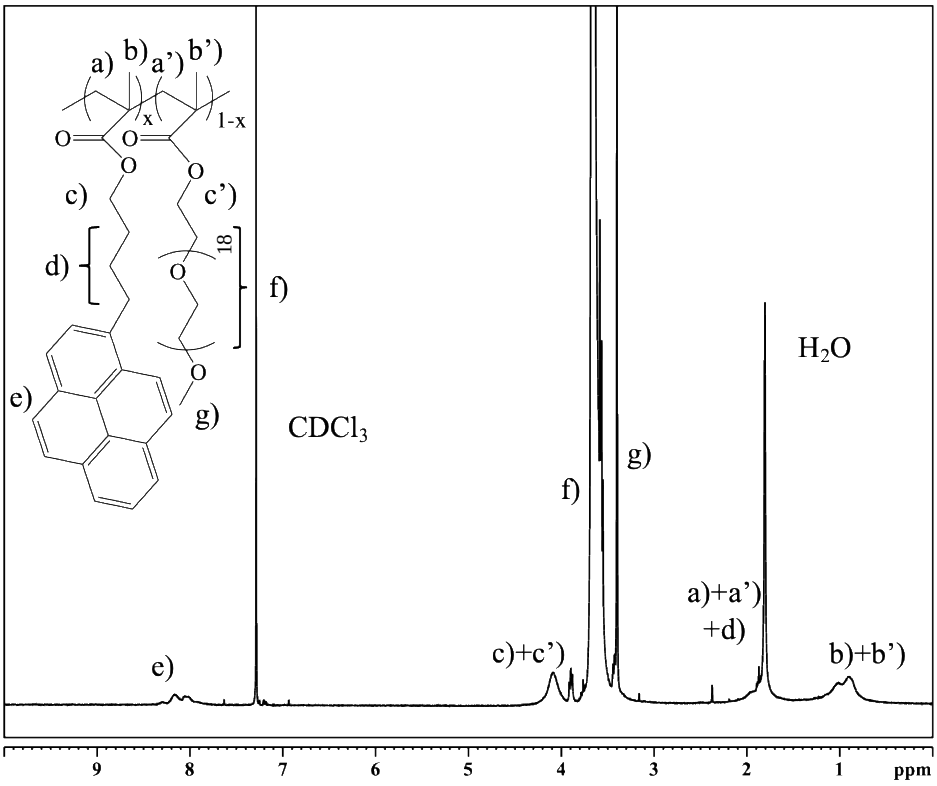

Figure S5.2. ^{1}H NMR spectrum of PyC_4-$PEG_{19}MA$ with a pyrene content of 7.4 mol %. (300 MHz, $CDCl_3$).

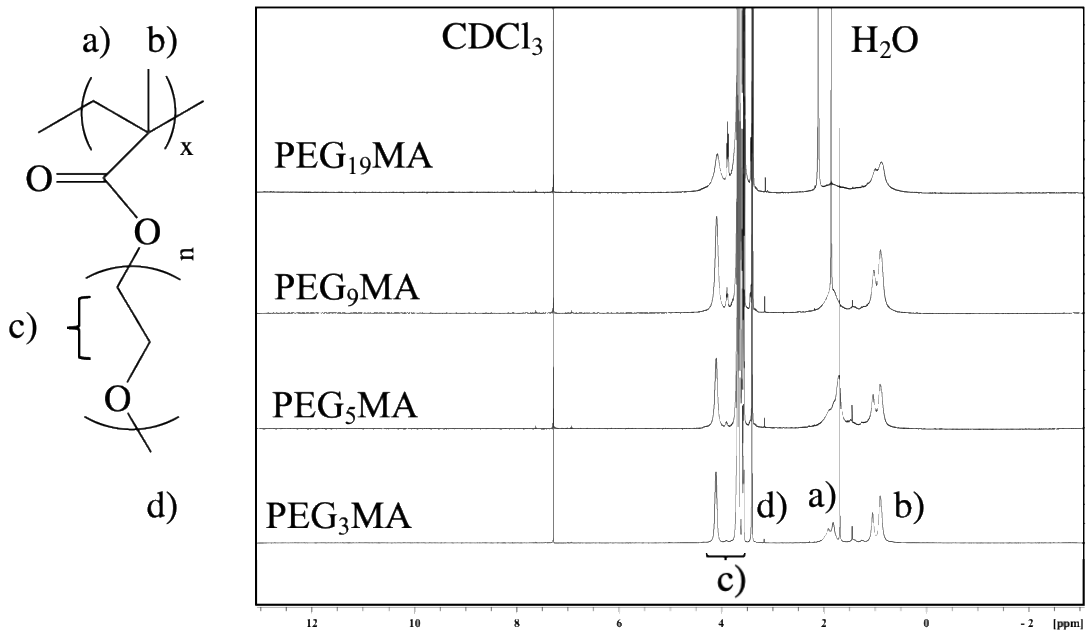

Figure S5.3. ^{1}H NMR spectrum of PEG$_n$MA polymers where n= 3, 5, 9, and 19. (300 MHz, $CDCl_3$).

Gel permeation chromatography (GPC) traces

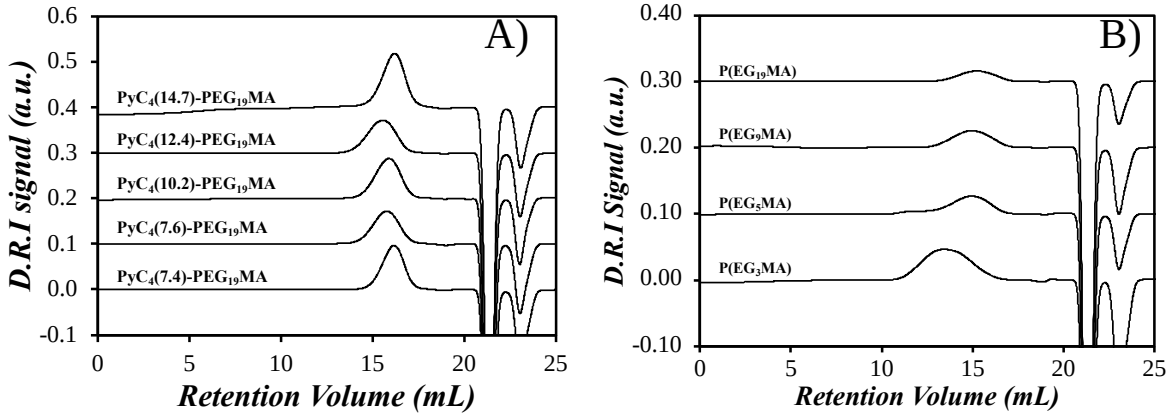

Figure S5.4. GPC traces acquired in DMSO for the A) $PyC_4(x)$-$PEG_{19}MA$ series where x = 7.4, 7.6, 10.2, 12.4, or 14.7 mol % pyrene labeling and the B) PEG_nMA homopolymers.

Steady-state fluorescence (SSF) spectra

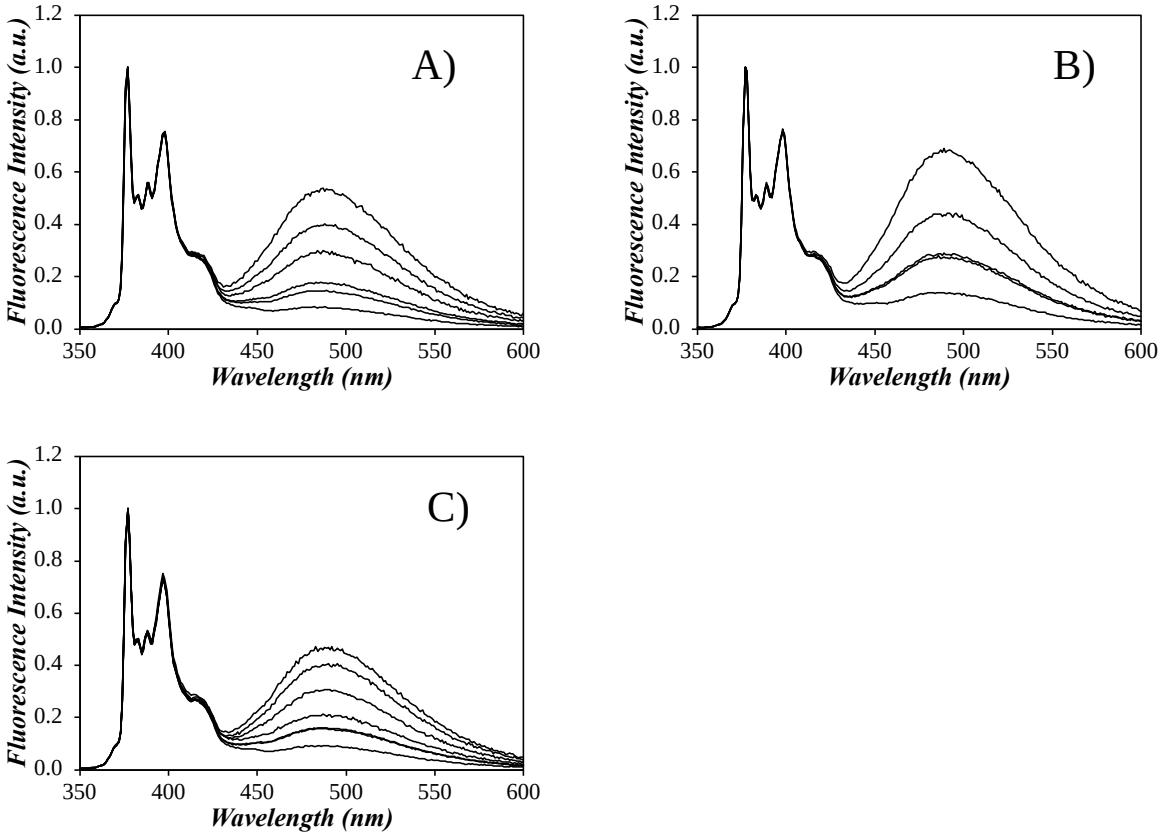

Figure S5.5. Steady state fluorescence spectra for the A) $PyEG_5$-PEG_3MA, B) $PyEG_5$-PEG_5MA, and C) $PyEG_5$-$PEG_{19}MA$ samples in water.

Concentration study

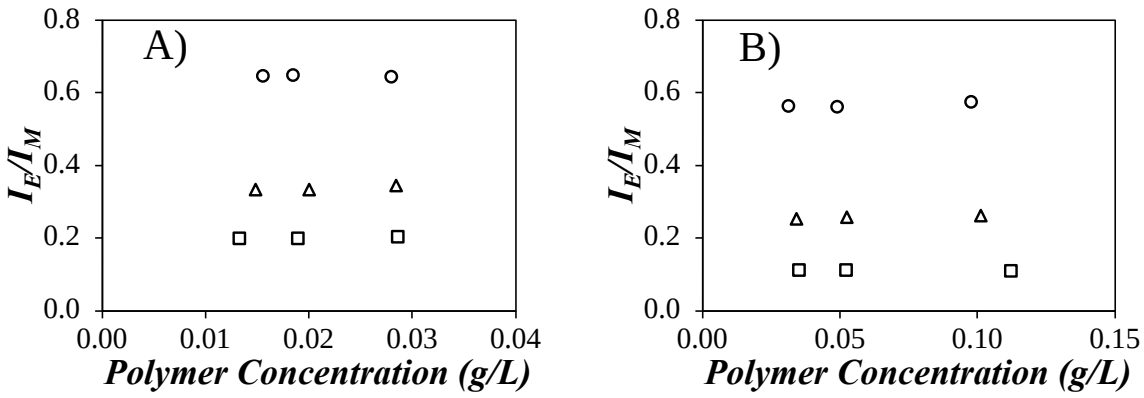

Figure S5.6. Effect of polymer concentration on the I_E/I_M ratio for A) $PyEG_5$-PEG_3MA with pyrene content of (□)2.0 mol %, (△) 3.0 mol %, and (○) 3.8 mol % and B) $PyEG_5$-$PEG_{19}MA$ with pyrene content of (□) 2.1 mol %, (△) 4.4 mol %, and (○) 6.6 mol % in water.

Molar extinction coefficient of pyrene

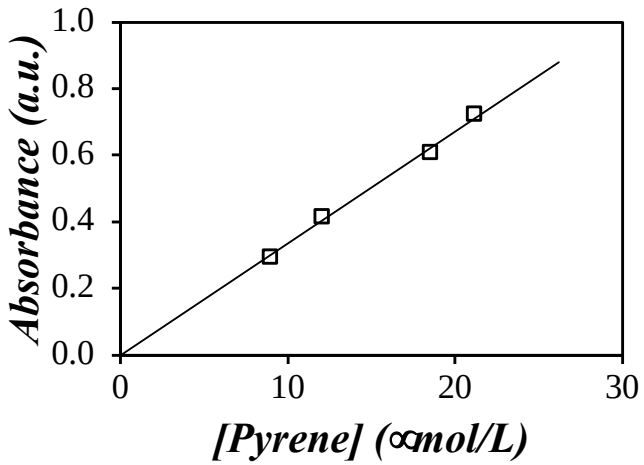

Figure S5.7. Plot of absorbance versus concentration of molecular pyrene in a 2.70 g/L aqueous solution of PEG_3MA. The line of best fit was found to equal 33,500 ± 400 $M^{-1}cm^{-1}$.

Sample fit of the global FBM analysis of the fluorescence decays

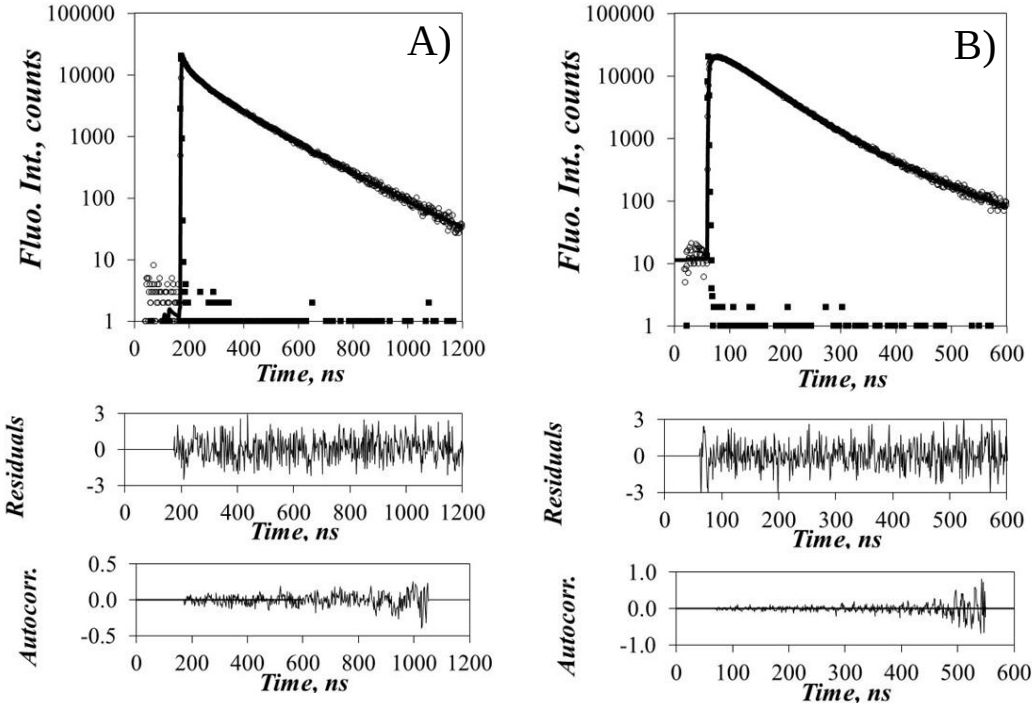

Figure S5.8. Global FBM analysis of the fluorescence decays of the pyrene A) monomer and B) excimer acquired at 375 nm and 510 nm, respectively, for $PyEG_5$-PEG_3MA with a pyrene content of 3.4 mol%. $\chi^2 = 1.09$, $\lambda_{ex} = 344$ nm.

Parameters retrieved from the FBM

Table S5.1. Parameters retrieved from the FBM analysis of the monomer decays for the $PyEG_5$-PEG_nMA and PyC_4-$PEG_{19}MA$ samples in water.

Sample	Mol%	k_{blob} ($10^6 s^{-1}$)	<n>	$k_e[blob]$ ($10^6 s^{-1}$)	f_{Mdiff}	f_{k2}	f_{Mfree}	χ^2
$PyEG_5$-PEG_3MA $k_2 = 1.42\times10^8$ s^{-1} τ_M = 210 ns	2.0	15.6	0.85	2.87	0.41	0.16	0.43	1.1
	2.1	13.4	0.86	2.23	0.36	0.13	0.51	1.1
	3.0	13.1	0.93	3.65	0.55	0.21	0.24	1.1
	3.4	11.9	1.06	2.94	0.58	0.26	0.16	1.1
	3.8	10.9	1.23	2.93	0.62	0.28	0.10	1.1
$PyEG_5$-PEG_5MA $k_2 = 1.46\times10^8$ s^{-1} τ_M = 215 ns	2.2	14.3	0.77	4.75	0.39	0.15	0.46	1.2
	3.6	13.2	0.91	4.46	0.48	0.24	0.28	1.1
	3.8	13.3	0.89	4.58	0.49	0.24	0.27	1.1
	4.8	12.3	1.06	4.22	0.52	0.30	0.19	1.1
	6.5	11.9	1.22	3.84	0.51	0.37	0.12	1.2
$PyEG_5$-PEG_9MA $k_2 = 1.58\times10^8$ s^{-1} τ_M = 213 ns	2.9	17.4	0.78	4.50	0.44	0.17	0.39	1.1
	5.2	14.7	0.94	3.01	0.54	0.27	0.19	1.1
	5.8	16.1	0.99	3.48	0.52	0.30	0.18	1.1
	7.4	14.5	1.16	3.81	0.51	0.37	0.12	1.1
	10.2	13.8	1.46	2.59	0.49	0.47	0.04	1.1
$PyEG_5$-$PEG_{19}MA$ $k_2 = 1.48\times10^8$ s^{-1} τ_M = 209 ns	2.1	17.8	0.89	2.60	0.27	0.13	0.60	1.2
	3.2	15.2	0.88	4.09	0.38	0.00	0.44	1.1
	4.4	24.4	0.96	3.67	0.48	0.22	0.30	1.1
	5.2	18.3	1.05	4.15	0.45	0.23	0.32	1.0
	6.3	12.1	1.11	3.01	0.52	0.28	0.20	1.1
	6.6	13.9	1.20	3.43	0.45	0.36	0.20	1.0
$PyC4$-$PEG_{19}MA$ $k_2 = 2.45\times10^8$ s^{-1} τ_M = 156 ns	7.4	15.7	1.12	4.93	0.50	0.24	0.24	1.1
	7.6	17.9	1.03	5.92	0.51	0.21	0.28	1.2
	10.2	16.7	1.24	4.34	0.54	0.33	0.13	1.1
	12.4	16.1	1.38	4.14	0.56	0.37	0.07	1.0
	14.7	16.8	1.48	4.19	0.49	0.43	0.08	1.0

Table S5.2. Parameters retrieved from the FBM analysis of the excimer decays for the $PyEG_5$-PEG_nMA and PyC_4-$PEG_{19}MA$ samples in water.

Sample	Mol %	f_{Ek2}	τ_{E0} (ns)	$f_{EdiffE0}$	f_{EE0}	τ_D (ns)	f_{EdiffD}	f_{ED}	χ^2
$PyEG_5$-PEG_3MA	2.0	0.19	49	0.30	0.30	82	0.21	0.00	1.1
	2.1	0.16	48	0.28	0.41	90	0.16	0.00	1.1
	3.0	0.21	48	0.39	0.23	73	0.15	0.03	1.1
	3.4	0.23	47	0.48	0.15	86	0.02	0.12	1.1
	3.8	0.23	43	0.30	0.13	64	0.22	0.13	1.1
$PyEG_5$-PEG_5MA	2.2	0.21	54	0.55	0.24	-	-	-	1.2
	3.6	0.24	55	0.49	0.27	-	-	-	1.1
	3.8	0.24	55	0.49	0.27	-	-	-	1.1
	4.8	0.26	55	0.26	0.30	-	-	-	1.1
	6.5	0.28	55	0.38	0.34	-	-	-	1.2
$PyEG_5$-PEG_9MA	2.9	0.20	52	0.53	0.17	36	0.00	0.09	1.1
	5.2	0.24	62	0.18	0.25	37	0.30	0.03	1.1
	5.8	0.25	59	0.26	0.31	36	0.17	0.02	1.1
	7.4	0.27	55	0.35	0.20	44	0.02	0.15	1.1
	10.2	0.28	38	0.21	0.01	63	0.08	0.41	1.1
$PyEG_5$-$PEG_{19}MA$	2.1	0.25	43	0.33	0.23	82	0.19	0.00	1.2
	3.2	0.24	60	0.45	0.25	97	0.05	0.00	1.1
	4.4	0.17	55	0.30	0.47	101	0.07	0.00	1.1
	5.2	0.19	53	0.33	0.44	85	0.04	0.00	1.0
	6.3	0.25	42	0.41	0.12	72	0.05	0.17	1.1
	6.6	0.29	48	0.31	0.26	74	0.04	0.10	1.0
PyC4-$PEG_{19}MA$	7.4	0.22	52	0.31	0.26	83	0.14	0.08	1.1
	7.6	0.19	56	0.34	0.28	88	0.14	0.05	1.2
	10.2	0.25	53	0.17	0.35	82	0.23	0.00	1.1
	12.4	0.24	54	0.17	0.39	86	0.20	0.00	1.0
	14.7	0.25	55	0.11	0.46	87	0.17	0.01	1.0

Table S5.3. Molar fractions retrieved from the FBM analysis of the monomer and excimer decays for the $PyEG_5$-PEG_nMA and PyC_4-$PEG_{19}MA$ samples in water.

Sample	Mol %	f_{free}	f_{agg}	f_{diff}	f_{k2}	χ^2
$PyEG_5$-PEG_3MA	2.0	0.28	0.21	0.37	0.14	1.1
	2.1	0.31	0.28	0.30	0.11	1.1
	3.0	0.15	0.22	0.46	0.18	1.1
	3.4	0.09	0.24	0.46	0.21	1.1
	3.8	0.05	0.24	0.49	0.22	1.1
$PyEG_5$-PEG_5MA	2.2	0.32	0.16	0.38	0.14	1.2
	3.6	0.16	0.23	0.41	0.20	1.1
	3.8	0.16	0.22	0.42	0.20	1.1
	4.8	0.07	0.34	0.29	0.29	1.1
	6.5	0.05	0.33	0.36	0.26	1.2
$PyEG_5$-PEG_9MA	2.9	0.26	0.20	0.40	0.15	1.1
	5.2	0.10	0.25	0.43	0.22	1.1
	5.8	0.09	0.30	0.39	0.23	1.1
	7.4	0.05	0.33	0.36	0.26	1.1
	10.2	0.01	0.42	0.29	0.28	1.1
$PyEG_5$-$PEG_{19}MA$	2.1	0.44	0.13	0.29	0.14	1.2
	3.2	0.28	0.18	0.36	0.18	1.1
	4.4	0.13	0.41	0.31	0.14	1.1
	5.2	0.15	0.37	0.32	0.16	1.0
	6.3	0.11	0.26	0.41	0.22	1.1
	6.6	0.08	0.33	0.33	0.26	1.0
PyC4-$PEG_{19}MA$	7.4	0.13	0.29	0.39	0.19	1.1
	7.6	0.16	0.28	0.40	0.16	1.2
	10.2	0.06	0.33	0.38	0.23	1.1
	12.4	0.03	0.38	0.35	0.24	1.0
	14.7	0.02	0.46	0.27	0.24	1.0

Table S5.4. Parameters retrieved from the FBM analysis of the monomer decays for PyC_4-PEG_nMA samples in THF.

Sample	Mol%	k_{blob} ($10^6 s^{-1}$)	<n>	$k_e[blob]$ ($10^6 s^{-1}$)	f_{Mdiff}	f_{k2}	f_{Mfree}	χ^2
PyC_4-$PEG_{19}MA$ $k_2 = 1.08\times10^8$ s^{-1} τ_M = 200 ns	7.4	7.9	1.24	3.22	0.66	0.22	0.12	1.2
	7.6	9.7	1.11	4.12	0.64	0.24	0.12	1.0
	10.2	9.3	1.46	3.69	0.64	0.31	0.05	1.1
	12.4	9.2	1.73	3.89	0.61	0.37	0.02	1.1
	14.7	8.6	2.14	2.47	0.53	0.45	0.02	1.1

Table S5.5. Parameters retrieved from the FBM analysis of the excimer decays for the PyC_4-PEG_nMA samples in THF.

Sample	Mol %	f_{Ek2}	τ_{E0} (ns)	$f_{EdiffE0}$	f_{EE0}	τ_D (ns)	f_{EdiffD}	f_{ED}	χ^2
PyC_4-$PEG_{19}MA$	7.4	0.24	44	0.46	0.01	71	0.25	0.04	1.2
	7.6	0.26	48	0.49	0.00	77	0.20	0.06	1.0
	10.2	0.31	62	0.43	0.06	38	0.21	0.00	1.1
	12.4	0.35	65	0.27	0.07	46	0.31	0.00	1.1
	14.7	0.42	47	0.33	0.00	68	0.17	0.09	1.1

Table S5.6. Molar fractions retrieved from the FBM analysis of the monomer and excimer decays for the PyC_4-PEG_nMA samples in THF.

Sample	Mol %	f_{free}	f_{agg}	f_{diff}	f_{k2}	χ^2
PyC_4-$PEG_{19}MA$	7.4	0.09	0.04	0.65	0.22	1.2
	7.6	0.08	0.06	0.63	0.23	1.0
	10.2	0.03	0.06	0.61	0.30	1.1
	12.4	0.01	0.07	0.57	0.35	1.1
	14.7	0.01	0.09	0.49	0.42	1.1